Leaf anatomy and photosynthesis:

Unravelling the CO_2 diffusion pathway in C_3 leaves

Herman Nicolaas Cornelis Berghuijs

Thesis committee

Promotors

Prof. Dr P.C. Struik

Professor of Crop Physiology

Wageningen University

Prof. Dr B.M. Nicolaï

Professor of Biosystems Engineering

KU Leuven, Belgium

Co-promotor

Dr X. Yin

Senior scientist, Centre for Crop Systems Analysis

Wageningen University

Other members

Prof. Dr J. Molenaar, Wageningen UR

Prof. Dr B.M. Mulder, Wageningen UR

Prof. Dr M. de Proft, KU Leuven, Belgium

Prof. Dr W. Saeys, KU Leuven, Belgium

This research was conducted under the joined auspices of the C.T. de Wit Graduate School for Production Ecology and Resource Conservation and the Arenberg Doctoral School.

Leaf anatomy and photosynthesis:

Unravelling the CO_2 diffusion pathway in C_3 leaves

Herman Nicolaas Cornelis Berghuijs

Thesis
submitted in fulfilment of the requirements for the joint degree of doctor at
Wageningen University
by the authority of the Rector Magnificus
Prof. Dr A.P.J. Mol
and doctor in de bio-ingenieurswetenschappen van de
KU Leuven
by the authority of the Director of the Arenberg Doctoral School
Prof. Dr G. Govers
in the presence of the
thesis committee appointed by
the Academic Board of Wageningen University
and
the Director of the Arenberg Doctoral School of the KU Leuven
to be defended in public
on Wednesday May 25, 2016
at 1:30 p.m. in the Aula, Wageningen University

Berghuijs, H.N.C.
Leaf anatomy and photosynthesis; unravelling the CO_2 diffusion pathway in C_3 leaves
Joint PhD thesis, Wageningen University, Wageningen, NL; KU Leuven, Leuven, BE (2016), 286 pages
With references, with summaries in English and Dutch
DOI: 10.18174/379249
ISBN: 978-94-6257-794-7

Abstract

Herman Nicolaas Cornelis Berghuijs (2016). Leaf anatomy and photosynthesis; unravelling the CO_2 diffusion pathway in C_3 leaves. PhD thesis. Wageningen University, Wageningen, The Netherlands, with summaries in English and Dutch. 286 pages

Optimizing photosynthesis can contribute to improving crop yield, which is necessary to meet the increasing global demand for food, fibre, and bioenergy. One way to optimize photosynthesis in C_3 plants is to enhance the efficiency of CO_2 transport from the intercellular air space to Rubisco. The drawdown of CO_2 between these locations is commonly modelled by Fick's first law of diffusion. This law states that the flux from the air spaces to Rubisco is proportional to the difference in partial pressure between these locations. The proportionality constant is the mesophyll conductance. Its inverse is mesophyll resistance. Mesophyll resistance is a complex trait, which lumps various structural barriers for CO_2 transport and processes that add or remove CO_2 along the diffusion pathway. In order to better understand how and to what extent these factors affect photosynthesis, it is necessary to find a more mechanistic description of CO_2 transport in the mesophyll. The aim of this dissertation is to investigate how leaf anatomical properties and CO_2 sources and sinks along the CO_2 diffusion pathway in C_3 leaves affect the photosynthetic capacity of these leaves. In this study, *Solanum lycopersicum* was used as a model organism. In a first approach, we developed a model in which we partitioned mesophyll resistance into two sub-resistances. The model assumed that CO_2 produced by respiration and photorespiration was released between the two sub-resistance components. By quantifying these resistances using measured thicknesses, exposed mesophyll and chloroplast surfaces, and assumed diffusive properties, we were able to simulate the effect of various anatomical properties on photosynthesis. A disadvantage of this two-resistance approach is that it assumes either that (photo)respiratory CO_2 release takes place in the outer cytosol or that there is no CO_2 gradient in the cytosol. Therefore, in a second approach we modelled CO_2 transport, production and consumption by use of a reaction-diffusion model. This model is more flexible in terms of determining the

location of CO_2 sources and sinks. We developed methods to estimate physiological parameters of this model using combined gas exchange and chlorophyll fluorescence measurements on leaves. The results suggest that the rate of respiration depends on the oxygen partial pressure, which is often not considered in previous photosynthesis models. We also presented a method to calculate the fraction of (photo)respiratory CO_2 that is re-assimilated. We found that this fraction strongly depends on both environmental factors (CO_2, irradiance), the location of mitochondria relative to the chloroplast, stomatal conductance and various physiological parameters. The reaction-diffusion model and associated methods presented in this study provide a more mechanistic framework to describe the CO_2 diffusion pathway in C_3 leaves. This model could, therefore, contribute to identifying targets to increase mesophyll conductance in future research.

Keywords: CO_2 diffusion, C_3 photosynthesis, mesophyll conductance, mesophyll resistance, re-assimilation, photorespiration, respiration, tomato

Table of contents

CHAPTER 1

General introduction

1.1 Introduction

Photosynthesis can be defined as the process in which light energy is converted into chemical energy (Reece *et al.*, 2011). This process is of vital importance for life on Earth; photosynthesis allows phototrophic organisms to convert sun light and inorganic carbon into biomass. More specifically, in green plants, photosynthesis refers to the conversion of CO_2 from the atmosphere into sugars and other organic compounds. This assimilation of CO_2 consumes energy. Green plants obtain this energy by the absorption of photosynthetically active radiation (PAR). Understanding the mechanisms of photosynthesis in green plants is of interest from an agronomical perspective. In 2009, the Food and Agricultural Organization (FAO) expected the global population to increase by 34% to 9 billion people in 2050 (FAO, 2009a). In order to fulfil this global demand for more food and production due to the growing world population, the FAO estimated that the global food production had to increase by 70% from 2009 to 2050 to meet the global demand for food, feed, and fibres (FAO, 2009b). This can be achieved in two ways; using larger areas of land for crop production or increasing the efficiency of the production process (Ort *et al.*, 2015). Increasing of the efficiency of the process can be done by increasing the efficiency of light absorption by crops, by increasing the conversion of absorbed light energy into biomass and by increasing the harvest index (Long *et al.*, 2006). During the second half of the 20th Century, there have already been major improvements in increasing the efficiency of the production process. Between 1960 and 2005, the global food production has been increased by 160%, while the total area of cropland has only increased by 27% (Burney *et al.*, 2010). This increase of the global food production can mainly be explained by the increase in harvest index. Although there is some potential to further increase the efficiency of light absorption and the harvest index, the scope of possibilities to further improve these is very limited (Long *et al.*, 2006). Therefore, further increase of crop yield can mainly be achieved by increasing the conversion efficiency of absorbed light into biomass; i.e. by optimizing photosynthesis. Zhu *et al.* (2010) identified several possibilities to further increase the efficiency of photosynthesis. These possibilities include alterations at the canopy level,

the leaf tissue (mesophyll) level, and the molecular level. One of the possibilities on the leaf level is the decrease of the resistance for CO_2 transport from the intercellular airspaces to the sites of CO_2 fixation. This resistance is determined by biochemical processes in the mesophyll, leaf anatomical properties, and environmental conditions. Since it is affected by such a wide variety of factors, it is hard to conceive how this property can be altered to optimize photosynthesis. Nevertheless, it can be very beneficial to examine the mechanism of mesophyll resistance. Zhu *et al.* (2010) estimated that decreasing the mesophyll resistance can potentially lead to an increase of 20% of the photosynthetic capacity. In this dissertation, I will contribute to this by investigating the mechanism of mesophyll resistance.

1.2 CO_2 consumption and production in leaves

The net CO_2 assimilation rate is the difference between the rates of CO_2 consumption and production in the leaves. In this section, I will briefly review each of the biochemical processes that consume or produce CO_2 in the mesophyll cells of leaves in C_3 plants.

1.2.1 CO_2 consumption by RuBP carboxylation

The Calvin cycle is a cycle of biochemical reactions, in which inorganic CO_2 is converted into sugars. Fig. 1.1 contains a schematic overview of the Calvin cycle. It takes place in the stroma ; the fluid filled cavity in a chloroplast outside the thylakoids (a system of interconnected membrane sacs). The first step in the Calvin cycle is the assimilation of inorganic carbon in the form of CO_2 by the carboxylation of ribulose-1,5-biphosphate (RuBP). This biochemical reaction is catalyzed by the enzyme ribulose-1,5-biphosphate carboxylase/oxygenase (Rubisco). The next steps in the Calvin cycle consist of a a series of redox reactions that result in the production of glyceraldehyde-3-phosphate (G3P). G3P is either converted into sugars or it is used to regenerate RuBP to close the biochemical cycle. Both the conversion of RuBP and CO_2 into G3P and the regeneration of RuBP require energy. The energy required for these processes are obtained by the absorption of PAR in the thylakoids, in which photons are absorbed by chlorophyll. This is the first step in a chain of redox reactions,

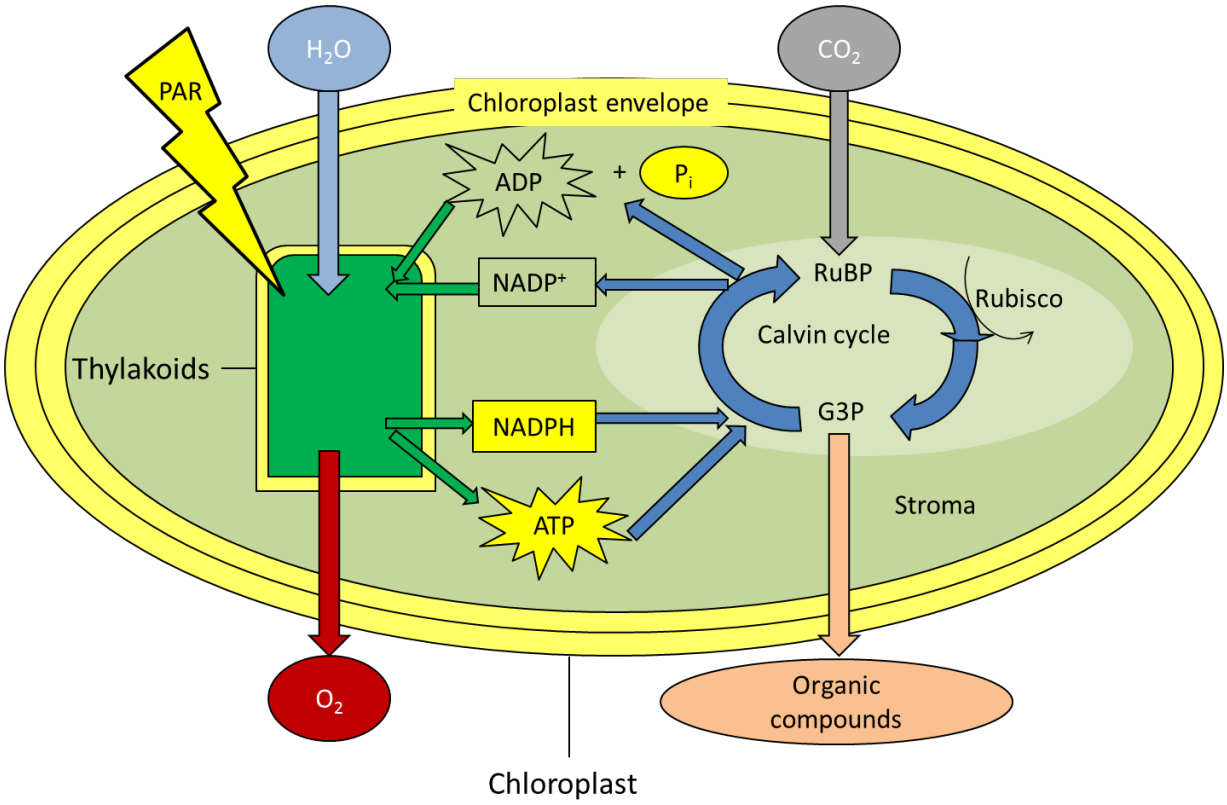

Figure 1.1: Schematic overview of fluxes of CO_2, O_2, and H_2O in a chloroplasts, the light reactions and the dark reactions within a chloroplast of a C_3 mesophyll cell.

which ultimately results in the production of oxygen (a waste product in this context) and the reduction of $NADP^+$ to NADPH. In the electron transport chain, energy is released, while electrons are transferred from one acceptor to the next one. This energy is used to phosphorylate adenosine-diphosphate (ADP) to adenosine-triphosphate (ATP). Both NADPH and ATP act as cofactors; they transfer energy to the Calvin cycle to support the production of G3P and the regeneration of RuBP.

1.2.2 CO_2 production by photorespiration

One source of CO_2 is photorespiration. Fig. 1.2 shows a schematic overview of this process. It also shows how photorespiration and photosynthesis are connected. Rubisco has affinity for both CO_2 and O_2. If Rubisco binds O_2, it will catalyse the oxygenation of RuBP instead of its carboxylation. The oxygenation initiates a chain of redox reactions, which results in the production of 2-phosphoglycolate (G2P) and G3P. Since this G3P is converted back to RuBP rather than converted into sugars,

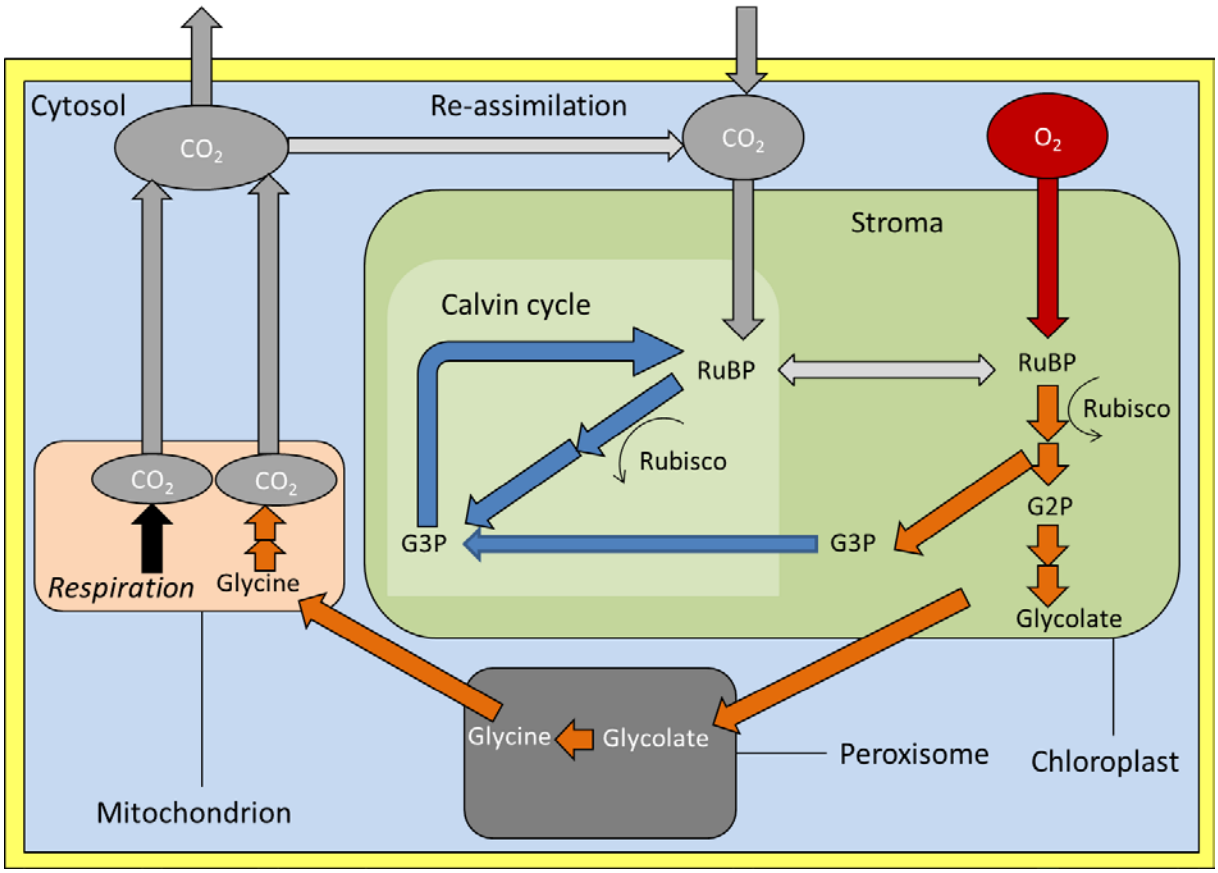

Figure 1.2: Schematic overview of fluxes of CO_2 in a C_3 mesophyll cell, the biochemical pathway, of photorespiration, how these processes are related to Rubisco and the Calvin cycles.

photorespiration consumes energy without contributing to the production of sugars. G2P is further converted into glycolate and transferred from the chloroplasts to peroxisomes. In the peroxisomes, glycolate is converted into glycine. Glycine is transferred from the peroxisomes to the mitochondria. In the mitochondria, glycine is further transformed to serine with the concurrent release of CO_2. Photorespiration is a wasteful process, since the carbon in the released CO_2 comes from RuBP and will most likely be lost to the atmosphere.

1.2.3 CO_2 production by respiration

Another source of CO_2 production is respiration (Fig. 1.3). This process takes place in the mitochondria. In this process, sugars are reduced to release energy to supply the production of the cofactors ATP and NADH. The reduction of sugars can be either

aerobic (cellular respiration) or anaerobic (fermentation). In either case, ultimately CO_2 is released from the mitochondria into the cytosol (Nobel, 2009).

1.3 Modelling CO_2 assimilation

In photosynthesis, plants absorb light energy and use this energy to assimilate CO_2. Therefore, the net CO_2 assimilation in a leaf strongly depends on the CO_2 partial pressure in the atmosphere around this leaf and the irradiance. A major step forward in the understanding of how the irradiance and the CO_2 partial pressure in C_3 plants affects its photosynthetic efficiency was the development of the Farquhar-von Caemmerer-Berry model (Farquhar *et al.*, 1980), which has been abbreviated in the literature as "FvCB model". This biochemical model states that the net rate of CO_2 consumption by RuBP carboxylation W is either limited by the number of binding sites and the turnover rate of Rubisco (Rubisco-limited RuBP carboxylation) or by the rate of RuBP regeneration which is assumed to be determined by the rate of electron transport J. For both limitations, Farquhar *et al.* (1980) derived mathematical expressions for the potential rates of RuBP carboxylation. The actual net CO_2 assimilation rate is the minimum of these two potential rates. If there is both a high level of CO_2 and light, RuBP carboxylation can also be limited by the rate at which triose phosphates are utilised in the synthesis of starch and sucrose. This is the rate of triose phosphate utilization. In order to consider this limitation as well, Sharkey (1985) expanded the FvCB model with a potential rate limited by the rate of triose phosphate utilization. In this extended form of the FvCB model, the actual rate of RuBP carboxylation is the minimum of three potential RuBP carboxylation rates. Throughout this dissertation, we will apply this form of the FvCB model.

1.4 CO_2 transport in leaves

CO_2 molecules in the atmosphere have to cross various barriers to reach Rubisco (Fig. 1.3). First, CO_2 from the turbulent atmosphere has to cross a laminar boundary layer to reach the leaf surface. Second, CO_2 can only diffuse from the leaf surface into the stomatal cavity in the interior part of the leaf through the pores of stomata. These pores are surrounded by guard cells. Plants can regulate the size of these pores by the

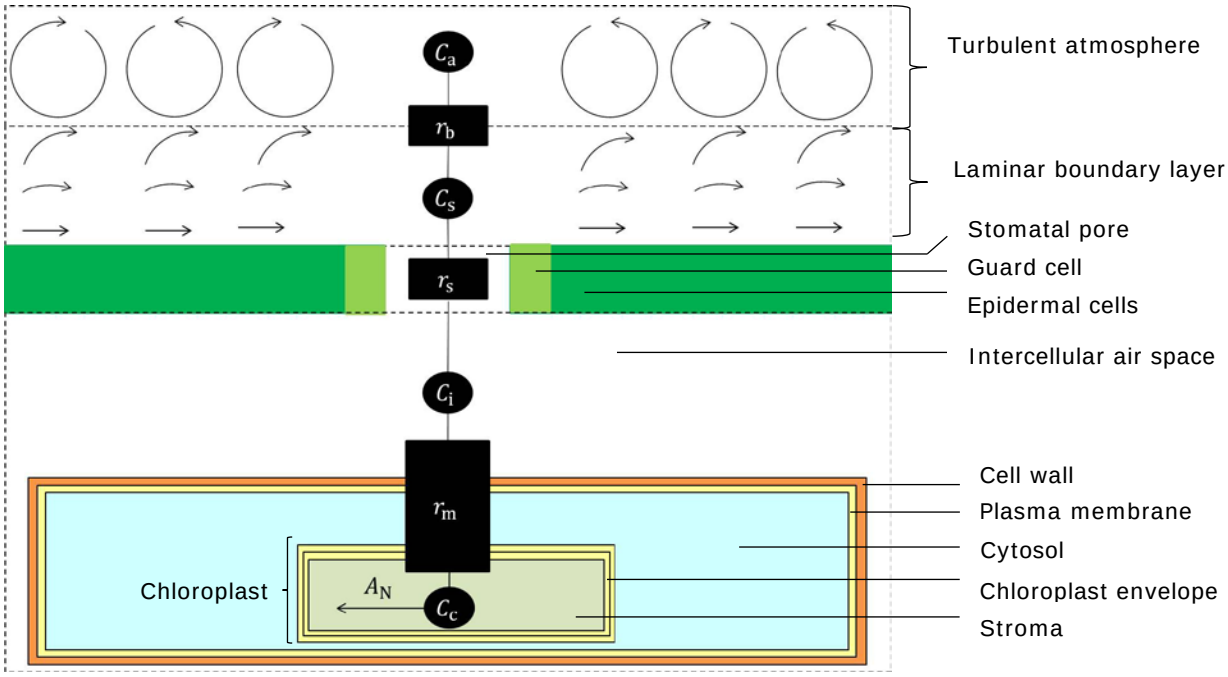

Figure 1.3: Schematic overview of the CO_2 diffusion pathway from the turbulent atmosphere to Rubisco in the stroma.

contraction and relaxation of the guard cells. Third, CO_2 molecules can further diffuse into the interior of the leaf through a network of interconnected intercellular air space. Fourth, CO_2 has to enter the mesophyll cells. These cells are partly exposed to the intercellular airspaces. In order to enter the mesophyll cells, CO_2 has to dissolve in the water filled pores of the cell wall. Once inside, CO_2 has to cross a number of subcellular structures before it reaches Rubisco in the chloroplast stroma. These subcellular barriers are the cell wall, the plasma membrane, the cytosol and the chloroplast envelope. While diffusing into the stroma, CO_2 molecules are finally assimilated by Rubisco. Besides diffusion, CO_2 transport in the plasma membrane, the cytosol, the chloroplast envelope and the stroma may be facilitated by the activity of carbon anhydrases. These enzymes catalyse the interconversion between CO_2 and HCO_3^-. This process makes new CO_2 available to replace CO_2 that is assimilated, thereby increasing the CO_2 partial pressure near Rubisco and the net CO_2 assimilation rate (Terashima *et al.*, 2011). The atmosphere is not the only source of CO_2 for assimilation. As stated earlier, respiration and photorespiration produce CO_2 in mitochondria and release this into the cytosol. This (photo)respired CO_2 can either

diffuse out of the leaf or into the chloroplast stroma, where it can be assimilated by Rubisco. This latter process is called re-assimilation.

1.5 CO_2 transport in leaves affects the net CO_2 assimilation rate

RuBP carboxylation in the chloroplast stroma is a strong sink of CO_2 and various structures that limit CO_2 diffusion in both the gas phase and the liquid phase of the diffusion path generate barriers to CO_2 transport from the atmosphere to Rubisco. Therefore, the CO_2 partial pressure near Rubisco is not the same as the CO_2 partial pressure in the atmosphere. When leaves are illuminated, the steady-state CO_2 partial pressure in chloroplast is smaller than in the atmosphere under most environmental conditions. Since the net CO_2 assimilation rate under both Rubisco-limited and electron transport-limited conditions depends on the CO_2 partial pressure near Rubisco, the various barriers for CO_2 transport in leaves constrain the assimilation of CO_2 as well. In photosynthesis models, these barriers are commonly modelled as resistances. In many studies, the overall resistance for CO_2 transport in leaves is partitioned into three resistances. These are the resistance of the boundary layer (r_b), the resistance of the stomata (r_s) and the resistance of the mesophyll (r_m). Fig. 1.3 shows the location of each of these resistances along the CO_2 diffusion pathway. Resistance models can be used to express the net rate of CO_2 assimilation A_N under steady state conditions as:

$$A_\mathrm{N} = \frac{(C_\mathrm{a} - C_\mathrm{s})}{r_\mathrm{b}} \tag{1.1}$$

$$A_\mathrm{N} = \frac{(C_\mathrm{s} - C_\mathrm{i})}{r_\mathrm{s}} \tag{1.2}$$

$$A_\mathrm{N} = \frac{(C_\mathrm{i} - C_\mathrm{c})}{r_\mathrm{m}} \tag{1.3}$$

where C_a is the CO_2 partial pressure in the turbulent atmosphere, C_s is the CO_2 partial pressure at the leaf surface, C_i is the CO_2 partial pressure in the intercellular air space, and C_c is the CO_2 partial pressure near Rubisco. These partial pressures can be expressed in Pa. A_N is the net CO_2 assimilation rate, expressed in μmol CO_2 m^{-2} leaf area s^{-1}. Gas exchange measurements can be used to measure A_N as the net CO_2 flux into the leaf for a certain C_a. Von Caemmerer and Farquhar (1981) exploited the fact that the diffusion pathways of CO_2 and water vapour from transpiration overlap in the stomata and the boundary layer. They derived equations to determine r_b and r_s from simultaneous gas exchange measurements of CO_2 and water vapour fluxes at the leaf surface. This framework allows the calculation of C_i from gas exchange measurements.

Determining r_m and C_c is more challenging, since there is currently no framework available to measure these variables directly *in vivo*. The simplest approach to deal with this is to assume that r_m is negligible (Aalto and Juurola, 2001), which allows to assume that $C_c = C_i$. However, this assumption will result in the overestimation of C_c if r_m is actually not negligible. Consequently, if the FvCB model is used to estimate photosynthetic parameters under his assumption from gas exchange measurements, these estimates are biased and can lead to wrong predictions of the net CO_2 assimilation rate (Niinemets *et al.*, 2009; Sun *et al.*, 2014). There are various methods to estimate r_m from gas exchange measurements, sometimes combined with measurements of chlorophyll fluorescence (Harley *et al.*, 1992a also reviewed by Yin and Struik (2009) and Pons *et al.* (2009)) or isotope discrimination (Pons *et al.*, 2009). These methods have certain limitations. First, they lump all biochemical processes and physical barriers in the mesophyll cells in a single parameter r_m. Second, they rely on the assumption that r_m does not vary with the irradiance and C_c. Several studies (Harley *et al.*, 1992a; Flexas *et al.*, 2007; Yin *et al.*, 2009; Tholen and Zhu, 2011; Tholen *et al.*, 2012) present proof that this latter assumption does not hold.

1.6 Objectives

The overview above shows that both biochemical processes and physical barriers on the CO_2 diffusion pathway in leaves can substantially reduce the the efficiency of photosynthesis. One major contribution to understand the relationship between environmental circumstances and photosynthesis was the development of the FvCB model (Farquhar *et al.*, 1980) that gives an accurate description of the kinetics of CO_2 assimilation by Rubisco. Another major contribution was the model from von Caemmerer and Farquhar (1981). This model allowed the calculation of r_s and r_b from gas exchange measurements. Both models are widely used (for instance, LI-COR (1999)) and contributed to a better understanding of how photosynthesis can be limited by the stomata. The remaining challenge is to understand what factors affect the last part of the CO_2 diffusion pathway between the atmosphere and Rubisco, i.e. the diffusion pathway in the mesophyll. The mechanism of how structural barriers and biochemical process within mesophyll cells constrain CO_2 transport from the intercellular air space to Rubisco in still largely unknown. The main aim of my PhD project is to investigate how anatomical properties along the CO_2 diffusion pathway in a C_3 leaf and biochemical processes that add or remove CO_2 to this diffusion path affect its photosynthetic capacity. In my view, the commonly used resistance models, (equations (1.1-1.3)), cannot fully capture the complexity of this relationship. I will demonstrate this in my dissertation. An alternative to these resistance models is reaction-diffusion models. These models are more flexible than resistance models, which makes it more feasible to include all processes and leaf anatomical structures separately that affect the efficiency of CO_2 transport in the mesophyll. Still, this type of models is considerably less frequently used than resistance models. A possible reason is that they are more complex from a mathematical point of view (Parkhurst, 1977, 1994). In this study, we apply this type of models as well to gain more insights into what biochemical and leaf anatomical factors affect the efficiency of CO_2 transport. I will answer the following questions in this dissertation:

Q1. How have mesophyll resistance models been used to study photosynthesis in previous work?

Q2. What leaf anatomical properties can potentially affect the net CO_2 assimilation rate?

Q3. How have reaction-diffusion models been used to study photosynthesis in previous work?

Q4. How can reaction-diffusion models be used as an alternative to resistance models?

Q5. How does the position of mitochondria relative to the chloroplasts affect the net CO_2 assimilation rate?

Q6. To what extent and under which combination of light, CO_2 and O_2 levels does the re-assimilation of CO_2 produced by respiration and photorespiration affect the net CO_2 assimilation rate of CO_2?

Throughout this dissertation, I will use various tomato (*Solanum lycopersicum* L.) cultivars as model organism to answer the research questions.

1.7 Outline of the thesis

Chapter 2 is a literature review, in which I will answer research questions Q1 and Q3. I will do so by explaining what the physical basis of both reaction-diffusion models and resistance models is, critically reviewing how both types of models have been used in the past, and comparing both types of models.

In Chapter 3, I will answer research question Q2. For this purpose, I will describe the development of a resistance model to study how photosynthesis is constrained by a variety of anatomical properties of mesophyll cells. In order to do so, I will partition mesophyll resistance into several sub-resistances for CO_2. Rather than estimating these resistances, I will directly calculate them based on measurements of leaf anatomical properties and assumed diffusive properties and curvature factors. In a sensitivity analysis, I will investigate how and under what light and CO_2 levels the net CO_2 assimilation rate is determined by leaf anatomical properties. I will also specify the assumptions of this model and analyse which assumptions can possibly be avoided by the use of reaction diffusion models.

In Chapter 4, I will describe the development and the validation of a reaction-diffusion model for CO_2 transport in leaves. In almost all the literature studies, a combination of the FvCB and a resistance model is used to determine photosynthetic parameters from gas exchange measurements. Rather than this common approach, I will use the reaction-diffusion model to directly estimate photosynthetic parameters from gas exchange measurements. By doing so, I will answer research question Q4. I will also answer research question Q5 by using the model to vary the position of (photo)respiratory CO_2 release relative to the chloroplasts and compare simulated light response curves and CO_2 response curves for these different positions.

In Chapter 5, I will answer research question Q6 by simulating how the fraction of CO_2 that is re-assimilated changes with different levels of CO_2, O_2, and light.

In Chapter 6, I will summarize the answers to the research questions, discuss implications and make recommendations for further research.

CHAPTER 2

Reaction-diffusion models extend our understanding of C_3 leaf photosynthesis: opportunities and challenges

Herman N.C. Berghuijs[1,2,3], Xinyou Yin[1,2], Q. Tri Ho[3], Steven M. Driever[1], Moges A. Retta[1,3], Bart M. Nicolaï[3], Paul C. Struik[1,2]

[1] Centre for Crop Systems Analysis, Wageningen University, Droevendaalsesteeg 1, 6708 PB Wageningen, The Netherlands

[2] BioSolar Cells, P.O. Box 98, 6700 AB Wageningen, The Netherlands

[3] Flanders Center of Postharvest Technology / BIOSYST-MeBioS, Katholieke Universiteit Leuven, Willem de Croylaan 42, B-3001, Leuven, Belgium

Abstract

One of the ways to increase global potential crop yield may be increasing mesophyll conductance g_m. This variable determines the difference between the CO_2 partial pressure in the intercellular air spaces C_i and near Rubisco C_c. There are various methods to determine g_m from gas exchange measurements, sometimes combined with measurements of chlorophyll fluorescence or carbon isotope discrimination. g_m lumps all biochemical and physical factors that determine the drawdown of C_c from C_i. Moreover, g_m appears to vary with C_i. This variability indicates that g_m does not satisfy the physical definition of a conductance according to Fick's first law. Uncertainty about the mechanisms that determine g_m can be limited to some extent by the use of analytical models that partition g_m into separate conductances. Yet such models are still not capable of capturing the full complexity of the CO_2 diffusion path in leaves. They also make implicit assumptions about the re-assimilation of (photo)respired CO_2. As an alternative, reaction-diffusion models could be used. Rather than quantifying g_m, these models explicitly account for factors that affect the efficiency of CO_2 transport in the mesophyll. Disadvantages of this approach are the uncertainties of diffusive properties and curvature factors, the need to collect leaf anatomical data, and higher computational costs. However, these models provide a mechanistic description of the CO_2 diffusion pathways, which can help to identify traits that can be improved to increase g_m and, thereby, global crop yield.

Keywords

CO_2, photosynthesis, mesophyll conductance, reaction-diffusion models, 3D models, C_3 plants

2.1. Introduction

In 2009, the FAO predicted that the global population will increase between 2009 and 2050 by 34% to 9 billion people (FAO, 2009a). Given this increase in global population and the change in dietary requirements, the global crop yield has to increase by 70% to meet the global demand for food, feed, fibres, and bioenergy (FAO, 2009b). Increasing the efficiency of photosynthesis could greatly contribute by increasing the global yield, given the limited availability of arable land or the limited scope of alternative possibilities to further increase the global yield, like increasing the harvest index or the efficiency of light absorption by crops (Long *et al.*, 2006; Ort *et al.*, 2015).

A major step in the understanding of leaf-level C_3 photosynthesis was the introduction of the Farquhar-von Caemmerer-Berry model (FvCB model hereafter), which relates the CO_2 partial pressure C_c near Rubisco to the net CO_2 assimilation rate (Farquhar *et al.*, 1980). C_c is, in most cases, lower than the CO_2 partial pressure in the atmosphere C_a outside the leaf. This can be explained by various structural barriers for CO_2 transport between the ambient air and the site of Rubisco (Von Caemmerer and Farquhar, 1981; Evans *et al.*, 2009; Tosens *et al.*, 2012b) and biochemical processes along the CO_2 diffusion pathway that produce or consume CO_2 (Tholen and Zhu, 2011; Tholen *et al.*, 2012). The CO_2 partial pressure in the leaf's intercellular air space C_i can be calculated directly from water vapour and CO_2 gas exchange measurements, since diffusion paths of CO_2 and water vapour overlap (Von Caemmerer and Farquhar, 1981). In contrast, C_c cannot be measured directly. C_c is commonly determined using mesophyll conductance models, but unfortunately these models do not explicitly describe the factors that cause the difference between C_i and C_c. However, it is very important to understand the mechanisms responsible for C_c and C_i differences, to find possibilities for improving mesophyll conductance to CO_2. For example, Zhu *et al.* (2010) estimated that increasing mesophyll conductance can potentially lead to an increase of photosynthetic capacity by as much as 20%.

In this review, we will show that current models for mesophyll conductance (Harley *et al.*, 1992a; Ethier and Livingston, 2004; Yin *et al.*, 2009; Tholen *et al.*, 2012) can only explain to a limited extent the mechanisms that cause the drawdown of the CO_2 partial pressure from the intercellular air space to Rubisco. Since reaction-diffusion models are more flexible than mesophyll conductance models (as described below), they provide an alternative to study the mechanisms that cause the drawdown between C_i and C_c. This literature review aims to discuss how reaction-diffusion models can be used to improve our understanding of CO_2 transport to Rubisco in comparison with the more common mesophyll conductance models. First, we describe how the net CO_2 assimilation rate depends on C_c. Second, we analyse the CO_2 diffusion pathway to Rubisco. Third, we explain what conductance models are, why these models are important to model photosynthesis, and discuss their usefulness and their limitations. Fourth, we will introduce reaction-diffusion models, their flexibility and how this type of model has been used in previous studies to simulate CO_2 transport in leaves. Finally, we reflect on the advantages and disadvantages of reaction-diffusion models compared with mesophyll conductance models and make recommendations for further research.

2.2. CO_2 consumption and production in leaves

The FvCB model states that the rate of CO_2 consumption through ribulose-1,4-biphosphate (RuBP) carboxylation by Rubisco is either limited either by the capacity of Rubisco to carboxylate RuBP or by the regeneration of RuBP, which depends on the rate of electron transport (Farquhar *et al.*, 1980). The FvCB model contains mathematical expressions for the corresponding potential rates of RuBP carboxylation. If there is a surplus of both CO_2 and light, the recycling of RuBP, which is determined by the rate of triose phosphate utilization, can limit RuBP carboxylation (Sharkey, 1985). The actual rate of RuBP carboxylation, *W*, is the minimum of the three.

$$W = \min\left(W_\mathrm{c}, W_\mathrm{j}, W_\mathrm{p}\right) \tag{2.1}$$

where W_c is the potential rate of RuBP carboxylation limited by Rubisco (μmol m^{-2} s^{-1}), W_j the potential rate of RuBP carboxylation limited by the rate of electron transport (μmol m^{-2} s^{-1}), and W_p the potential rate of RuBP carboxylation limited by triose phosphate utilization (μmol m^{-2} s^{-1}).

Besides the consumption of CO_2, CO_2 is produced by respiration and photorespiration. Respiration is CO_2 production due to the aerobic and anaerobic reduction of sugars in mitochondria. In photorespiration, Rubisco's dual affinity (for both CO_2 and O_2) allows the oxygenation of RuBP, instead of its carboxylation. The net CO_2 assimilation rate is defined as the difference between the rate of CO_2 consumption by RuBP carboxylation W and the rates of CO_2 production by respiration R_d and photorespiration R_p. R_p can be calculated as $\frac{\Gamma^*}{C_c}W$ (Long and Bernacchi, 2003). Here Γ^* is the CO_2 compensation point, i.e., the CO_2 partial pressure near Rubisco at which the amount of CO_2 produced by photorespiration equals the amount of CO_2 consumed by RuBP carboxylation. The net CO_2 assimilation rate can be expressed as:

$$A_N = W - R_p - R_d = \left(1 - \frac{\Gamma^*}{C_c}\right)\min\left(W_c, W_j, W_p\right) - R_d \tag{2.2}$$

After substitution of the mathematical expressions for the potential rates of RuBP carboxylation in equation (2.2), the full FvCB model (Farquhar *et al.*, 1980), extended with triose-phosphate-limited RuBP carboxylation (Sharkey, 1985), can be written as:

$$A_N = \left(1 - \frac{\Gamma^*}{C_c}\right)\min\left(\frac{C_c V_{cmax}}{C_c + K_{mC}\left(1 + \frac{O}{K_{mO}}\right)}, \frac{C_c J}{4C_c + 8\Gamma^*}, \frac{3T_p}{1 - \frac{\Gamma^*}{C_c}}\right) - R_d \tag{2.3}$$

where O is the oxygen partial pressure and V_{cmax} the maximum rate of RuBP carboxylation by Rubisco. The term $K_{mC}(1 + O/K_{mO})$ represents the apparent Michaelis-Menten constant for RuBP carboxylation by Rubisco, in presence of both

O_2 and CO_2. The term implies that CO_2 and O_2 compete for Rubisco binding sites. Within this term, K_{mC} is the Michaelis-Menten constant for RuBP carboxylation by Rubisco in absence of oxygen and K_{mO} represents the Michaelis-Menten constant for RuBP oxygenation by Rubisco in absence of carbon dioxide. T_{p} is the rate of triose phosphate utilization. J is the rate of electron transport. The relationship between J and the irradiance I_{inc} can be described as a non-rectangular hyperbole (Johnson and Thornley, 1984; Yin *et al.*, 2004; Yin *et al.*, 2009). One of the forms of this relationship is presented by Yin *et al.* (2009) as:

$$J = \frac{\kappa_{2\mathrm{LL}} I_{\mathrm{inc}} + J_{\mathrm{max}} - \sqrt{(\kappa_{2\mathrm{LL}} I_{\mathrm{inc}} + J_{\mathrm{max}})^2 - 4\theta J_{\mathrm{max}} \kappa_{2\mathrm{LL}} I_{\mathrm{inc}}}}{2\theta} \tag{2.4}$$

where $\kappa_{2\mathrm{LL}}$ is the conversion factor of incident radiation into linear electron transport, J_{max} is the maximum rate of linear electron transport and θ is a convexity factor.

2.3. CO_2 diffusion pathway in leaves

In order to reach Rubisco, CO_2 molecules have to diffuse first from the turbulent atmosphere through the laminar boundary layer at the leaf surface (Raschke, 1956). Next, they have to pass through the stomatal pores in the epidermis to reach the sub-stomatal cavity inside the leaf. The efficiency of the latter transfer depends on the stomatal density, the radius of the stomatal pore and the length of the stomatal tube. Plants can regulate the radius of the stomatal pores and the size of the stomatal tube by changing the conformation of the guard cells that surround the stomatal pores (Nobel, 2009) and, thereby, control both the influx of CO_2 and the efflux of water vapour produced by transpiration (Hall and Schulze, 1980). Once inside the leaf in the sub-stomatal cavity, CO_2 molecules will spread through the leaf by diffusion through the intercellular air space. From the intercellular air space, CO_2 molecules can only enter mesophyll cells by dissolving in the water of water-filled pores of cell walls that are exposed to the intercellular air space. Hence, the surface area of mesophyll cells

exposed to the intercellular air space (S_m) is an important determinant of the amount of CO_2 that can be taken up by the mesophyll cells (Nobel *et al.*, 1975; Nobel, 1977). Since CO_2 molecules can only be assimilated in chloroplasts, von Caemmerer and Evans (1991) and Tholen *et al.* (2008) argued that the surface area of chloroplasts that is facing the intercellular air space, S_c, is a better determinant than S_m for the extent of CO_2 uptake from the intercellular air space by mesophyll cells. Once CO_2 has dissolved in the water of the pores of the cell wall, it diffuses, either in the form of dissolved CO_2 or HCO_3^-, through various liquid phase compartments of the mesophyll. These compartments consist of the pore network of the cell wall, the plasma membrane, the aqueous cytosol, the chloroplast envelope, and the stroma (Flexas *et al.*, 2008; Evans *et al.*, 2009; Nobel, 2009). CO_2 can pass a membrane (plasma membrane or chloroplast envelope) through either the lipid phase or the aquaporins (Terashima *et al.*, 2011). After passing the chloroplast envelope, CO_2 enters the stroma. While in the stroma, CO_2 can be fixed through RuBP carboxylation. Besides CO_2 from the atmosphere, there is a second source of CO_2 that can be used for RuBP carboxylation. Inside the mesophyll cells CO_2 is produced by both respiration and photorespiration. The CO_2 molecules produced by these processes, may diffuse from the mitochondria (in the cytosol) into the chloroplast stroma, to be assimilated by RuBP carboxylation. This is usually called re-assimilation of CO_2 produced by respiration and photorespiration, and may be especially important if chloroplasts are packed close together (Sage and Sage, 2009). Various studies (Loreto *et al.*, 1999; Haupt-Herting *et al.*, 2001; Pärnik and Keerberg, 2007; Tholen *et al.*, 2012; Busch, 2013; Ho *et al.*, 2016) have estimated the percentages of re-assimilation of (photo)respired CO_2. There is great variety in the reported values of re-assimilation, ranging from 14%-18% in sunflower (Pärnik and Keerberg, 2007) to 100% in tomato (Loreto *et al.*, 1999). This illustrates that re-assimilation of (photo)respired CO_2 may vary and increases the uncertainty for estimating the actual C_c, particularly when CO_2 assimilation rates are low.

2.4. The physical definition of conductance

Equations for the conductance of a physical barrier for transport of dissolved particles can be derived from Fick's first law. According to Fick (1855), the direction of the diffusive flux of any type of particle is from high- to low concentration, which is similar to the movement of heat from high- to low-temperature regions. In a one-dimensional space, Fick's first law can be written as:

$$\varphi = -D\frac{\mathrm{d}c}{\mathrm{d}x} \tag{2.5}$$

where φ is the flux and D is the diffusion coefficient, a proportionality constant between the flux of a particle and its gradient. Equation (2.5) can be discretized ($\mathrm{d}c/\mathrm{d}x \cong \Delta c/\Delta x$) and rewritten to describe the flux between locations x_2 and x_1 ($\Delta x = x_2 - x_1$) with concentrations c_1 and c_2:

$$\varphi = \frac{D}{x_2 - x_1}(c_1 - c_2) \tag{2.6}$$

where $D/(x_1 - x_2)$ is the conductance (m s^{-1}). In photosynthesis research, densities of CO_2 are more commonly expressed as partial pressures p rather than in molar concentrations c. In order to express the flux as a function of the concentration difference, the ideal gas law is applied by substituting p/RT for the concentrations c_1 and c_2 in equation (2.6). Some rearranging yields:

$$\varphi = \frac{D}{LRT}(p_1 - p_2) = g(p_1 - p_2) \tag{2.7}$$

$$g = \frac{D}{LRT} \tag{2.8}$$

where L is the thickness of the compartment ($L = |x_1 - x_2|$) through which the flux goes, T is the temperature (K) and R is the universal gas constant (8.314 Pa m^3 K^{-1} s^{-1}). g is the conductance expressed in mol m^{-2} s^{-1} Pa^{-1}. The inverse of g is called the resistance.

2.5. Application of gas exchange measurements to determine mesophyll conductance

According to Gaastra (1959), the overall conductance for CO_2 transport can be partitioned into three conductances, namely the boundary layer conductance g_b, the stomatal conductance g_s and the conductance of the mesophyll g_m. This partitioning of the leaf conductance is still commonly used in most C_3 photosynthesis studies. Since the diffusion pathway of CO_2 and water vapour are overlapping in the gas phase, g_b and g_s can be calculated from gas exchange measurements from equations derived by Von Caemmerer and Farquhar (1981) and are commonly used in gas exchange measurements (LI-COR, 1999). From the measured net CO_2 assimilation rate A_N, C_i can be calculated as:

$$C_\mathrm{i} = C_\mathrm{a} - \left(\frac{1}{\frac{1}{g_\mathrm{s}} + \frac{1}{g_\mathrm{b}}} \right) A_\mathrm{N} \tag{2.9}$$

This equation assumes that the conductance of the intercellular air space is infinite. This assumption has been questioned in the past (Parkhurst, 1994). We will adopt this assumption for now, but we will discuss it later on. Determination of C_c is considerably more challenging. C_c can be expressed as:

$$C_c = C_i - \frac{A_N}{g_m} \tag{2.10}$$

g_m cannot be calculated directly from gas exchange measurements, because it does not share a diffusion pathway with water and can, therefore, not be determined from the transpiration rate. Consequently, equation (2.10) has two unknown variables: C_c and g_m. Gaastra (1959) assumed $C_c = 0$, which reduces the number of unknowns in equation (2.10) to one, allowing calculation of g_m. If this specific calculation of g_m is used, it should be considered as a serial conductance that lumps the mesophyll conductance and the carboxylation conductance. With the introduction of the widely used FvCB model (Farquhar *et al.*, 1980), this assumption was rejected (Flexas *et al.*, 2008) and g_m no longer includes the carboxylation conductance. Instead, Farquhar *et al.* (1980) assumed that $g_m = \infty$ and, thereby, that $C_c = C_i$. This assumption was adopted in various studies, which used the FvCB model to estimate photosynthetic parameters (Harley *et al.*, 1992b; Wullschleger, 1993; Aalto and Juurola, 2001; Lenz *et al.*, 2010). However, it has been shown in recent work that the estimates of the parameter values for V_{cmax} can be considerably underestimated if g_m is assumed infinite, while actually finite (Niinemets *et al.*, 2009; Gu and Sun, 2014; Sun *et al.*, 2014a; Sun *et al.*, 2014c). Such an assumption can also lead to an underestimation of J_{max}, but to a much lesser extent, if it is also estimated from gas exchange measurements. It can be argued that this bias may not be a problem, because the lower estimates for V_{cmax} and J_{max} will compensate for the absence of mesophyll conductance in models that predict CO_2 response curves. However, several studies showed that this can lead to wrong predictions. Niinemets *et al.* (2009) estimated V_{cmax}, J_{max}, and T_p from CO_2 response curves using models that either assumed a finite or an infinite mesophyll conductance. Next, they used these estimates to predict how the net CO_2 assimilation rate varies over a day in leaves from plants in the field. They noticed that the model performs considerably better in predicting the midday drop in the net CO_2 assimilation rate if g_m is not assumed to be infinite and if V_{cmax}

and $J_{\max}$ are estimated with a model including this non-infinite g_{m}. Sun *et al.* (2014b) showed that global climate models can considerably underestimate the response of the global terrestrial productivity to increasing CO_2 levels in the atmosphere, if g_{m} is considered infinite. These studies show that g_{m} should not be assumed infinite in photosynthesis models, and highlight the importance of a reliable estimation of g_{m}.

There are various methods in the literature to determine g_{m}, without adopting the assumption from early studies that either $C_{\mathrm{c}} = 0$, or has a fixed value close to zero. Most recent methods are based on gas exchange measurements, often combined with measurements of either chlorophyll fluorescence or carbon isotope discrimination.

One commonly used method based on gas exchange methods and chlorophyll fluorescence is the constant J method (Harley *et al.*, 1992a), in which the term for C_{c} in equation (2.10) is substituted for C_{c} in W_{j} in equation (2.3). This equation is subsequently solved for J, which results in:

$$J = (A_{\mathrm{N}} + R_{\mathrm{d}}) \frac{4\left(\left(C_{\mathrm{i}} - \frac{A_{\mathrm{N}}}{g_{\mathrm{m}}}\right) + 2\Gamma^{*}\right)}{\left(C_{\mathrm{i}} - \frac{A_{\mathrm{N}}}{g_{\mathrm{m}}}\right) - \Gamma^{*}} \tag{2.11}$$

First R_{d} and Γ^{*} are determined. Next, the range of at least three different C_{i} points in $A - C_{\mathrm{i}}$ curve is identified, based on chlorophyll fluorescence data which indicate that J is constant (normally the last few points of $A - C_{\mathrm{i}}$ curve). Then, a test value of g_{m} is used to calculate J using equation (2.11) at each C_{i}. The average value of J for these points (J_{a}) with this test g_{m} is thereof obtained. J_{a} is then used to calculate the variance $\sum_i^n (J_{\mathrm{i}} - J_{\mathrm{a}})^2/(n-1)$, where J_{i} is J for a single point in the $A - C_{\mathrm{i}}$ curve, n is the total number of points used in this analysis. This is repeated for a number of test values for g_{m}. The test value for g_{m} that minimizes the variance is considered as the final estimate of g_{m}.

Another method is the variable J method. In this method, equation (2.11) is further rewritten to express g_{m}:

$$g_{\mathrm{m}} = \frac{A_{\mathrm{N}}}{C_{\mathrm{i}} - \frac{\Gamma^{*}\left(J + 8(A_{\mathrm{N}} + R_{\mathrm{d}})\right)}{J - 4(A + R_{\mathrm{d}})}} \tag{2.12}$$

where J is determined from an empirical relationship for J with the irradiance and the quantum yield of Photosystem II, determined from chlorophyll fluorescence data. An advantage of the variable J method is that J does not have to be constant for different values of C_{i}. Both the variable J method and the constant J method are only valid if the rate of RuBP carboxylation is limited by the rate of electron transport, as explained by Yin and Struik (2009).

Ethier and Livingston (2004) and Ethier *et al.* (2006) derived equations to express both the net CO_2 assimilation rate under Rubisco-limited conditions (A_{c}) and under RuBP-limited conditions (A_{j}) in a generic model as:

$$A_{\mathrm{N}} = \min\left(A_{\mathrm{c}}, A_{\mathrm{j}}\right) \tag{2.13}$$

$$A_{\mathrm{N}} = \frac{-\mathscr{b} + \sqrt{\mathscr{b}^2 - 4ac}}{2a} \tag{2.14a}$$

$$a = -\frac{1}{g_{\mathrm{m}}} \tag{2.14b}$$

$$\mathscr{b} = \begin{cases} \dfrac{(V_{\mathrm{cmax}} - R_{\mathrm{d}})}{g_{\mathrm{m}}} + C_{\mathrm{i}} + K_{\mathrm{mC}}\left(1 + \dfrac{O}{K_{\mathrm{mO}}}\right) & \text{if } A_{\mathrm{N}} = A_{\mathrm{c}} \\ \dfrac{\left(\frac{1}{4}J - R_{\mathrm{d}}\right)}{g_{\mathrm{m}}} + C_{\mathrm{i}} + 2\Gamma^{*} & \text{if } A_{\mathrm{N}} = A_{\mathrm{j}} \end{cases} \tag{2.14c}$$

$$c = \begin{cases} R_{\mathrm{d}}\left(C_{\mathrm{i}} + K_{\mathrm{c}}\left(1 + \dfrac{O}{K_{\mathrm{mO}}}\right) - V_{\mathrm{cmax}}(C_{\mathrm{i}} - \Gamma^{*})\right) & \text{if } A_{\mathrm{N}} = A_{\mathrm{c}} \\ \dfrac{\left(\frac{1}{4}J - R_{\mathrm{d}}\right)}{g_{\mathrm{m}}} + C_{\mathrm{i}} + 2\Gamma^{*} & \text{if } A_{\mathrm{N}} = A_{\mathrm{j}} \end{cases} \quad (2.14\mathrm{d})$$

A_{c} and A_{j} are the potential net CO_2 assimilation rate, limited by RuBP carboxylation and electron transport respectively. Equations (14a-d) are used to simultaneously estimate g_{m} with R_{d}, V_{cmax}, and J_{max} from photosynthetic response curves by non-linear regression (Ethier *et al.*, 2006). In order to do so, a certain cut-off value for C_{i} has to be defined; below this value, $A_{\mathrm{N}} = A_{\mathrm{c}}$, above this value, $A_{\mathrm{N}} = A_{\mathrm{j}}$. This method to determine g_{m} is called the curve-fitting method. Yin *et al.* (2009) presented an extension of this framework with the possibility to estimate g_{m} from a combination of gas exchange and chlorophyll fluorescence measurements. This extension includes methods to determine Γ^{*}, R_{d}, and J_{max} from this combination of measurements under photorespiratory and non-photorespiratory conditions *a priori*. After determination of these parameters, only two parameters remain to be estimated (V_{cmax}, g_{m}). This limited number of parameters allows simultaneous estimation of V_{cmax} and g_{m} using the whole model (equation (2.13-2.14a-d)) directly, rather than defining an arbitrary cut-off value for C_{i}.

The constant and variable J methods (Harley *et al.*, 1992a) and the curve fitting methods to estimate g_{m} (Ethier *et al.*, 2006; Yin *et al.*, 2009) are all based on substitution of a term for C_{c} in the FvCB model. In contrast, methods to estimate mesophyll conductance from gas exchange models combined with carbon isotope discrimination methods can be used to determine C_{c}. The obtained term for C_{c} can subsequently be used to calculate g_{m} (Evans *et al.*, 1986; Evans and von Caemmerer, 1996). For this purpose, carbon isotope discrimination needs to be measured, as the change of ^{12}C:^{13}C in CO_2 of air after exposure to a leaf (Δ_{13}). According to Farquhar and Cernusak (2012), the model of Farquhar *et al.* (1982) can be expressed by the sum

of all processes that affect this ratio due to differences in diffusion coefficient or differences in biochemical reaction rates for $^{12}CO_2$ and $^{13}CO_2$:

$$\Delta_{13} = \frac{1}{1-t}\left(a_\mathrm{b}\frac{C_\mathrm{a}-C_\mathrm{s}}{C_\mathrm{a}} + a'\frac{C_\mathrm{s}-C_\mathrm{i}}{C_\mathrm{a}}\right) + \frac{1+t}{1-t}\left((b_\mathrm{s}+a_\mathrm{l})\frac{C_\mathrm{i}-C_\mathrm{c}}{C_\mathrm{a}} + b\frac{C_\mathrm{c}}{C_\mathrm{a}} - \frac{\alpha_b}{\alpha_e}e\frac{R_\mathrm{d}}{k}\frac{C_c}{C_\mathrm{a}} - \frac{\alpha_b}{\alpha_f}f\frac{\Gamma^*}{C_\mathrm{a}}\right) \quad (2.15)$$

where a_b is the fractionation due to boundary layer diffusion. a' is the fractionation due to diffusion in the air. b_s is the fractionation due to CO_2 entering the liquid phase. a_1 is the fractionation due to CO_2 diffusion in the liquid phase. b is the fractionation due to RuBP carboxylation. k is the carboxylation efficiency. e and f are the fractionations due to respiration and photorespiration respectively. a_b, a_e and a_f are $1+b$, $1+e$ and $1+f$, respectively. This model contains a parameter $t$for a ternary correction (Farquhar and Cernusak, 2012), which accounts for the influence of transpiration on the CO_2 diffusion from the air to the intercellular air space. t is defined as:

$$t = \frac{\alpha_{ac}E}{2g_\mathrm{b}} \quad (2.16)$$

where E is the transpiration rate, a_ac is $1+\bar{a}$, the weighted diffusion fraction across the leaf boundary layer and stomata:

$$\bar{a} = \frac{a_b(C_a-C_s)+a'(C_s-C_i)}{C_s-C_i} \quad (2.17)$$

Although values for e and f are still under debate, g_{m} can be estimated when combining the above with measurements of leaf gas exchange, on the basis that the measured Δ_{13} are lower than predicted, when assuming $C_{\mathrm{c}} = C_{\mathrm{i}}$. For this, an infinite g_{m} can be assumed to derive the predicted Δ_{13}:

$$\Delta_{\mathrm{i}} = \frac{1}{1-t}\left[a_b \frac{C_a - C_s}{C_a} + a_s \frac{C_s - C_i}{C_a}\right] + \frac{1+t}{1-t}\left[b \frac{C_i}{C_a} - \frac{\alpha_b}{\alpha_e} e \frac{R_d}{A + R_d} \frac{C_i - \Gamma^*}{C_a} - \frac{\alpha_b}{\alpha_f} f \frac{\Gamma^*}{C_a}\right] \tag{2.18}$$

To allow for the estimation of Δ_{i} from measurement of leaf gas exchange (A_{N}), Equation (2.18) is modified from Equation (2.15) by substituting C_{c} for C_{i} and $C_{\mathrm{c}}/k/k$ for $(C_{\mathrm{i}} - \Gamma^*)/(A_{\mathrm{N}} + R_{\mathrm{d}})$. The resulting difference between Δ_{i} (from gas exchange) and Δ_{13} (from carbon isotope discrimination) then yields g_{m}:

$$g_m = \frac{1+t}{1-t}\left(\frac{b - (b_s - a_l) - \frac{a_b}{a_e} e \frac{R_d}{A_{\mathrm{N}} + R_d}}{\Delta_{\mathrm{i}} - \Delta_{13}}\right)\frac{A_{\mathrm{N}}}{P C_{\mathrm{a}}} \tag{2.19}$$

where *P* is the atmospheric pressure. It should be noted that this approach assumes that any respired CO_2 from mitochondria would have to diffuse through the chloroplasts, implying complete re-assimilation.

2.6. Determination of g_{m} based on leaf anatomical properties

A disadvantage of the methods described above is that g_{m} should be considered as an apparent variable as it lumps the effect of any individual leaf anatomical properties on CO_2 transport in the mesophyll. Therefore, these models cannot be used directly to assess how individual leaf anatomical properties affect the photosynthesis. An

alternative is to calculate g_{m} from leaf anatomical properties, curvature factors, and assumed diffusion coefficients and/or conductances. In these models, the physical definition of a conductance g (equation (2.8)) is directly applied to quantify the conductance of some of the components in the liquid phase for CO_2 transport in the mesophyll (Evans *et al.*, 1994; Niinemets and Reichstein, 2003; Evans *et al.*, 2009; Peguero-Pina *et al.*, 2012; Tosens *et al.*, 2012a; Tosens *et al.*, 2012b; Tomas *et al.*, 2013) in order to calculate g_{m}. Once the conductance of each component is quantified, the liquid phase conductance, g_{liq} can be calculated as (Tosens *et al.*, 2012b; Tomas *et al.*, 2013):

$$g_{\mathrm{liq}} = \frac{1}{\frac{1}{g_{\mathrm{wall}}} + \frac{1}{g_{\mathrm{mem}}} + \frac{1}{g_{\mathrm{cyt}}} + \frac{1}{g_{\mathrm{env}}} + \frac{1}{g_{\mathrm{str}}}} \tag{2.20}$$

where g_{wall}, g_{mem}, g_{cyt}, g_{env}, and g_{str} are the conductances of the cell wall, the plasma membrane, the cytosol, the chloroplast envelope, and the chloroplast stroma respectively. Note that each of these conductances is expressed in mol m^{-2} *exposed chloroplast surface area* s^{-1} Pa, instead of mol m^{-2} *leaf area* s^{-1}. In order to calculate expressed g_{liq}', the liquid phase conductance in mol m^{-2} leaf area s^{-1}, g_{liq} has to be multiplied with S_{c}/S, which is the ratio of the area of chloroplast surface exposed to the intercellular air space to the leaf area. A common way to determine this parameter is to first measure the ratio of L_{m}/L and $L_{\mathrm{c}}/L_{\mathrm{m}}$ from TEM (transmission electron microscopy) or light microscopic images. L_{m}/L represents the length ratio of the exposed mesophyll surface to total length of the section. $L_{\mathrm{c}}/L_{\mathrm{m}}$ represents the ratio of the length of the part of the chloroplast facing the intercellular air space to the total length of the mesophyll in the image. The length ratio L_{m}/L can be converted to the equivalent surface ratio S_{m}/S by determining the curvature factor of the tissue from a series of paradermal and transversal sections and multiply this factor with L_{m}/L (Thain, 1983; Evans *et al.*, 1994). g_{liq}' is then calculated as:

$$g_{\mathrm{liq}}{}' = \frac{S_{\mathrm{c}}}{S} g_{\mathrm{liq}} = \frac{S_{\mathrm{m}}}{S} \frac{S_{\mathrm{c}}}{S_{\mathrm{m}}} g_{\mathrm{liq}} = \frac{S_{\mathrm{m}}}{S} \frac{L_{\mathrm{c}}}{L_{\mathrm{m}}} g_{\mathrm{liq}} \tag{2.21}$$

Strictly speaking, there is no reason to assume that the length ratio $L_{\mathrm{c}}/L_{\mathrm{m}}$ equals its equivalent surface area ratio $S_{\mathrm{c}}/S_{\mathrm{m}}$. Nevertheless, this assumption is made in all aforementioned studies that determined S_{c}/S. g_{m} is defined as a gas phase conductance, while g_{liq} is a liquid phase conductance. Therefore, Henry's law has to be applied, which states that the ratio between the concentrations of a chemical species in a gas and in an adjacent solvent is constant at steady state conditions (Ho *et al.*, 2010; Tosens *et al.*, 2012b):

$$g_{\mathrm{m}} = \frac{H}{RT} g_{\mathrm{liq}}{}' \tag{2.22}$$

where H is Henry's law constant for CO_2. There are a couple of disadvantages to this approach. First, the collection of all microscopic images required to determine the curvature factors for the calculations of S_{m}/S is laborious. There are alternative methodologies to determine S_{m}/S mentioned in literature; (1) they can be measured directly from a tomography obtained by X-ray synchrotron microscopy (Verboven *et al.*, 2015) or by the reconstruction of the three-dimensional structure from light microscopic images of macerated palisade and spongy parenchyma cells (Ivanova and Pyankov, 2002; Ivanova *et al.*, 2006; Ivanova, 2012). (2) the conductance of each mesophyll component in equation (2.20) either has to be measured directly or to be calculated by equation (2.8). Still, measuring the conductance or the diffusion coefficients of these components directly is very challenging and the amount of published data is very limited (Evans *et al.*, 2009). (3) The diffusion path length of the cell wall and the cytosol can be set equal to the measured thickness of these components. However, this is not valid for the stroma, since CO_2 molecules can be

carboxylated by Rubisco while they are diffusing in the mesophyll, resulting in a diffusion path length shorter than the chloroplast thickness. Various studies (Peguero-Pina *et al.*, 2012; Tosens *et al.*, 2012a; Tosens *et al.*, 2012b; Tomas *et al.*, 2013) assumed that the diffusion path length of CO_2 in the stroma is half its thickness. However, this implies that the local CO_2 partial pressure linearly decreased with the distance that the molecules diffuse in the stroma. This is unlikely as the ratio of the stromal CO_2 diffusion path length to the stromal thickness is probably considerably smaller than 0.5 (Tholen and Zhu, 2011) and may depend on the sink strength. The power of this type of models is the fact that they can link mesophyll conductance directly to leaf anatomical properties by modelling these properties explicitly. They have recently been used to investigate how g_{m} is affected by leaf development and light and water availability (Tosens *et al.*, 2012b), to explain differences in g_{m} between two *Abies* species (Peguero-Pina *et al.*, 2012), and to check whether leaf anatomical properties can explain differences in g_{m} among different levels of drought stress (Tomas *et al.*, 2013; Tomas *et al.*, 2014). However, there are also limitations to this approach. Several of these limitations, i.e. the uncertainty of the length of the CO_2 diffusion path in the stroma and the absence of variability of g_{m} with C_{i}, can be solved by the use of reaction-diffusion models. We will discuss this type of models in sections 2.9-2.12 of this chapter.

2.7. Variability of g_{m}

One of the fundamental assumptions of models for the conductance of a material for a certain chemical species is that it does not change with the concentration of this chemical species, since diffusive transport only depends on the diffusion coefficient, the thickness of the material, and the temperature (equation (2.8)). The assumption that g_{m} does not change with C_{i} was confirmed in a recent study (Tazoe *et al.*, 2009) in wheat, but several other recent studies report considerable changes in the estimate of g_{m} if the above methods to determine it are applied at different CO_2 levels (Flexas *et al.*, 2007; Hassiotou *et al.*, 2009; Vrabl *et al.*, 2009; Bunce, 2010; Douthe *et al.*, 2011; Tazoe *et al.*, 2011) as reviewed by Flexas *et al.* (2012). Importantly, this reported variability violates the definition of a physical conductance and implies that g_{m} is not

a lumped conductance but instead an apparent variable that depends on C_i. The mechanism of the dependence of g_m on C_i is largely unclear (Flexas *et al.*, 2012), which makes it hard to mechanistically model it. One solution to this issue is to describe the variability of g_m by a phenomenological model instead (Yin *et al.*, 2009):

$$g_\mathrm{m} = \frac{\delta(A + R_\mathrm{d})}{C_\mathrm{c} - \Gamma^*} \tag{2.23}$$

where parameter δ defines the C_c:C_i ratio at saturating light as $(C_\mathrm{c} - \Gamma^*)/(C_\mathrm{i} - \Gamma^*) = 1/(1 + 1/\delta)$. Substitution of this term in the curve-fitting method equation (2.14a-d) and considerable re-arranging yields:

$$A_\mathrm{N} = \frac{-\mathcal{B} + \sqrt{\mathcal{B}^2 - 4\mathcal{A}\mathcal{C}}}{2\mathcal{A}} \tag{2.24a}$$

$$\mathcal{A} = X_2 + \Gamma^* + \delta(C_\mathrm{i} + X_2) \tag{2.24b}$$

$$\mathcal{B} = -\{(X_2 + \Gamma^*)(X_1 - R_\mathrm{d}) + (C_\mathrm{i} + X_2)[\delta(X_1 - R_\mathrm{d})] + \delta[(X_1(C_\mathrm{i} - \Gamma^*) - R_\mathrm{d}(C_\mathrm{i} + X_2)]\} \tag{2.24c}$$

$$\mathcal{C} = \delta(X_1 - R_\mathrm{d})[X_2(C_\mathrm{i} - \Gamma^*) - R_\mathrm{d}(C_\mathrm{i} + X_2)] \tag{2.24d}$$

$$X_1 = \begin{cases} V_\mathrm{cmax} & \text{if } A_\mathrm{N} = A_\mathrm{c} \\ \frac{1}{4}J & \text{if } A_\mathrm{N} = A_\mathrm{j} \end{cases} \tag{2.24e}$$

$$X_2 = \begin{cases} K_\mathrm{mC}\left(1 + \frac{O}{K_\mathrm{mO}}\right) & \text{if } A_\mathrm{N} = A_\mathrm{c} \\ 2\Gamma^* & \text{if } A_\mathrm{N} = A_\mathrm{j} \end{cases} \tag{2.24f}$$

Yin *et al.* (2009) demonstrated that equations (2.24a-f) can be used to estimate δ and V_cmax and subsequently to simulate how g_m varies with C_i as:

$$g_{\mathrm{m}} = \frac{A_{\mathrm{N}} - \delta(A_{\mathrm{N}} + R_{\mathrm{d}})}{C_{\mathrm{i}} - \Gamma^*} \tag{2.25}$$

The advantage of this model is that it allows the estimation of photosynthetic parameters, while still considering the variability of g_{m}. However, since this is a phenomenological model, it does not explain any of the mechanisms that determine g_{m}. Tholen *et al.* (2012) designed a mathematical framework to show that this variability may be explained by the release of (photo)respiratory CO_2 from the mitochondria in the cytosol. In this framework g_{m} is partitioned into two serial conductances g_{wp} (serial conductance of cell wall and plasma membrane) and g_{chl} (serial conductance of chloroplast envelope and stroma). According to this framework, g_{m} can be expressed as:

$$g_{\mathrm{m}} = \frac{g_{\mathrm{wp}} g_{\mathrm{chl}}}{g_{\mathrm{chl}} + g_{\mathrm{wp}} \left(1 + \frac{R_{\mathrm{d}} + R_{\mathrm{p}}}{A_{\mathrm{N}}}\right)} \tag{2.26}$$

An interesting feature of this model for g_{m} is that it gives a more mechanistic explanation for the variability of g_{m} with the CO_2 partial pressure than the Yin *et al.* (2009) model, although it explains only the initial part of the commonly recorded variability (i.e., the increase of g_{m} with increasing C_{i}). It can also be parameterized from gas exchange methods combined with isotope discrimination, so leaf anatomical measurements and assumed diffusion coefficients for CO_2 in mesophyll compartments are not required to quantify g_{wp} and g_{chl}. Nevertheless, it has an important limitation as it is assumed implicitly that CO_2 release by (photo)respiration takes place in a cytosol compartment between the cell wall and the chloroplast envelope. Subsequently, this CO_2 shares its diffusion pathway with CO_2 taken up from the atmosphere from the cytosol to Rubisco. This either implies that (1) diffusion of CO_2 in the cytosol is so fast, compared to CO_2 diffusion in the stroma, that there is no gradient of CO_2 in the cytosol (Tholen *et al.*, 2014) or that (2) (photo)respired CO_2

release is restricted to a layer of cytosol between the cell wall and the part chloroplast envelope facing the intercellular air space. In case (1), the placement of mitochondria in relation to chloroplasts does not have any effect on the re-assimilation of (photo)respired CO_2. In case (2), the re-assimilation of (photo)respired CO_2 may be underestimated, because the diffusion distance of (photo)respired CO_2 between the mitochondria is then very short, compared to a situation in which they are placed between the part of the chloroplast envelope facing the vacuole and the tonoplast. Fig. 2.1 shows a schematic overview of the description of the CO_2 diffusion path by (a) an unpartitioned mesophyll conductance model, (b) a partitioned mesophyll conductance model assuming that CO_2 produced by respiration and photorespiration is released in the outer layer of the cytosol. (c) a partitioned mesophyll conductance model assuming that CO_2 produced by respiration and photorespiration can be released anywhere and that CO_2 diffusion in the cytosol is very fast.

2.8. Mesophyll conductance; potentials and limitations

Mesophyll conductance models have a large number of applications as described in the two sections above. They are particularly useful for the estimation of parameters. Their use prevents the underestimation of photosynthetic parameters in the FvCB model (Farquhar *et al.*, 1980) and prevent the propagation of such errors if the FvCB model is used for further predictions after parameterization (Niinemets *et al.*, 2009; Sun *et al.*, 2014b). Moreover, mesophyll conductance can be partitioned into sub-conductances, which allows modelling of the effects of leaf anatomical properties on mesophyll conductance (Evans *et al.*, 1994; Tosens *et al.*, 2012b) and photosynthesis (Tholen *et al.*, 2012). However, the various types of mesophyll conductance models have several limitations. (1) Models that determine g_m from gas exchange measurements, sometimes combined with chlorophyll fluorescence or isotope discrimination methods, are prone to statistical artefacts that may lead to errors in the estimates of photosynthetic parameters (Yin and Struik, 2009; Gu and Sun, 2014; Sun *et al.*, 2014a; Sun *et al.*, 2014c; Sharkey, 2015). (2) These models do not give a mechanistic explanation on which processes and structures that determine g_m and, thereby, C_c and the net CO_2 assimilation rate. Models that quantify g_m by anatomical measurements

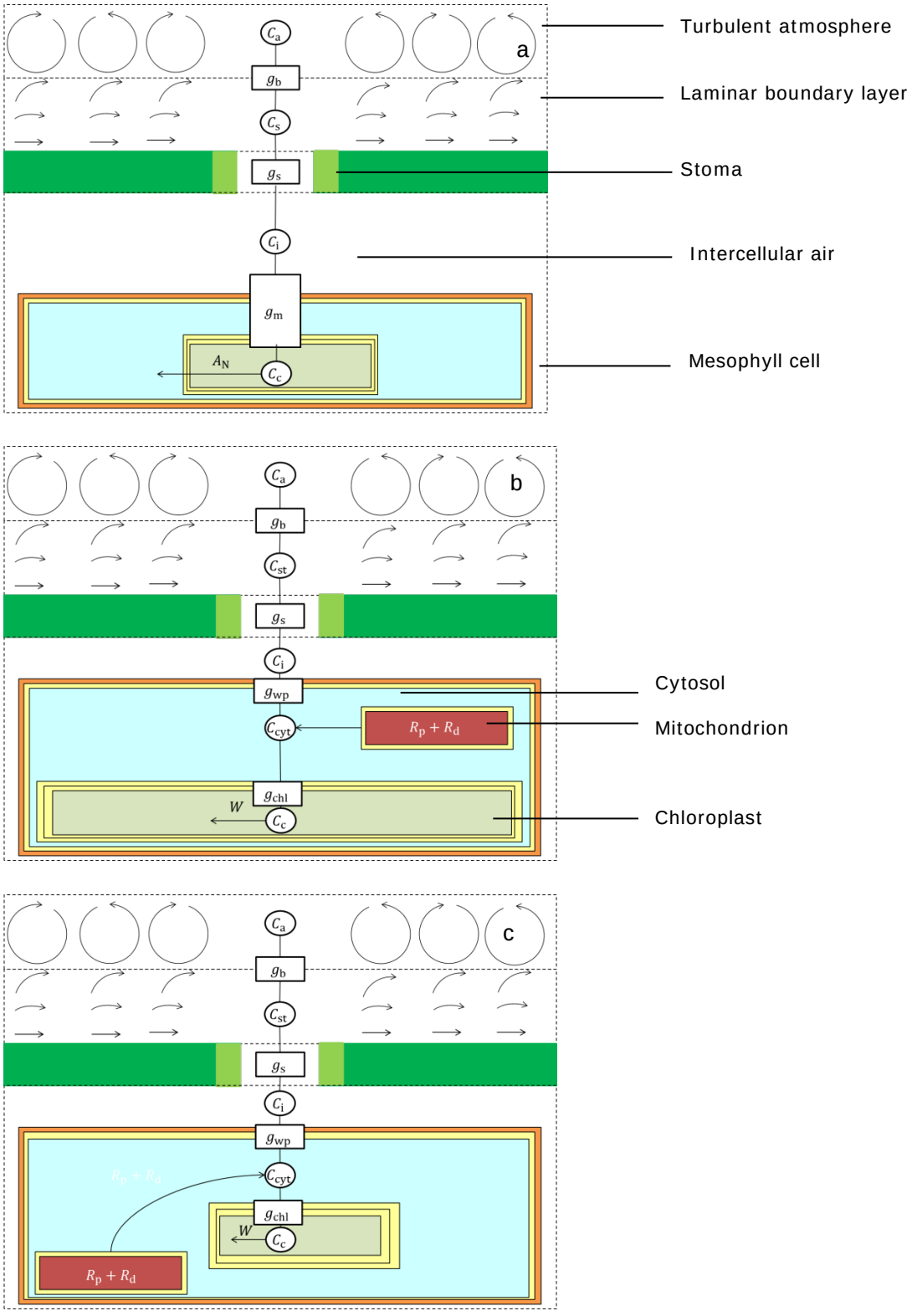

Figure 2.1: Schematic overview of the CO_2 diffusion path according to the framework that assumes that a): the drawdown of of the CO_2 partial pressure between the intercellular air space and Rubisco is determined by a single conductance g_m, b): mesophyll conductance is partitioned into two subconductances g_{wp} and g_{chl}. Mitochondria in the outer cytosol layer release (photo)respired CO_2 between these two conductances. c) Mitochondria at any location release CO_2 between the two subresistances assuming that diffusion in the cytosol is very fast.

and assumed diffusive properties can be used to study the relationship between leaf structures and g_m. However, both models that determine g_m from gas exchange measurements and from leaf anatomical measurements do not contain a mechanistic explanation for the variability of g_m with C_i. According to the conductance model of Tholen *et al.* (2012), the variability of g_m can be partly explained by the release of (photo)respired CO_2 in the cytosol. However, this model either restricts the position of the mitochondria relative to the chloroplasts to an outer cytosol layer between the cell wall and the chloroplast envelope facing the intercellular air space or assumes that there is no CO_2 gradient in the cytosol. Both assumptions have implications for predictions of the amount of (photo)respired CO_2 being re-assimilated. Lastly, (3), mesophyll conductance models are inflexible. Adding various forms of complexity to conductance models makes the mathematical expressions for g_m and A_N complex and, therefore, cumbersome to use (Parkhurst, 1977). For instance, the curve fitting method of Ethier *et al.* (2006) requires substitution of $C_c = C_i - \frac{A_N}{g_m}$ in the FvCB model, which lead to the complex set of equations (2.13) and (2.14a-d). These terms become even more complicated, when a phenomenological model for the variability of g_m is added (Yin *et al.*, 2009) (equations (2.24a-f,2. 25)). The inflexibility and the algebraic complexity of mesophyll conductance models make it hard to understand the model's behaviour and the lack of a mechanistic description makes it hard to interpret the results of these models. Therefore, it may be worthwhile to find an alternative for the g_m type of models. The alternatives that we review in the next sections are reaction-diffusion type models, which overcome the above-mentioned limitations.

2.9. Fundamentals of reaction-diffusion models

The accumulation of the concentration of a certain substance can be defined as the difference between the rate of concentration increase due to the net production of this substance (source term S) and the rate of concentration decrease due to the net outflux (formulated as the gradient of the outflux $-\nabla\varphi$) of this substance. This can be described by a reaction-diffusion equation:

$$\frac{\partial c}{\partial t} = -\nabla\varphi + S \tag{2.27}$$

where t is the time. Substitution of φ in equation 27 as defined by Fick's first law, results in Fick's second law (Fick, 1855).

$$\frac{\partial c}{\partial t} = \nabla \cdot D\nabla c + S \tag{2.28}$$

Equation (2.28) can be solved over an arbitrary geometry called a computational domain. The exact expression of the gradient operator ∇ (expressed in m^{-1}) depends on the coordinate system and the number of dimensions. Solving equation (2.28) also requires boundary conditions that define either the net flux or the concentration at the boundary of the computational domain. The steady state distribution can be calcuated by setting $\partial c/\partial t = 0$ in equation (2.24):

$$\nabla \cdot D\nabla c + S = 0 \tag{2.29}$$

Almost all reaction-diffusion models for leaf photosynthesis in the literature are steady-state models, just like all mesophyll conductance models. So, they satisfy equation (2.29). Solving this equation can be done analytically in certain simple cases (Parkhurst, 1977; Rand, 1977, 1978). More commonly, they have to be solved numerically by the means of finite element or finite volume methods (Lewis *et al.*, 2004). The power of reaction-diffusion models is that they are very flexible. It is possible to solve them over any geometry, explicitly define in which subdomain specific sinks or sources are present, and to define the diffusion coefficient for each subdomain.

2.10. Early reaction-diffusion models for photosynthesis

To the best of our knowledge, the earliest reaction-diffusion models for CO_2 transport in leaves were published in the 1970s (Parkhurst, 1977; Rand, 1977; Sinclair *et al.*, 1977). Parkhurst (1977) simulated a "leaf plug" as a rectangular cuboid. This 3D domain is modelled as a homogeneous medium, in which the diffusion coefficient is calculated as the weighted average diffusion coefficient in the gas phase and liquid phase. The CO_2 uptake was calculated as the ratio of the concentration difference between the air space and the site of carboxylations to the sum of the "carboxylation resistance" and the resistance of the intracellular liquid. This model predicted a gradient of CO_2 from the stomata to the internal leaf parts. In a later study, the stomatal pore was explicitly modelled. Parkhurst (1984) modelled a stomatal pore explicitly as a cylindrical tube attached to a larger cylinder representing the mesophyll. He varied the size of this pore to assess how the CO_2 profile is affected. There are three problems with the concepts of the models described above. First, none of the models described above, except for Parkhurst and Mott (1990), were validated with data. This limits their use to strictly theoretical analyses and may result in wrong conclusions, if the assumed parameter values are unrealistic. Second, some of the models above assume that C_c is constant under all environmental conditions and is considered to be very small, a concept that was frequently used before the era of the FvCB model. This leads to large concentration differences between the intercellular air space and the binding sites of Rubisco. Therefore, the net influx of CO_2 in mesophyll cells is large, which can lead to overstimation of the net CO_2 assimilation rate. This limitation can be overcome by adding a source term that considers RuBP carboxylation (Parkhurst and Mott, 1990). Thirdly, another limitation is the porous medium approximation. It assumes that CO_2 can be assimilated at any place in the media, since only CO_2 transport in the gas phase is explicitly modelled. This results in a simulated CO_2 gradient (Parkhurst, 1977; Rand, 1977, 1978) from the stomatal opening to the internal parts of the leaf and may lead to the conclusion that the air space may contribute substantially to the overall mesophyll conduction. In reality, CO_2 consumption by RuBP carboxylation is limited to the chloroplasts, which only fill a

small fraction of the whole mesophyll. They are almost always concentrated near the interface between the intercellular air space and the exposed mesophyll surface area (Haberlandt, 1904). Consequently, the real diffusion path length in the liquid phase is very short, compared to the diffusion path length in the gas phase. The concentration of chloroplasts near the exposed mesophyll surface area also makes the diffusion path one-dimensional; this means that the CO_2 gradient is mainly from the exposed cell wall to the binding sites of Rubisco and not, as simulated by porous media approaches, from the adaxial to the abaxial leaf surface. More recent reaction-diffusion models for CO_2 transport in leaves generally model the liquid phase and the gas phase for CO_2 transport explicitly (Vesala *et al.*, 1996; Aalto *et al.*, 1999; Aalto and Juurola, 2002; Juurola *et al.*, 2005; Tholen and Zhu, 2011; Ho *et al.*, 2012; Ho *et al.*, 2016), which allows separation of the CO_2 gradient in the liquid phase and the gas phase.

2.11. Modern reaction-diffusion models for CO_2 transport

The first reaction-diffusion model for CO_2 in leaves that separates the gas phase and liquid phase of CO_2 transport is proposed by Vesala *et al.* (1996). They modelled a leaf as a stoma and a stomatal cavity, connected by a stomatal pore (Vesala *et al.*, 1995). The stomatal cavity was flanked with liquid phase compartments that formed the liquid phase of CO_2 transport, in which RuBP carboxylation takes place. A reaction-diffusion model was solved over this structure and the net CO_2 assimilation rate of the leaf and the CO_2 concentration profile was calculated. This distribution showed a substantial decline of the CO_2 concentration from the interface of the stomatal pore and the stomatal cavity to the bottom of the stomatal cavity. According to Vesala *et al.* (1996), this result comfirmed the hypothesis of Parkhurst (1994) that the intercellular air space can be a major barrier for CO_2 transport. However, this conclusion is controversial, as Vesala *et al.* (1996) modelled all mesophyll below the stomatal cavity as a liquid phase compartment. They state that this assumption ignores the air channels between the pallisade and spongy parenchyma, which interconnects these tissues. To compensate for that, they assumed that the diffusion coefficient of CO_2 in the liquid phase was ten times as large as for water. Consequently, the conductance of the liquid phase for CO_2 transport is much higher than suggested in

most studies. Aalto *et al.* (1999) used a similar model to run a senstivity analysis for the diffusion coefficient of CO_2 in the liquid phase. Indeed, they found that the gradient of CO_2 in the intercellular air space becomes steeper when the diffusion coefficient of CO_2 in the liquid phase is increased.

Aalto and Juurola (2002) presented a new reaction-diffusion model. In this model, the palisade and spongy parenchyma cells were represented as simple geometrical shapes (cylinders with half-spherical caps and spheres, respectively) and the epidermis cells were represented as a rectangular cuboids. The abaxial epidermis contained a stomatal air filled pore, modelled as a cylindrical hole. Stomatal conductance could be regulated by varying the radius of the stomatal pore. This was the first reaction-diffusion model, in which loose chloroplasts are modelled near the mesophyll surface area exposed to the intercellular air space. Unlike previous models that assumed very high liquid phase diffusion coefficients (Vesala *et al.*, 1996; Aalto *et al.*, 1999), the diffusion coefficient of CO_2 in the liquid phase compartments was now set to the one in water. The calculated CO_2 concentration profile revealed that there was no CO_2 gradient under ambient CO_2 levels from interface between the stomatal pore and the intercellular air space and the upper side of the leaf. In contrast, there was a strong gradient from the exposed mesophyll surface area to the centre of the chloroplasts. This finding rejected the hypothesis of a strong CO_2 gradient in the air space.

Besides studying CO_2 gradients in the air phase and liquid phase of CO_2 transport, the model from Aalto and Juurola (2002) provided various other insights that cannot be obtained by previously described mesophyll conductance models. Juurola *et al.* (2005) expanded the model with the temperature dependency of various photosynthetic parameters, with diffusion coefficients and with the solubility of CO_2 in the liquid phase. They used the model to re-estimate photosynthetic parameters and parameters for their temperature dependence. The parameter estimates were sometimes remarkably different from the estimates based on the same data in a previous study (Aalto and Juurola, 2001), in which an infinite mesophll conductance was assumed while estimating photosynthetic parameters. This supports the statement that g_{m} cannot be ignored. It was the first time that a reaction-diffusion model is directly used

to estimate photosynthetic parameters and their temperature dependencies. This allowed separation of temperature dependencies of physical parameters (diffusion coefficients, CO_2 solubility) and biochemical parameters (K_{mC}, K_{mO}, V_{cmax}, J_{max} R_{d}). Juurola *et al.* (2005) stated that the temperature dependencies of each of these parameters may be partly lumped in g_{m}, in case a mesophyll conductance model is used (Bernacchi *et al.*, 2002; Scafaro *et al.*, 2011) . The temperature dependencies may be even more biased, if it is assumed that g_{m} is negligible (Harley *et al.*, 1992b; Aalto and Juurola, 2001).

Tholen and Zhu (2011) developed another reaction-diffusion model. Their computational domain consisted of a sphere that represented a single mesophyll cell. This sphere was further subdivided into subdomains representing loose spherical chloroplasts, mitochondria, and a spherical centrale volume, which is the vacuole. The remaining space was the cytosol. Tholen and Zhu (2011) aimed to address all factors that affect mesophyll resistance and, thereby, C_{c} and the net rates of CO_2 assimilation. These factors included the diffusion coefficient of various compartments and CO_2 facilitation by carbonic anhydrases. This was also one of the first studies proved that a reaction-diffusion model describes gas exchange measurements, in this case an $A_{\mathrm{N}} - C_{\mathrm{i}}$ curve, reasonably well.

Another reaction-diffusion model was developed by Ho *et al.* (2016). The geometry used in this study was directly obtained from a 3-D tomography of a leaf obtained by 3-D X-ray synchrotron microscopy (Verboven *et al.*, 2015). This geometry was subdivided into subdomains (chloroplasts, cytosol, vacuole, intercellular air space, epidermis). Within this highly complex 3-D computational domain a gas exchange model was solved. The high degree of realism of the internal structure of the mesophyll in the tomography allowed to solve a Monte Carlo ray tracing model to simulate light propagation through the leaf (Watté *et al.*, 2015). This resulted in similar profiles as measured for photosynthetic capacity (Sun *et al.*, 1998; Vogelmann and Evans, 2002; Evans and Vogelmann, 2003). Ho *et al.* (2016) used this combined CO_2 and light transport model to simulate how the distribution of chloroplasts (“face” or “profile”) (Tholen *et al.*, 2008) affects the light distribution profile in the leaf and its

photosynthesis. They also used this model to comfirm that the net CO_2 assimilation is optimal if the gradient of the photosynthetic capacity follows the light absorption gradient. Local CO_2 concentrations in the intercellular air space, that appeared to be highly interconnected, were about the same throughout the intercellular air space. On the other hand, strong gradients of CO_2 were found in the cytosol and the chloroplasts. Again, this comfirmed that the conductance of the intercellular air space is very high compared to the conductance of the remaining part of the mesophyll. It was also the first time that such a reaction-diffusion model was explored to calculate the amount of refixation of CO_2 produced by respiration and photorespiration. The model from Ho *et al.* (2016) allowed to study processes related to photoynthesis at small scale in greater detail than ever before. Nevertheless, this approach also has some disadvantages. First, the model requires a high resolution 3-D tomography, which requires access to advanced equipment, like X-ray microscopy (Verboven *et al.*, 2008; Verboven *et al.*, 2015). Second, this tomography cannot be systematically changed. Consequently, if a new leaf type is studied, a new tomography has to be made. Third, the model requires a very dense mesh due to the very detailed geometry. This makes the model very computationally expensive and, therefore, limited by the number of simulations that can be done. Using such a model requires access to powerful supercomputers. Some of these problems may become less of an issue in the future, when computers have become more powerful or if it is easier to frequently access high resolution 3-D visualisation facilities like 3-D X-ray synchrotron microscopy. In the next paragraph, we will discuss for which purposes mesophyll conductance models can be used in future research and for which purposes we think it is necessary to use reaction-diffusion models as an alternative.

2.12 Why (not) use reaction-diffusion models as an alternative to mesophyll conductance models?

If mesophyll resistance is simply ignored during the estimation of FvCB model parameters (Farquhar *et al.*, 1980), V_{cmax} and J_{max} can be underestimated considerably. Climate and crop models that use these biased parameters for predictions may

underestimate the CO_2 uptake by plants considerably and, therefore, generate wrong predictions (Niinemets *et al.*, 2009; Sun *et al.*, 2014b). Although mesophyll conductance models have often been used to determine C_c, they have some disadvantages. First, the models that estimate g_m are prone to statistical artefacts (Yin and Struik, 2009), which can result in wrong estimation of photosynthetic parameters as well. Second, they lump both biochemical processes and leaf anatomical structures in a single parameter. This makes it impossible to assess to what extent each structure and biochemical process affects C_c and A_N, particulalry in response to environmental variables. This problem can be tackeled somewhat by the partitioning of mesophyll conductance in subconductances (Evans *et al.*, 1994; Niinemets and Reichstein, 2003; Peguero-Pina *et al.*, 2012; Tosens *et al.*, 2012a; Tosens *et al.*, 2012b; Tomas *et al.*, 2013), but these models do not consider variability of g_m with C_i. Mesophyll conductances are useful to estimate parameters of the FvCB model. It is possible to consider the variability of g_m with C_i in estimation procedures, if a phenomological model is used to describe this variability (Yin *et al.*, 2009; Gu *et al.*, 2012). However, mesophyll conductance models are not flexible enough to give a mechanistic description of the CO_2 diffusion pathway. If one is interested to identify individual factors that affect CO_2 transport from the intercellular air space, reaction-diffusion models could be used as an alternative.

Reaction diffusion models have various advantages over mesophyll conductance models. (1) They are more flexible than mesophyll conductance models, which makes it easier to extend them with additional factors, like CO_2 transport facilitation by carbonic anhydrase activity (Tholen and Zhu, 2011) or light propagation (Watté *et al.*, 2015; Ho *et al.*, 2016). (2) They can be used to study the effect of S_c/S_m or the position of mitochondria on the net CO_2 assimilation and the re-assimilation of (photo)respired CO_2 (Ho *et al.*, 2016). (3) They can be used to give a mechanistic explanation on why the efficiency of CO_2 transport depends on environmental conditions, rather than lumping all factors that cause this in a single parameter g_m. (4) They can separately describe the effects of physical and biochemical factors on the efficiency of CO_2 transport in leaves.

It is important to simulate the gas phase and the liquid phase separately, because a porous volume approach, used in the older reaction-diffusion models, may overestimate the gradient of CO_2 between the stomatal pore and the internal leaf parts. This limitation has been solved by the introduction of methods to model the liquid phase and the gas phase separately (Vesala *et al.*, 1996; Aalto and Juurola, 2002). Nevertheless, reaction-diffusion models do have other limitations, which do not necessarily occur in mesophyll conductance models. The most important limitations are (1) that the diffusion coefficients and the diffusion path length in the stroma are uncertain. Although reaction diffusion models are physically more realistic and provide a more mechanistic description of CO_2 transport, the downside is that some of the physical parameters are uncertain. Therefore, we emphasize that reaction-diffusion models need to be validated after parameterization, whenever possible. Also, (2) they require leaf anatomical data to reconstruct the computational domain. The collection of these data is considerably more laborious than gas exchange measurements if it is done by TEM and/or light microscopy (Thain, 1983; Evans *et al.*, 1994; Peguero-Pina *et al.*, 2012; Tosens *et al.*, 2012a; Tosens *et al.*, 2012b; Tomas *et al.*, 2013) or it requires access to advanced 3-D visualization technology like X-ray synchrotron microscopy (Verboven *et al.*, 2008; Verboven *et al.*, 2015). This latter problem may become obsolete over the years due to technological advancement of visualization technology. Finally, (3) there is a trade-off between the degree of realism of the desired geometry in the computational domain and the computational time. Again, this problem may become obsolete over time, if the speed of computers further increases.

The prediction from Zhu *et al.* (2010) that the photosynthetic efficiency can be increased by 20% by increasing g_{m} opens great possibilities to increase crop productivity and meet the global demand for food, fibres and bioenergy. Nevertheless, in this review we explained that in current models, this parameter lumps a large number of biochemical factors and physical factors. In order to examine ways to increase g_{m}, we therefore have to understand which of these factors we may have to alter to achieve increases of g_{m}. In our view, the possibilities to do so with conventional mesophyll conductance models are very limited, due to restricted

capability to provide a mechanistic description of the CO_2 diffusion path in the mesophyll. Even though reaction-diffusion models also have their limitations, their separation of biochemical and physical factors are key to identifying targets to increase g_m and photosynthesis, to ultimately find ways to increase global crop productivity.

CHAPTER 3

Modelling the relationship between CO_2 assimilation and leaf anatomical properties in tomato leaves

Herman N.C. Berghuijs[1,2,3], Xinyou Yin[1,2], Q. Tri Ho[3], Peter E.L. van der Putten[1,2], Pieter Verboven[3], Moges A. Retta[1,3], Bart M. Nicolaï[3], Paul C. Struik[1,2]

[1] Centre for Crop Systems Analysis, Wageningen University, Droevendaalsesteeg 1, 6708 PB Wageningen, The Netherlands

[2] BioSolar Cells, P.O. Box 98, 6700 AB Wageningen, The Netherlands

[3] Flanders Center of Postharvest Technology / BIOSYST-MeBioS, Katholieke Universiteit Leuven, Willem de Croylaan 42, B-3001, Leuven, Belgium

Abstract

The CO_2 concentration near Rubisco and, therefore, the rate of CO_2 assimilation, is influenced by both leaf anatomical factors and biochemical processes. Leaf anatomical structures act as physical barriers for CO_2 transport. Biochemical processes add or remove CO_2 along its diffusion pathway through mesophyll. We combined a model that quantifies the diffusive resistance for CO_2 using anatomical properties, a model that partitions this resistance and an extended version of the Farquhar-von Caemmerer-Berry model. We parametrized the model by gas exchange, chlorophyll fluorescence and leaf anatomical measurements from three tomato cultivars. There was generally a good agreement between the predicted and measured light and CO_2 response curves. We did a sensitivity analysis to assess how the rate of CO_2 assimilation responds to changes in various leaf anatomical properties. Next, we conducted a similar analysis for assumed diffusive properties and curvature factors. Some variables (diffusion pathway length in stroma, diffusion coefficient of the stroma, curvature factors) substantially affected the predicted CO_2 assimilation. We recommend more research on the measurements of these variables and on the development of 2-D and 3-D gas diffusion models, since these do not require the diffusion pathway length in the stroma as predefined parameter.

Key words: Leaf anatomy, photosynthesis, diffusion, mesophyll resistance, mesophyll conductance, C_3

Published in: *Plant Science* **238 (**2015), 297-311

3.1. Introduction

The biochemical model of Farquhar, von Caemmerer & Berry ('the FvCB model' hereafter) (Farquhar *et al.*, 1980) has been widely used to study leaf physiology and to predict leaf photosynthesis under various environmental conditions. This model states that Rubisco-limited and electron-transport-limited rates of CO_2 assimilation depend on the CO_2 partial pressure at the carboxylation sites of Rubisco, C_c (see Table 3.1 for the definition of symbols used in this study). Assessing C_c is complicated by the mesophyll resistance that substantially constrains CO_2 diffusion from the intercellular air space to Rubisco (Flexas *et al.*, 2008; Niinemets *et al.*, 2009; Tholen *et al.*, 2012b; Sun *et al.*, 2014).

Traditionally, mesophyll resistance r_m is defined as a lumped resistance as:

$$r_m = \frac{(C_i - C_c)}{A_N} \tag{3.1}$$

where C_i is CO_2 partial pressures in intercellular air-spaces, and A_N is the net rate of CO_2 assimilation. The inverse of mesophyll resistance is mesophyll conductance g_m. Various methods have been developed to estimate r_m indirectly with either chlorophyll fluorescence measurements (Yin and Struik, 2009) or ^{13}C isotope discrimination methods (Pons *et al.*, 2009). One of the most widely used methods to estimate r_m based on chlorophyll fluorescence measurements is the variable J method (Harley *et al.*, 1992). This method, when applied to various C_i or light levels, often shows an initial increase and then decrease of g_m with an increasing C_i or of a continuous increase of g_m with an increasing irradiance I_{inc} (Flexas *et al.*, 2008; Yin and Struik, 2009). This method is, in principle, only valid for the electron-transport-limited CO_2 assimilation, and caution is needed when applying it to Rubisco or triose-phosphate-utilization-limited CO_2 assimilation. For example, that the variable J method may

Table 3.1. List of variables and their units

Variable	Definition	Unit
A_{N}	Net rate of CO_2 assimilation	μmol CO_2 m^{-2} leaf s^{-1}
C_{a}	CO_2 partial pressure in the atmosphere	μbar CO_2
C_{i}	CO_2 partial pressure in the intercellular air space	μbar CO_2
C_{i0}	CO_2 partial pressure in the intercellular air space if $I_{\mathrm{inc}} = 0$	μbar CO_2
C_{c}	CO_2 partial pressure near Rubisco	μbar CO_2
$D_{\mathrm{CO_2,i}}$	Diffusion coefficient of CO_2 in component i	m^2 s^{-1}
$D_{\mathrm{CO_2,water}}$	Diffusion coefficient of CO_2 in water	m^2 s^{-1}
f_{i}	Fraction of the diffusive path length of component i and its thickness	-
f_{pal}	Fraction of the exposed mesophyll surface area that belongs to the palisade parenchyma	-
F	Rate of photorespiratory CO_2 release	μmol CO_2 m^{-2} leaf s^{-1}
G_{mem}	Permeability of the cell wall	m s^{-1}
G_{env}	Permeability of the chloroplast envelope	m s^{-1}
H	Henry's law constant for CO_2	Pa m^{-3} mol^{-1}
I_{inc}	Irradiance incident at the leaf surface	μmol photons m^{-2} leaf s^{-1}
J	Rate of electron transport through Photosystem II	μmol e^- m^{-2} leaf s^{-1}
J_{max}	Maximum rate of electron transport through Photosystem II at saturating light	μmol e^- m^{-2} leaf s^{-1}
K_{mC}	Michaelis-Menten constant of Rubisco for CO_2	μbar CO_2
K_{mO}	Michaelis-Menten constant of Rubisco for O_2	mbar O_2
L_{i}	Diffusion path length of component i	m
$\left(\frac{L_{\mathrm{m}}}{L}\right)_{\mathrm{tissue}}$	Fraction of exposed mesophyll length relative to the width of the section at one side of the leaf in a certain tissue (either palisade parenchyma or spongy parenchyma)	m m^{-1}
O	O_2 partial pressure	mbar O_2
$p_{\mathrm{eff,i}}$	Effective porosity of component i	-
q	Power in the power law that describes the empirical relationship between C_{i} and I_{inc}	
r_{i}	Resistance for CO_2 transport of component i in the mesophyll	m^2 leaf s bar CO_2 mol^{-1} CO_2
r_{chl}	Lumped resistance for CO_2 transport of the chloroplast envelope and the stroma, and half the resistance of the cytosol	m^2 leaf s bar CO_2 mol^{-1} CO_2
r_{diff}	Total resistance for CO_2 transport of the physical barriers in the mesophyll	m^2 leaf s bar CO_2 mol^{-1} CO_2
r_{m}	Apparent mesophyll resistance	m^2 leaf s bar CO_2 mol^{-1} CO_2
r_{wp}	Lumped resistance for CO_2 transport of the cell wall, the plasma membrane, and half the resistance of the cytosol	m^2 leaf s bar CO_2 mol^{-1} CO_2
R	Universal gas constant	J K^{-1} mol^{-1}
R_{d}	Rate of mitochondrial respiration in the light	μmol CO_2 m^{-2} leaf s^{-1}
R_{i}	Resistance for CO_2 transport of component i in the mesophyll	s m^{-1}
s	Slope of the assumed linear relationship between A_{N} and $\frac{1}{4} I_{\mathrm{inc}} \Phi_2$ under strictly electron-transport-limited conditions	-
$\frac{S_{\mathrm{c}}}{S}$	Fraction of the exposed chloroplast surface area of the palisade parenchyma and the spongy parenchyma relative to leaf surface area at one side of the leaf	m^2 chloroplast m^{-2} leaf
$\frac{S_{\mathrm{c}}}{S_{\mathrm{m}}}$	Fraction of the exposed chloroplast surface area of the palisade parenchyma and the spongy parenchyma relative to the exposed mesophyll surface area of these tissues	m^2 chloroplast m^{-2} mesophyll
$S_{\mathrm{C/O}}$	Relative CO_2/O_2 specificity factor of Rubisco	mbar O_2 μbar^{-1} CO_2

$\frac{S_m}{S}$	Fraction of the exposed mesophyll surface area of the palisade parenchyma and the spongy parenchyma relative to leaf surface area at one side of the leaf	m^2 mesophyll m^{-2} leaf
t_i	Weighted average thickness of a mesophyll component i in the palisade and the spongy parenchyma	m
T	Temperature	K
T_p	Rate of triose phosphate utilization	µmol phosphate m^{-2} leaf s^{-1}
α_{2LL}	Quantum yield of electron transport through Photosystem II under strictly electron-transport-limiting conditions on the basis of light absorbed by both Photosystem I and Photosystem II	mol e^- mol^{-1} photon
γ_{tissue}	Curvature factor of a certain tissue (either palisade parenchyma or spongy parenchyma)	-
Γ^*	CO_2 compensation point	µbar CO_2
θ	Convexity factor of the response of J to I_{inc}	-
ζ_i	Reduction factor of the diffusion coefficient of CO_2 relative to $D_{CO_2,water}$ in component i due to the higher viscosity of i	
κ_{2LL}	Conversion factor of incident irradiance into electron transport under electron-transport-limited conditions	mol e^- mol^{-1} photon
Φ_2	Quantum yield of electron transport through Photosystem II	mol e^- mol^{-1}photon
ω	Ratio of r_{chl} to r_{diff}	-

underestimate g_m for the low C_i range where CO_2 assimilation is limited by Rubisco activity (Yin *et al.*, 2009).

Nevertheless, the variability of g_m with C_i in the low C_i range can at least partially be explained by the release of photorespired CO_2 (Tholen *et al.*, 2012b; Tholen *et al.*, 2014). Photorespiration starts in the stroma with the production of phosphoglycolate through RuBP oxygenation by Rubisco. Phosphoglycolate is converted to glycolate, which is transferred from the stroma to the peroxisomes. In the peroxisome, glycolate is converted to glycine, which is then transferred to a mitochondrion, where glycine is converted to serine and CO_2. Additionally, mitochondrial respiration also releases CO_2. The CO_2 concentration difference between the cytosol and intercellular air space is, therefore, smaller than one would expect.

Tholen *et al*. (Tholen *et al.*, 2012b) developed a framework to calculate C_c, in which they distinguished the different physical barriers for CO_2 transported from the intercellular air-spaces and CO_2 released from (photo)respiration. They defined r_{diff} as the lumped constant resistance for CO_2 transport due to these barriers in the diffusion pathway of the mesophyll:

$$r_{\mathrm{diff}} = r_{\mathrm{wp}} + r_{\mathrm{chl}} \tag{3.2}$$

where r_{wp} is defined as the lumped resistance of the cell wall and plasma membrane, and r_{chl} is defined as the lumped diffusive resistance of the chloroplast envelope and the stroma. Based on their framework, C_{c} can be expressed as:

$$C_{\mathrm{c}} = C_{\mathrm{i}} - r_{\mathrm{diff}}\left(A_{\mathrm{N}} - \omega(F + R_{\mathrm{d}})\right) \tag{3.3}$$

where $\omega = \frac{r_{\mathrm{chl}}}{r_{\mathrm{diff}}}$, F and R_{d} are rates of photorespired and respired CO_2 release, respectively (see also Cano *et al.* (2014)).

A number of studies (Peguero-Pina *et al.*, 2012; Tosens *et al.*, 2012a; Tosens *et al.*, 2012b; Tomas *et al.*, 2013) have been conducted to investigate the possibility to further partition r_{chl} and r_{wp} and calculate each of these resistances based on leaf anatomical measurements and assumptions related to the diffusivity for CO_2 of each of these components. These authors found that there was a mismatch between the values for r_{m} calculated by the variable J method and the values for r_{diff} at ambient CO_2 levels and saturating light. This mismatch may be explained by the framework of Tholen *et al.* (2012b) that r_{m} is variable with C_{i} and that this variability can be associated with the varying levels in the release of photorespired CO_2.

In summary, C_{c}, and thereby the rate of CO_2 assimilation, is influenced by both leaf anatomical features that act as physical barriers for CO_2 transport and biochemical processes that act as sources and sinks for CO_2 along the CO_2 diffusion pathway in leaves. To the best of our knowledge, there has been no report on predicting the rate of CO_2 assimilation by combining gas exchange, chlorophyll fluorescence, and leaf anatomical measurements. We present a model that combines the model of Tosens *et al.* (2012b) quantifying r_{diff} from leaf anatomical measurements, the model of Tholen *et al.* (2012b) partitioning r_{diff}, and an extended version of the original FvCB model

(Farquhar *et al.*, 1980; Sharkey, 1985; Yin *et al.*, 2009). We will use this combined model to investigate to what extent various leaf anatomical traits affect the net rate of CO_2 assimilation at various light and CO_2 levels. We will also use the model for a sensitivity analysis with regard to mesophyll curvature factors and a number of diffusive properties of subcellular components. The results of this analysis demonstrate that some of these parameters substantially affect the net rate of CO_2 assimilation and that their values should therefore not be taken for granted.

3.2. Materials and methods

3.2.1 Plant material and growth conditions

We carried out an experiment in a UNIFARM glasshouse of Wageningen University, using three cultivars of tomato (*Solanum lycopersicum* L.): Admiro (Syngenta, The Netherlands), Doloress (De Ruiter Seeds, The Netherlands) and Growdena (Syngenta, The Netherlands). All measurements involved four replicates. In order to spread the measurements over time, seeds were sown in small pots in a staggered way, i.e., on February 18, February 27, March 11, and March 21 of 2013, providing plants of the four replicates, respectively. The plants were grown on substrate blocks saturated with UNIFARM standard tomato nutrient solution (0.854% Calsal^{TM}, 0.15% Amnitra^{TM}, 0.36% Sulfakal^{TM}, 0.682% Bascal^{TM}, 0.864% Magnesul^{TM} ; all from Yara Benelux, The Netherlands), 0.43% 6 M nitric acid and 0.118% 6 M phosphoric acid. The nutrient solution was supplied by a hydroponic irrigation system. The photoperiod in the greenhouse was 16 h. During day time, supplemental light from 600 W HPS Hortiflux Schréder lamps (Monster, South Holland, The Netherlands, 0.4 lamps m^{-2}) were switched off as soon as the intensity of the global solar radiation dropped below 400 W m^{-2}. Day and night temperatures were kept at 21^{o}C and 16^{o}C (±3^{o}C), respectively. All measurements were carried out on plants that were at least 42 days old, using distal leaflets of the compound leaves that were 15 days old or 25 days old (typically at the fifth and the ninth nodes from the bottom).

3.2.2 Simultaneous gas exchange and chlorophyll fluorescence measurements

We used the LI-6400XT Portable Photosynthesis System (Li-Cor BioSciences, Lincoln, NE, USA) to simultaneously measure gas exchange and chlorophyll fluorescence. We measured both light and CO_2 response curves. During all measurements, the leaf temperature was kept at 25^{o}C, and the leaf-to-air vapour pressure difference was kept at 1.0-1.6 kPa.

We measured the CO_2 response curves under an incident irradiance (I_{inc}) of 1500 μmol m^{-2} s^{-1} under both 21% and 2% O_2 conditions. The low O_2 condition was created using a gas mixture of 2% O_2 and 98% N_2, and the IRGA calibration was adjusted for the O_2 composition of the gas mixture. The leaflet was consecutively exposed to different levels of CO_2), i.e., 400, 300, 200, 100, 50, 400, 600, 800, 1000, 1200, 1600, and 2000 μmol mol^{-1}. For light response curves, two sets of conditions were used. First, the light response curve was measured when C_{a} was kept constant at 400 μmol mol^{-1} combined with 21% O_2. The light response was also obtained under a non-photorespiratory condition, using 1000 μmol mol^{-1} C_{a} combined with the 2% O_2 gas mixture. During the light response measurements, the leaflet was consecutively exposed to I_{inc} levels of 1500, 1000, 750, 500, 300, 150, 100, 50, and 25 μmol m^{-2} s^{-1}. During all measurements, the plant was allowed to adapt to a new level of CO_2 or light for three minutes, except for the transfer from $C_{\mathrm{a}} = 50\ \mu\mathrm{mol\ mol}^{-1}$ to $C_{\mathrm{a}} = 400\ \mu\mathrm{mol\ mol}^{-1}$. In the latter case, the plant was allowed to adapt for 12 minutes. Preliminary measurements had indicated that such an interval was long enough to obtain steady-state values reliably. Each combination of measured values for A_{N} and C_{i} was corrected for leakage in and out of the cuvette, using thermally killed leaves, as described by Flexas *et al.* (2007).

At each light or CO_2 step during the measurements, the steady-state fluorescence F_{s} was measured. Next, a saturating light pulse (8500 μmol m^{-2} s^{-1}) was applied for less than a second to measure the maximum fluorescence F_{m}'. These parameters were used

to calculate the apparent operating quantum yield of Photosystem II as $\Phi_2 = \frac{F'_m - F_s}{F_m'}$ (Genty *et al.*, 1989).

3.2.3 Sample preparation for light and transmission electron microscopy

After the gas exchange and chlorophyll fluorescence measurements, small leaflet samples (5 x 1 mm^2) were cut parallel to the main vein. The samples were vacuum infiltrated in 3% glutaraldehyde in 0.1 M phosphate buffer (pH =7.2), postfixed in 1% osmium tetroxide in 0.1 M phosphate buffer (pH=7.2), and dehydrated in an ethanol series. They were then infiltrated and embedded with Spurr's resin (Spurr, 1969). The samples were put in an oven for 8 h at 70^{o}C for polymerization.

3.2.4 Light microscopy

Sections of 1 μm thick were cut using an ultramicrotome (Leica EM UC6), and they were stained using methylene blue. The sections were viewed and photographed by a digital inverted microscope (VOS, AMC-3206) at 20x magnification. The microscopic images were digitized using in house MATLAB (The Mathworks Inc, Natick, Massachusetts, USA) software (Mebatsion *et al.*, 2006). The digitized images were subsequently loaded into COMSOL 3.5a (COMSOL AB, Stockholm, Sweden). The ratio of the length of the mesophyll exposed to the intercellular air space L_m to the length of the section L was calculated using measurements from these images. The exposed mesophyll surface area per unit of leaf area $\frac{S_m}{S}$ was calculated for both the palisade parenchyma and the spongy parenchyma as:

$$\left(\frac{S_m}{S}\right)_{tissue} = \gamma_{tissue}\left(\frac{L_m}{L}\right)_{tissue} \tag{3.4}$$

where the subscript tissue indicates either palisade parenchyma or spongy parenchyma tissue, and γ_{tissue} is the curvature factor (Thain, 1983; Evans *et al.*, 1994) of the tissue. We adopted γ_{tissue} values for *S. lycopersicum* leaves determined by

Galmes *et al*. (Galmes *et al.*, 2013): 1.497 and 1.281 for the palisade and the spongy parenchyma, respectively.

3.2.5 Measurements using transmission electron microscopy

Sections of 80 nm thick were cut using an ultramicrotome, stained by lead citrate, and photographed using a transmission electron microscope (TEM Zeiss EM 900). The ratio of the length of chloroplasts exposed to intercellular air space L_{c} to the length of exposed mesophyll L_{m} was measured for both the palisade and the spongy parenchyma. The exposed mesophyll surface area covered by chloroplast per unit of leaf area was calculated as:

$$\frac{S_{\mathrm{c}}}{S} = \left(\frac{L_{\mathrm{c}}}{L_{\mathrm{m}}}\right)_{\mathrm{pal}} \left(\frac{S_{\mathrm{m}}}{S}\right)_{\mathrm{pal}} + \left(\frac{L_{\mathrm{c}}}{L_{\mathrm{m}}}\right)_{\mathrm{spo}} \left(\frac{S_{\mathrm{m}}}{S}\right)_{\mathrm{spo}} \tag{3.5}$$

where the subscripts ‘pal′ and ‘spo’ indicate palisade parenchyma and spongy parenchyma, respectively.

Cell wall thickness t_{wall}, cytosol thickness t_{cyt}, and chloroplast stroma thickness t_{str} were measured from these images (Fig. 3.1). The thickness of the cytosol was measured as the average distance between the cell wall and the chloroplast envelope. For each compartment i, the overall thickness t_{i} was calculated as a weighted average between the thickness of compartment i in the palisade parenchyma and the spongy parenchyma:

$$t_{\mathrm{i}} = f_{\mathrm{pal}} t_{\mathrm{i,pal}} + \left(1 - f_{\mathrm{pal}}\right) t_{\mathrm{i,spo}} \tag{3.6}$$

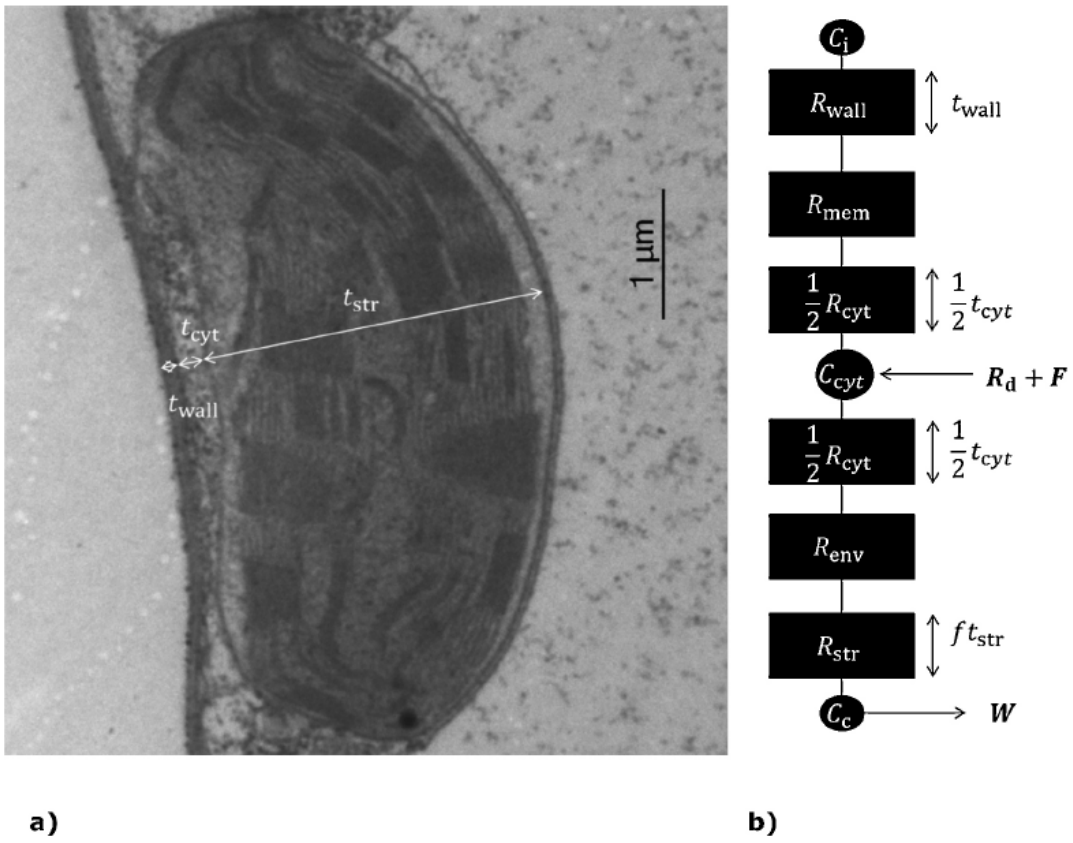

Figure 3.1:

a): Sample TEM image. A single chloroplast in the palisade parenchyma in a 25-day-old *S. lycopersicum* L. cv. Admiro leaf. The double arrows represent the thicknesses of the cell wall t_{wall}, the cytosol t_{cyt} and the chloroplast t_{str}.

b): Schematic representation of the resistance model used in this study. The circles represent CO_2 partial pressures in the intercellular air space (C_i), in the middle of the cytosol (C_{cyt}) and in the stroma near Rubisco (C_c). The boxes represent the resistances of the cell wall (R_{wall}), the plasma membrane (R_{mem}), the two compartments of the cytosol (R_{cyt}), the chloroplast envelope (R_{env}) and the stroma (R_{str}). The double arrows show the assumed thickness of the resistances of the cell wall, the cytosol and the stroma. The single arrows show the CO_2 sink (rate of CO_2 carboxylation W) and the sources (rate of mitochondrial respiration in the light R_d and the rate of photorespiration F).

where f_{pal} is the fraction of exposed mesophyll surface area covered by chloroplast in the palisade parenchyma relative to the total mesophyll surface area covered by chloroplasts.

3.2.6 Model to calculate the sub-resistances in the mesophyll

Sub-resistance components in the mesophyll, R_{wall}, R_{cyt} and R_{str}, were calculated as described by Niinemets and Reichstein (2003) and Tosens *et al.* (Tosens *et al.*, 2012b):

$$R_{\mathrm{i}} = \frac{f_{\mathrm{i}}\, t_{\mathrm{i}}}{p_{\mathrm{eff,i}} \zeta_{\mathrm{i}} D_{\mathrm{CO_2,water}}} \tag{3.7}$$

where R_{i} is the resistance of component i. t_{i} is the thickness of component i. $D_{\mathrm{CO_2,water}}$ is the diffusion coefficient of CO_2 in pure water at standard pressure and temperature ($D_{\mathrm{CO_2,water}} = 1.79 \cdot 10^{-9}$ m^2 s^{-1}, $P = 101325$ Pa, $T = 298.15$ K). $p_{\mathrm{eff,i}}$ is the effective porosity for CO_2. ζ_{i} is a reduction factor of the diffusion coefficient of CO_2 relative to that of water due to a higher viscosity. f_{i} is the fraction of the effective diffusion path length in component i. We assumed that ζ_{i} is 1.0 for the cell wall and 0.5 for the cytosol (i.e., $\zeta_{\mathrm{wall}} = 1$, $\zeta_{\mathrm{cyt}} = 0.5$) following Tholen and Zhu (2011) and Ho *et al.* (2016). It was also assumed that $\zeta_{\mathrm{i}} = 0.5$ for the stroma (Ho *et al.*, 2016), $f_{\mathrm{str}} = 0.25$ (Tholen and Zhu, 2011), $f_{\mathrm{i}} = 1$ for other components, and $p_{\mathrm{eff,i}} = 1$ for the cytosol and the chloroplast stroma. Finally, we assumed that $p_{\mathrm{eff,i}} = 0.2$ for the cell wall (Fanta *et al.*, 2012; Ho *et al.*, 2016). By applying equation (3.7), we adopt the commonly used assumption (Peguero-Pina *et al.*, 2012; Tosens *et al.*, 2012a; Tosens *et al.*, 2012b; Tomas *et al.*, 2013) that the cell wall thickness measured from transmission electron micrographs is not affected by the dehydration and embedding procedures of the sample preparation (von Caemmerer and Furbank, 2003).

While there are only few data available, reported values of the permeability of the plasma membrane G_{mem} and the chloroplast envelope G_{env} varied considerably (Evans *et al.*, 2009). Gutknecht *et al.* (1977) found that the permeability of an artificial lipid bilayer membrane that consists of egg lecithin and cholesterol had a permeability of $3.5 \cdot 10^{-3}$ m s^{-1}. Due to the lack of data, we set G_{mem} equal to this value. Since the chloroplast envelope is a double membrane, we assumed that $G_{\mathrm{env}} = \frac{1}{2} G_{\mathrm{mem}} = 1.75 \cdot 10^{-3}$ m s^{-1}. G_{mem} lumps the permeability of aquaporins and the bulk plasma membrane (Terashima *et al.*, 2006).

During gas exchange measurements, the rate of photosynthesis is commonly expressed in μmol CO_2 m^{-2} leaf s^{-1} and the CO_2 level is in μbar CO_2. Consequently, the unit of diffusive mesophyll resistance is m^2 leaf s bar CO_2 mol^{-1} CO_2, rather than in s m^{-1} for $R_{\text{diff,}}$ resulting from anatomical measurements. We calculated the resistance, expressed in m^2 s bar mol^{-1}, from the resistances expressed in s m^{-1}. For this purpose, we used equation (3.8) to calculate this resistance for the cell wall, plasma membrane and cytosol and equation (3.9) for the chloroplast envelope and the stroma:

$$r_{\text{i}_1} = \left(\frac{S_{\text{m}}}{S}\right)^{-1} \frac{H}{10^5} \frac{f_{\text{i}}\, t_{\text{i}}}{p_{\text{eff,i}} \zeta_{\text{i}} D_{\text{CO}_2,\text{water}}} \tag{3.8}$$

$$r_{\text{i}_2} = \left(\frac{S_{\text{c}}}{S}\right)^{-1} \frac{H}{10^5} \frac{f_{\text{i}}\, t_{\text{i}}}{p_{\text{eff,i}} \zeta_{\text{i}} D_{\text{CO}_2,\text{water}}} \tag{3.9}$$

where H is Henry's law constant for CO_2 ($H = 2941$ Pa m^3 mol^{-1} at $T = 298.15$ K and standard pressure. 10^5 is a conversion factor to convert Pascals to bars. Its unit is Pa bar^{-1}. In equation (3.8), the subscript 1 refers to the first set of resistance components (i.e., the cell wall, the plasma membrane and the cytosol). The subscript 2 in equation (3.9) refers to the second set of resistance components (i.e., chloroplast envelope, stroma). We describe the derivation of equations (3.8) and (3.9) in Appendix 3.1. Equation (3.9) implies that we assume that only chloroplasts that are exposed to the intercellular air space affect the net rate of CO_2 assimilation. It is also important to emphasize that we scaled resistances of the cell wall, the plasma membrane and the cytosol with the exposed mesophyll surface area (equation (3.8)) and the resistance of the chloroplast envelope and stroma with the exposed chloroplast surface area. This modification of the original resistance model presented by Tosens *et al*. (Tosens *et al.*, 2012b) was necessary to correct for the fact that the mesophyll surface area available for CO_2 uptake is larger than the chloroplast surface area (Tomas *et al.*, 2013).

3.2.7 Model to calculate ω

The diffusive resistance of the mesophyll r_{diff} (expressed in $\text{m}^2\ \text{s bar mol}^{-1}$) can be considered as a series of sub-resistances. These sub-resistances are resistances of the cell wall, plasma membrane, cytosol, chloroplast envelope, and chloroplast stroma (Evans *et al.*, 2009):

$$r_{\text{diff}} = r_{\text{wall}} + r_{\text{mem}} + r_{\text{cyt}} + r_{\text{env}} + r_{\text{str}} \tag{3.10}$$

where r_{wall}, r_{mem}, r_{cyt}, r_{env} and r_{str} are the resistances of the cell wall, plasma membrane, cytosol, chloroplast envelope and chloroplast stroma (Tholen *et al.*, 2014). Since we assume that the source for (photo)respired CO_2 release is located halfway in the diffusion pathway in the cytosol (Fig. 3.1), we can calculate ω as:

$$\omega = \frac{r_{\text{env}} + r_{\text{str}} + \frac{1}{2} r_{\text{cyt}}}{r_{\text{diff}}} \tag{3.11}$$

Note that the diffusive resistance r_{diff} is not the same as the previously defined mesophyll resistance r_{m} (Tholen *et al.*, 2014). The first one is the sum of the resistances to CO_2 diffusion of all cellular components; the latter one, as defined by equation (3.1), lumps the effect of r_{diff} and biochemical processes on the overall resistance to CO_2 transport from the intercellular air space to Rubisco [10].

3.2.8 The FvCB model to calculate the rate of photosynthesis

The generic form of the FvCB model is:

$$A_{\mathrm{N}} = \left(1 - \frac{\Gamma^*}{C_{\mathrm{c}}}\right)\left(\frac{C_{\mathrm{c}} X_1}{C_{\mathrm{c}} + X_2}\right) - R_{\mathrm{d}} \tag{3.12}$$

where R_{d} is day respiration (i.e., the CO_2 release other than by photorespiration), and Γ^* is CO_2 compensation point in the absence of R_{d}. In equation (3.12), $X_1 = V_{\mathrm{cmax}}$ and $X_2 = K_{\mathrm{mC}}\left(1 + \frac{O}{K_{\mathrm{mO}}}\right)$ if the rate of carboxylation is limited by Rubisco, where V_{cmax} is the maximum rate of carboxylation by Rubisco, K_{mC} and K_{mO} are the Michaelis-Menten kinetic constants of Rubisco for RuBP carboxylation and oxygenation, respectively. If the rate of carboxylation is limited by the rate of electron transport J and this rate is limited by NADPH production rather than ATP production, $X_1 = \frac{1}{4}J$ and $X_2 = 2\Gamma^*$. J can be calculated as:

$$J = \frac{\kappa_{2\mathrm{LL}} I_{\mathrm{inc}} + J_{\mathrm{max}} - \sqrt{(\kappa_{2\mathrm{LL}} I_{\mathrm{inc}} + J_{\mathrm{max}})^2 - 4\theta J_{\mathrm{max}} \kappa_{2\mathrm{LL}} I_{\mathrm{inc}}}}{2\theta} \tag{3.13}$$

where I_{inc} is the incident irradiance; $\kappa_{2\mathrm{LL}}$ is the efficiency of converting incident irradiance to electron transport under limiting light; J_{max} is the maximum rate of electron transport; and θ is a convexity factor. If the rate of CO_2 assimilation is limited by the rate of triose phosphate utilization T_{p} (Sharkey, 1985), $X_1 = 3T_{\mathrm{p}}$ and $X_2 = -\Gamma^*$.

3.2.9 Parameters of the FvCB model

The CO_2 compensation point Γ^* can be calculated as $\Gamma^* = \frac{0.5O}{S_{\mathrm{C/O}}}$, where $S_{\mathrm{C/O}}$ is the relative CO_2/O_2 specificity factor of Rubisco. We adopted the values $S_{\mathrm{C/O}} = 3.26\ \mathrm{mbar\ \mu bar^{-1}}$, $K_{\mathrm{mC}} = 267\ \mu\mathrm{bar}$ and $K_{\mathrm{mO}} = 164\ \mathrm{mbar}$ (Ho *et al.*, 2016). The cultivars used in this study were the same as in our study. The parameter R_{d} was calculated by linear regression as the intercept of the line $A_{\mathrm{N}} = s(I_{\mathrm{inc}}\Phi_2/4) - R_{\mathrm{d}}$ as described by Yin *et al.* (2009), using data of the electron-transport-limited range of the $A - I_{\mathrm{inc}}$ ($I_{\mathrm{inc}} \leq 200\ \mu\mathrm{mol\ m^{-2}\ s^{-1}}$) curve under non-photorespiratory conditions. The

slope *s* of this linear regression was used as a calibration factor to calculate values of electron transport rate: $J = sI_{\mathrm{inc}}\Phi_2$ (Yin *et al.*, 2009). We estimated the efficiency of photosystem II under light limiting conditions ($\Phi_{2\mathrm{LL}}$) according to the method described by Yin *et al.* (2009). We calculated $\kappa_{2\mathrm{LL}}$ as $\kappa_{2\mathrm{LL}} = s\Phi_{2\mathrm{LL}}$. We then used the calculated values for $\kappa_{2\mathrm{LL}}$ as an input to estimate $J_{\max}$ and θ for each leaf type by fitting the calculated J ($J = sI_{\mathrm{inc}}\Phi_2$) to equation (3.13).

3.2.10 Coupling of the FvCB model with the gas diffusion model

Combining the FvCB model, equation (3.12), with the CO_2 diffusion model, equation (3.3), results in:

$$A_{\mathrm{N}} = \frac{-\mathcal{B} - \sqrt{\mathcal{B}^2 - 4\mathcal{A}\mathcal{C}}}{2\mathcal{A}} \tag{3.14}$$

with

$$\mathcal{A} = X_2 + \Gamma^*(1-\omega) \tag{3.15}$$

$$\mathcal{B} = -\Big\{[X_2 + \Gamma^*(1-\omega)](X_1 - R_{\mathrm{d}}) - \omega(R_{\mathrm{d}}X_2 + \Gamma^*X_1) + (C_{\mathrm{i}} + X_2)\left[\frac{1}{r_{\mathrm{diff}}}(X_2 + \Gamma^*)\right]\Big\} \tag{3.16}$$

$$\mathcal{C} = -\omega(R_{\mathrm{d}}X_2 + \Gamma^*X_1)(X_1 - R_{\mathrm{d}}) + \frac{1}{r_{\mathrm{diff}}}(X_2 + \Gamma^*)[X_1(C_{\mathrm{i}} - \Gamma^*) - R_{\mathrm{d}}(C_{\mathrm{i}} + X_2)] \tag{3.17}$$

Equations (3.14-3.17) were applied to calculate the net rate of CO_2 assimilation limited by Rubisco ($A_{\mathrm{N,c}}$) or by electron transport ($A_{\mathrm{N,j}}$). We calculated the net rate of CO_2 assimilation limited by triose phosphate utilization ($A_{\mathrm{N,p}}$) as $A_{\mathrm{N,p}} = 3T_{\mathrm{p}} - R_{\mathrm{d}}$. The actual net rate of CO_2 assimilation was the minimum of these three potential rates.

This model was used to estimate V_{cmax} and T_{p}, using already estimated or measured parameter values as input.

3.2.11 Relationship between C_{i} and I_{inc}

In order to interpolate the rate of photosynthesis for light levels that were not measured, it is necessary to know C_{i}. An empirical relationship between C_{i} and I_{inc} was found by fitting data for C_{i} and I_{inc} to a power law:

$$C_{\mathrm{i}} = C_{\mathrm{i0}} {I_{\mathrm{inc}}}^{q} \tag{3.18}$$

Next, we simulated two additional light response curves for 25-day-old Admiro leaves for both ambient and low oxygen levels. In each of these curves, C_{i} is fixed to the average of all C_{i} measurements in the light response curve measurements rather than that calculated by equation (3.18).

3.2.12 Sensitivity analysis

We simulated light and CO_2 response curves for 15-day-old Admiro leaves at ambient O_2 levels using different assumed parameter values (γ_{pal}, γ_{spo}, $p_{\mathrm{eff,wall}}$, G_{mem}, ζ_{cyt}, G_{env}, f_{str} and ζ_{str}) and measured leaf anatomical properties (t_{wall}, t_{cyt}, t_{str}, $\frac{L_{\mathrm{m}}}{L}$, $\frac{L_{\mathrm{c}}}{L_{\mathrm{m}}}$). Each time, one of these properties was changed by -25%, and +25%, respectively, while keeping the remaining variables at their default value.

3.3. Results

3.3.1 Leaf anatomical measurements

Table 3.2 shows the ratio of the measured length of mesophyll exposed to the intercellular air space to the total width of the section $\frac{L_{\mathrm{m}}}{L}$. The values of $\frac{L_{\mathrm{m}}}{L}$ varied between 4.87 and 6.01 in the palisade parenchyma and between 6.28 and 7.06 in the

spongy parenchyma. The ratio of the length of chloroplasts exposed to the intercellular air space to the length of exposed mesophyll $\frac{L_c}{L_m}$ was also measured.

We calculated values for $\frac{S_c}{S}$ for the palisade parenchyma, the spongy parenchyma and the whole mesophyll (Table 3.2). The values for $\frac{S_c}{S}$ in the mesophyll ranged from 14.3 to 16.4.

The thicknesses of the mesophyll components were measured for each cultivar, leaf age, and tissue type. Table 3.3 shows the weighted average thicknesses of the mesophyll components (see equation (3.6)). The average cell wall thickness ranged from 0.089 µm to 0.208 µm. The weighted average thickness of the cytosol ranged from 0.172 µm to 0.492 µm and of the stroma from 2.035 µm to 2.708 µm.

3.3.2 Determination of R_i, r_{diff}, and ω

The thicknesses of the cell wall, cytosol and stroma and the assumed values of p_{eff}, f_i and ζ_i were used to calculate the resistance for each component in the mesophyll (R_i; see equation (3.7)). Since we assumed that the permeability of the membranes $G_{mem} = G_{env} = 3.5 \cdot 10^{-3}$ m s^{-1} was the same for all leaf types, their resistances were the same as well. Table 3 shows the values of these partitioned resistances. We used equation (3.8) and (3.9) to convert the unit for the resistance of each component. from s m^{-1} to m^2 s bar mol^{-1}. Table A3.2.2 shows the values of these partitioned resistances. We applied equation (3.10) and (3.11) to calculate r_{diff} and ω. Table 3.4 shows the calculated values of these variables. The values for ω varied between 0.62 and 0.67 (Table 4). For all cultivars, ω was higher for 15-day-old leaves than for 25-day-old leaves. The values for r_{diff} varied between 3.85 and 5.09 m^2 s bar mol^{-1}. For all cultivars r_{diff} was higher for 15-day-old leaves than for 25-day-old leaves.

3.3.3 Parameters relationship between I_{inc} and C_i

Table A3.2.3 displays the estimates for C_{i0} and q that describe the relationship between I_{inc} and C_i. At $O = 210$ mbar and $C_a = 400$ µbar, C_{i0} varies between 617

Table 3.2. Measurements of the ratio of $\frac{S_c}{S}$ for each cultivar (Admiro, Doloress, Growdena), leaf age (15 days and 25 days after appearance) and tissue type (palisade parenchyma and spongy parenchyma and total mesophyll).

Cultivar	Leaf age (days)	Tissue type	$\frac{S_{\mathrm{m}}}{S}$	$\frac{L_c}{L_{\mathrm{m}}}$	$\frac{S_{\mathrm{c}}}{S}$
Admiro	15	pal[1]	8.99	0.96	8.66
		spo[2]	8.04	0.87	7.00
		mes[3]	17.04		15.66
	25	pal	8.29	0.98	8.09
		spo	8.31	0.84	6.96
		mes	16.61		15.05
Doloress	15	pal	8.29	0.94	7.87
		spo	8.94	0.95	8.51
		mes	17.23		16.38
	25	pal	8.37	0.96	8.00
		spo	9.04	0.90	8.13
		mes	17.41		16.13
Growdena	15	pal	8.70	0.94	8.14
		spo	8.91	0.87	7.81
		mes	17.64		15.96
	25	pal	7.29	0.90	6.55
		spo	8.97	0.87	7.78
		mes	16.26		14.34

[1] pal: palisade parenchyma
[2] spo: spongy parenchyma
[3] mes: whole mesophyll

and 862 µbar and q varies between -0.126 and -0.218. At $O = 20$ mbar and $C_{\mathrm{a}} = 1000$ µbar, C_{i0} varies between 1224 µbar and 1949 µbar and q varies between -0.070 and -0.204. Fig. A3.2.2 shows the simulated and the measured relationship between I_{inc} and C_i.

3.3.4 Estimation of photosynthetic parameters

The estimated values for R_{d} varied from 1.35 µmol $\mathrm{m}^{-2}\,\mathrm{s}^{-1}$ to 2.65 µmol $\mathrm{m}^{-2}\,\mathrm{s}^{-1}$, and the values for s varied from 0.413 to 0.529 (Table A3.2.4). For all cultivars and leaf ages, Φ_{2LL} was larger at $O = 210$ mbar than at $O = 20$ mbar (Table A.3.2.5). The estimated values for J_{max} ranged from 157.1 to 263.7 µmol $\mathrm{m}^{-2}\,\mathrm{s}^{-1}$ at $O = 210$ mbar and $C_{\mathrm{a}} = 400$ µbar, and from 149.8 to 179.8 µmol $\mathrm{m}^{-2}\,\mathrm{s}^{-1}$ at $O = 20$ mbar and $C_{\mathrm{a}} = 1000$ µbar (Table A3.2.5). The values for J_{max} were higher in 15-

Table 3.3. Average thicknesses (± the standard errors of the mean) of the cell wall, cytosol and stroma for all studied cultivars (Admiro, Doloress, Growdena), leaf ages (15 days and 25 days after emergence) and tissue types (palisade and spongy parenchyma and total mesophyll).

			Component thickness (µm)		
Cultivar	Leaf age (days)	Tissue type	Cell wall	Cytosol	Stroma
Admiro	15	pal[1]	0.120 ± 0.006[5]	0.256 ± 0.036	2.691 ± 0.211
		spo[2]	0.117 ± 0.010	0.229 ± 0.019	2.366 ± 0.186
		mes[3,4]	0.119	0.243	2.55
	25	pal	0.168 ± 0.020	0.257 ± 0.035	2.273 ± 0.153
		spo	0.170 ± 0.022	0.235 ± 0.021	2.613 ± 0.771
		mes	0.169	0.246	2.43
Doloress	15	pal	0.104 ± 0.008	0.172 ± 0.023	2.691 ± 0.394
		spo	0.151 ± 0.026	0.263 ± 0.042	2.577 ± 0.571
		mes	0.128	0.212	2.63
	25	pal	0.146 ± 0.008	0.184 ± 0.027	2.552 ± 0.633
		spo	0.145 ± 0.015	0.269 ± 0.044	2.213 ± 0.340
		mes	0.145	0.231	2.38
Growdena	15	pal	0.089 ± 0.005	0.194 ± 0.041	2.218 ± 0.266
		spo	0.125 ± 0.009	0.304 ± 0.098	2.035 ± 0.158
		mes	0.107	0.250	2.13
	25	pal	0.177 ± 0.022	0.404 ± 0.098	2.708 ± 0.691
		spo	0.208 ± 0.023	0.492 ± 0.093	2.550 ± 0.356
		mes	0.193	0.453	2.62

[1] pal: palisade parenchyma
[2] spo: spongy parenchyma
[3] mes: total mesophyll
[4] The values represent the weighted average thicknesses of these compartments in the palisade and the spongy parenchyma.
[5] standard error of the mean

day-old leaves than in 25-day-old leaves only under $O = 20$ mbar. The values for θ ranged from 0.760 to 0.851 (Table A3.2.5). Finally, Table A3.2.5 shows the calculated values of $\kappa_{2\mathrm{LL}}$ (as $\kappa_{2\mathrm{LL}} = s\Phi_{2\mathrm{LL}}$). The estimates for V_{cmax} and T_{p} are shown in Table A3,2,6. The estimates for V_{cmax} vary between 219 µmol m^{-2} s^{-1} and 274 µmol m^{-2} s^{-1}. The standard errors of the estimates of V_{cmax} are relatively high.

This may either reflect that the number of data points in the Rubisco-limited range was limited, or that anatomical data on r_{diff} and ω may not match the curvature of the initial part of $A - C_{\mathrm{i}}$ curves from gas exchange measurements, or both. The estimates for T_{p} vary between 12.6 µmol m^{-2} s^{-1} and 13.6 µmol m^{-2} s^{-1}. There was no triose-phosphate-limitation for 25-day-old Doloress leaves.

Table 3.4. Values for ω and r_{diff} calculated for each cultivar (Admiro, Doloress, Growdena) and leaf age (15 days and 25 days after leaf appearance)

Cultivar	Leaf age (days)	ω	r_{diff} ($\mathrm{m^2\ s\ bar\ mol^{-1}}$)
Admiro	15	0.67	3.94
	25	0.63	4.27
Doloress	15	0.66	3.85
	25	0.64	3.86
Growdena	15	0.66	3.59
	25	0.62	5.09

3.3.5 Comparison of measured and simulated CO_2 and light response curves

Fig. 3.2 displays both the measured and modelled CO_2 response curve for each leaf type and oxygen level. Fig. 3.3 shows both the measured and simulated light response curves for each leaf type and condition (either $O = 210\ \mathrm{mbar}$ and $C_{\mathrm{a}} = 400\ \mu\mathrm{bar}$ or $O = 20\ \mathrm{mbar}$ and $C_{\mathrm{a}} = 1000\ \mu\mathrm{bar}$). In general, the model reasonably fitted to the data, although the model underestimates the net rate of CO_2 assimilation at high CO_2 and light levels for 25-day-old Doloress leaves except for the light response curves measured at ambient O_2 and CO_2 levels. The underestimation of the net CO_2 assimilation rate may be caused by the estimate of s (Table A3.2.4). The estimate of s for 25-day-old Doloress leaves ($s = 0.413$) and, thereby, the calculated value of $\kappa_{2\mathrm{LL}}$ ($\kappa_{2\mathrm{LL}} = s\Phi_{2LL}$) are considerably lower than in the other five leaf types (between 0.462 and 0.529). This may have resulted in an underestimation of J_{max}, which may explain the mediocre fit of the model with the data at high CO_2 and light levels. This suggests that the s estimate for this leaf type from the lower part of the $A - I_{\mathrm{inc}}$ curve under the non-photorespiratory condition does not represent the situation across the high light and CO_2 ranges. The model also predicted that the rate of CO_2 assimilation somewhat decreased with increased irradiances. This contradicts the measurements that did not show this trend.

3.3.6 Sensitivity analysis of CO_2 response curves

The left panels of Figs. 3.4-3.7 display simulated $A - C_{\mathrm{i}}$ curves for each leaf type at ambient oxygen and $I_{\mathrm{inc}} = 1500\ \mu\mathrm{mol\ m^{-2}\ s^{-1}}$ In each simulated curve, one of the

model parameters was either increased or decreased by 25%, while the remaining parameter values were kept at their default values. Not surprisingly, in the parts of the simulated curves limited by triose-phosphate-utilization, the rate of CO_2 assimilation was the same for any parameter value. In the remaining parts of the simulated curves, the response of A_N to 25% changes in any parameter value shows the following pattern. Initially, at low CO_2 levels the difference between the predicted rate of CO_2 assimilation with an adjusted parameter value and the rate of CO_2 assimilation with the default parameter value increased with C_i. At higher CO_2 levels, this difference decreased with C_i. The predicted rate of CO_2 assimilation increased with $\frac{L_m}{L}$, $\frac{L_c}{L_m}$ p_{eff}, G_{mem}, ζ_{cyt}, G_{env}, ζ_{str}, γ_{pal} and γ_{spo} in the non-triose-phosphate-utilization-limited parts of the simulated curves. In contrast, the predicted rate of CO_2 assimilation decreased with t_{wall}, t_{cyt}, t_{str} and f_{str}. We did not show the simulated $A - C_i$ curves for 25% changes of t_{wall}, t_{cyt}, p_{eff}, and G_{mem}because 25% change in these parameters only resulted in a small response of the net rate of CO_2 assimilation, which can hardly be made visible in these figures. We did not increase $\frac{L_c}{L_m}$ by 25%, because the value of this parameter cannot be larger than 1. Table 3.5 shows for the sensitivity analysis of each parameter what the maximum difference in the predicted A_N between changed parameter values and default parameter values was. CO_2 assimilation was most sensitive to 25% changes in the values of $\frac{L_m}{L}$ and $\frac{L_c}{L_m}$.

3.3.7 Sensitivity analysis of light response curves

The right panels of Figs. 3.4-3.6 display simulated $A - I_{inc}$ curves for each leaf type at ambient CO_2 and O_2 levels, when one of the model parameters was either increased or decreased by 25% while the remaining parameter values were kept at their default values. The response of CO_2 assimilation to 25% changes in any of the parameter values showed the following pattern. The difference between A_N predicted using an

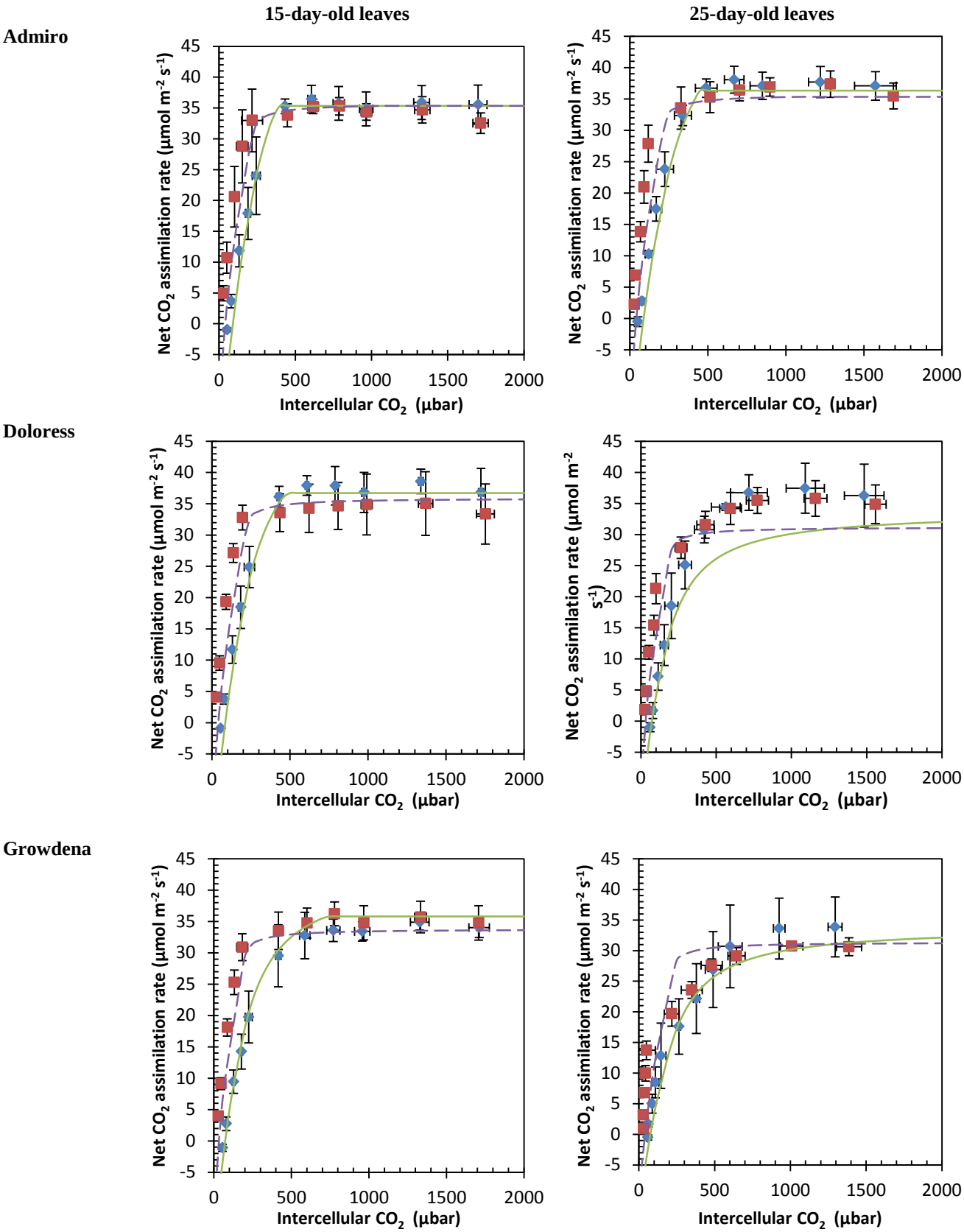

Figure 3.2: Measured and simulated CO_2 response curves at saturating light (I_{inc} = 1500 µmol m^{-2} s^{-1}). Measured rates of net CO_2 assimilation at O = 210 mbar (diamonds±one standard error) and at O = 20 mbar and (squares±one standard error) for three cultivars (Admiro, Doloress, Growdena) and two leaf ages (15 days and 25 days after emergence). Simulated rates of net CO_2 assimilation at O = 210 mbar (solid lines) and at O = 20 mbar (squares).

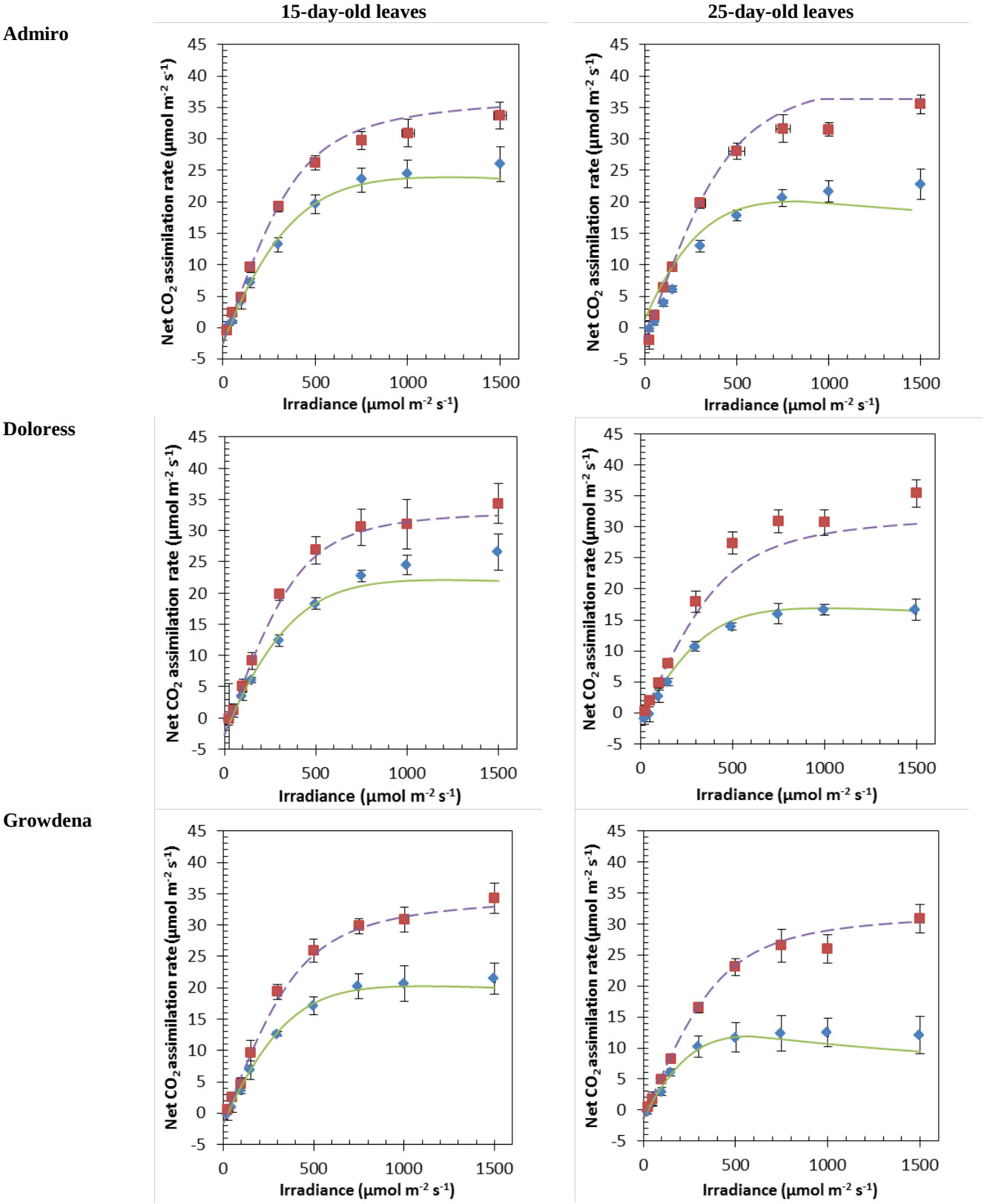

Figure 3.3: Measured and simulated light response curves. Measured rates of net CO_2 assimilation at $O = 210$ mbar and $C_a = 400$ µbar (diamonds±one standard error) and at $O = 20$ mbar and $C_a = 1000$ µbar (squares±one standard error) for three cultivars (Admiro, Doloress, Growdena) and two leaf ages (15 days and 25 days after emergence). Simulated rates of net CO_2 assimilation at $O = 210$ mbar and $C_a = 400$ µbar (solid lines) and at $O = 20$ mbar and $C_a = 1000$ µbar (squares)

Table 3.5. Maximum difference in A_N and the corresponding C_i in simulated $A - C_i$ curves, if a parameter ϱ is 25% increased or decreased.

Parameter	$\max(\Delta A_n)$ $\varrho = (1 - 0.25)\varrho_{default}$ [1]		$\max(\Delta A_n)$ $\varrho = (1 + 0.25)\varrho_{default}$	
	C_i	ΔA_N	C_i	ΔA_N
$\frac{L_m}{L}$ [2]	245	-4.97	218	3.47
$\frac{L_c}{L_m}$ [3]	245	-3.63	- [4]	- [4]
t_{wall}	241	0.335	245	-0.457
t_{cyt}	241	0.481	245	-0.474
t_{str}	234	1.65	245	-1.59
p_{eff}	245	-0.605	241	0.370
G_{mem}	245	-0.524	241	0.319
ζ_{cyt}	245	-0.629	241	0.383
G_{env}	245	-1.70	238	1.06
ζ_{str}	245	-2.09	234	1.32
f_{str}	234	-1.64	245	-1.59
γ_{pal}	245	-2.46	226	2.02
γ_{spo}	245	-2.17	230	1.81

[1] ϱ denotes the parameter which was varied. $\varrho_{default}$ denotes the default value of this parameter.

[2] Both $\left(\frac{L_m}{L}\right)_{pal}$ and $\left(\frac{L_m}{L}\right)_{spo}$ were respectively decreased or increased by 25%.

[3] Both $\left(\frac{L_c}{L_m}\right)_{pal}$ and $\left(\frac{L_c}{L_m}\right)_{spo}$ were respectively decreased or increased by 25%.

[4] Since $\left(\frac{L_c}{L_m}\right)_{pal}$ and $\left(\frac{L_c}{L_m}\right)_{spo}$ cannot be larger than 1, we did not increase this parameter by 25%.

adjusted parameter value and A_N using the default value increased with I_{inc}. Table 6 shows the maximum difference between the simulated value of A_N for default parameters values and for parameter values for which one is 25% increased or decreased. CO_2 assimilation was most sensitive to 25% changes in the values of $\frac{L_m}{L}$ and $\frac{L_c}{L_m}$. We did not show the simulated $A - I_{inc}$ curves for 25% changes of t_{wall}, t_{cyt}, ζ_{cyt}, p_{eff}, and G_{mem}, because 25% change in these parameters only resulted in a small response of the net rate of CO_2 assimilation, which can hardly be made visible in these figures. We found that setting $\frac{L_c}{L_m}$ to 1 (Fig. 3.4) for both the palisade and the spongy parenchyma results in an increase in the net rate of CO_2 assimilation of 0.87 μmol m^{-2} s^{-1} at 1500 μmol m^{-2} s^{-1}.

Table 3.6. Maximum difference in A_N and the corresponding C_i in simulated $A - I_{inc}$ curves (in all cases $I_{inc} = 1500$ µmol m^{-2} s^{-1}), if a parameter ϱ is 25% increased or decreased.

Parameter	$\max(\Delta A_n)$ $\varrho = (1 - 0.25)\varrho_{default}$ [1]	$\max(\Delta A_n)$ $\varrho = (1 + 0.25)\varrho_{default}$ [1]
	ΔA_N	ΔA_N
$\frac{L_m}{L}$ [2]	-4.91	2.94
$\frac{L_c}{L_m}$ [3]	-3.59	- [4]
t_{wall}	0.466	-0.449
t_{cyt}	0.479	-0.470
t_{str}	1.44	-1.57
p_{eff}	-0.595	0.371
G_{mem}	-0.515	0.319
ζ_{cyt}	-0.621	0.384
G_{env}	-1.68	0.960
ζ_{str}	-2.07	1.17
f_{str}	1.44	-1.57
γ_{pal}	-2.43	1.76
γ_{spo}	-2.14	1.59

[1] ϱ denotes the parameter which was varied. $\varrho_{default}$ denotes the default value of this parameter.

[2] Both $\left(\frac{L_m}{L}\right)_{pal}$ and $\left(\frac{L_m}{L}\right)_{spo}$ were respectively decreased or increased by 25%.

[3] Both $\left(\frac{L_c}{L_m}\right)_{pal}$ and $\left(\frac{L_c}{L_m}\right)_{spo}$ were respectively decreased or increased by 25%.

[4] Since $\left(\frac{L_c}{L_m}\right)_{pal}$ and $\left(\frac{L_c}{L_m}\right)_{spo}$ cannot be larger than 1, we did not increase this parameter by 25%.

3.4 Discussion

In this study, we combined the leaf anatomical model described by Tosens *et al*. (2012b) and the biochemical models for C_3 photosynthesis described by Farquhar *et al*. (1980) and Yin *et al*. (2009) and the CO_2 diffusion model of Tholen *et al*. (2012). We used this combined model to directly calculate the rate of CO_2 assimilation based on a combination of leaf anatomical and photosynthetic parameters. The model generally agreed well with the data, although the net rate of CO_2 assimilation tended to slightly decrease as the light intensity increased at high light levels. We used the model to simulate how the net rate of CO_2 assimilation responds to changes in thickness of mesophyll subcellular components,

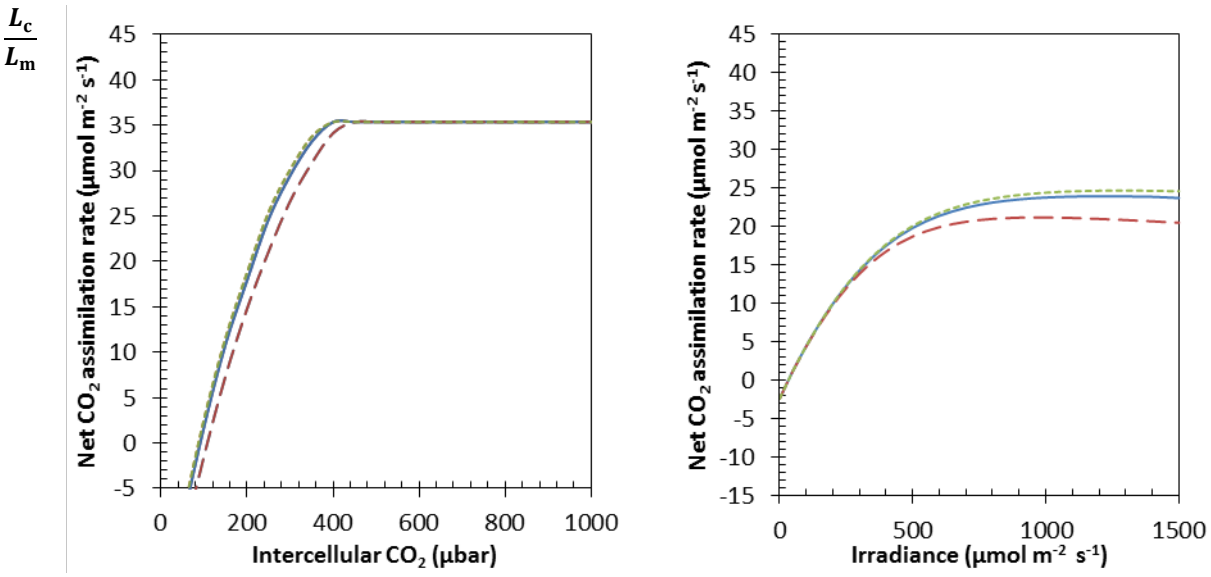

Figure 3.4: Sensitivity analysis $A - C_i$ curve and $A - I_{inc}$ curve for $\frac{L_c}{L_m}$. Parameter $\frac{L_c}{L_m}$ of the model is either decreased by 25% (dashed line) or set to 1 (short dashed line). The continuous line represents the simulated $A - C_i$ curve for default parameter values.

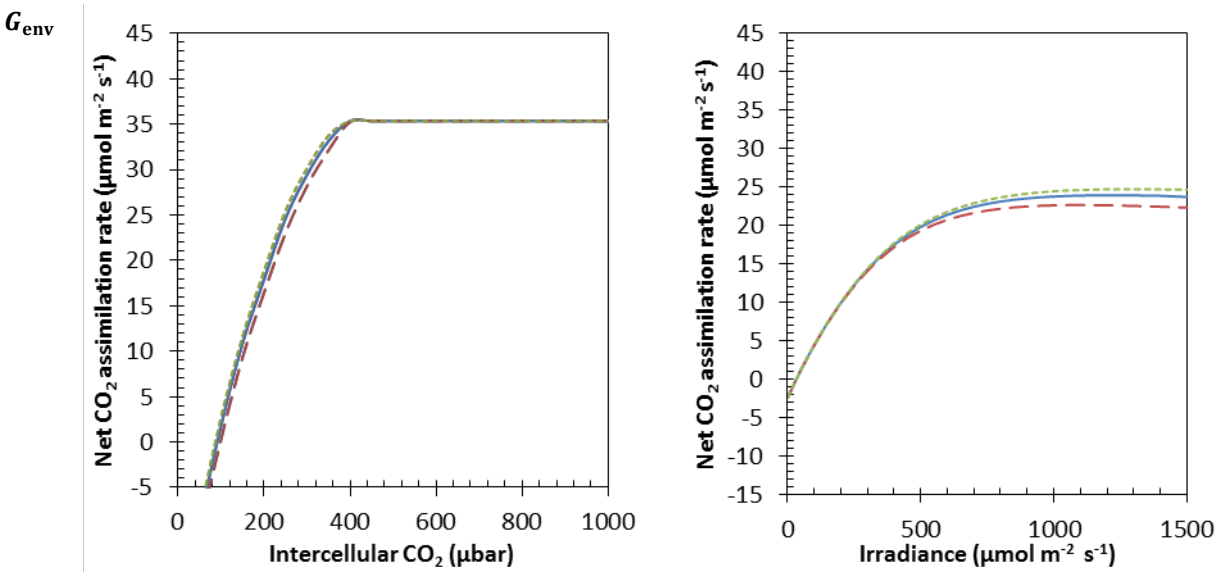

Figure 3.5: Sensitivity analysis $A - C_i$ curve and $A - I_{inc}$ curve for G_{env}. Parameter $\frac{L_c}{L_m}$ of the model is either decreased by 25% (dashed line) or increased by 25% (short dashed line). The continuous line represents the simulated $A - C_i$ curve for default parameter values.

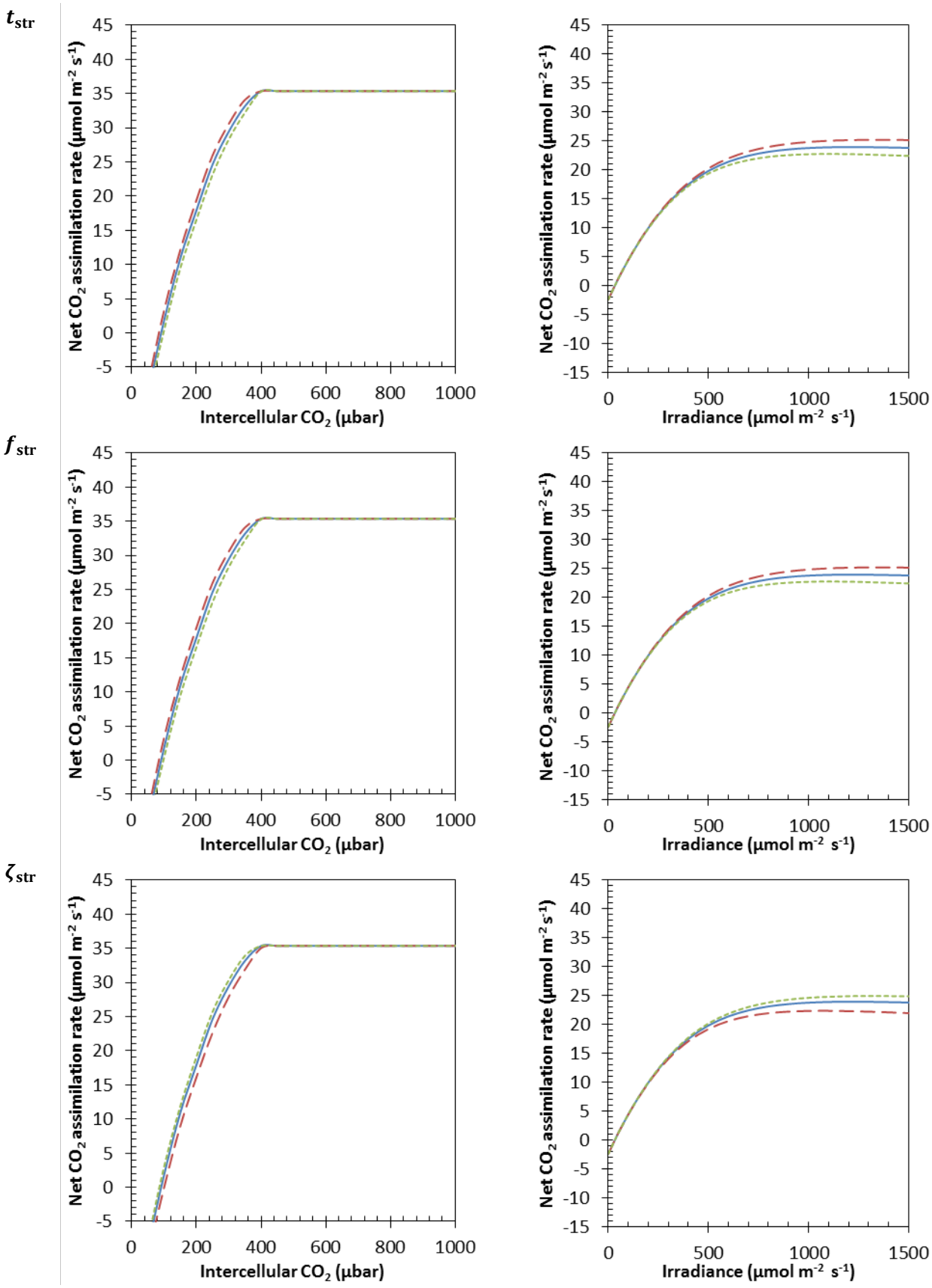

Figure 3.6: Sensitivity analysis $A - C_i$ curves and $A - I_{inc}$ curves for t_{str}, f_{str} and ζ_{str}. Model parameters are either decreased by 25% (long dashed line) or increased by 25 (short dashed line). The continuous line represents the simulated $A - C_i$ curve for default parameter values.

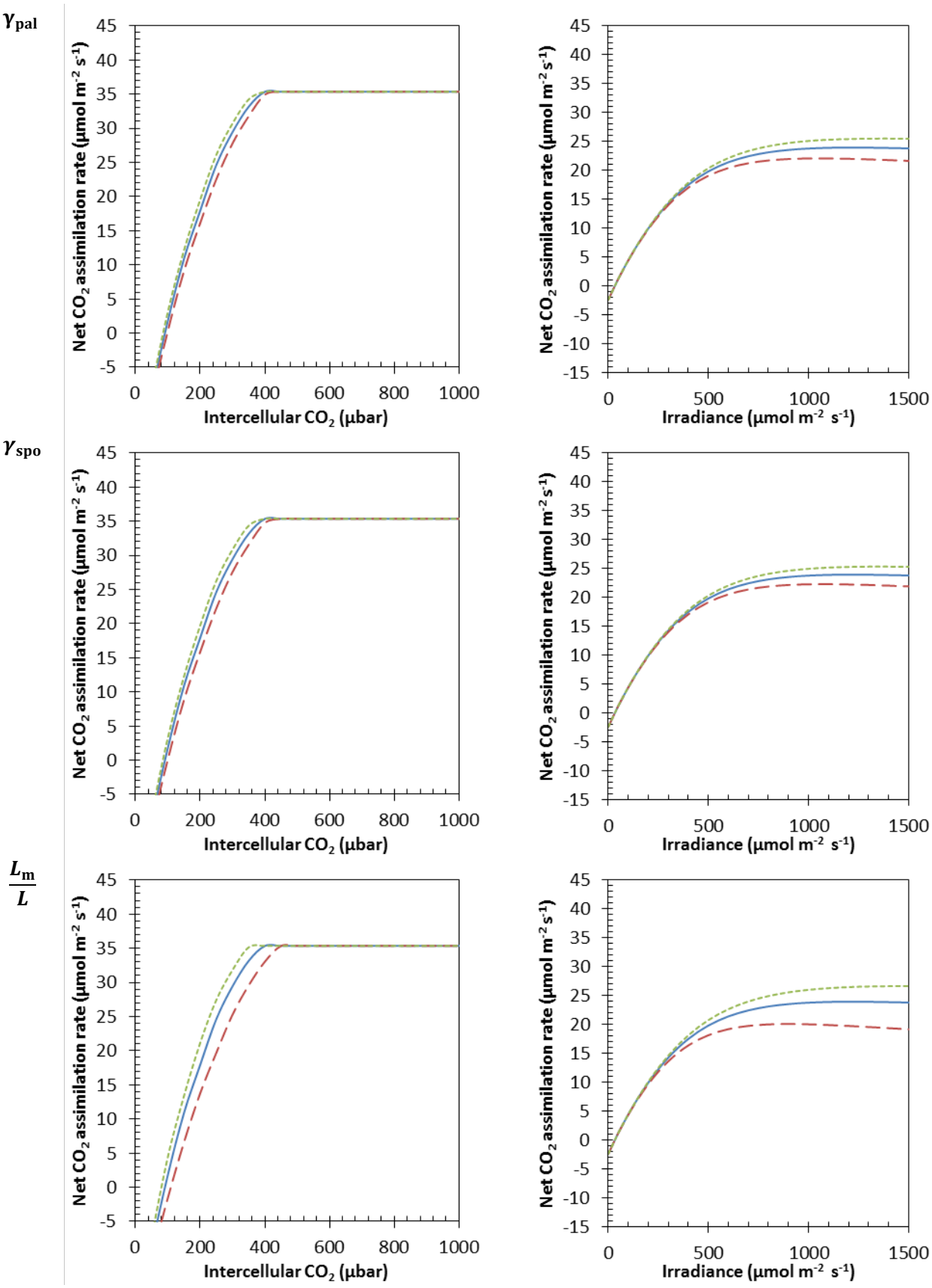

Figure 3.7: Sensitivity analysis $A - C_i$ curves and $A - I_{inc}$ curve for γ_{pal},γ_{spo} and $\frac{L_m}{L}$. Model parameters are either decreased by 25% (long dashed line) or increased by 25 (short dashed line). The continuous line represents the simulated $A - C_i$ curve for default parameter values.

exposed mesophyll and chloroplast surface areas, palisade and spongy mesophyll curvature factors, and a range of assumed diffusive properties. Although there were large differences between the extent of the response of the rate of CO_2 assimilation to each parameter, we found two overall trends. At low C_i levels, the increase or decrease of the rate of CO_2 assimilation in response to changing a parameter value initially increased with C_i. For higher CO_2 levels, it later decreased with C_i. Second, this increase or decrease increased with I_{inc}. These two findings have important consequences. Tholen *et al.* (2012a) reviewed the progress of genetic engineering of specific leaf anatomical traits to improve the efficiency of CO_2 transport in leaves. The results of our sensitivity analysis indicate that the potential gain of photosynthetic capacity by changing leaf anatomical traits may strongly depend on the CO_2 and light levels in the environments of such an enhanced plant.

Since this is the first study that uses a resistance model to directly calculate the net CO_2 assimilation rate based on leaf anatomical measurements, we found it was necessary to compare our results with the overall mesophyll conductances calculated in earlier studies. Therefore, we first used our current model to calculate C_c by combining equations (3.3) and (3.12). Second, we calculated the overall mesophyll conductance as $g_m = \frac{A_N}{(C_i - C_c)}$ at $I_{inc} = 1500$ µmol m^{-2} s^{-1} and ambient O_2 and CO_2. The results are shown in Table S6. According to our analysis, g_m varies between 0.085 mol m^{-2} s^{-1} bar^{-1} and 0.223 mol m^{-2} s^{-1} bar^{-1}. There is quite some variation in g_m for tomato. Galmes *et* al. (2013) calculated the overall mesophyll conductance (g_m) by the variable J method (Harley *et al.*, 1992a) in a range of Mediterranean accessions grown under well-watered conditions. They reported that g_m varies between 0.170 mol m^{-2} s^{-1} bar^{-1} and 0.289 mol m^{-2} s^{-1} bar^{-1} under saturating light and ambient CO_2. We also used the variable J method to calculate g_m from another data-set consisting of combined gas exchange and chlorophyll fluorescence measurements on the same cultivars as the ones used in this study (Ho *et al.*, 2016). We found that g_m varied between 0.0718 mol m^{-2} s^{-1} bar^{-1} and 0.246 mol m^{-2} s^{-1} bar^{-1}. The values for g_m,

calculated by the model presented in the current study, are within the range of the values determined from these earlier studies.

The results of the sensitivity analysis model indicate that $\frac{S_m}{S}$ and $\frac{S_c}{S_m}$ are the most important anatomical properties in determining photosynthetic capacity. The most important assumed diffusive properties are G_{mem}, ζ_{str} and f_{str}. The results of our sensitivity analysis showed that changing t_{wall} had less influence on the net CO_2 assimilation rate. This may contradict with the results from Tosens *et al*. (Tosens *et al.*, 2012b), which suggest that the cell wall determines more than half of r_{diff}. This may be explained by the fact that the range of t_{wall} for the species used in their study was considerably higher (from 252 nm to 420 nm) than in our study (119 nm to 193 nm). It may also be explained by the value of p_{eff} that we chose, which is higher than that assumed in their study. It is important to emphasize that assumptions on the diffusive properties of the different components of the liquid phase of the mesophyll may affect the calculated value for r_{diff}. These properties are hard to measure and uncertain (Evans *et al.*, 2009). Evans *et al*. (2009) argued that the value of $p_{eff,wall}$ varies between 0.02 and 0.2. In our model, we assumed that $p_{eff,wall} = 0.2$ and $\zeta_{str} = 0.5$. The latter value is considerably higher than the ones applied in a number of other studies (Niinemets and Reichstein, 2003; Peguero-Pina *et al.*, 2012; Tosens *et al.*, 2012b; Tomas *et al.*, 2013). These authors all assumed that the reduction factor of the diffusion coefficient for CO_2 in the stroma relative to water is equal to the ratio of the effective water self-diffusion coefficients in duck embryo and in water [24]. However, the application of their assumed values of ζ_{str} resulted in considerable underestimations of the rate of CO_2 assimilation at high light or low CO_2 levels (Fig. A3.2.1a-b) in 15-day-old Admiro leaves at both $p_{eff,wall}$=0.02 and $p_{eff,wall} = 0.2$. When we changed ζ_{str} from 0.294 to 0.5, while keeping $p_{eff,wall}$ at 0.02, the underestimation of the rate of CO_2 assimilation became considerably less. We conclude that the rate of CO_2 assimilation is sensitive to the diffusion coefficient of the stroma for the whole range of biologically relevant values of p_{eff} (Evans *et al.*, 2009). This makes the assumed diffusive properties that make up this diffusion coefficient; f_{str} and ζ_{str}, important parameters. In the resistance model described by

Tosens *et al*. (Tosens *et al.*, 2012b), it is assumed that the diffusion path length of CO_2 molecules in the chloroplasts is half the total thickness of the chloroplasts ($f_{\mathrm{str}} = 0.5$). In contrast, results from CO_2 diffusion simulations in a virtual 3D cell (Tholen and Zhu, 2011) suggest that $f_{\mathrm{str}} = 0.25$ at saturating light and a CO_2 intercellular partial pressure of 30 Pa. In our model, we adopted the latter value as the default value for f_{str}. Figs. A3.2.1c-d in Appendix 3.2 show $A - C_{\mathrm{i}}$ curves and $A - I_{\mathrm{inc}}$ curves for different combinations of values for $p_{\mathrm{eff,wall}}$ and ζ_{str} if we would have assumed that $f_{\mathrm{str}} = 0.5$, as suggested by Tosens *et al*. (Tosens *et al.*, 2012b). These curves show that the net rate of CO_2 assimilation at 21% O_2 is underestimated, even if we assume high values for ζ_{str} and p_{eff}. This analysis shows that f_{str} and, therefore, the length of the diffusion pathway, is an important parameter to determine the net rate of CO_2 assimilation. Additionally, the diffusion pathway length of CO_2 in the stroma may depend on the CO_2 sink, i.e. RuBP carboxylation, which depends on C_{c} and I_{inc}. This suggests that f_{str} may vary with environmental conditions. We recommend more research on both the diffusion coefficient for CO_2 and the length of the diffusion pathway in the stroma. The uncertainty of the CO_2 diffusion pathway length can be tackled by the use of 2D (Ho *et al.*, 2012) or 3D models (Parkhurst, 1977; Aalto and Juurola, 2002; Tholen and Zhu, 2011; Ho *et al.*, 2016) to simulate CO_2 transport in mesophyll cells, since these models do not require a predefined value for f_{str}.

Other assumed diffusive properties may also be important. Uehlein *et al*. (Uehlein *et al.*, 2008) attempted to measure the permeability of the plasma membranes and the chloroplast envelopes for CO_2 in *Nicotiana tabacum* L. from isolated vesicles from these membranes, and found that these permeability values were $8 \cdot 10^{-5}$ m s^{-1} and $2 \cdot 10^{-5}$ m s^{-1}, respectively. However, these methods have a number of shortcomings which may result in large underestimation of the permeability values of membranes (Tholen and Zhu, 2011). Gutknecht *et al*. (1977) estimated that the permeability of lipid bilayers was $3.5 \cdot 10^{-3}$ m s^{-1} based on $^{14}CO_2$ flux measurements through artificial lipid bilayer membranes that consisted of egg lecithin and cholesterol. Due to a lack of data, we adopted this value for G_{mem} and assumed that $G_{\mathrm{env}} = \frac{1}{2} G_{\mathrm{mem}}$,

because the chloroplast envelope is a double membrane. We also assumed that both G_{mem} and G_{env} are parallel resistances that lump the permeabilities of aquaporines and the remaining parts of the membranes (Terashima *et al.*, 2006).

Our model requires the calculation of $\frac{S_{\mathrm{m}}}{S}$. Evans *et al* (Evans *et al.*, 1994) described how $\frac{S_{\mathrm{m}}}{S}$ can be calculated, after the determination of curvature factors (Thain, 1983) from a combination of paradermal and transversal leaf sections. In our measurements, no paradermal sections were collected. We adopted the curvature factors γ_{pal} and γ_{spo} for the palisade and the spongy parenchyma of tomato from a previous study (Galmes *et al.*, 2013). We showed in our sensitivity analysis that the simulated rate of photosynthesis was sensitive to changes of γ_{pal} and γ_{spo}. Tomas *et al*. (Tomas *et al.*, 2013) measured both curvature factors for 15 different species with a wide range of foliage characteristics. They found that γ_{pal} varied from 1.4 to 1.5 and γ_{spo} from 1.16 to 1.4. Combined with the results of our sensitivity analysis, this suggests that it is important to measure this parameter for unknown species, if one wants to relate $\frac{S_{\mathrm{m}}}{S}$ to the photosynthetic capacity of these leaves. The need for a method to calculate curvature factors to calculate $\frac{S_{\mathrm{m}}}{S}$ can be circumvented by measuring exposed mesophyll surfaces directly from 3D leaf images. One way to obtain these images is to use synchrotron radiation X-ray tomography. Verboven *et al*. (2015) used this technique to measure $\frac{S_{\mathrm{m}}}{S}$ directly and also validated the method of Thain (1983) by determining the curvature factors from 2D sections of the tomography. An advantage of this method over the method of Thain (1983) is that it does not require a fixed orientation of all samples and that it requires fewer samples. This technique or other 3-D imaging techniques may be used in future research to determine $\frac{S_{\mathrm{m}}}{S}$ as an alternative to the method of Thain (1983).

Both in the framework of Tholen *et al.* (2012b) and in our model, it is assumed that all CO_2 produced by normal respiration and photorespiration is released by mitochondria in the cytosol between the plasma membrane and the chloroplast envelope. It is not clear where the mitochondria are located in the cytosol (either between chloroplast

envelope and plasma membrane, between chloroplast envelope and tonoplast, or both), but their location may strongly affect the reassimilation of (photo)respired CO_2. Tholen *et* al. (2014) pointed out that if the mitochondria are located between the tonoplast and the chloroplast envelope, the effect of (photo)respiration on mesophyll resistance may be small or even insignificant. We observed that the model predicts a slightly decreasing rate of CO_2 assimilation with increasing I_{inc} at high light levels and ambient oxygen and CO_2 levels in 25-day-old leaves (Fig. 3.3). In contrast, we did not see this behaviour at non-photorespiratory conditions ($C_{\mathrm{a}} = 1000$ µbar, $O = 20$ mbar). Our assumptions about the location of mitochondria may partly explain this behaviour. If the predicted rate of photorespiration is high, there is a considerable release of CO_2 in the cytosol. This CO_2 release will decrease the concentration difference between the cytosol and the intercellular air space and, thereby, will decrease the predicted CO_2 flux over the plasma membrane and the cell wall. An alternative explanation is that we described the relationship between I_{inc} and C_{i} by equation (3.18) (Fig. A3.2.2). This empirical relationship predicts that C_{i} can decrease with I_{inc}, a commonly observed trend that is possibly a consequence of regulation set by stomatal resistance. This decrease in C_{i} means an increase in the rate of photorespiration under these high light conditions. If we set ω equal to 0, we implicitly assume that (photo)respired CO_2 release and CO_2 consumption by photosynthesis take place in the same compartment (i.e. the stroma). In this specific case, there is no longer a CO_2 source halfway the diffusion path in the cytosol, so any decrease of net CO_2 assimilation can fully be explained by equation (3.18). Fig. A3.2.3 shows a simulated light response curve for 25-day-old Growdena leaves for $\omega = 0$. The decrease of the net CO_2 assimilation rate with I_{inc} (Fig. A3.2.3) is strongly reduced compared to assuming the default value for ω. This suggests that the empirical relationship between C_{i} and I_{inc} used in this model can only partly explain the simulated decrease of the CO_2 assimilation rate with I_{inc}. We therefore suspect that at least part of the mitochondria may be located between the chloroplast envelope and the tonoplast. In future studies, the effect of different locations of mitochondria may be better studied in 2D (Ho *et al.*, 2012) or 3D modelling approaches (Parkhurst, 1977; Aalto and Juurola,

2002; Tholen and Zhu, 2011; Ho *et al.*, 2016). These models are much more flexible in terms of changing the modelled leaf structure than resistance models (Parkhurst, 1994) like the one used in this study.

It has been frequently debated whether or not carbonic anhydrases (CA) facilitate CO_2 transport in the mesophyll (Evans *et al.*, 2009; Terashima *et al.*, 2011; Flexas *et al.*, 2012). Results from studies on *Nicotiana tabacum* mutants, in which CA activity was knocked out by antisense RNA, suggest that the rate of CO_2 assimilation is not affected at ambient CO_2 at both saturating light (Price *et al.*, 1994) and lower light (150 – 400 μmol m^{-2} s^{-1}) conditions (Williams *et al.*, 1996) compared with wild type individuals. On the other hand, Gillon and Yakir (2000) suggest that CA activity in the chloroplasts has an influence on the CO_2 assimilation rate in species with high $\frac{r_{\mathrm{wp}}}{r_{\mathrm{chl}}}$ ratios like *Quercus robur* (oak) where they found that $\frac{r_{\mathrm{wp}}}{r_{\mathrm{chl}}} = 3.2$. Our anatomical data and assumed diffusive properties show for different cultivars and ages after emergence that $\frac{r_{\mathrm{wp}}}{r_{\mathrm{chl}}}$ is between 0.48 and 0.62. These values are all even smaller than the ratio $\frac{r_{\mathrm{wp}}}{r_{\mathrm{chl}}} = 0.8$ found in *N. tabacum*, in which no significant reduction of the net rate of CO_2 assimilation was found in several studies (Price *et al.*, 1994; Williams *et al.*, 1996; Gillon and Yakir, 2000). We therefore surmise that CA facilitation only has a limited effect on the net rate of CO_2 assimilation in the leaves used in this study and, therefore, we did not model CA facilitation explicitly. Evans *et al.* (Evans *et al.*, 2009) argued that CA facilitation mainly takes place in the cytosol and the stroma. Therefore, if CA facilitation does occur, its effect on CO_2 transport is lumped in the parameters ζ_{cyt} and ζ_{str} of our model.

To the best of our knowledge, this study presents the first attempt to quantify the rate of CO_2 assimilation by combining a resistance model based on leaf anatomical measurements and diffusive properties, and simultaneous gas exchange and chlorophyll fluorescence measurements. This approach can potentially contribute a lot to understand the relationship between leaf anatomy and leaf photosynthesis, but it relies on a number of unknown diffusive properties and curvature factors. We

demonstrated that the diffusion path length for CO_2 and its diffusion coefficient in the stroma, and the curvature factors of palisade and spongy parenchyma substantially affect the predicted net CO_2 assimilation rate. We therefore recommend more research to measure these parameters and to develop sophisticated 2-D or 3-D models that do not require the diffusion path length of the stroma as an input factor.

Acknowledgements

We thank Tiny Franssen-Verheijen (Wageningen University, Laboratory of Virology) and Norbert de Ruiter (Wageningen University, Laboratory of Cell Biology) for advice and technical support during sample preparation, An Vandoren (KU Leuven, Laboratory of Socioecology and Social Evolution) for cutting the sections of the light and electron microscopy samples, Johan Billen (KU Leuven, Laboratory of Socioecology and Social Evolution) for granting access to a transmission electron microscope and for support in making TEM images, Metadel Abera (KU Leuven, Flanders Centre for Post Harvest / MeBios) for his assistance to digitize the leaf images, and all employees of UNIFARM (Wageningen University) for assisting in cultivating the plants used in this study. Wageningen based authors thank the BioSolar Cells programme (project C3B3) for financial support. Leuven based authors thank the Research Council of the KU Leuven (project OT 12/055) for financial support.

Appendix 3.1: Calculation of resistances of mesophyll components

A3.1.1 Introduction

Equations (3.8-3.9) describe how the resistance of a subcomponent of the mesophyll can be calculated, expressed in $\mathrm{m^2\ s\ bar\ mol^{-1}}$. The aim of this section is to derive these equations. It is based on the explanation about fluxes provided by Nobel (2009) and the anatomical resistance model described by Tosens *et al.* (2012) and Evans *et al.* (2009).

A3.1.2 Fundamentals of Fick's first law of diffusion

Fick's first law of diffusion (Fick, 1855) states that particles move from higher concentrations to lower concentrations. In other words, the direction of the flux of these particles is in the opposite direction of the direction of the gradient of these particles. Mathematically, this can be expressed as:

$$\varphi = -D\nabla c \tag{A3.1.1}$$

where c is the concentration (mol m^{-3}), φ is the flux (mol m^{-2} s^{-1}) and ∇ is the gradient operator (m^{-1}). Parameter D (m^2 s^{-1}) is the diffusion coefficient. In 1D space, equation (A3.1.1) can be expressed as:

$$\varphi = -D\frac{\mathrm{d}c}{\mathrm{d}x} \tag{A3.1.2}$$

Equation (A3.1.2) can be discretized and rearranged as:

$$\varphi = -D\frac{\mathrm{d}c}{\mathrm{d}x} \cong -D\frac{c(x+\Delta x)-c(x)}{\Delta x} = \frac{D}{\Delta x}(c(x)-c(x+\Delta x)) \tag{A3.1.3}$$

where equation (A3.1.3) describes the flux between a point x and a point $x+\Delta x$ in 1D space. In equation (A3.1.3), the concentration difference is multiplied by a factor $\frac{D}{\Delta x}$. This factor is called the permeability or the conductance for diffusion G_{diff} (m s^{-1}). The inverse of G_{diff} is the resistance for diffusion R_{diff}.

A3.1.3 Fick's first law applied to sub-resistances in the mesophyll

Equation (A3.1.3) can be applied to calculate the flux of CO_2 through a component i of the mesophyll:

$$\varphi = \frac{D_{\mathrm{CO_2,i}}}{\Delta x}\left([\mathrm{CO_2}](x)-[\mathrm{CO_2}](x+\Delta x)\right) \tag{A3.1.4}$$

$[\mathrm{CO_2}]$ is the CO_2 concentration, x is the end location of the component i facing the outer side of the cell and $x+\Delta x$ the other end of component i facing the inner side of the cell. The conductance and the resistance of component i can be calculated as:

$$G_{\mathrm{diff,i}} = \frac{D_{\mathrm{CO_2,i}}}{\Delta x}, \qquad R_{\mathrm{diff,i}} = \frac{1}{G_{\mathrm{i}}} = \frac{\Delta x}{D_{\mathrm{CO_2,i}}} \tag{A3.1.5}$$

If the solvent for CO_2 in component i is water, the diffusion coefficient of CO_2 in this component can be expressed as:

$$D_{\mathrm{CO_2,i}} = p_{\mathrm{eff},i}\zeta_{\mathrm{i}} D_{\mathrm{CO_2,water}} \quad \text{(A3.1.6)}$$

where $p_{\mathrm{eff,i}}$ is the effective porosity of component i and ζ_{i} is a reduction factor of the diffusion coefficient due to the higher viscosity of component i relative to pure water. Substitution of the term for $D_{\mathrm{CO_2,i}}$ in equation (A3.1.6) into equation (A3.1.5) results in the following term for the resistance of component i:

$$R_{\mathrm{i}} = \frac{\Delta x}{p_{\mathrm{eff},i}\zeta_{\mathrm{i}} D_{\mathrm{CO_2,water}}} \quad \text{(A3.1.7)}$$

The term Δx in equation (A3.1.7) is the diffusion path length for CO_2 in component i. If there is no source or sink for CO_2 in component i, Δx is the same as the measured thickness of the component t_{i}. However, if there is a sink for CO_2 on the diffusion pathway, for example CO_2 assimilation, it can no longer be assumed that $t_{\mathrm{i}} = \Delta x$. Instead, Δx is a fraction f of the total thickness t_{i}. Substitution of $\Delta x = f t_{\mathrm{i}}$ in equation (A3.1.7) results in equation (A3.1.8):

$$R_{\mathrm{i}} = \frac{f \mathrm{t}_i}{p_{\mathrm{eff},i}\zeta_{\mathrm{i}} D_{\mathrm{CO_2,water}}} \quad \text{(A3.1.8)}$$

In the context of CO_2 assimilation, densities of CO_2 are usually expressed in partial pressures (Pa or µbar) rather than CO_2 concentrations (mol CO_2 m^{-3}). The ideal gas law can be stated for CO_2 as:

$$p_{\mathrm{CO_2,gas}} = [\mathrm{CO_2}]_{\mathrm{gas}} RT \quad \text{(A3.1.9)}$$

where p is the partial pressure of a gas CO_2 (Pa), $[CO_2]_{gas}$ is the concentration of CO_2 in the gas phase (mol m^{-3}), R is the universal gas constant (8.314 Pa m^3 K^{-1} mol^{-1}), and T is the temperature (K). Since CO_2 is dissolved in the liquid phase, we have to apply Henry's law as well to calculate the CO_2 concentration in the liquid phase. Henry's law states that at steady state, the ratio between free and dissolved molecules of a gas at a constant temperature at an interface between a gas phase and a liquid phase is a constant. This law can be applied on CO_2, expressed as:

$$[CO_2]_{liq} = \frac{RT}{H}[CO_2]_{gas} \quad \text{(A3.1.10)}$$

where $[CO_2]_{liq}$ is the concentration of CO_2 in the liquid phase and H is Henry's law constant (Pa m^3 mol^{-1}). Rearrangement of equation (A3.1.10) and substitution in equation (A3.1.9) and results in:

$$p_{CO_2,gas} = H[CO_2]_{liq} \quad \text{(A3.1.11)}$$

Equation (A3.1.11) can be rearranged as:

$$[CO_2]_{liq} = \frac{p_{CO_2,gas}}{H} \quad \text{(A3.1.12)}$$

Substitution of equation (A3.1.12) for c in equation (A3.1.2) gives:

$$\varphi = -\frac{D_{\mathrm{CO_2}}}{H}\frac{\mathrm{d}p_{\mathrm{CO_2i,gas}}}{\mathrm{d}x} \tag{A3.1.13}$$

Discretization of equation (A3.1.13) for x and some rearrangement gives:

$$\varphi = -\frac{D_{\mathrm{CO_2}}}{H}\frac{\mathrm{d}p_{\mathrm{CO_2,gas}}}{\mathrm{d}x} \cong \frac{D_{\mathrm{CO_2,liq}}}{H\Delta x}\left(p_{\mathrm{CO_2i,gas}}(x) - p_{\mathrm{CO_2i,gas}}(x+\Delta x)\right) \tag{A3.1.14}$$

In the manuscript, the CO_2 partial pressures C are expressed in μbar. Since 1 bar is equal to 10^5 Pa ($C = 10^5 p_{\mathrm{CO_2}}$), equation (A3.1.14) satisfies:

$$\varphi \cong 10^5 \frac{D_{\mathrm{CO_2,liq}}}{H\Delta x}\left(C(x) - C(x+\Delta x)\right) \tag{A3.1.15}$$

where the unit of 10^5 is Pa bar^{-1}. Equation (A3.1.15) describes the CO_2 flux of over either the mesophyll surface (flux through the cell wall, the plasma membrane or the cytosol) $\varphi_1{}'$ or the chloroplast surface exposed to the intercellular air space (through the chloroplast envelope or the stroma) $\varphi_2{}'$:

$$\varphi_1' \cong 10^5 \left(\frac{S_{\mathrm{m}}}{S}\right)\frac{D_{\mathrm{CO_2,liq}}}{H\Delta x}\left(C(x) - C(x+\Delta x)\right) \tag{A3.1.16}$$

$$\varphi_2{}' \cong 10^5 \left(\frac{S_{\mathrm{c}}}{S}\right)\frac{D_{\mathrm{CO_2,liq}}}{H\Delta x}\left(C(x) - C(x+\Delta x)\right) \tag{A3.1.17}$$

However, net flux of CO_2 is commonly described as the amount of CO_2 per second per unit of leaf area. In order to express the fluxes through the mesophyll components

in these units as well, $\varphi_1{}'$ and $\varphi_2{}'$ have to be rescaled again by $\frac{S_\mathrm{m}}{S}$ and $\frac{S_\mathrm{c}}{S}$ respectively. This yields the amount of CO_2 per second per unit of leaf area φ_1 and φ_2 through the mesophyll components:

$$\varphi_1 \cong 10^5 \left(\frac{S_\mathrm{m}}{S}\right) \frac{D_{\mathrm{CO_2,liq}}}{H\Delta x}\big(C(x) - C(x+\Delta x)\big) \tag{A3.1.18}$$

$$\varphi_2 \cong 10^5 \left(\frac{S_\mathrm{c}}{S}\right) \frac{D_{\mathrm{CO_2,liq}}}{H\Delta x}\big(C(x) - C(x+\Delta x)\big) \tag{A3.1.19}$$

The terms $10^5 \left(\frac{S_\mathrm{m}}{S}\right) \frac{D_{\mathrm{CO_2,water}}}{H\Delta x}$ and $10^5 \left(\frac{S_\mathrm{c}}{S}\right) \frac{D_{\mathrm{CO_2,water}}}{H\Delta x}$ in A3.1.18 and A3.1.19 can be considered as conductances, the inverse of these terms can be considered to be resistances analogous to R_i as defined in equation (A3.1.8).

$$r_{\mathrm{i}_1} = \left(\frac{S_\mathrm{m}}{S}\right)^{-1} \frac{H}{10^5} R_{\mathrm{i}_1} \tag{A3.1.20}$$

$$r_{\mathrm{i}_2} = \left(\frac{S_\mathrm{c}}{S}\right)^{-1} \frac{H}{10^5} R_{\mathrm{i}_2} \tag{A3.1.21}$$

Combining equations (A3.1.20) and (A3.1.1) with equations (A3.1.6), (A3.1.7) and (A3.1.8) gives:

$$r_{\mathrm{i}_1} = \left(\frac{S_\mathrm{m}}{S}\right)^{-1} \frac{H}{10^5} \frac{f_{\mathrm{i}_{1_1}}\, t_{i_{1_1}}}{p_{\mathrm{eff},i_1} \zeta_{\mathrm{i}_1} D_{\mathrm{CO_2,water}}} \tag{A3.1.22}$$

$$r_{\mathrm{i}_2} = \left(\frac{S_\mathrm{c}}{S}\right)^{-1} \frac{H}{10^5} \frac{f_{\mathrm{i}_2}\, t_{i_2}}{p_{\mathrm{eff},i_2} \zeta_{\mathrm{i}_2} D_{\mathrm{CO_2,water}}} \tag{A3.1.23}$$

which correspond to equations (3.8-3.9) in the main text.

Appendix 3.2: supplementary tables and figures

Table A3.2.1: Calculated resistances for each subcomponent of the mesophyll for each cultivar and leaf age

		Resistance (s m^{-1})				
Cultivar	Leaf age (days)	Cell wall	Plasma membrane	Cytosol	Chloroplast envelope	Stroma
Admiro	15	331	286	272	571	711
	25	472	286	275	571	679
Doloress	15	359	286	237	571	735
	25	406	286	258	571	665
Growdena	15	300	286	279	571	594
	25	542	286	506	571	732

Table A3.2.2: Calculated resistances for each subcomponent of the mesophyll for each cultivar and leaf age

		Resistance (m^2 s bar mol^{-1})				
Cultivar	Leaf age (days)	Cell wall	Plasma membrane	Cytosol	Chloroplast envelope	Stroma
Admiro	15	0.571	0.493	0.469	1.07	1.34
	25	0.836	0.506	0.487	1.12	1.33
Doloress	15	0.612	0.488	0.404	1.03	1.32
	25	0.686	0.483	0.435	1.04	1.21
Growdena	15	0.500	0.476	0.465	1.05	1.10
	25	0.981	0.517	0.914	1.17	1.50

Table A3.2.3: Estimated parameter values for C_{i0} and q describing the empirical relationship between I_{inc} and C_i in $A - I_{inc}$ curves for each cultivar (Admiro, Doloress, Growdena), leaf age (15 and 25 days after emergence) and conditions (either $C_a = 400$ µbar and $O = 210$ mbar or $C_a = 1000$ µbar and $O = 20$ mbar)

Cultivar	Leaf age	Conditions		C_{i0}	q	r^2
		C_a	O			
	(days)	(µbar)	(mbar)	(µbar CO_2)		
Admiro	15	400	210	617.1	-0.128	0.940
		1000	20	1225.9	-0.074	0.859
	25	400	210	683.9	-0.152	0.910
		1000	20	1260.3	-0.077	0.869
Doloress	15	400	210	615.03	-0.126	0.946
		1000	20	1224.1	-0.070	0.775
	25	400	210	862.5	-0.205	0.909
		1000	20	1639.4	-0.150	0.782
Growdena	15	400	210	653.7	-0.142	0.936
		1000	20	1429.5	-0.113	0.518
	25	400	210	844.1	-0.218	0.947
		1000	20	1949.4	-0.204	0.902

Table A3.2.4: Estimates of R_d and s for each cultivar (Admiro, Doloress, Growdena) and each leaf age (days after emergence)

Cultivar	Leaf age	R_d	s
	(days)	(µmol m^{-2} s^{-1})	
Admiro	15	2.46	0.529
	25	1.98	0.520
Doloress	15	2.65	0.514
	25	1.48	0.413
Growdena	15	1.57	0.462
	25	1.35	0.480

Table A3.2.5: Estimates of Φ_{2LL}, J_{max}, θ and their standard errors (SE), the calculated value for κ_{2LL} for each cultivar, leaf age, and conditions

Cultivar	Leaf age	Conditions		Φ_{2LL}		J_{max} ($\mu mol\ e^-\ m^{-2}\ s^{-1}$)		θ		κ_{2LL}
		C_a	O	Estimate	SE	Estimate	SE	Estimate	SE	
	(days)	(µbar)	(mbar)							
Admiro	15	400	210	0.721	0.0078	263.7	9.73	0.760	0.0411	0.381
		1000	20	0.662	0.0105	162.7	5.59	0.838	0.0416	0.350
	25	400	210	0.709	0.00484	242.6	6.53	0.789	0.0291	0.370
		1000	20	0.664	0.0075	179.3	5.00	0.837	0.0302	0.345
Doloress	15	400	210	0.696	0.0089	223.3	11.05	0.797	0.0545	0.357
		1000	20	0.669	0.0116	164.0	7.31	0.851	0.0511	0.343
	25	400	210	0.691	0.0040	157.1	0.838	0.834	0.0148	0.285
		1000	20	0.666	0.0141	140.8	5.02	0.833	0.0410	0.275
Growdena	15	400	210	0.710	0.0061	191.3	6.20	0.835	0.0340	0.328
		1000	20	0.684	0.0076	151.9	2.83	0.826	0.0228	0.316
	25	400	210	0.673	0.0178	149.8	11.50	0.851	0.0899	0.323
		1000	20	0.614	0.0094	141.9	5.29	0.819	0.0463	0.295

Table A3.2.6: Estimates of the parameters V_{cmax} and T_{p} and their standard errors (SE) for each cultivar (Admiro, Doloress, Growdena) and leaf age (15 days and 25 days after emergence)

Cultivar	Leaf age (days)	V_{cmax} (µmol $\mathrm{m^{-2}\ s^{-1}}$)		T_{p} (µmol $\mathrm{m^{-2}\ s^{-1}}$)	
		Estimate	SE	Estimate	SE
Admiro	15	256	29	12.6	0.10
	25	257	131	12.8	0.44
Doloress	15	274	80	13.6	0.31
	25	219	67	None	None
Growdena	15	236	53	12.3	0.17
	25	259	45	12.5	0.20

Table A3.2.7: Apparent mesophyll conductance (g_{m}) calculated by the model at ambient CO_2 levels ($C_{\mathrm{a}} = 400$ µbar) and saturating irradiance (I_{inc})

Cultivar	Leaf age (Days after emergence)	g_{m} (mol $\mathrm{m^{-2}\ s^{-1}\ bar^{-1}}$)
Admiro	15	0.170
	25	0.137
Doloress	15	0.173
	25	0.207
Growdena	15	0.223
	25	0.085

$f_{str} = 0.25$

a)

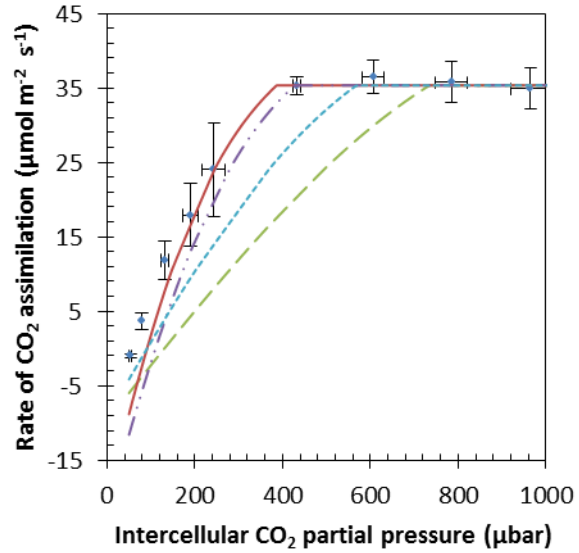

b)

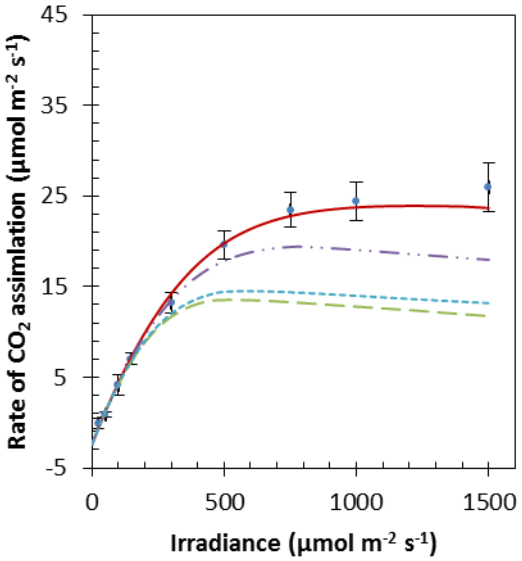

$f_{str} = 0.5$

c)

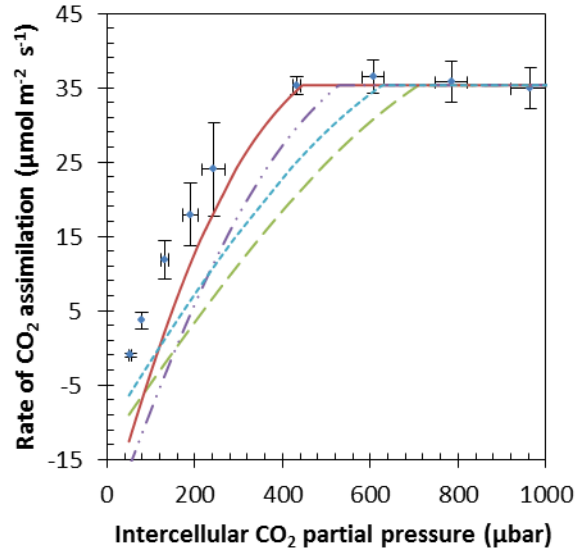

d)

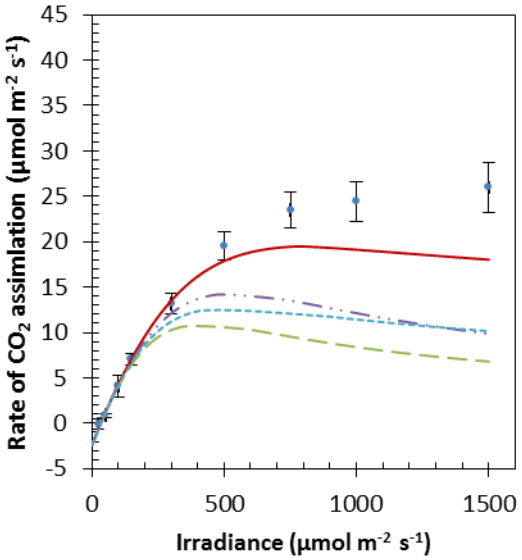

Figure A3.2.1: Simulated light and CO_2 response curves for alternative assumed diffusive properties. Measured (dots) and simulated $A - C_i$ (a+c) and $A - I_{inc}$ (b+d) curves for 15-day-old Admiro leaves under ambient O_2 (210 mbar) and CO_2 (400 µbar). In panel a and b, $f_{str} = 0.25$. In panel c and d, $f_{str} = 0.5$. The simulated response curves were simulated for different combinations of values for $p_{eff,wall}$ and ζ_{str}: $\{p_{eff,wall} = 0.02, \zeta_{str} = 0.294\}$ (dashed line), $\{p_{eff,wall} = 0.2, \zeta_{str} = 0.294\}$(dotted line), $\{p_{eff,wall} = 0.02, \zeta_{str} = 0.5\}$ (dashed dotted line), $\{p_{eff,wall} = 0.2, \zeta_{str} = 0.5\}$ (continuous line, default parameter values for $p_{eff,wall}$ and ζ_{str}).

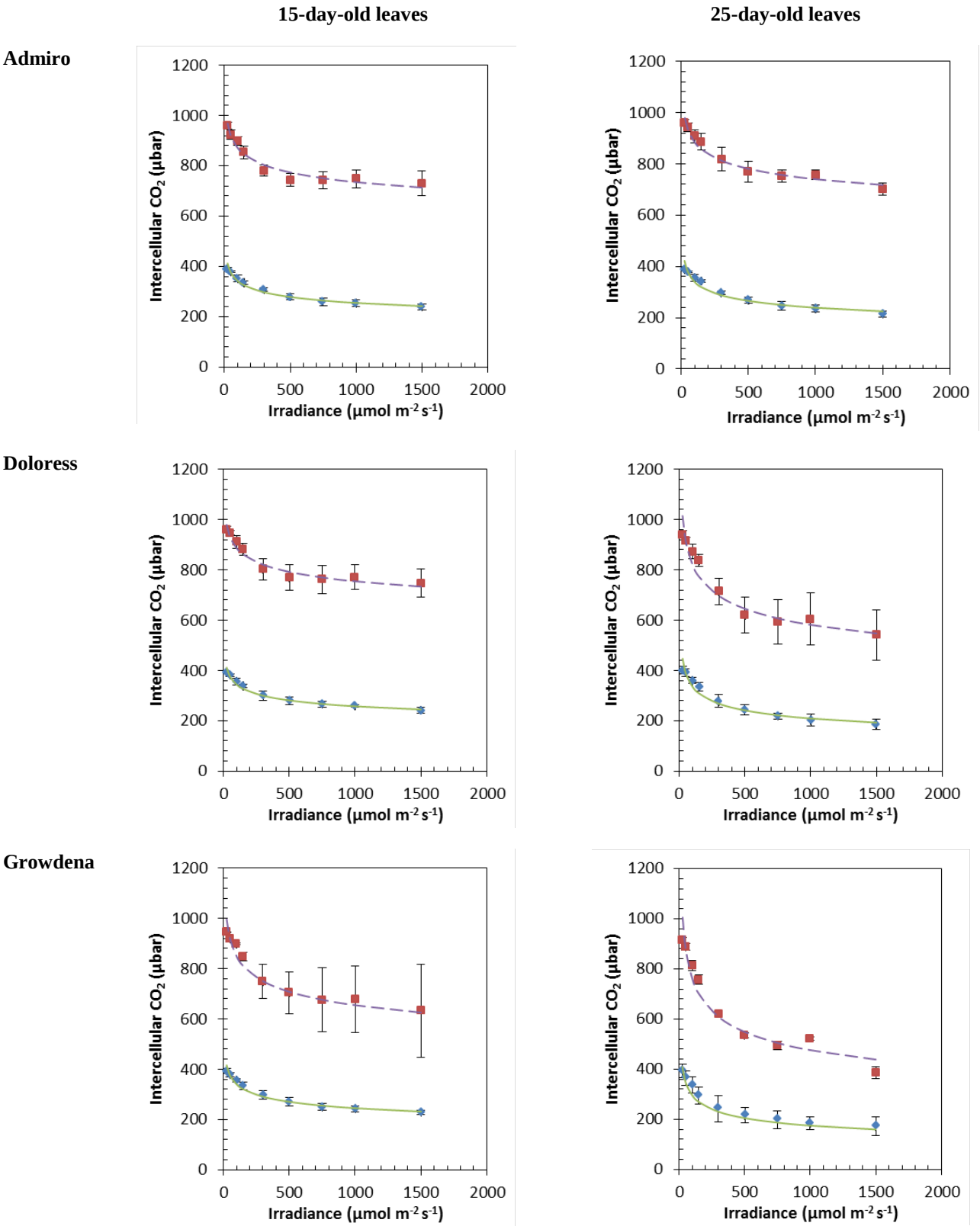

Figure A3.2.2: Measured and simulated C_i-I_{inc} relationships. Measured C_i-I_{inc} relationships at $O = 210$ mbar and $C_a = 400$ µbar (diamonds±one standard error) and at $O = 20$ mbar and $C_a = 1000$ µbar (squares±one standard error) for three cultivars (Admiro, Doloress, Growdena) and two leaf ages (15 days and 25 days after emergence). Simulated C_i-I_{inc} at $O = 210$ mbar and $C_a = 400$ µbar (solid lines) and at $O = 20$ mbar and $C_a = 1000$ µbar (dotted lines).

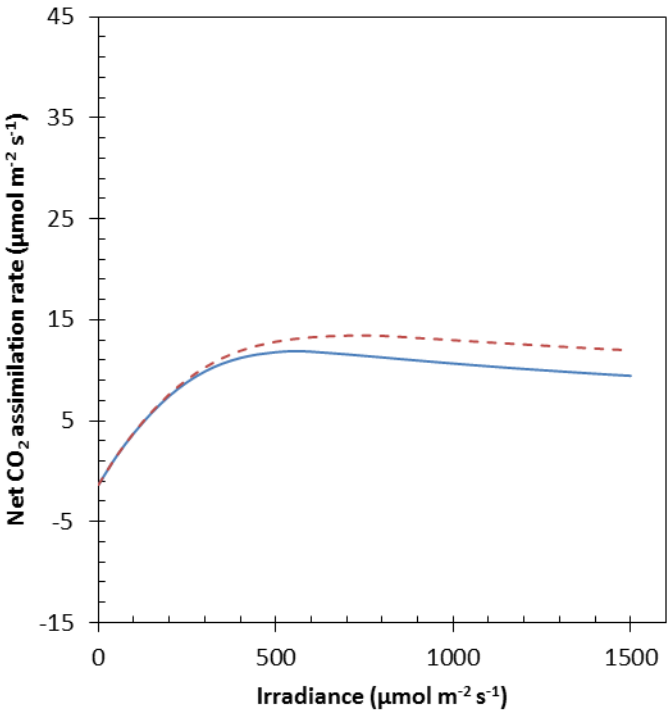

Figure A3.2.3: Light response curve with and without cytosol as separate compartment. Simulated $A - I_{\mathrm{inc}}$ curves for a 25-day-old Growdena leaf at the default value for ω ($\omega = 0.70$) (continuous line) and at $\omega = 0$ (dashed line)

CHAPTER 4

Localization of (photo)respiration and CO_2 re-assimilation in tomato leaves investigated with a reaction-diffusion model

Herman N.C. Berghuijs [1,2,3], Xinyou Yin[1,2], Q. Tri Ho[3], Moges A. Retta[1,3], Pieter Verboven[3], Bart M. Nicolaï[3], Struik P.C.[1,2]

[1] Centre for Crop Systems Analysis, Wageningen University, Droevendaalsesteeg 1, 6708 PB Wageningen, The Netherlands

[2] BioSolar Cells, P.O. Box 98, 6700 AB Wageningen, The Netherlands

[3] Flanders Center of Postharvest Technology / BIOSYST-MeBioS, Katholieke Universiteit Leuven, Willem de Croylaan 42, B-3001, Leuven, Belgium

Abstract

The CO_2 partial pressure near Rubisco, C_c, is commonly calculated by models using the overall mesophyll resistance. A disadvantage of such models is that they do not provide a mechanistic explanation for the CO_2 concentration difference between the intercellular air space and the carboxylation site. This study provides an alternative by presenting a reaction-diffusion model for CO_2 transport, production and fixation in leaves. It is parameterized by both leaf physiological and leaf anatomical data. The anatomical data consisted of the thickness of the cell wall, cytosol and stroma, and the area ratios of mesophyll exposed to the intercellular air space to leaf surfaces (S_m/S) and exposed chloroplast to exposed mesophyll surfaces (S_c/S_m). The model was used directly to estimate photosynthetic parameters from a part of the measured light and CO_2 response curves; the remaining data were used for validation. The model predicted light and CO_2 response curves reasonably well for 15 days old tomato (cv. Admiro) leaves, if (photo)respiratory CO_2 release was assumed to take place in the inner cytosol or in the gaps between the chloroplasts. The model was also used to calculate the fraction of CO_2 produced by (photo)respiration that is re-assimilated in the stroma, and this fraction ranged from 56 to 76%. In future research, the model should be further validated to better understand how the re-assimilation of (photo)respired CO_2 is affected by environmental conditions and physiological parameters.

Keywords: CO_2 diffusion, internal conductance, leaf anatomy, mesophyll conductance, mesophyll resistance, re-assimilation, re-fixation, reaction-diffusion model, photorespiration

Submitted to *Plos Computational Biology*

4.1 Introduction

The mesophyll of C_3 plants can substantially constrain CO_2 transport from the intercellular air space to Rubisco (Harley *et al.*, 1992a; Flexas *et al.*, 2008; Niinemets *et al.*, 2009; Flexas *et al.*, 2012). This results in a significant drawdown between the CO_2 partial pressures in the intercellular air space (C_i) and near the binding sites of Rubisco (C_c) where CO_2 is fixed. C_c is an input variable for the widely used Farquhar-von Caemmerer-Berry model (Farquhar *et al.*, 1980) (abbreviated as "FvCB model") that is used to predict the net rate of CO_2 assimilation (A_N) of a leaf. In order to calculate C_c, the mesophyll resistance (r_m) to CO_2 transport is commonly introduced as:

$$C_c = C_i - r_m A_N \tag{4.1}$$

This approach has several limitations. r_m, or its inverse (mesophyll conductance g_m), in equation (4.1) needs to be estimated by one of the various gas exchange-based methods described in literature (see Pons et al. (2009) for a review). This makes this method prone to measurement errors and statistical artefacts (Yin and Struik, 2009; Gu and Sun, 2014). Additionally, it has been shown that the mesophyll resistance is not constant, but possibly varies with light and CO_2 levels (Flexas *et al.*, 2007). One way to incorporate this variability in equation (4.1) is to use a Leuning-type phenomenological model (Leuning, 1995) that describes the correlation between C_c and g_m (Yin *et al.*, 2009; Gu *et al.*, 2012). However, this approach does not provide a mechanistic explanation for the variability of r_m with light and CO_2 levels.

Tholen *et al.* (2012) provided a mathematical framework to allow for the fact that CO_2 fixation takes place in chloroplasts whereas respiratory and photorespiratory CO_2 is released in mitochondria that are in the cytosol. Using this framework, they showed that the variability of r_m with CO_2 levels can at least partly be explained by the difference in the diffusion pathway between the (photo)respired CO_2 and the CO_2

coming from the intercellular air space. Their model assumes that CO_2 production by (photo)respiration takes place in a cytosol compartment between the cell wall and the chloroplast envelope and that there is CO_2 influx from the intercellular air space into this compartment. This implies that CO_2 from the intercellular air space and CO_2 produced by (photo)respiration share the diffusion pathway from the cytosol to Rubisco, where CO_2 is fixed. However, there can only be a shared diffusion pathway of these two sources of CO_2 if one of the following two conditions is met. Either, the mitochondria releasing (photo)respired CO_2 are located between the plasma membrane and the chloroplasts (instead of between the tonoplast and the chloroplasts) or CO_2 in the cytosol is completely mixed. Tholen *et al.* (2014) commented on their earlier framework (Tholen *et al.*, 2012) that this latter assumption was made. Complete mixture of CO_2 from the atmosphere and CO_2 produced by (photo)respiration implies that CO_2 diffusion in the cytosol is much faster than diffusion in the combined cell wall and plasma membrane and in the chloroplast. Physically, this means that under these assumptions the location of mitochondria does not affect C_c and that the Tholen *et al.* (2012) framework cannot be used to investigate the effect of the placement of mitochondria. However, the position of mitochondria relative to the chloroplast may affect net CO_2 assimilation rate. If most of the (photo)respired CO_2 is produced between the chloroplast envelope and the tonoplast, the released CO_2 will likely be re-assimilated. This is especially the case when the space between the chloroplasts is small (Sage and Sage, 2009; Busch *et al.*, 2013). The exposed mesophyll surface that is not covered by chloroplasts may provide a pathway for CO_2 to escape to the intercellular air space.

In order to deal with most of the limitations of the concept of mesophyll resistance and to study the influence of several leaf structural and biochemical properties on leaf photosynthesis separately, it may be necessary to move beyond resistance models. Several reaction-diffusion models of a leaf have been produced. Parkhurst (1977) modelled a leaf as a porous volume and modelled CO_2 transport and assimilation within this volume. In later studies, the leaf structure was modelled more explicitly to study the effect of stomatal opening state and pore size, gradients of CO_2 in the

intercellular air space (Parkhurst and Mott, 1990; Vesala *et al.*, 1996; Aalto and Juurola, 2002), and the effect of temperature dependency of carbon anhydrase activity, CO_2 solubility and diffusion related parameters (Aalto *et al.*, 1999; Aalto and Juurola, 2002; Juurola *et al.*, 2005) on CO_2 assimilation. A limitation of these models is that they assume that (photo)respiration and CO_2 assimilation take place in the same compartments. More recent reaction-diffusion models (Tholen and Zhu, 2011; Ho *et al.*, 2016) describe the structure in more detail in order to compartmentalize these processes, allowing mechanistic modelling of the contribution of (photo)respired CO_2 to the calculated mesophyll resistance. An advantage of these models, compared with resistance models that use anatomical properties to calculate r_{m} and C_{c} (Tosens *et al.*, 2012; Tomas *et al.*, 2013) is that these models do not require a predefined diffusion distance in the chloroplasts. Tholen and Zhu (2011) implemented a 3-D reaction-diffusion model for CO_2 and HCO_3^- into a detailed representation of a single mesophyll cell. Ho *et al.* (2016) described a similar model, but incorporated the geometry of leaf tissue based on synchrotron computed laminography images. This complexity has consequences. The model of Tholen and Zhu (2011) describes a very detailed cell microstructure. Therefore, it may become computationally expensive if a whole mesophyll tissue sample is modelled in this way. This feature is important, because the computationally expensive models are unattractive to use for procedures that require a large number of model runs, like optimization or parameter estimation procedures. The 3-D leaf geometry from Ho *et al.* (2016) is a direct reconstruction of a whole leaf section, which makes it impossible to change to structure of mesophyll cells. The computational time of this model is also very high.

In the current study, we first present a simple microstructural model of a leaf, in which CO_2 transport, CO_2 production by (photo)respiration, and CO_2 consumption by carboxylation is modelled. The mesophyll microstructures in the model are very simple and flexible. This makes the model easy to apply to a wide range of C_3 species and also computationally inexpensive. We will demonstrate that by directly using the model to analyse simultaneously measured data for gas exchange and chlorophyll fluorescence. The model can contribute to the understanding of the mechanisms that

determine C_c. We will demonstrate this by investigating how the position of the sites of (photo)respiration relative to the chloroplast stroma affect the net rate of CO_2 assimilation and the re-assimilation of CO_2 produced by (photo)respiration.

4.2 Material and methods

4.2.1 Plant material and experimental data

The experiment was carried out in a UNIFARM glasshouse of Wageningen University, using three cultivars of tomato (*Solanum lycopersicum* L.). In this experiment, a LI-6400XT Portable Photosynthesis System (Li-Cor BioSciences, Lincoln, NE, USA) was used to simultaneously measure gas exchange and chlorophyll fluorescence. CO_2 response curves were measured at an incident irradiance (I_{inc}) of 1500 μmol m^{-2} s^{-1} under both 21% and 2% O_2 conditions. The same leaf material was used to prepare samples for both light microscopy and transmission electron microscopy (TEM). From the obtained light microscopic images, L_m/L (the ratio of the length of the exposed mesophyll cell to the total length of the image) was measured. Subsequently, curvature factors (Thain, 1983; Evans *et al.*, 1994) were adopted from Galmes *et al.* (2013), to calculate the ratio of the exposed mesophyll surface to the leaf surface S_m/S. From the obtained transmission electron microscopic images, S_c/S_m (the ratio of the chloroplast surface area exposed to the intercellular air space to the exposed mesophyll surface area, the thickness of the cytosol, the stroma and the cell wall were determined. More detailed information on the experimental procedure is described in Chapter 3. For our present study, we only used the gas exchange, chlorophyll fluorescence and leaf anatomical data for 15-days old leaves of cv. ‘Admiro’.

4.2.2 Overall description of the model

The model consists of two main parts; a description of the geometry of the computational domain and a mathematical formulation, in the form of partial differential equations and boundary conditions, of the processes that are simulated

within this geometry. The next two sections describe the geometry and the mathematical formulation of processes, respectively.

4.2.3 Geometry description

The computational domain consists of a rectangular section with dimensions $l \times h$ of a mesophyll cell exposed to the intercellular space (Fig. 4.1). This section contains a single chloroplast. CO_2 enters the domain by diffusing through the cell wall and plasma membrane into the outer cytosol (thickness $t_{\mathrm{cyt,out}}$). From there, it diffuses through the double chloroplast membrane into the stroma (thickness t_{str}). Part of the CO_2 may diffuse through cytosol gaps between the chloroplasts (height h_{gap}) and enter the inner cytosol (thickness $t_{\mathrm{cyt,in}}$). CO_2 may be produced through (photo)respiration in either the outer cytosol, inner cytosol or the cytosol gaps between the chloroplasts, depending on where mitochondria are located. (Photo)respired CO_2 either escapes towards the intercellular space, or diffuses back into the chloroplasts, being re-assimilated. For reasons of symmetry, the height of the cytosol gap at the bottom and the top of the computational domain was half of that of the total gap height (h_{gap}); similarly, it is assumed that $t_{\mathrm{cyt,in}} = t_{\mathrm{cyt,out}}$ (hereafter they are denoted collectively as t_{cyt}). More details on the reconstruction of the geometry can be found in Supplementary text 1. The chloroplast envelope was modelled as a thin film diffusion barrier. Since preliminary simulations showed that the presence of a vacuole did barely affect the net CO_2 assimilation rate, Fig. 4.1 does not include a vacuole. An insulated boundary condition (net flux is zero) was applied over the tonoplast, which is the membrane between the inner cytosol and the vacuole.

In all simulations an assumption from Tholen and Zhu (2011) was adopted; namely, the aspect ratio q of the chloroplasts (in this study, $q = \frac{t_{\mathrm{str}}}{h_{\mathrm{str}}}$) was constant and equal to 2.5. The gap width h_{gap} was varied in order to produce geometries with different values of $S_{\mathrm{c}}/S_{\mathrm{m}}$. It can be expressed as:

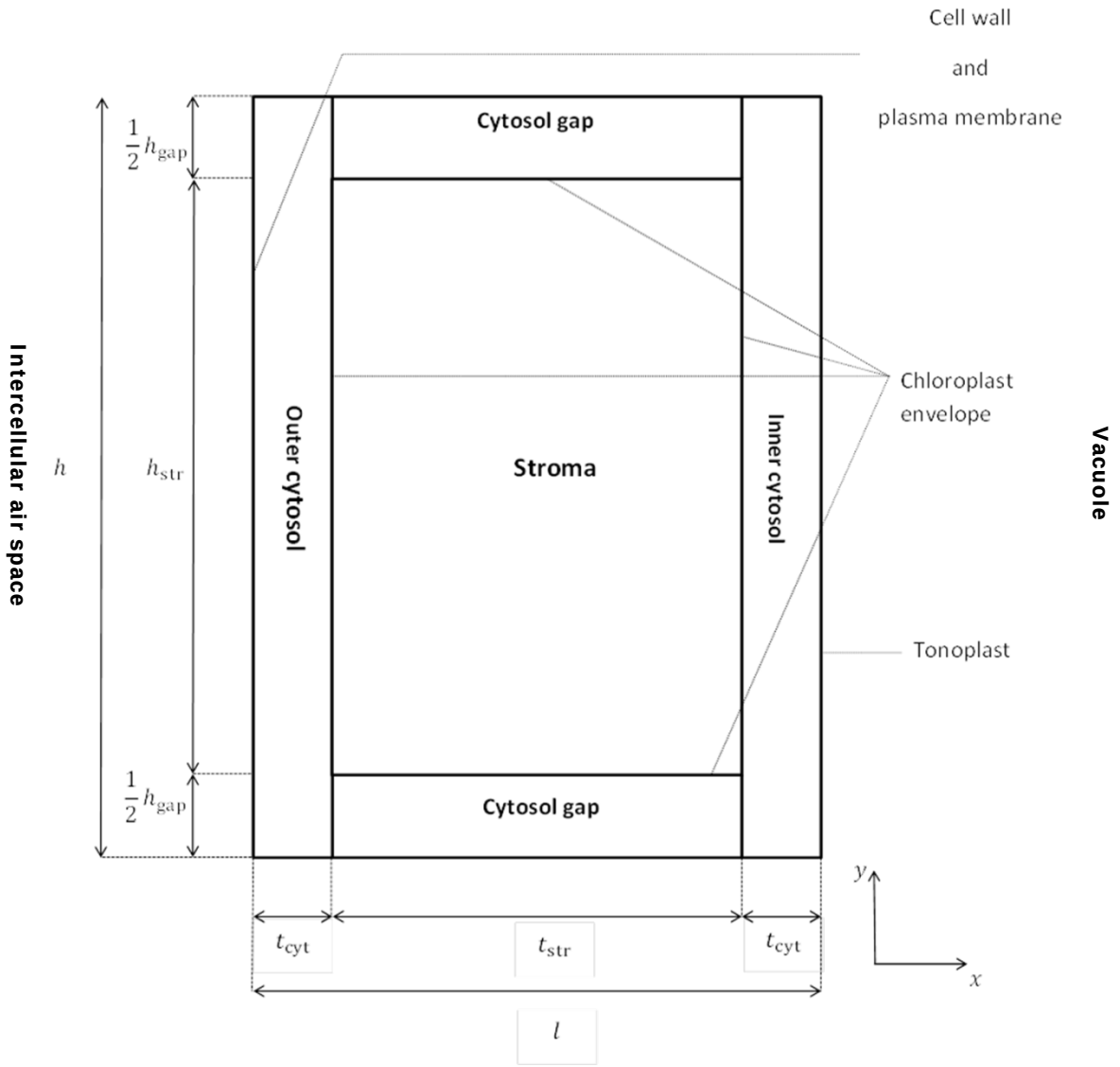

Figure 4.1: Schematic drawing of the computational domain and its position relative to the intercellular air space and the vacuole.

$$h_{\mathrm{gap}} = q t_{\mathrm{str}} \left(\left(\frac{S_{\mathrm{c}}}{S_{\mathrm{m}}} \right)^{-1} - 1 \right) \tag{4.2}$$

More details on the derivation of equation (4.2) can be found in Supplementary text 2. By applying this geometry, it is assumed that all anatomical parameters ($S_{\mathrm{c}}/S_{\mathrm{m}}$, t_{str}, t_{cyt}, and q) are uniform in the paradermal direction.

4.2.4 Process description

Diffusion equation for CO_2 transport

In a steady state, CO_2 diffusion, consumption and production should be in balance as:

$$\nabla \cdot D_{\mathrm{CO_{2,i}}} \nabla[\mathrm{CO_2}] = w_{\mathrm{i}} - r_{\mathrm{p,i}} - r_{\mathrm{d,i}} \tag{4.3}$$

where the subscript 'i' denotes the medium (either a cytosol compartment or the stroma). $D_{\mathrm{CO_{2,i}}}$ is the diffusion coefficient of CO_2 ($m^2\ s^{-1}$)in compartment i. w is the volumetric rate of carboxylation by Rubisco (mol CO_2 m^{-3} s^{-1}), which is only non-zero in the stroma. r_{p} is the volumetric rate of photorespiration (mol CO_2 m^{-3} s^{-1}), which is only non-zero in the cytosol. r_{d} is the volumetric rate of respiration (mol CO_2 m^{-3} s^{-1}) that is only non-zero in the cytosol and was taken as a constant. $[\mathrm{CO_2}]$ is the CO_2 concentration (mol m^{-3}). ∇ (m^{-1}) is the gradient operator. The diffusion coefficient for CO_2 transport depends on the porosity and the viscosity of the medium. For the cytosol and the stroma, the diffusion coefficient for CO_2 was calculated as (Tosens *et al.*, 2012):

$$D_{\mathrm{CO_{2,i}}} = p_{\mathrm{eff,i}} \zeta_{\mathrm{i}} D_{\mathrm{CO_{2,water}}} \tag{4.4}$$

where p_{eff} is the effective porosity of the medium. It is assumed that the effective porosity of the cytosol and the stroma is 1.0. ζ_{i} is a reduction factor in the medium compared to pure water due to a higher viscosity of the media compared to water. It is assumed to be 0.5 for the stroma and the cytosol and 1.0 for the cell wall (Ho *et al.*, 2016). Table 4.1 shows physical parameter values used in this study and their units.

Table 4.1: Physical and biochemical constants

Symbol	Explanation	Value	Source
$D_{\mathrm{CO_2,water}}$	Diffusion coefficient of CO_2 in water at $T = 298.13$ K	$1.79 \cdot 10^{-9}$ m^2 s^{-1}	Tosens *et al.* (2012)
G_{mem}	Plasma membrane permeability	$3.5 \cdot 10^{-3}$ m s^{-1}	Gutknecht *et al.* (1977)
G_{env}	Chloroplast envelope permeability	$\frac{1}{2}\, G_{\mathrm{mem}}$	Ho *et al.* (2016)
g_{s}	Stomatal conductance at ambient CO_2 and O_2, and saturating light	1.53 mol m^{-2} s^{-1} Pa^{-1}	
H	Henry's constant for CO_2 at $T = 298.13$ K	2941 Pa m^3 mol^{-1}	Sander (2014)
K_{mC}	Michaelis-Menten constant for RuBP carboxylation by Rubisco	26.7 Pa	Bernacchi *et al.* (2002)
K_{mO}	Michaelis-Menten constant for RuBP oxygenation by Rubisco	16.4 kPa	Bernacchi *et al.* (2002)
$p_{\mathrm{eff,wall}}$	Effective porosity of the cell wall	0.2	Evans *et al.* (2009)
R	Universal gas constant	8.314 Pa m^3 mol^{-1} K^{-1}	Nobel (2009)
$S_{\mathrm{C/O}}$	Rubisco specificity factor	2.6 mmol μmol^{-1}	Tholen *et al.* (2012)
T	Temperature (constant at room temperature in this study)	298.13 K	
ζ_{cyt}	Fraction of CO_2 diffusion coefficient in cytosol to CO_2 diffusion coefficient in water	0.5	Tosens *et al.* (2012)
ζ_{str}	Fraction of CO_2 diffusion coefficient in stroma to CO_2 diffusion coefficient in water	0.5	Tosens *et al.* (2012)

Carboxylation rate

The FvCB model (Farquhar *et al.*, 1980), expanded with triose phosphate utilization limited carboxylation (Sharkey, 1985), was used to quantify the rate of carboxylation by Rubisco w in the stroma:

$$w = \min\left(\frac{[\mathrm{CO_2}]v_{\mathrm{cmax}}}{[\mathrm{CO_2}] + k_{\mathrm{mC}}\left(1 + \frac{[\mathrm{O_2}]}{k_{\mathrm{mO}}}\right)}, \frac{j[\mathrm{CO_2}]}{4[\mathrm{CO_2}] + 8\gamma^*}, \frac{3t_{\mathrm{p}}}{1 - \frac{\gamma^*}{[\mathrm{CO_2}]}}\right) \tag{4.5}$$

where v_{cmax} is the maximum volumetric rate of carboxylation by Rubisco (mol m^{-3} s^{-1}); k_{mC} and k_{mO} are the Michaelis-Menten constants of Rubisco (mol m^{-3}) for carboxylation and oxygenation, respectively; j is the volumetric rate of electron transport (mol m^{-3} s^{-1}); t_{p} is the volumetric rate of triose phosphate utilization (mol m^{-3} s^{-1}); and γ^* is the CO_2 compensation point, the CO_2 concentration (mol m^{-3}) in the

stroma at which the amount of CO_2 consumed by carboxylation equals the amount of CO_2 released by photorespiration.

Photorespiration rate

The rate of CO_2 production due to photorespiration was modelled as (Tholen and Zhu, 2011):

$$r_{\mathrm{p}} = \left(\iint_{\mathrm{Stroma}} \frac{\gamma^{*} w}{[\mathrm{CO_2}]} \mathrm{d}x \, \mathrm{d}y \right) \left(\iint_{\mathrm{(Photo)respiration}} \mathrm{d}x \, \mathrm{d}y \right)^{-1} \tag{4.6}$$

where "Stroma" is the stroma compartment in the computational domain. "(Photo)respiration" is the location in the computational domain, in which CO_2 release by (photo)respiration is assumed to take place. Three different scenarios for the location for CO_2 release by (photo)respiration were considered: either (1) the inner cytosol, or (2) the outer cytosol, or (3) the cytosol gaps between the chloroplasts.

Unit conversions

The variables $v_{\mathrm{cmax}}, r_{\mathrm{d}}, r_{\mathrm{p}}, t_{\mathrm{p}}, j,$ and w in equations (4.3), (4.5) and (4.6) are rates per unit of volume. Their equivalents expressed in rate per unit of leaf area (mol $\mathrm{m^{-2}\ s^{-1}}$) are denoted here in capitals; $V_{\mathrm{cmax}}, R_{\mathrm{d}}$, R_{p}, T_{p}, J, and W. In order to calculate j, v_{cmax} and t_{p}, J, V_{cmax} and T_{p} are multiplied with the ratio S/V_{str}, which is the ratio of the leaf area to the total volume of the stroma in a leaf. Supplementary texts 2 and 3 explain how this term is derived mathematically; r_{d} is calculated by multiplying R_{d} with $S/V_{\mathrm{cyt,inner}}$, $S/V_{\mathrm{cyt,outer}}$, or $S/V_{\mathrm{cyt,gap}}$, depending on the scenario. Table 4.2 shows mathematical expressions for these surface to volume fractions. There are also a number of parameters that represent concentrations (k_{mC}, k_{mO}, γ^{*}, $[\mathrm{O_2}]$, $[\mathrm{CO_2}]$) expressed in mol $\mathrm{m^{-3}}$. In most photosynthesis research, these parameters

Table 4.2: Overview of surface to volume ratios and parameterizations

Symbol	Unit	Mathematical expression	Meaning of ratios
$\frac{S}{V_{\mathrm{str}}}$	m^{-1}	$\frac{1}{t_{\mathrm{str}}}\left(\frac{S_{\mathrm{m}}}{S}\right)^{-1}\left(\frac{S_{\mathrm{c}}}{S_{\mathrm{m}}}\right)^{-1}$	Leaf area to total chloroplast volume
$\frac{S}{V_{\mathrm{cyt,inner}}}$	m^{-1}	$\frac{1}{t_{\mathrm{cyt}}}\left(\frac{S_{\mathrm{m}}}{S}\right)^{-1}$	Leaf area to total volume of the inner cytosol
$\frac{S}{V_{\mathrm{cyt,outer}}}$	m^{-1}	$\frac{1}{t_{\mathrm{cyt}}}\left(\frac{S_{\mathrm{m}}}{S}\right)^{-1}$	Leaf area to total volume of the outer cytosol
$\frac{S}{V_{\mathrm{cyt,gap}}}$	m^{-1}	$\frac{1}{t_{\mathrm{str}}}\left(\frac{S_{\mathrm{m}}}{S}\left(1-\frac{S_{\mathrm{c}}}{S_{\mathrm{m}}}\right)\right)^{-1}$	Leaf area to total volume of the cytosol gaps

are expressed as partial pressures instead (here written as K_{mC}, K_{mO}, Γ^{*}, O). These parameters are expressed in Pa. The ideal gas law and Henry's law were applied (Ho *et al.*, 2010) to convert all mentioned partial pressure parameters, expressed in gas phase (K_{mC}, K_{mO}, Γ^{*}), into concentrations in the liquid phase.

4.2.5 Quantification of parameters

Quantification of leaf anatomical parameters

Leaf anatomical parameters (t_{cyt}, t_{str}, $S_{\mathrm{c}}/S_{\mathrm{m}}$, S_{m}/S, t_{wall}) for 15-day-old Admiro leaves were adopted from Chapter 3. $S_{\mathrm{c}}/S_{\mathrm{m}}$, t_{cyt}, and t_{str} were used to generate a unique geometry for this leaf, as described in Supplementary materials 1-3. The model was solved for the combination of input parameter values for each leaf type. The anatomical parameter values are listed in Table 4.3. The measured cytosol thicknesses in Table 4.3 are considerably smaller than the thickness of mitochondria assumed by Tholen and Zhu (2011). To the best of our knowledge, there have been no systematic measurements of diameters of mitochondria and some sample images from a number of studies (Busch *et al.*, 2013; Gielwanowska *et al.*, 2015; Moser *et al.*, 2015) suggest that this diameter can vary considerably. Due to lack of data, we assumed that the thickness is equal to the cytosol thickness measured on the TEM images from Chapter 3.

Table 4.3: Values of leaf anatomical properties

Symbol	Unit	Explanation	Value	Source
q		Ratio of the height of a chloroplast to its thickness	2.50	Assumed
$\frac{S_{\mathrm{m}}}{S}$	-	Ratio of the area of the mesophyll cell surface, exposed to the intercellular air space, to the leaf surface area	17.0	Chapter 3
$\frac{S_{\mathrm{c}}}{S_{\mathrm{m}}}$	-	Ratio of the area of the chloroplast surface, facing the intercellular air space, to the mesophyll surface area, exposed to the intercellular air space	0.919	Chapter 3
t_{wall}	m	Cell wall thickness	$1.18 \cdot 10^{-7}$	Chapter 3
t_{cyt}	m	Cytosol thickness	$1.18 \cdot 10^{-7}$	Chapter 3
t_{str}	m	Stroma thickness	$2.54 \cdot 10^{-6}$	Chapter 3

Quantification of Rubisco kinetic parameters

We adopted the Michaelis-Menten constants for carboxylation (K_{mC}) and oxygenation (K_{mO}) by Rubisco from Bernacchi *et al.* (2002). We further assumed that the specificity factor of Rubisco for CO_2 and O_2, $S_{\mathrm{c/o}}$, equals 2.6 (Tholen *et al.*, 2012). For $S_{\mathrm{C/O}}$, we calculated the CO_2 compensation point Γ^* as:

$$\Gamma^* = \frac{0.5O}{S_{\mathrm{c/o}}} \tag{4.7}$$

Determination of the rate of electron transport

We used $A_{\mathrm{N}} - I_{\mathrm{inc}}$ data measured at 2% O_2 under limiting irradiance conditions (I_{inc} equal to 25, 50, 100, and 150 µmol m^{-2} s^{-1}) to fit A_{N} against $\frac{1}{4}\Phi_2 I_{\mathrm{inc}}$ by linear regression (where Φ_2 is the measured quantum yield of Photosystem II). Based on the estimated slope of this regression (s), we calculated the rate of electron transport J for each combination of measured values for I_{inc} and Φ_2 as in (Yin *et al.*, 2009):

$$J = s\Phi_2 I_{\mathrm{inc}} \tag{4.8}$$

4.2.6 Boundary conditions

In the model, it is assumed that the resistance of the intercellular air space for CO_2 transport is negligible. The cell wall and the plasma membrane were not modelled as separate domains, because they were very thin. Together with the stomata, they were incorporated in the boundary conditions of the combined cell wall and plasma membrane (Fig. 4.1) instead. The following convection boundary conditions were thus assigned to these edges:

$$\phi_{\mathrm{wp}} = \frac{1}{\frac{1}{G_{\mathrm{s}}} + \frac{t_{\mathrm{wall}}}{p_{\mathrm{eff,wall}} D_{\mathrm{CO_2,water}}} + \frac{1}{G_{\mathrm{mem}}}} \left(\frac{RT}{H} [\mathrm{CO_2}]_{\mathrm{a}} - [\mathrm{CO_2}] \right) \tag{4.9}$$

where ϕ_{wp} is the net flux of CO_2 over the cell wall from the intercellular air space normal to the mesophyll surface; $[\mathrm{CO_2}]_{\mathrm{a}}$ is the CO_2 concentration at the leaf surface; G_{mem} is the plasma membrane conductance (m s^{-1}); t_{wall} is the cell wall thickness; p_{eff} is the effective porosity of the cell wall; R is the universal gas constant; T is the temperature; and H is Henry's law constant for CO_2 at temperature T and standard pressure. The term RT/H represents the dimensionless Henry's law constant that is used to convert gas phase concentrations into liquid phase concentrations (Ho *et al.*, 2010; Tosens *et al.*, 2012). It is assumed that $G_{\mathrm{mem}} = 3.5 \cdot 10^{-3}$ m s^{-1} (Gutknecht *et al.*, 1977) and $p_{\mathrm{eff,wall}} = 0.2$ (Fanta *et al.*, 2012; Ho *et al.*, 2016). G_{s} represents the stomatal conductance expressed in m s^{-1}. It was calculated from the measured stomatal conductance, expressed in mol m^{-2} s^{-1} Pa^{-1}, as:

$$G_{\mathrm{s}} = g_{\mathrm{s}} \left(\frac{S_{\mathrm{m}}}{S} \right)^{-1} RT \tag{4.10}$$

The flux over the chloroplast envelope was modelled as a resistance with conductance $G_{\mathrm{env}} = \frac{1}{2} G_{\mathrm{mem}}$. Since the chloroplast envelope is a double membrane, it was assumed that its conductance was half that of the plasma membrane. By applying equations (4.9) and (10), it was assumed that the resistance of the intercellular air space was negligible. All other boundaries of the computational domain were insulated as explained earlier.

4.2.7 Estimation of leaf physiological parameters

We used the reaction-diffusion model directly to estimate the parameters R_{d} and V_{cmax}.

Estimation of R_{d}

We estimated R_{d}, based on the assumed location of (photo)respiratory CO_2 release (inner cytosol, outer cytosol, or cytosol gaps between chloroplasts). For this estimation, we only used the A_{N} and g_{s} measurements from $A_{\mathrm{N}} - I_{\mathrm{inc}}$ curve measurements at I_{inc} set at 25, 50, 100, and 150 μmol m^{-2} s^{-1}. For this range of light levels, we estimated R_{d} by minimizing the squared difference between average measured net rates of CO_2 assimilation and the ones for each light level simulated by the reaction-diffusion model. For these light levels, the RuBP carboxylation rate is always limited by electron transport; so, R_{d} is expected to be estimated using J and Γ^* as inputs.

Determination of T_p

In order to calculate T_{p}, we first determined the triose-phosphate-utilization-limited net CO_2 assimilation rate A_{p} as the average measured net CO_2 assimilation rate at $C_{\mathrm{a}} = 200$ Pa, $O = 21$ kPa and $I_{\mathrm{inc}} = 1500$ μmol m^{-2} s^{-1}. From that average net CO_2 assimilation rate, we calculated T_{p} as:

$$T_{\mathrm{p}} = \frac{\left(A_{\mathrm{p}} + R_{\mathrm{d}}\right)}{3} \tag{4.11}$$

where we used the previously estimated values of R_d as input for equation (4.11).

Estimation of V_{cmax}

For the estimation of V_{cmax}, we only used the A_N and C_i measurements from $A_N - C_i$ curves measured at $I_{inc} = 1500$ µmol m^{-2} s^{-1} $O = 21$ kPa and C_a equal to 5, 10, 15, and 20 Pa. We estimated V_{cmax} by minimizing the squared difference between the average measured and simulated net CO_2 assimilation rates at these ambient CO_2 levels, assuming that the net CO_2 assimilation rate is limited by Rubisco. During this procedure, we used the previously determined values for R_d and T_p as input variables. In order to do this estimation, we used COMSOL 5.1 with MATLAB livelink (COMSOL AB, Stockholm, Sweden) to convert the COMSOL model into a MATLAB 2014b (The Mathworks, Natick, USA) script to allow optimization.

4.2.8 Validation

We did not use the measurements of the $A_N - C_i$ at ambient CO_2 levels if the leaf was exposed to CO_2 partial pressures between 40 Pa and 160 Pa for the estimation of s, R_d, T_p, and V_{cmax}. Neither did we use the $A_N - I_{inc}$ measurements at irradiances between 300 and 1500 µmol m^{-2} s^{-1}. We used these remaining combinations of measured values for O, I_{inc} and C_i to predict the net CO_2 assimilation rate and compared these predictions with the experimental data.

4.2.9 Solving the model and post-processing

The model was implemented and solved in the finite element software COMSOL Multiphysics 5.1. After solving the model, the rate of CO_2 production by RuBP carboxylation rate W, expressed as the rate per unit of leaf area per second, was calculated by multiplying the average volumetric rate of RuBP carboxylation by the total stroma volume and dividing this by the leaf surface area:

$$W = \left(\frac{S}{V_{\text{str}}}\right)^{-1} \left(\iint_{\text{Stroma}} w \, \mathrm{d}x \, \mathrm{d}y \right) \left(\iint_{\text{Stroma}} \mathrm{d}x \, \mathrm{d}y \right)^{-1} \tag{4.12}$$

The rate of CO_2 production per unit of leaf area by photorespiration was calculated as:

$$R_{\text{p}} = \left(\frac{S}{V_{\text{str}}}\right)^{-1} \left(\iint_{\text{Stroma}} \frac{w\gamma^*}{[\text{CO}_2]} \, \mathrm{d}x \, \mathrm{d}y \right) \left(\iint_{\text{Stroma}} \mathrm{d}x \, \mathrm{d}y \right)^{-1} \tag{4.13}$$

The net rate of CO_2 assimilation was calculated as:

$$A_{\text{N}} = W - R_{\text{p}} - R_{\text{d}} \tag{4.14}$$

4.2.10 Estimating re-assimilation of (photo)respired CO_2

The model was used to calculate the fraction (f_{rec}) of CO_2 produced by (photo)respiration that is re-assimilated. The method to achieve this is largely based on the method described by Ho *et al.* (2016), who used their model to conduct an *in silico* experiment mimicking the *in vivo* experiment described by Haupt-Herting *et al.* (2001). In Haupt-Herting *et al.*'s experiment, a leaf was adapted to ambient CO_2 levels and saturating light. Under ambient conditions, atmospheric CO_2 mainly consists of $^{12}CO_2$ isotopes. After adaptation, the leaf was exposed to air that contained $^{13}CO_2$, but no $^{12}CO_2$. The concentrations of $^{12}CO_2$ and $^{13}CO_2$ at the leaf surface reached new equilibrium concentrations after about 12 seconds. Although no atmospheric $^{12}CO_2$ is taken up, the assimilates still contain mainly ^{12}C isotopes, so all CO_2 produced by (photo)respiration consists of $^{12}CO_2$. It takes a longer period (20-30 s) than the 12-seconds adaptation time before measureable amounts of $^{13}CO_2$ are released by (photo)respiration. Haupt-Herting *et al.* (2001) exploited this fact by stating that $^{12}CO_2$

and $^{13}CO_2$ are in quasi steady state during this period of 12 seconds. Since all (photo)respired CO_2 consists of $^{12}CO_2$, the measured net $^{13}CO_2$ assimilation rate ${}^{13C}A_N$ equals the carboxylation rate W. Next they measured the $^{12}CO_2$ and $^{13}CO_2$ concentrations in the intercellular air space. The total CO_2 concentration ($[{}^{12}CO_2] + [{}^{13}CO_2]$ is constant during the experiment. Since the discrimination of $^{13}CO_2$ is very small (0.27%) (Farquhar *et al.*, 1982), Haupt-Herting *et al*. therefore assumed it to be negligible and stated that ${}^{12}A_N = \frac{[{}^{12}CO_2]_i}{[{}^{13}CO_2]_i} {}^{13}A_N$. The symbols $[{}^{12}CO_2]_i$ and $[{}^{13}CO_2]_i$ represent the concentrations of $^{12}CO_2$ and $^{13}CO_2$ respectively, in the intercellular air space. Since all assimilated CO_2 produced by (photo)respiration consists of $^{12}CO_2$, ${}^{12}A_N$ is also the rate of CO_2 re-assimilation.

For the *in silico* experiment in this study, equation (4.3) was replaced by separate reaction-diffusion equations for $^{12}CO_2$ and $^{13}CO_2$ transport. Since all CO_2 production by (photo)respiration consists of $^{12}CO_2$, the partial differential equations for $^{12}CO_2$ and $^{13}CO_2$ can be expressed as:

$$\nabla \cdot D_{CO_2,i} \nabla [{}^{12}CO_2] = w_{12} - r_d - r_p \tag{4.15}$$

$$\nabla \cdot D_{CO_2,i} \nabla [{}^{13}CO_2] = w_{13} \tag{4.16}$$

Since the total CO_2 concentration does not change after $^{12}CO_2$ in the air near the leaf surface was replaced by $^{13}CO_2$, $[{}^{12}CO_2] + [{}^{13}CO_2]$ were substituted for $[CO_2]$ in equations (4.5) and (4.6). The volumetric consumption of $^{12}CO_2$ and $^{13}CO_2$ by RuBP carboxylation (w_{12} and w_{13}) were expressed as:

$$w_{12} = \frac{[{}^{12}CO_2]}{[{}^{12}CO_2] + [{}^{13}CO_2]} w \tag{4.17}$$

$$w_{13} = \frac{\left[^{13}\mathrm{CO_2}\right]}{\left[^{12}\mathrm{CO_2}\right] + \left[^{13}\mathrm{CO_2}\right]} w \tag{4.18}$$

In order to determine the rate of CO_2 re-assimilation, it is necessary to know what the concentration of $^{12}CO_2$ in the intercellular air space is. It cannot be assumed to be 0, because this would imply that once $^{12}CO_2$ enters the intercellular air space, it cannot be re-assimilated anymore. Instead, it is assumed that the $^{12}CO_2$ concentration at the leaf surface is zero and applied the following conditions at the mesophyll cell surface, in analogy to equation (4.9)

$$\phi_{\mathrm{wp},^{12}\mathrm{CO_2}} = -\frac{1}{\frac{1}{G_\mathrm{s}} + \frac{t_\mathrm{wall}}{p_\mathrm{eff,wall} D_{\mathrm{CO_2,water}}} + \frac{1}{G_\mathrm{mem}}} \left[^{12}\mathrm{CO_2}\right] \tag{4.19}$$

$$\phi_{\mathrm{wp},^{13}\mathrm{CO_2}} = \frac{1}{\frac{1}{G_\mathrm{s}} + \frac{t_\mathrm{wall}}{p_\mathrm{eff,wall} D_{\mathrm{CO_2,water}}} + \frac{1}{G_\mathrm{mem}}} \left(\frac{RT}{H}\left[^{13}\mathrm{CO_2}\right]_\mathrm{a} - \left[^{13}\mathrm{CO_2}\right]\right) \tag{4.20}$$

where $\phi_{\mathrm{wp},^{12}\mathrm{CO_2}}$ and $\phi_{\mathrm{wp},^{13}\mathrm{CO_2}}$ are the net fluxes of $^{12}CO_2$ and $^{13}CO_2$ respectively over the stomata, the intercellular air space, the cell wall and the plasma membrane; $\left[^{13}\mathrm{CO_2}\right]_\mathrm{a}$ is the concentration of $^{13}CO_2$ at the leaf surface.

The re-assimilation rate was calculated, equivalent to the rate $^{12}CO_2$ consumption due to RuBP carboxylation W_{12}, as:

$$W_{12} = \left(\frac{S}{V_\mathrm{str}}\right)^{-1} \left(\iint_\mathrm{Stroma} w_{12}\, \mathrm{d}x\, \mathrm{d}y\right) \left(\iint_\mathrm{Stroma} \mathrm{d}x\, \mathrm{d}y\right)^{-1} \tag{4.21}$$

The fraction of CO_2 produced by (photo)respiration that is re-assimilated is calculated as (Ho *et al.*, 2016):

$$f_{\mathrm{rec}} = \frac{W_{12}}{R_{\mathrm{d}} + R_{\mathrm{p}}} \tag{4.22}$$

4.2.11 Additional analyses

Supplementary text 4 contains the description of a sensitivity analysis for $t_{\mathrm{cyt,in}}$ and $t_{\mathrm{cyt,out}}$ to assess how these parameters may affect A_{N} and f_{rec}. Supplementary material 5 contains a description of an analysis in which the mitochondria were modelled explicitly to assess to what extent modelling loose mitochondria may change the calculated values of A_{N} and f_{rec}.

4.3. Results

4.3.1 Estimates of R_{d}, T_{p}, and V_{cmax}

Table 4.4 shows the value of s estimated by the Yin *et al.* (2009) method, the parameter values R_{d} and V_{cmax} and their standard errors estimated by our model, and the calculated values of T_{p}. The estimate of s was 0.529. The estimates for R_{d} were 3.43 $\mu\mathrm{mol\,m^{-2}\,s^{-1}}$, 3.36 $\mu\mathrm{mol\,m^{-2}\,s^{-1}}$, and 3.41 $\mu\mathrm{mol\,m^{-2}\,s^{-1}}$ assuming the (photo)respired CO_2 takes place in the inner cytosol, the outer cytosol and the cytosol gap compartments, respectively. These R_{d} and the measured A_{j} values were used to calculate T_{p}, which was 13 $\mu\mathrm{mol\,m^{-2}\,s^{-1}}$ for each assumed location of (photo)respiration. The estimates of V_{cmax} were 174 $\mu\mathrm{mol\,m^{-2}\,s^{-1}}$, 177 $\mu\mathrm{mol\,m^{-2}\,s^{-1}}$, and 227 $\mu\mathrm{mol\,m^{-2}\,s^{-1}}$ assuming (photo)respiratory CO_2 release in the inner cytosol, the outer cytosol and the cytosol gaps respectively. Although the standard errors of the estimates of V_{cmax}, assuming (photo)respired CO_2 release in the inner cytosol or cytosol gap were small relative to the parameter value, the standard

Table 4.4: Estimated values of parameters of the FvCB model for each scenario for (photo)respired CO_2 release (it takes either place in the inner cytosol, in the outer cytosol, or in the cytosol gap)

Symbol	Unit	Explanation	(Photo)respired CO_2 release in:		
			Inner cytosol	Outer cytosol	Cytosol gaps
s	-	Slope of the assumed linear relationship between J and $I_{\mathrm{inc}}\Phi_2/4$ at low light levels and low O_2 levels	0.529	0.529	0.529
R_{d}	μmol m^{-2} s^{-1}	Rate of normal respiration	3.44±0.36	3.36±0.36	3.41±0.36
T_{p}	μmol m^{-2} s^{-1}	Rate of triose phosphate utilization	13.39	13.38	13.38
V_{cmax}	μmol m^{-2} s^{-1}	Rate of RuBP carboxylation by Rubisco	174±29	177±251	227±29

errors were larger than the estimated parameter value assuming (photo)respired CO_2 in the outer cytosol.

4.3.2 Validation

Figure 4.2 shows a comparison between the simulated and measured net CO_2 assimilation rates. Only the lower parts of the $A - I_{\mathrm{inc}}$ curve ($I_{\mathrm{inc}} \leq 200$ μmol m^{-2} s^{-1}) and the $A - C_{\mathrm{a}}$ curves were used for the estimation of photosynthetic parameters ($C_{\mathrm{a}} \leq 30$ Pa) of s and R_{d}. Only the measurements at $C_{\mathrm{a}} = 200$ Pa in the $A - C_{\mathrm{a}}$ curve were used to determine T_{p}. The model was validated by predicting A_{N} for the remaining levels of C_{a} and I_{inc} that were used in the experiment. If (photo)respired CO_2 is released in the inner cytosol, the model predictions of A_{N} generally agrees well with the measurements. The same is true if (photo)respired CO_2 release is assumed to take place in the cytosol gap compartment, although the model tends to slightly underestimate A_{N} for intermediate C_{a} levels in the $A - C_{\mathrm{a}}$ curve. This underestimation is considerably higher if (photo)respired CO_2 is assumed to take place in the outer cytosol. Additionally, if $I_{\mathrm{inc}} \geq 500$ μmol m^{-2} s^{-1}, the predicted A_{N} is substantially lower than the measured A_{N}, if (photo)respiratory CO_2 release takes place in the outer cytosol.

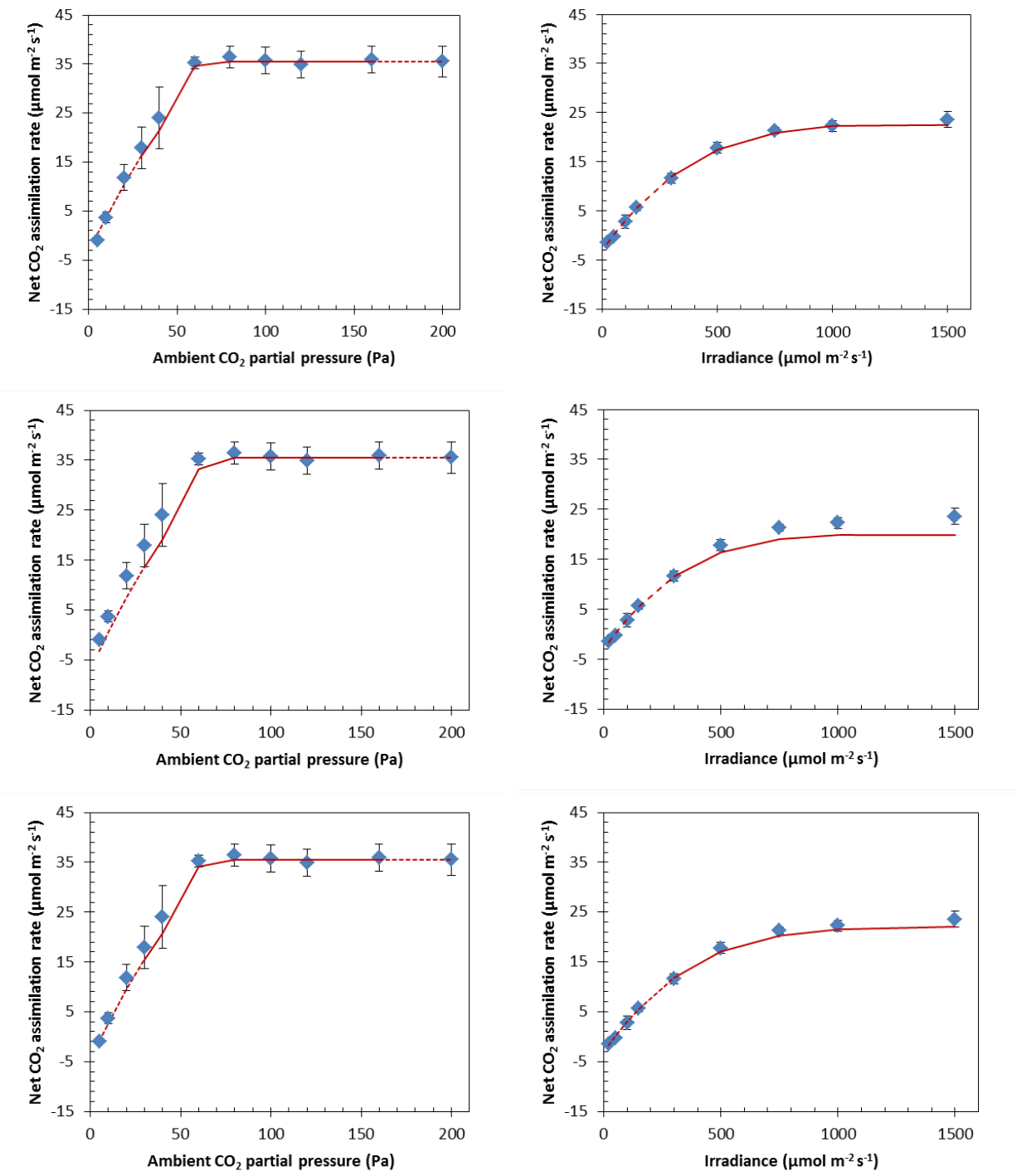

Figure 4.2: Measured (symbols) and simulated (lines) $A - C_a$ (left) and $A - I_{inc}$ (right) curves for different scenarios for the location of (photo)respiratory CO_2 release. The error bars represent one standard deviation. In the simulated $A - C_i$ curves, (photo)respiration either takes place in the inner cytosol (upper panels), in the outer cytosol (middle panels) or in the cytosol gaps (lower panels). The solid line represents the predicted net CO_2 assimilation rates for values of C_a and I_{inc} that were neither used in the estimation procedure of R_d and V_{cmax} nor for the determination of T_p. The dashed lines connect the predicted net CO_2 assimilation rates under the remaining values of C_a and I_{inc} with the solid curve.

4.3.3 CO_2 concentration profiles

Fig. 4.3 shows CO_2 concentration profiles at ambient CO_2 levels ($C_a = 40$ Pa) and saturating light ($I_{inc} = 1500\ \mu mol\ m^{-2}\ s^{-1}$) for three scenarios. It is assumed that (photo)respiratory CO_2 is released in the inner cytosol (Fig. 4.3A), in the outer cytosol (Fig. 4.3B) or in the cytosol gaps (Fig. 4.3C). If CO_2 is released in the outer cytosol, the CO_2 partial pressure decreases along the diffusion pathway from the cell wall to the tonoplast. If CO_2 is released in the inner cytosol or in the cytosol gap, the CO_2 partial pressure also decreases along the diffusion pathway from the cell wall to near the inner chloroplast envelope. However, in these two scenarios, it slightly increases again in the inner cytosol (Fig. 4.3).

4.3.4 Re-assimilation of CO_2

The fraction of re-assimilation of CO_2 produced by (photo)respiration, f_{rec}, was calculated under ambient CO_2 levels ($C_a = 40$ Pa) and saturating light ($I_{inc} = 1500\ \mu mol\ m^{-2}\ s^{-1}$). The highest values for f_{rec} were obtained if (photo)respired CO_2 release took place in the inner cytosol ($f_{rec} = 0.75$). The lowest values were obtained if it took place in the outer cytosol ($f_{rec} = 0.56$). If it took place in the cytosol gap, $f_{rec} = 0.69$.

4.4 Discussion

In this study, a microstructural model for photosynthesis was developed based on a simplified geometry of a mesophyll cell consisting of three layers (outer cytosol, chloroplasts, inner cytosol) (Fig. 4.1). The microstructural model was parameterized by the measured leaf anatomical properties S_c/S_m, t_{cyt}, and t_{str} (Table 4.3), which were determined from transmission electron microscopic images (Chapter 3), and an assumed value for the aspect ratio of a chloroplast. Within the microstructural model, a reaction-diffusion model was solved for CO_2. The model was used directly to estimate the parameters R_d and V_{cmax} for each scenario of (photo)respired CO_2 release. By estimating R_d with the model, the estimation method does not make the assumption

A)

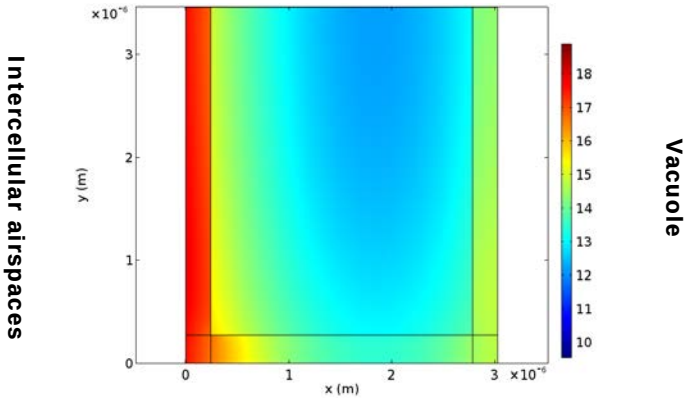

B)

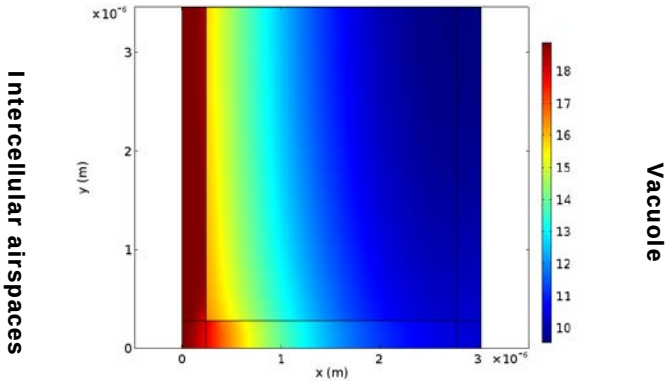

C)

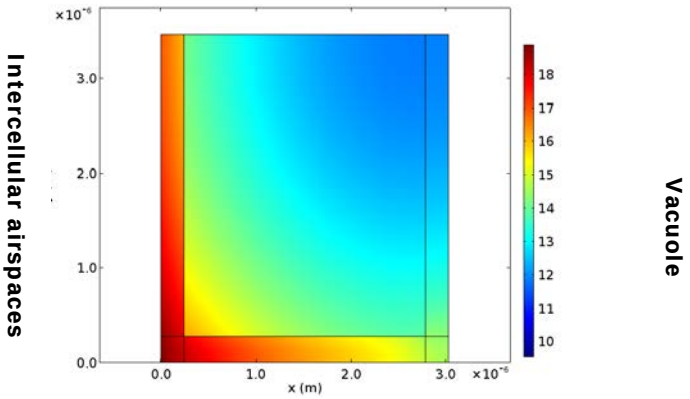

Figure 4.3: CO_2 partial pressure profile within half the computational domain at $C_i = 25$ Pa levels and saturating light ($I_{inc} = 1500$ µmol m^{-2} s^{-1}). The color bar displays partial pressures (Pa). (Photo)respired CO_2 is produced in either the inner cytosol (A), the outer cytosol (B), or the cytosol gaps (C).

that there is no re-assimilation of (photo)respired CO_2, which is made implicitly in simpler models to estimate R_d (Kok, 1948, 1949; Laisk, 1977; Yin *et al.*, 2009; Yin *et al.*, 2011). Current models for mesophyll resistance models either made the implicit assumption that CO_2 release by (photo)respiration takes place in the stroma itself (Harley *et al.*, 1992a; Ethier and Livingston, 2004; Pärnik and Keerberg; Yin *et al.*, 2009), in the outer cytosol (Chapter 3) or that there is no CO_2 gradient in the cytosol (Tholen *et al.*, 2012; Tholen *et al.*, 2014). By estimating V_{cmax} with the 2-D model, the estimation method also avoids the assumption that respiration, photorespiration and RuBP carboxylation take place in the same compartment.

The model was validated by comparing the predicted A_N with measurements for A_N that were not used for estimation of R_d and V_{cmax} or the determination of T_p (Fig. 4.2). The model described the data well for both the light and the CO_2 response curves, if it is assumed that (photo)respiratory CO_2 release takes place in the inner cytosol. In the other two simulated cases for the location of (photo)respiration (outer cytosol and cytosol gap), the model tended to predict lower values for the net CO_2 assimilation rate for high light levels and/or low CO_2 levels than in the case of (photo)respiratory CO_2 release in the inner cytosol. The estimate of V_{cmax} for the scenario that assumes release of (photo)respired CO_2 in the cytosol gaps is higher than in the scenario that assumes release of (photo)respired CO_2 in the inner cytosol (Table 4.4). An explanation for the difference between both V_{cmax} estimates is that the model that assumes (photo)respired CO_2 release in the cytosol gaps attempts to compensate the shorter diffusion path for (photo)respired CO_2 with a more efficient RuBP carboxylation. The very high standard error in the scenario of the model that assumes (photo)respired CO_2 release in the outer cytosol suggests that V_{cmax} cannot be properly estimated by this scenario. An explanation is that the model cannot sufficiently compensate the short length of the diffusion path by increasing the efficiency of RuBP carboxylation by estimating a higher V_{cmax} value. These results suggests that CO_2 release by (photo)respiration is more likely to take place in the inner cytosol or the cytosol gaps than in the outer cytosol.

After validation, the model was extended to allow simulating the transport, consumption and production of $^{12}CO_2$ and $^{13}CO_2$ simultaneously. This approach allowed us to implement *in silico* experiments to determine the percentage for re-assimilation of CO_2 produced by (photo)respiration. Our results show that the re-assimilation percentage varied from 56% to 75%, on the scenario. The range of reported values for f_{rec} in literature is large. Haupt-Herting *et al.* (2001) determined that 23%-29% of the (photo)respired CO_2 is recycled. However, this percentage is likely underestimated, because they assumed in their calculations that the ratio of the concentrations $^{12}CO_2$ to $^{13}CO_2$ in the intercellular air space is the same as in the chloroplasts, which is very unlikely (Ho *et al.*, 2016). Tholen *et al.* (2012) used a resistance model to calculate that this percentage is between 25% and 40% in tobacco. However, they assumed that the CO_2 concentration is completely mixed throughout the cytosol. Results from our study clearly show that this is not the case (Fig. 4.3). Loreto *et al.* (1999) found that 100% of the (photo)respired CO_2 is re-assimilated in tomato and over 80% is re-assimilated in a number of other species. Pärnik and Keerberg (2007) found re-assimilation percentages between 14% and 18% in sunflower and rye and between 42% and 50% in wheat. This summary shows that the range of possible values for f_{rec} is considerable and that the use of different species, and methodologies and their assumptions affects the calculated or measured value of f_{rec}. In future research, this model can be used to determine f_{rec} for different species without these assumptions.

An advantage of the 2-D model presented in this study is that it does not require to determine mesophyll resistances, because several factors that determine mesophyll resistance are explicitly modelled. However, the model requires a number of assumed values of diffusion coefficients and permeabilities of several mesophyll cell compartments. The permeability of both the plasma membrane and the chloroplast envelope was adopted from (Gutknecht *et al.*, 1977). We assumed that this permeability lumps the permeability for CO_2 of aquaporins and the phospholipid bilayer in these membranes (Terashima *et al.*, 2006). We also assumed that the permeability of the chloroplast envelope is twice as low as the plasma membrane.

Values for the effective porosity of the cell wall $p_{\text{eff,wall}}$ were adopted from Fanta *et al.* (2012) and effective diffusion coefficients from the stroma and cell wall from Ho *et al.* (2016). Since there are only a very few measurements of these assumed diffusive properties and permeabilities available (Evans *et al.*, 2009), it can be argued that these uncertainties can result in large errors in the predicted net CO_2 assimilation rate. Nevertheless, validation of the model showed that the model predicted the net CO_2 assimilation rate reasonably well for both the case that (photo)respiration takes place in the inner cytosol and in the cytosol gap (Fig. 4.2). This suggests that even though each single assumed permeability or diffusion coefficient can be biased, the combination of these assumptions results in reasonable predictions of light and CO_2 response curves.

Compared with other recent reaction-diffusion models for CO_2 transport in leaves (Tholen and Zhu, 2011; Watté *et al.*, 2015; Ho *et al.*, 2016), we made a number of simplifications in both the modelled leaf structure and in the processes. These simplifications are as follows. (i) The compartment in which (photo)respiratory CO_2 is released is a compartment in which mitochondria and cytosol are lumped, rather than modelling individual mitochondria like (Tholen and Zhu, 2011) did. (ii) It is assumed that the resistance of the intercellular air space is negligible, rather than explicitly model the intercellular air space like (Ho *et al.*, 2016). (iii) The leaf model is 2-D, instead of 3-D as was done by Ho *et al.* (2016) and Tholen and Zhu (2011) did. (iv) The leaf structure is reduced to simple geometrical shapes. (v) The light absorption gradient is not explicitly modelled like Watté *et al.* (2015) and Ho *et al.* (2016) did. (vi) The activity of carbonic anhydrases is lumped in the apparent diffusion coefficient of the stroma and the cytosol, rather than modelling its activity and HCO_3^- transport explicitly. We have made these simplifications, because adding more complexity requires also additional assumed parameter values, that cannot easily be measured. Adding complexity will also make the model less flexible and more computational demanding, which makes the model cumbersome and unattractive to use. Nevertheless, any of these simplifications can potentially have a substantial impact on the predictions. We therefore checked how these simplifications may affect

the predicted net CO_2 assimilation rate. We investigated simplification (1) in supplementary material 5 where we presented a modified version of the model in which we modelled individual mitochondria explicitly and compared the predicted net CO_2 assimilation rate and f_{rec} with the predictions of the default model. We saw that modelling loose mitochondria barely changes these predictions. The assumption of no CO_2 gradient in the intercellular air space (2) is reasonable for tomato leaves. The intercellular air space in tomato leaves are highly interconnected (Verboven *et al.*, 2015). This high interconnectivity, combined with the fact that the diffusion coefficient of CO_2 in air is about 10^4 times as large as in water at room temperature (Nobel, 2009), makes it very unlikely that there is a CO_2 gradient in the intercellular air space in tomato leaves or any other homobaric leaf with highly interconnected air space. This was demonstrated by Aalto and Juurola (2002). They used a 3-D model to simulate CO_2 diffusion in both the intercellular air space and within mesophyll cells. There was only a stomatal pore modelled at the abaxial leaf surface. They found that the CO_2 concentration difference between the upper and lower boundary was less than 0.1%. In order to discuss the impact of modelling a 2-D leaf structure (3), instead of 3-D leaf structure, we will first discuss potential problems of a 2-D approach and then how we dealt with these issues. If a digitized transversal leaf image is used as a computational domain (Pachepsky *et al.*, 1995; Ho *et al.*, 2012), it is implicitly assumed that the length ratio of the exposed mesophyll surface area to the length of the section L_{m}/L, measured from leaf transversal sections, equals S_{m}/S. This assumption will result in the underestimation of the exposed mesophyll surface available for CO_2 uptake (Thain, 1983; Evans *et al.*, 1994) and, thereby, the net CO_2 assimilation rate. In our model, we dealt with this issue by modelling the leaf as a rectangular geometry in two dimensions and assuming that each of the leaf anatomical parameters (t_{wall}, t_{cyt}, t_{str}, q, $S_{\mathrm{c}}/S_{\mathrm{m}}$, S_{m}/S) does not change in the direction of the third dimension. A consequence of this 2-D approach is that air spaces seem isolated if they are not in 3-D space. Another assumption of a 2-D reaction model from a previous study (Ho *et al.*, 2012b) was that air spaces that seemed isolated in 2-D microscopic images from transversal leaf sections were also isolated in three dimensional space. This makes these the mesophyll surface exposed to these isolated

air spaces unavailable for CO_2 uptake, which lower the net CO_2 assimilation rate even more. Ho *et al.* (2012b) solved these two limitations by estimating the diffusion coefficients for CO_2 in the epidermis and the cell wall from gas exchange measurement data. This resulted in diffusion coefficients for CO_2 that were about 100 times as large as water. Although applying these diffusion coefficients resulted in a reasonable fit of gas exchange measurements with simulated $A_N - C_i$ and $A_N - I_{inc}$ curves, their concentration profiles show that the cell wall and the interface between the epidermal cells and the mesophyll cells are a major diffusion pathways for CO_2, which is very unlikely. In the current 2-D model, the issue of isolated air spaces solved by assuming that the resistance for CO_2 transport in the intercellular air space is negligible and by implementing stomatal conductance in the boundary conditions of the outer border of the computational domain. In supplementary material 6, we checked whether our other assumptions, namely, the reduction of the leaf structure to simple geometrical shapes (4) and not explicitly modelling the light gradient (5) and carbonic anhydrase activity (6), affect the predicted net CO_2 assimilation rate. We did so by comparing simulated $A - C_a$ curves modelled by a complex 3-D model that does not have any of these simplifications (Ho *et al.*, 2016) with $A - C_a$ curves modelled by the model from this study. The net CO_2 assimilation rates were about the same. All these analyses above show that the simplifications in our model, at least for tomato, do not affect the predictions of the net CO_2 assimilation rate.

To the best of our knowledge, this study is the first attempt to directly assess how the localization of released CO_2 produced by (photo)respiration could affect both the net rate of CO_2 assimilation and re-assimilation. This is important, because previous resistance models (Harley *et al.*, 1992a; Yin *et al.*, 2009; Tholen *et al.*, 2012; Tholen *et al.*, 2014; Yin *et al.*), and the model described in Chapter 3, make implicit assumptions about the location of (photo)respiration or about the CO_2 gradients in the cytosol. A finding of our study is that it is unlikely that (photo)respiratory CO_2 release takes place in the outer cytosol and also that it is unlikely that there is no CO_2 gradient in the cytosol. Additionally, none of the aforementioned models allows to model CO_2 diffusion through the gaps between the chloroplasts, which can affect the predicted net

CO_2 assimilation rate and about the re-assimilation of CO_2. Since the parameter estimates in this study are directly estimated by the model, for each estimate it is clear what the assumed location of (photo)respiration is. As far as the authors know, the only attempt in which a reaction diffusion model is directly used to estimate FvCB parameters is described by Juurola *et al.* (2005). They estimated parameters for the FvCB model and parameters for the temperature response of these FvCB model parameters by both a 3-D model (Aalto and Juurola, 2002) and by a simple photosynthesis model (Aalto and Juurola, 2001). They found that the estimates can be quite different, because their 3-D model is capable of partitioning the temperature response of photosynthesis due to physical (solubility of CO_2 in the liquid phase, temperature response of the diffusion coefficient of CO_2 in water) and biochemical (temperature dependency of kinetic constants of Rubisco) parameters. Our model also has the capability to distinguish how CO_2 transport is affected by biochemical processes and leaf structural barriers. Therefore it can be interesting to use the model in future research to re-examine the temperature response of various photosynthetic parameters. It would also be interesting to further validate the model for other tomato cultivars, species and environmental conditions and subsequently investigate how this affects the re-assimilation of (photo)respired CO_2 and the estimates of photosynthetic parameters. Finally, the results of the validation of the 2-D model in this study suggest that it is possible to simplify both the structures and the processes, while the model still is capable of predicting the net CO_2 assimilation well.

Acknowledgements

Wageningen based authors thank the BioSolar Cells programme (project C3B3) for financial support. Leuven based authors thank the Research Council of the KU Leuven (project OT 12/055) for financial support. The authors thank Ruud Börger (COMSOL BV, Zoetermeer, The Netherlands), Durk de Vries (COMSOL BV, Zoetermeer, The Netherlands) and Tycho van Noorden (COMSOL Multiphysics BV, Zoetermeer, The Netherlands) for their advices to construct the model presented in this study. The authors also want to thank dr. Steven Driever (Wageningen UR, Centre for Crop Systems Analysis, Wageningen, The Netherlands) for useful discussions on isotope

discrimination and re-assimilation, and Alejandro Morales Sierra MSc and Laurens Krah BSc for comments on an early version of the manuscript.

Appendix 4.1: Construction of the 2-D computational domain

The computational domain represents a section of a mesophyll cell that contains a single chloroplast surrounded by cytosol. It consists of an $l \times h$ rectangle Ω_0 with boundaries Γ_1 (length l), Γ_2 (length h), Γ_3 (length l), and Γ_4 (length h). Boundary Γ_2 represents the tonoplast. Boundary Γ_4 represents the combined cell wall and plasma membrane (Fig. A4.1.1).

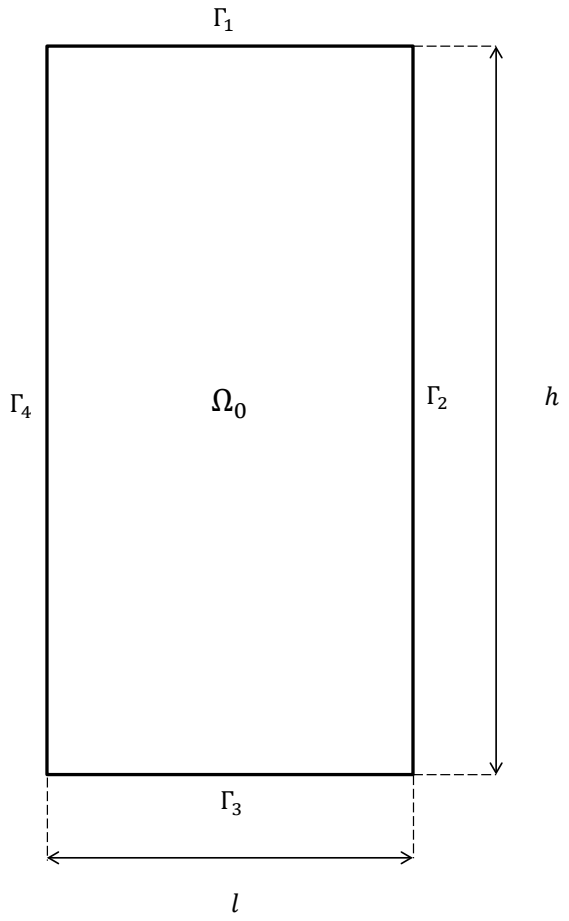

Figure A4.1.1: Schematic drawing of the $l \times h$ computational domain Ω_0 and its outer edges Γ_1, Γ_2, Γ_3, and Γ_4, before compartmentation. Γ_2 represents the tonoplast and Γ_4 represents the cell wall and the plasma membrane. Γ_1 and Γ_3 represent the upper and the lower edges of the computational domain.

Ω_0 was subdivided into three rectangular subdomains Ω_1, Ω_2, and Ω_3. The dimensions of Ω_1, Ω_2, and Ω_3 are $t_{\mathrm{cyt}} \times h$, $t_{\mathrm{str}} \times h$ and $t_{\mathrm{cyt}} \times h$ respectively, where t_{cyt} represents

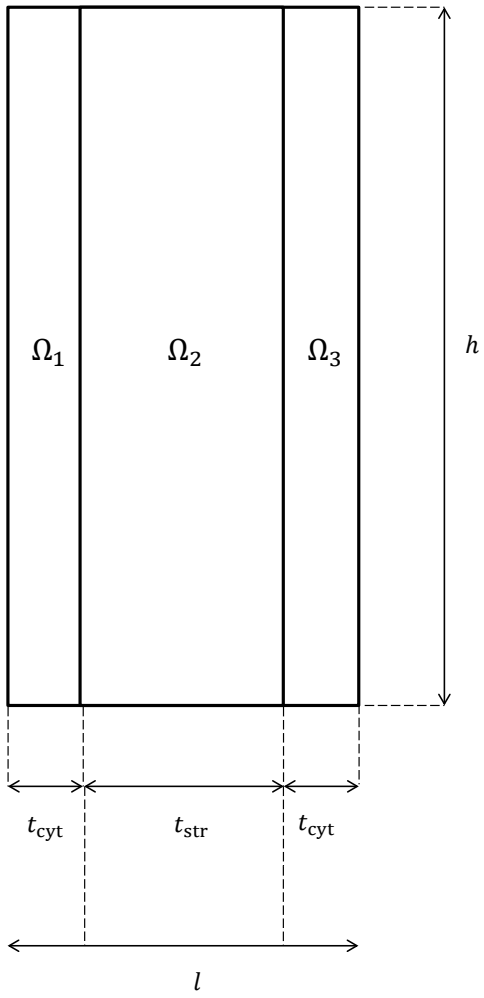

Figure A4.1.2: Schematic drawing of the computational domain, after compartmentation of Ω_0 into inner cytosol compartment Ω_1 and outer cytosol compartment Ω_3 , and a subdomain Ω_2 between Ω_1 and Ω_3

the thickness of the cytosol and t_{str} represents the thickness of the stroma. Subdomain Ω_1 represents the outer cytosol. Subdomain Ω_3 represents the inner cytosol. Subdomain Ω_2 lies between Ω_1 and Ω_3 (Fig. A4.1.2).

Ω_2 was further subdivided into a rectangular stroma compartment Ω_4 and two half rectangular cytosol gaps Ω_5 and Ω_6. The two $t_{\mathrm{str}} \times \frac{1}{2} h_{\mathrm{gap}}$ half cytosol gaps Ω_5 and Ω_6 are adjacent to Γ_1 and Γ_3, respectively. The remaining part of Ω_2 consists of the $t_{\mathrm{str}} \times h_{\mathrm{str}}$ stroma compartment Ω_4. The boundaries of the stroma compartments form the chloroplast envelope. Supplementary Fig. A4.1.3 shows the final geometry of the computational domain.

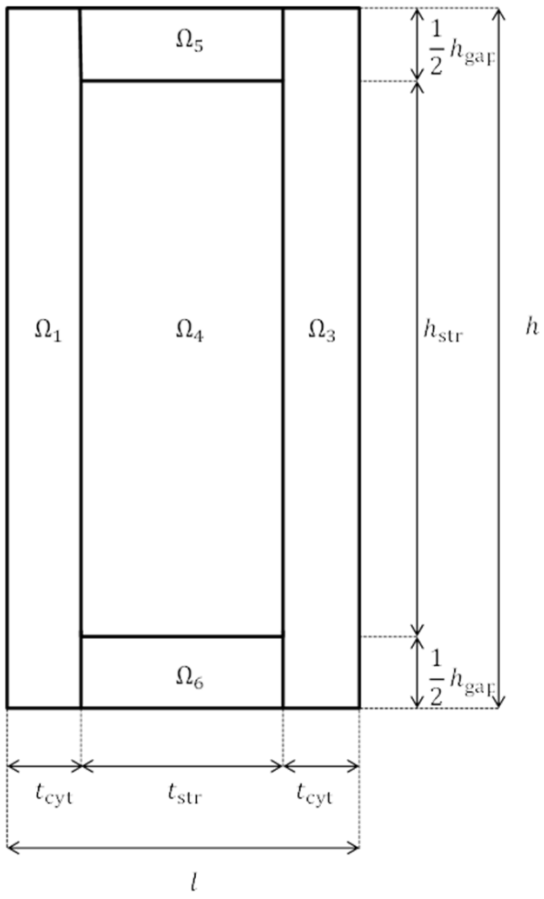

Figure A4.1.3: Schematic drawing of the computational domain, after compartmentation of Ω_2 into a stromal compartment Ω_4 and two cytosol gaps Ω_5 and Ω_6.

Appendix 4.2: Parameterization of the 2-D computational domain

Several studies use measurements of t_{cyt} and t_{str} to quantify the resistance of the cytosol and stroma, respectively. Some studies also describe the measurements of $S_{\mathrm{c}}/S_{\mathrm{m}}$, the ratio of the chloroplast surface area facing the intercellular air space to the mesophyll surface area facing the intercellular air space. This ratio is a measure to what extent the exposed mesophyll surface is covered with chloroplasts. The aim of this section is to design a flexible geometry that can be generated by different combinations of values for anatomical parameters t_{str}, t_{cyt}, and $S_{\mathrm{c}}/S_{\mathrm{m}}$. For this purpose, the length of a number of boundaries (h, h_{gap}, h_{str}) in Fig. A4.1.3 has to be written as a function of these parameters.

A4.2.1 Parameterization h_{str}

The height of the stroma compartment h_{str} can be written as a function of t_{str}:

$$h_{\mathrm{str}} = q t_{\mathrm{str}} \tag{A4.2.1}$$

A4.2.2 Parameterization h_{gap}

It our model, it is a assumed that the 2-D computational domain is a cross section of a 3-D rectangular cuboid. Therefore, the ratio of length of the chloroplast exposed to the intercellular air space to the length of the mesophyll exposed to the intercellular air space is:

$$\frac{h_{\mathrm{str}}}{h} = \frac{q t_{\mathrm{str}}}{h} = \frac{S_{\mathrm{c}}}{S_{\mathrm{m}}} \tag{A4.2.2}$$

which can be rewritten as:

$$h = \left(\frac{S_\mathrm{c}}{S_\mathrm{m}}\right)^{-1} q t_\mathrm{str} \tag{A4.2.3}$$

From equations (A4.2.1) and (A4.2.2), the height of the gaps between two chloroplast can be expressed as:

$$h_\mathrm{gap} = h - h_\mathrm{str} = \left(\left(\frac{S_\mathrm{c}}{S_\mathrm{m}}\right)^{-1} - 1\right) q t_\mathrm{str} \tag{A4.2.4}$$

A4.2.3 Parameterization l

The distance l between the cell wall and the tonoplast of the computational domain can be expressed as:

$$l = 2t_\mathrm{cyt} + t_\mathrm{str} \tag{A4.2.5}$$

Appendix 4.3: Parameterization of volume to volume and area to volume ratios

The process model contains several rate parameters and variables, expressed in mol m^{-3} s^{-1}. In this study, these parameters are called "volumetric rate parameters". These volumetric rate parameters are the rates of CO_2 production by respiration in the light and photorespiration (r_d and r_p), the maximum rate of RuBP carboxylation (v_cmax), the Rubisco limited rate of RuBP carboxylation (w), the rate of electron transport (j), and the rate of triose phosphate utilization (t_p) These parameters can be calculated from the parameters W, R_d, R_p, V_cmax, J, and T_p. These parameters can be determined by combined gas exchange and chlorophyll fluorescence measurements and are expressed in mol m^{-2} leaf s^{-1}. In this study, the volumetric rate parameters need to be calculated from some of the rate parameters expressed in mol m^{-2} leaf s^{-1}, and *vice versa*. For this purpose, the volumes of the compartments in the computational domains, in which each process takes place, need to be expressed mathematically.

4.3.1 Parameterization of area to volume fractions

Since it is assumed that the 2-D computational domain is a cross section of a rectangular cuboid, the total volume of chloroplasts is equal to $S_\mathrm{c} t_\mathrm{str}$, Here, S_c is the total surface area of chloroplast exposed to the intercellular air space for a leaf area S. The ratio of the leaf area to the chloroplast volume could be expressed as:

$$\frac{S}{V_\mathrm{str}} = \frac{S}{t_\mathrm{str} S_\mathrm{c}} = \frac{1}{t_\mathrm{str}} \left(\frac{S_\mathrm{m}}{S}\right)^{-1} \left(\frac{S_\mathrm{c}}{S_\mathrm{m}}\right)^{-1} \quad \text{(A4.3.1)}$$

Similarly, the volume of either the inner or the outer cytosol can be expressed as $S_\mathrm{m} t_\mathrm{cyt}$. Here, S_m is the total surface area of mesophyll exposed to the intercellular air space for a leaf area S. The ratio of the leaf area to either the inner or the outer cytosol volume can be expressed as:

Table A4.3.1: Overview of volume to volume, area to volume, length to area fractions, and length to length ratios used for the sensitivity analysis for $t_{\mathrm{cyt,in}}$ and $t_{\mathrm{cyt,out}}$

Symbol	Unit	Mathematical expression	Meaning of ratios
q	-	$\frac{h_{\mathrm{str}}}{t_{\mathrm{str}}}$	Stroma height to stroma thickness
$\frac{S}{V_{\mathrm{c}}}$	m^{-1}	$\frac{1}{t_{\mathrm{str}}}\left(\frac{S_{\mathrm{m}}}{S}\right)^{-1}\left(\frac{S_{\mathrm{c}}}{S_{\mathrm{m}}}\right)^{-1}$	Leaf area to total chloroplast volume
$\frac{S}{V_{\mathrm{cyt,in}}}$	m^{-1}	$\frac{1}{t_{\mathrm{cyt,in}}}\left(\frac{S_{\mathrm{m}}}{S}\right)^{-1}$	Leaf area to total volume inner cytosol
$\frac{S}{V_{\mathrm{cyt,out}}}$	m^{-1}	$\frac{1}{t_{\mathrm{cyt,out}}}\left(\frac{S_{\mathrm{m}}}{S}\right)^{-1}$	Leaf area to total volume outer cytosol

$$\frac{S}{V_{\mathrm{cyt,inner}}} = \frac{S}{V_{\mathrm{cyt,outer}}} = \frac{S}{t_{\mathrm{cyt}} S_{\mathrm{m}}} = \frac{1}{t_{\mathrm{cyt}}}\left(\frac{S_{\mathrm{m}}}{S}\right)^{-1} \tag{A4.3.2}$$

Since the cytosol gaps are also rectangular cuboids, we can express the ratio of the leaf area to the cytosol gap as:

$$\frac{S}{V_{\mathrm{gap}}} = \frac{S}{t_{\mathrm{str}}(S_{\mathrm{m}} - S_{\mathrm{c}}) =} = \left(t_{\mathrm{str}}\frac{S_{\mathrm{m}} - S_{\mathrm{c}}}{S}\right)^{-1} = \left(t_{\mathrm{str}}\left(\frac{S_{\mathrm{m}}}{S} - \frac{S_{\mathrm{c}}}{S_{\mathrm{m}}}\frac{S_{\mathrm{m}}}{S}\right)\right)^{-1} \tag{A4.3.3}$$

$$= \frac{1}{t_{\mathrm{str}}}\left(\frac{S_{\mathrm{m}}}{S}\left(1 - \frac{S_{\mathrm{c}}}{S_{\mathrm{m}}}\right)\right)^{-1}$$

Appendix 4.4 Sensitivity analysis of f_{rec} and A_N to $t_{cyt,in}$ and $t_{cyt,out}$

In the main text, it is assumed that $t_{cyt,in} = t_{cyt,out} = t_{cyt}$ and that the thickness of the cytosol compartments equals the ones measured from TEM images. Mitochondria compartments were not modelled explicitly, because this would increase the computational time considerably and because the dimensions of mitochondria are very uncertain. It was not possible to systematically measure the thickness from the TEM images from Chapter 3, because the mitochondria were often hard to distinguish from the cytosol or from other organelles. As far as the authors know, there have been no previous studies that systematically measured the dimensions of mitochondria in mesophyll cells. Some sample images from a number of studies (Busch *et al.*, 2013; Gielwanowska *et al.*, 2015; Moser *et al.*, 2015) suggest that these dimensions can vary considerably. In some cases, the thickness reported is larger than the assumed cytosol thicknesses in this study. In this section, a sensitivity analysis will be done for $t_{cyt,in}$ and $t_{cyt,out}$ to assess how uncertainty in the thickness of the inner and the outer cytosol could affect the net CO_2 assimilation rate and the re-assimilation of (photo)respired CO_2.

A4.4.1 Re-parameterization of the geometry

In order to conduct sensitivity analyses for $t_{cyt,in}$ and $t_{cyt,out}$ separately, it can no longer be assumed that $t_{cyt,in} = t_{cyt,out} = t_{cyt}$. This has implications for all parameterized ratios in Table 4.2 that depend on the cytosol thickness. First, $t_{cyt,inner}$ was substituted for t_{cyt} in the mathematical term for the ratio $S/V_{cyt,inner}$. Second, substituted $t_{cyt,out}$ was substituted for t_{cyt} in the term for the ratio $S/V_{cyt,out}$. Supplementary table S1 shows the updated mathematical terms for all volume to volume, length to volume and surface to volume ratios.

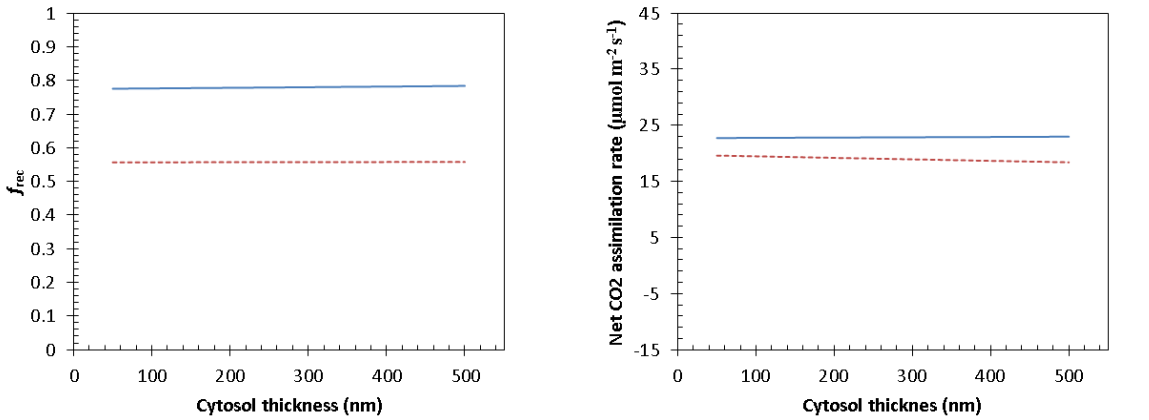

Figure A4.4.1: Simulated values of f_{rec} (left) and the net CO_2 assimilation rate (right) for different cytosol thicknesses, under the condition of ambient CO_2 (C_a = 40 Pa) and O_2 (O = 21 kPa) and saturating light levels (I_{inc} = 1500 µmol m^{-2} s^{-1}). The solid lines represent simulations assuming that (photo)respiratory CO_2 is released in the inner cytosol. The dashed lines are simulations which assume (photo)respiratory CO_2 release in the outer cytosol.

A4.4.2 Sensitivity analysis of A_N and f_{rec} to $t_{cyt,in}$ and $t_{cyt,out}$

For this analysis, the net CO_2 assimilation rate under ambient CO_2 and O_2 levels and saturating light levels was simulated for two scenarios. (Photo)respiratory CO_2 release takes either place in the inner or in the outer cytosol. During this analysis, the thickness (either $t_{cyt,inner}$ or $t_{cyt,outer}$) of the compartment in which (photo)respiration was assumed to take place was varied. Fig. A4.4.1A shows these simulated values of A_N. Additionally, a sensitivity analysis of f_{rec} was done under ambient CO_2 ($C_a = 40$ Pa) and saturating light ($I_{inc} = 1500$ µmol m^{-2} s^{-1}) by varying either $t_{cyt,in}$ or $t_{cyt,out}$. Fig. A4.4.1B shows the result of this analysis. f_{rec} and A_N hardly change with an increase in $t_{cyt,inner}$. Additionally, f_{rec} hardly changes with an increase in $t_{cyt,outer}$. f_{rec} does decrease with an increase in $t_{cyt,outer}$, but the rate of decrease is relatively low.

Appendix 4.5: Modelling individual mitochondrial compartments

In the main text, loose mitochondria are not modelled explicitly. Instead, the cytosol compartment in which (photo)respiration takes place (inner cytosol, outer cytosol or gap) is lumped with the mitochondria. The volume, in which (photo)respiration takes place, is larger than in the case in which loose mitochondria would have been modelled within this compartment. The volumetric rates of (photo)respiration r_{d} and r_{p} may therefore be underestimated, which can lead to an overestimation of the re-assimilation fraction of CO_2 produced by (photo)respiration. In this section, it is described how loose mitochondria can be added to the model to see to what extent distinguishing the cytosol and the mitochondria may affect the predicted net CO_2 assimilation rates and the fraction of re-assimilated (photo)respired CO_2.

4.5.1 Reconstruction 2-D computational domain

The 2-D computational domain was reconstructed as described in Supplementary texts 1 and 2 to obtain the geometry shown in Fig. A4.1.3. Two loose mitochondria were modelled as $\frac{1}{2}t_{\mathrm{cyt}} \times \frac{1}{2}qt_{\mathrm{cyt}}$ rectangular subdomains Ω_7 and Ω_8. We placed the left bottom corner of Ω_7 at different positions $(x_{\mathrm{p}}, y_{\mathrm{p}})$ in either the inner or the outer cytosol. The left bottom corners of mitochondria Ω_7 and Ω_8 were placed at locations (See also Fig. A4.5.1):

A). Ω_7: $(x_{\mathrm{p}}, y_{\mathrm{p}}) = \left(\frac{5}{4}t_{\mathrm{cyt}} + t_{\mathrm{str}}, \frac{1}{2}h_{\mathrm{gap}}\right)$

Ω_8: $(x_{\mathrm{p}}, y_{\mathrm{p}}) = \left(\frac{5}{4}t_{\mathrm{cyt}} + t_{\mathrm{str}}, \frac{1}{2}h_{\mathrm{gap}} + h_{\mathrm{str}} - \frac{1}{2}qt_{\mathrm{cyt}}\right)$

B). Ω_7: $(x_{\mathrm{p}}, y_{\mathrm{p}}) = \left(\frac{1}{4}t_{\mathrm{cyt}}, \frac{1}{2}h_{\mathrm{gap}}\right)$

Ω_8: $(x_{\mathrm{p}}, y_{\mathrm{p}}) = \left(\frac{1}{4}t_{\mathrm{cyt}}, \frac{1}{2}h_{\mathrm{gap}} + h_{\mathrm{str}} - \frac{1}{2}qt_{\mathrm{cyt}}\right)$

C). Ω_7: $(x_\mathrm{p}, y_\mathrm{p}) = \left(\frac{5}{4}t_\mathrm{cyt} + t_\mathrm{str}, \frac{1}{2}h_\mathrm{gap} + \frac{1}{2}h_\mathrm{str} - \frac{1}{2}qt_\mathrm{cyt}\right)$.

Ω_8: $(x_\mathrm{p}, y_\mathrm{p}) = \left(\frac{5}{4}t_\mathrm{cyt} + t_\mathrm{str}, \frac{1}{2}h_\mathrm{gap} + \frac{1}{2}h_\mathrm{str}\right)$

D). Ω_7: $(x_\mathrm{p}, y_\mathrm{p}) = \left(\frac{1}{4}t_\mathrm{cyt}, \frac{1}{2}h_\mathrm{gap} + \frac{1}{2}h_\mathrm{str} - \frac{1}{2}qt_\mathrm{cyt}\right)$

Ω_8: $(x_\mathrm{p}, y_\mathrm{p}) = \left(\frac{1}{4}t_\mathrm{cyt}, \frac{1}{2}h_\mathrm{gap} + \frac{1}{2}h_\mathrm{str}\right)$

These letters A, B, C, D correspond to the letters in Fig. A4.5.1.

4.5.2 Re-parameterization

In the original model without loose chloroplasts, the volumetric respiration rate r_d was calculated by multiplying R_d by the ratio of the leaf area S to the volume to the compartment V_resp, in which (photo)respiratory CO_2 release is assumed to take place. It was also assumed that the mitochondria and the cytosol are a lumped compartment. The fraction of the leaf area to the total volume, in which (photo)respiratory CO_2 release takes places, S/V_resp, could equal $S/V_\mathrm{cyt,inner}$, $S/V_\mathrm{cyt,outer}$ or $S/V_\mathrm{cyt,gap}$. This depends on the assumed location of (photo)respiratory CO_2 release. Supplementary text 3 contains a derivation of a mathematical formulation of these terms expressed in leaf anatomical properties. For the simulations described in this supplementary material - respiration and (photo)respiration are now restricted to loose mitochondria - it is necessary to further multiply S/V_resp by the fraction of the S/V_mit, which is the fraction of the leaf area to the volume of mitochondria. Since both the compartment in which (photo)respiratory CO_2 release takes place and the mitochondria are modelled as rectangular cuboids and it is further assumed that the mitochondria structure does not change with the third dimension, we express $V_\mathrm{resp}/V_\mathrm{mit}$ as:

$$\frac{V_{\text{resp}}}{V_{\text{mit}}} = \left(\iint_{\text{Respiration default}} \mathrm{d}x\ \mathrm{d}y \right) \left(\iint_{\text{Mitochondria}} \mathrm{d}x\ \mathrm{d}y \right)^{-1} \tag{A4.5.1}$$

where "Respiration default" is the volume in which (photo)respiratory CO_2 release takes place, in the default model in which the mitochondria are not explicitly modelled. In this analysis, two mitochondria are only placed in either the inner cytosol or the outer cytosol. These compartments have, aside from the analysis in Supplementary text 4, the same volume. Since $\iint_{\text{Respiration default}} \mathrm{d}x\ \mathrm{d}y = t_{\text{cyt}}\left(h_{\text{str}} + h_{\text{gap}}\right)$ and $\left(\iint_{\text{Mitochondria}} \mathrm{d}x\ \mathrm{d}y\right)^{-1} = 2 \cdot \frac{1}{2} t_{\text{cyt}} \cdot \frac{1}{2} q t_{\text{cyt}}$, we can express $\frac{V_{\text{resp}}}{V_{\text{mit}}}$ as:

$$\frac{V_{\text{resp}}}{V_{\text{mit}}} = \frac{t_{\text{cyt}}\left(h_{\text{str}} + h_{\text{gap}}\right)}{\frac{1}{2} t_{\text{cyt}} q t_{\text{cyt}}} \tag{A4.5.2}$$

Substitution of equation (A4.2.1) and (A4.2.4) for h_{str} and h_{gap} respectively in equation (A4.5.2), results in:

$$\frac{V_{\text{resp}}}{V_{\text{mit}}} = \frac{t_{\text{cyt}}\left(\left(\left(\frac{S_{\text{c}}}{S_{\text{m}}}\right)^{-1} - 1\right) q t_{\text{str}} + q t_{\text{str}}\right)}{\frac{1}{2} t_{\text{cyt}} q t_{\text{cyt}}} \tag{A4.5.3}$$

which can be rearranged to:

$$\frac{V_{\mathrm{resp}}}{V_{\mathrm{mit}}} = 2\,\frac{t_{\mathrm{str}}}{t_{\mathrm{cyt}}}\left(\frac{S_{\mathrm{c}}}{S_{\mathrm{m}}}\right)^{-1} \qquad \text{(A4.5.4)}$$

4.5.3 Results

The model was used to calculate A_{N} and f_{rec} under saturating light and and ambient CO_2 and O_2 concentrations for each of the simulated positions of the mitochondria mentioned in the section "Reconstruction computational domain". Figs. A4.5.7A-D show the CO_2 concentration profiles and the calculated values of A_{N} and f_{rec} for different positions of loose mitochondria in the outer cytosol (Fig. A4.5.7A-B) and inner cytosol (Fig. A4.5.7C-D). Figs A4.5.7E and AS4.5.7F show the CO_2 concentration profile in A_{N} and f_{rec} for the default model, in which the mitochondria are lumped with either the outer (E) or the inner (F) cytosol compartment. A_{N} and f_{rec} are about the same for the model that assumes (photo)respiratory CO_2 release in the inner cytosol and the model that assumes that this CO_2 release takes place in mitochondria located in the inner cytosol. A_{N} and f_{rec} are also about the same for the model that assumes (photo)respiratory CO_2 release in the outer cytosol and the model that assumes that this CO_2 release takes place in mitochondria located in the outer cytosol. The results suggest that modelling loose mitochondria will not substantially change A_{N} or f_{rec} and can therefore be lumped with the cytosol compartment and the mitochondria.

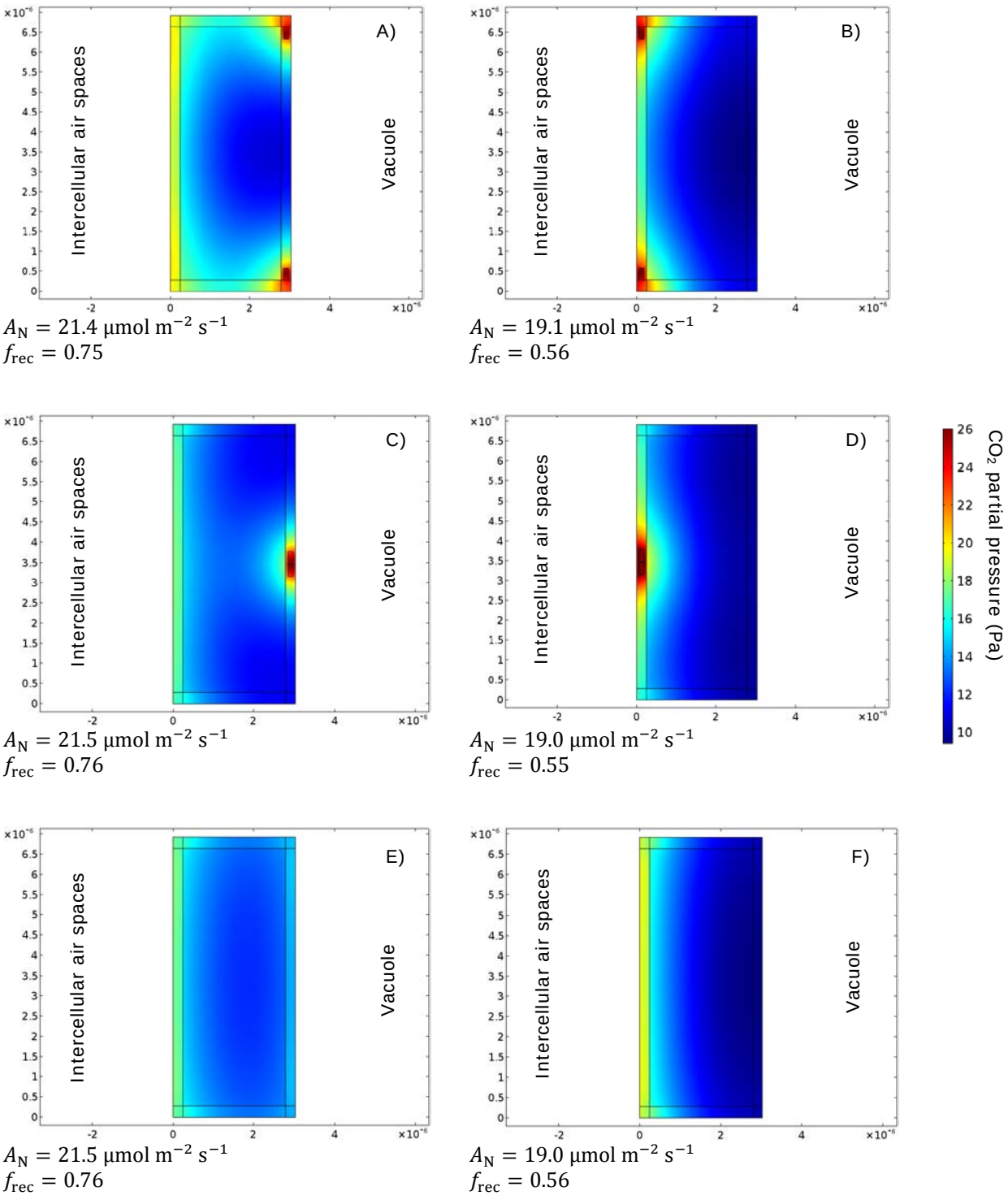

$A_N = 21.4$ µmol m^{-2} s^{-1}
$f_{rec} = 0.75$

$A_N = 19.1$ µmol m^{-2} s^{-1}
$f_{rec} = 0.56$

$A_N = 21.5$ µmol m^{-2} s^{-1}
$f_{rec} = 0.76$

$A_N = 19.0$ µmol m^{-2} s^{-1}
$f_{rec} = 0.55$

$A_N = 21.5$ µmol m^{-2} s^{-1}
$f_{rec} = 0.76$

$A_N = 19.0$ µmol m^{-2} s^{-1}
$f_{rec} = 0.56$

Figure A4.5.1: CO_2 concentration profiles in case loose mitochondria are modelled explicitly (A-D) or if they are lumped with a cytosol compartment (E-F). It is either assumed that loose mitochondria are located in the inner cytosol (A,C) or in the outer cytosol (B,D) or that they are lumped with the inner cytosol (E) or with the outer cytosol (F). The loose mitochondria, if present, are either placed near the cytosol gap (A,C) or as far away as possible from the cytosol gap (B, D) Below each curve, the calculated values of A_N and f_{rec} are displayed.

Appendix 4.6: The impact of simplifications in the leaf geometry and transport processes on A_N and f_{rec}

The model described in the main text of this manuscript makes various simplifications about both the leaf structure and the processes that take place in the leaf. These simplifications are:

1). It is assumed that (photo)respiration takes place in a cytosol compartment, rather than a loose mitochondrion in this compartment

2). It is assumed that the light absorption does not vary with the leaf depth.

3). It is assumed that there is full CO_2 transport facilitation by carbon anhydrase.

4). It is assumed that q, S_m/S, S_c/S_m, t_{wall}, t_{cyt} and t_{str} do not vary in the z-dimension.

In Supplementary text 5, it is already shown that modelling loose mitochondria in either the inner cytosol or outer cytosol hardly affects the values of A_N and f_{rec} predicted by the default model. This demonstrates that, in the case of tomato, simplification 1 is reasonable. The aim of the current supplementary text is to show that the remaining three limitations also will not affect A_N. This will be done by comparing the values of A_N predicted by the model in this study with the values predicted by the model from Ho *et al.* (2016) that does not have simplifications 2,3, and 4.

A4.6.1 Summary description model from Ho *et al.* (2016)

The model described by Ho *et al.* (2016) describes CO_2 transport, production, and consumption in tomato leaves. The leaf geometry is a discretized 3-D tomography (Ho *et al.*, 2016), which was obtained by X-ray synchrotron microscopy (Verboven *et al.*, 2015). Next, the mesophyll cells from the obtained 3-D leaf geometry was compartmented into a chloroplast layer that is exposed to the intercellular air space, a

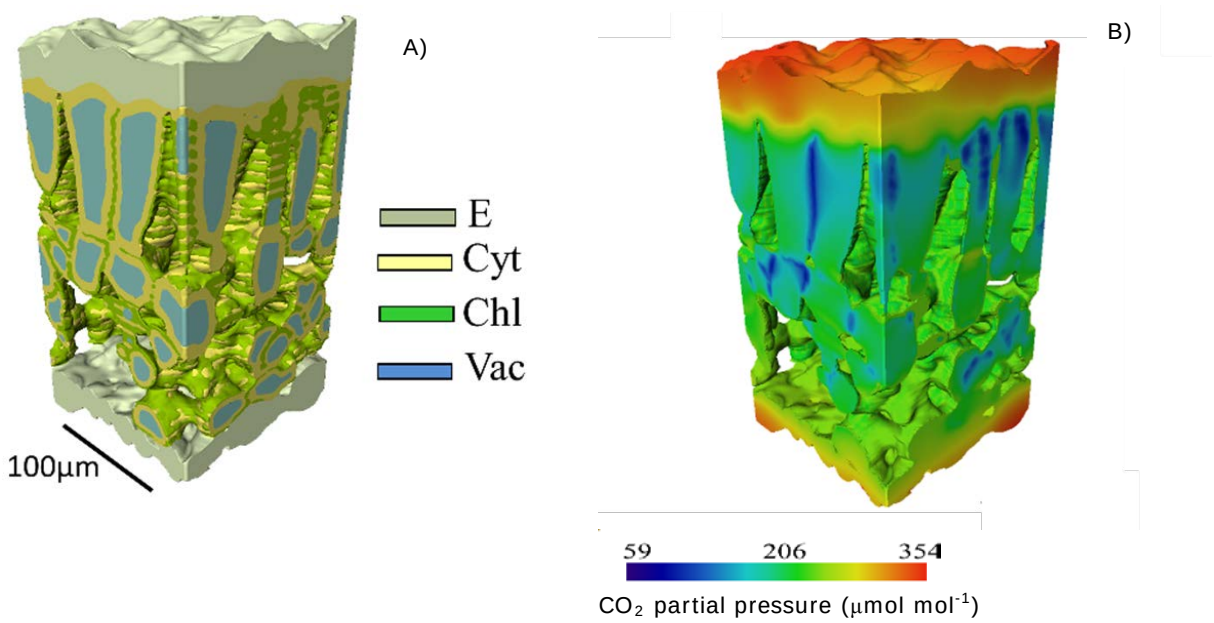

Figure A4.6.1: A) 3D microstructure of the liquid phase of a section of a tomato leaf ("cv Admiro lower leaf"), which is compartmented into epidermis (E), cytosol (Cyt), chloroplasts (Chl) and vacuole (Vac). B) The simulated steady CO_2 concentration profile at $C_a = 380$ µmol mol^{-1}, $O = 210$ mmol mol^{-1}, and $I_{inc} = 1000$ µmol m^{-2} s^{-1}using the microstructure in Fig. A4.6.1A and the reaction-diffusion model. These images are originally published by Ho *et al.* (2016).

cytosol layer, and a vacuole. Finally, the chloroplast layer was subdivided into spherical chloroplasts and cytosol compartments in between. Additionally, the remaining compartments were subdivided into intercellular air space and the epidermis. Fig. A4.6.1A shows how the obtained microstructure looked like. Monte-Carlo ray tracing was applied to calculate the light absorption gradient within this geometry (Watté *et al.*, 2015). Stomatal opening was modelled by making a cylindrical air hole in the epidermis that connects the intercellular air space with the ambient air. This air hole is the stomatal aperture. Over this discretized geometry, a system of partial differential equations for CO_2 transport and HCO_3^- transport were solved. The equations that were used are listed below; the notation of symbols is adjusted in such a way that the notation is the same as the symbols used in the 2-D model from the current study:

$$\nabla \cdot D_{CO_2,gas} \nabla [CO_2] = 0 \qquad \text{(A4.6.1)}$$

$$\nabla \cdot p_{\mathrm{eff,i}} \zeta_{\mathrm{i}} D_{\mathrm{CO_2,water}} \nabla[\mathrm{CO_2}] - w_{\mathrm{i}} + r_{\mathrm{p,i}} + r_{\mathrm{d,i}} - B = 0 \quad \text{(A4.6.2)}$$

$$\nabla \cdot p_{\mathrm{eff,i}} \zeta_{\mathrm{i}} D_{\mathrm{HCO_3,water}} \nabla[\mathrm{HCO_3}] + B = 0 \quad \text{(A4.6.3)}$$

where B is the conversion rate of CO_2 into HCO_3^-. The subscript i indicates that the value depends on the compartment. $D_{\mathrm{CO_2,gas}}$ is the diffusion coefficient of CO_2 in the gas phase.

For the simulations with the 3-D model that are considered in this supplementary text, it is assumed that CO_2 transport is facilitated by carbon anhydrases in the cytosol and the stroma. In the presence of carbon anhydrases, B was represented as (Tholen and Zhu, 2011; Ho *et al.*, 2016):

$$B = \frac{k_{\mathrm{CA}}[\mathrm{CA}]\left([\mathrm{CO_2}] - \frac{[\mathrm{H^+}][\mathrm{HCO_3^-}]}{K_{\mathrm{eq}}}\right)}{K_{\mathrm{CA,CO_2}} + \frac{K_{\mathrm{CA,CO_2}}[\mathrm{HCO_3^-}]}{K_{\mathrm{CA,HCO_3^-}}} + [\mathrm{CO_2}]} \quad \text{(A4.6.4)}$$

where k_{CA}, K_{eq}, and $[\mathrm{CA}]$ are the turnover rate, the equilibrium constant and the concentration of carbon anhydrases respectively. $K_{\mathrm{CA,CO_2}}$ and $K_{\mathrm{CA,HCO_3^-}}$ are the Michaelis-Menten constants of hydration and dehydration, respectively. Equation (A4.6.4) implicitly assumes that the further dehydration of HCO_3^- into CO_3^{2-} is negligible under the pH levels in leaves.

A4.6.2 Quantification parameter values in the 2-D model and in the 3-D model

The parameter values in equation (A4.6.1 - A4.6.4) can be found in the supplementary material of the study from Ho *et al.* (2016). For the simulations in the current study, the same parameter values were used for s, $S_{\mathrm{c\backslash O}}{}^*$, R_{d}, V_{cmax}, and T_{p} as by (Ho *et al.*, 2016). For the anatomical parameters, it was assumed that $S_{\mathrm{m}}/S = 16$, $t_{\mathrm{str}} = 2.5$ µm, and $t_{\mathrm{cyt}} = 250$ nm. The values $t_{\mathrm{wall}} = 200$ nm and $S_{\mathrm{c}}/S_{\mathrm{m}} = 0.90$ were adopted from Ho *et al.* (2016). In the 3-D model by Ho *et al.* (2016), it is assumed that the radius of

the stomatal pore does not change with increased C_a. Unlike the 2-D model in the current study, the 3-D model does not use stomatal conductance as an implicit input value in the 3-D model. In order to use the same stomatal conductance as input for the 2-D model as for the model from Ho *et al.* (2016), first C_i and A_N were calculated for each value of C_a from the solution of the 3-D model:

$$W = \left(\iiint_{\text{Stroma}} \text{w} \, \text{d}x \, \text{d}y \, \text{d}z \right) S^{-1} \tag{A4.6.5}$$

$$R_p = \left(\iiint_{\text{Stroma}} \frac{w\gamma^*}{[CO_2]} \, \text{d}x \, \text{d}y \, \text{d}z \right) S^{-1} \tag{A4.6.6}$$

$$R_d = \left(\iiint_{\text{Cytosol}} r_d \, \text{d}x \, \text{d}y \, \text{d}z \right) S^{-1} \tag{A4.6.7}$$

$$C_i = RT \left(\iiint_{\text{Intercellular air space}} [CO_2] \, \text{d}x \, \text{d}y \, \text{d}z \right) \left(\iiint_{\text{Intercellular air space}} \text{d}x \, \text{d}y \, \text{d}z \right)^{-1} \tag{A4.6.8}$$

$$A_N = W - R_p - R_d \tag{A4.6.9}$$

$$g_s = \frac{A_N}{C_a - C_i} \tag{A4.6.10}$$

Fig. A4.6B shows a CO_2 concentration profile in Admiro lower leaves for $C_a = 380$ µmol mol^{-1}, $O = 210$ µmol mol^{-1}. and $I_{inc} = 1000$ µmol m^{-2} s^{-1}.

A4.6.3 Comparison of simple 2-D model to complex 3-D model

For each combination of C_a calculated values of g_s (equations (A4.6.5-S6.10)) were used as input values for the 2-D model. Furthermore, the values of J, calculated by the 3-D model, were used as input for the 2-D model. The calculations are done for

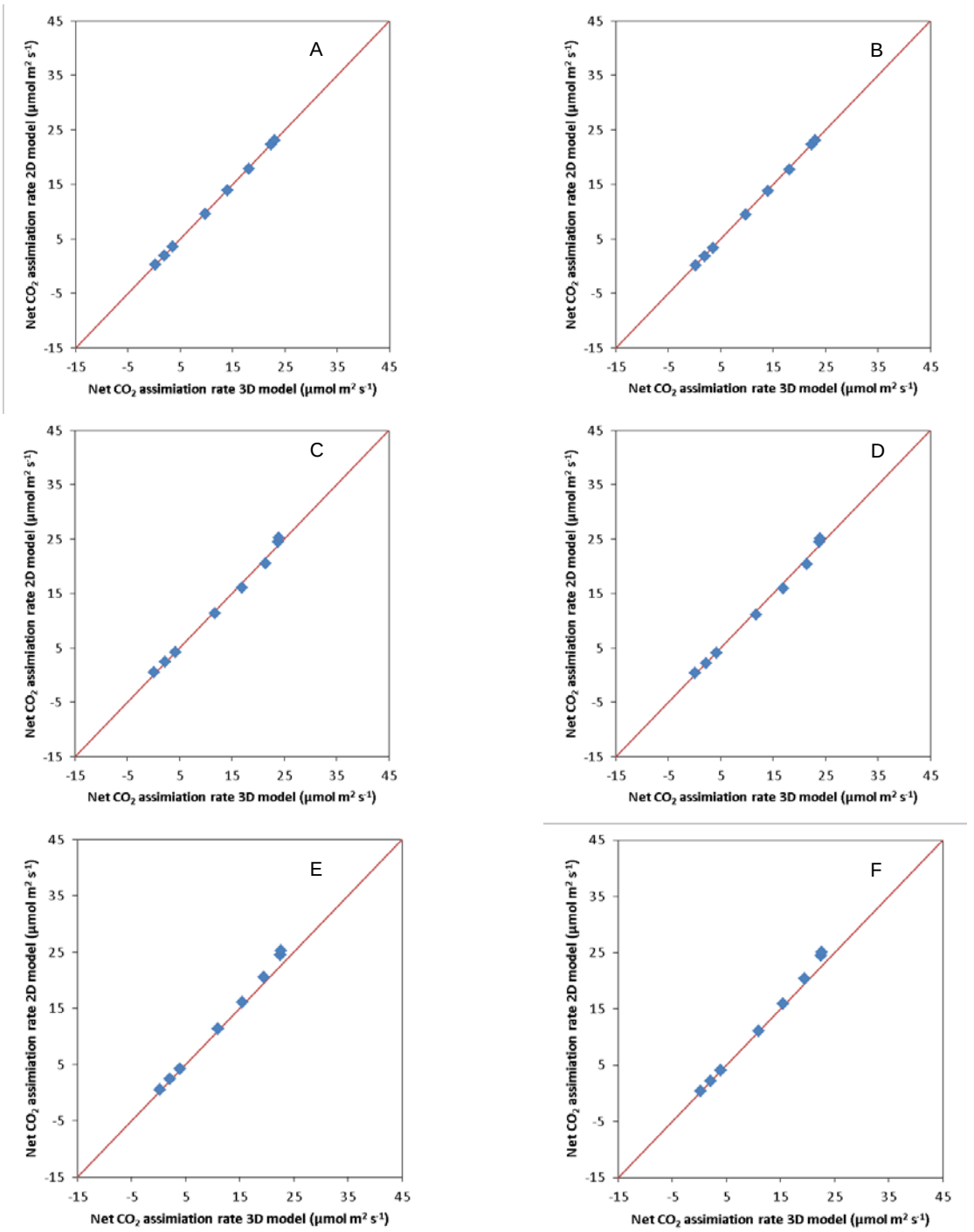

Figure A4.6.2: Net CO_2 assimilation rate predicted by the 2-D model is plotted against the net CO_2 assimilation rate predicted by the 3-D model from Ho *et al.* (2016) for three leaf types. These are "Admiro lower leaf" (A,D), "Doloress lower leaf" (B,E), "Growdena lower leaf" (C, F). Simulation with the 2-D model were run for two scenarios; (photo)respiratory CO_2 release takes place in the inner cytosol (A-C) or in the cytosol gaps (D-F). The solid line is the 1 to 1 line.

three of the six tomato leaf types examined by Ho *et al.* (2016). These leaf types are "Admiro lower leaf", "Doloress lower leaf", and "Growdena lower leaf". Fig. A4.6.1 shows diagrams, in which the values of A_{N} for each value of C_{a} predicted by the 2-D model are plotted against A_{N} values for the same C_{a} predicted by the 3-D model. This shows that all values of A_{N}, with a possible exception of the highest values of C_{a} ($C_{\mathrm{a}} = 100$ Pa and $C_{\mathrm{a}} = 150$ Pa) for Doloress lower leaf and Growdena lower leaf, are about the same for both the 2-D and the 3-D model.

CHAPTER 5

Quantitative analysis of the effects of environmental and physiological factors on the re-assimilation of (photo)respired CO_2, using a reaction-diffusion model

Herman N.C. Berghuijs[1,2,3], Xinyou Yin[1,3], Q. Tri Ho[2], Moges A. Retta[1,2], Bart M. Nicolaï[2], Paul C. Struik[1,3]

[1] Centre for Crop Systems Analysis – Wageningen University and Research Centre, Droevendaalsesteeg 1, 6708 PB Wageningen, The Netherlands

[2] Flanders Center of Postharvest Technology / BIOSYST-MeBioS, Katholieke Universiteit Leuven, Willem de Croylaan 42, B-3001, Leuven, Belgium

[3] BioSolar Cells, P.O. Box 98, 6700 AB Wageningen, The Netherlands

Abstract

Current methods to estimate the rates of respiration C_3 leaves do not consider the re-assimilation of respired CO_2. This may result in an underestimation of the rate of respiration in the light of R_d. Additionally, determining the rate of RuBP carboxylation and photorespiration is even more complex due to their dependence on the CO_2 partial pressure near Rubisco C_c. Although mesophyll conductance models can be used to calculate C_c, they do not explain the various factors along the CO_2 diffusion pathway that determine C_c. Reaction-diffusion models can be used to overcome these limitations. In this study, we demonstrate how such a model can be used to analyse gas exchange and chlorophyll fluorescence data on tomato and how such a model can be validated. We found that, under non-photorespiratory conditions (low O_2 and high CO_2), the re-assimilation at low light levels is very low and that the estimate of R_d is not affected by this process. We also found that R_d under photorespiratory conditions is substantially higher than under non-photorespiratory conditions, which suggests that R_d is oxygen dependent. Next, we investigate how the fraction of (photo)respired CO_2 that is re-assimilated, is affected by physiological factors and environmental conditions. We found that stomatal conductance, the sink strength for CO_2 and the location of mitochondria could strongly affect this fraction. Further research should focus on measuring the diffusion coefficients of the various mesophyll components along the CO_2 diffusion pathway and on validating this model for other species as well.

To be submitted

5.1 Introduction

According to the widely used Farquhar-von Caemmerer-Berry model ('FvCB model') (Farquhar *et al.*, 1980), the net CO_2 assimilation rate A_N can be calculated as the difference between the rates of CO_2 consumption for RuBP carboxylation W and the net CO_2 production by respiratory processes. The rate of respiratory processes is the sum of the rate of photorespiration (R_p) and the rate of CO_2-release by processes other than photorespiration (the latter commonly denoted as respiration with rate R_d):

$$A_N = W - R_p - R_d \tag{5.1}$$

Both photorespiration and respiration can substantially reduce the net CO_2 uptake in C_3 plants. Yin and Struik (2015) estimated that at room temperature and under ambient O_2 and a CO_2 partial pressure C_c near Rubisco of 25 Pa, the rate of photorespiration can be 35% of the rate of CO_2 consumption by RuBP carboxylation, thereby substantially reducing the efficiency of CO_2 assimilation. Although ratio of the amount of CO_2 that is produced by leaf respiration to the amount of CO_2 fixed at moderate irradiance is rather small (Nobel, 2009), this ratio can rapidly increase with decreased irradiance. Therefore, it is important to reliably determine R_p and R_d.

R_p can be calculated from the RuBP carboxylation rate as $R_p = \frac{\Gamma^*}{C_c} W$ (Long and Bernacchi, 2003). Here, C_c is the CO_2 partial pressure near Rubisco and Γ^* is the CO_2 compensation point; this is the CO_2 partial pressure at which the amount of CO_2 produced by photorespiration equals the amount of CO_2 consumed by RuBP carboxylation. In order to quantify W and, thereby, R_p, parameters of the FvCB model have to be estimated. This requires an accurate value for R_d. There are various methods reported in literature to estimate R_d in C_3 plants from gas exchange measurements (Kok, 1948, 1949; Laisk, 1977), sometimes combined with chlorophyll fluorescence measurements (Yin *et al.*, 2009). The Laisk method requires several

$A_N - C_i$ curves (C_i is the intercellular CO_2 partial pressure), measured at different irradiances (I_{inc}). The curves are typically obtained at low C_i levels where the response of A_N to C_i is linear. The negative net CO_2 assimilation rate at the point at which the linear $A_N - C_i$ curves intersect is the rate of R_d estimated by the Laisk method. The Kok method (Kok, 1948) exploits the fact that the response of the net CO_2 assimilation rate to irradiance is approximately linear at low irradiances. R_d is calculated as the intercept of this linear relationship. The Yin *et al.* (2009) method also exploits this linear relationship. It requires $A_N - I_{inc}$ curves measured at low irradiance, combined with simultaneously measured chlorophyll fluorescence to assess the quantum yield of Photosystem II (Φ_2). R_d is estimated as the intercept of the relationship between A_N and $\frac{1}{4}\Phi_2 I_{inc}$. In contrast to the Kok method, which assumes that Φ_2 is invariant with changing I_{inc}, the Yin *et al*. method accommodates for the commonly observed fact that Φ_2 decreases with increasing I_{inc} even within the limiting irradiance range (Yin *et al.*, 2014). Because of such a difference, the value of R_d estimated by the Yin *et al*. method is somewhat higher than that estimated by the Kok method (Yin *et al.*, 2011). Each of the methods mentioned above has limitations, as described by Yin *et al.* (2011). Additionally, each of these methods implicitly assumes that all CO_2 produced by respiration and photorespiration escapes into the atmosphere. Since this recycling of CO_2 is not accounted for in most methods to determine R_d, the true R_d is possibly underestimated. This also implies that W and R_p may also be incorrectly calculated, if underestimated values for R_d are used to estimate other photosynthetic parameters from $A_N - C_i$ and/or $A_N - I_{inc}$ curves. In fact, there is both experimental (Loreto *et al.*, 1999; Haupt-Herting *et al.*, 2001; Pärnik and Keerberg, 2007; Busch *et al.*, 2013) and theoretical (Tholen *et al.*, 2012; Ho *et al.*, 2016) evidence that a substantial fraction of the CO_2 produced by (photo)respiration is used for RuBP carboxylation in the chloroplasts, before it can escape to the atmosphere. According to the resistance model of Tholen *et al.* (2012), the fraction of re-assimilation of (photo)respired CO_2 depends on the CO_2 sink and source strengths in mesophyll cells. Since these source and sink strengths also depend on the CO_2 concentration and the irradiance, the re-assimilation is also affected by the

environment. In this study, we will investigate to what extent re-assimilation depends on these sources and sink strengths and to what extent the re-assimilation is affected by environmental circumstances.

Besides re-assimilation of (photo)respired CO_2, determining the actual rates of RuBP carboxylation and photorespiration is even more complicated due to the fact that they both depend on C_c. C_c can be calculated as (Harley *et al.*, 1992):

$$C_c = C_i - \frac{A_N}{g_m} \tag{5.2}$$

where g_m is the mesophyll conductance. This parameter is apparent, because it lumps various factors that affect CO_2 transport from the intercellular air spaces to Rubisco. g_m can be estimated from gas exchange measurements (Harley *et al.*, 1992; Ethier and Livingston, 2004), gas exchange measurements combined with chlorophyll fluorescence (Yin and Struik, 2009) or by gas exchange measurements combined with isotope discrimination methods (Farquhar *et al.*, 1982; Evans *et al.*, 1986; Farquhar and Cernusak, 2012; Evans and Von Caemmerer, 2013). Most of these methods consider that the mesophyll conductance does not change with an increase in CO_2 concentration or irradiance. However, it has been shown that g_m varies considerably with CO_2 concentration and irradiance (Flexas *et al.*, 2007). Yin *et al.* (2009) and Gu *et al.* (2012) tried to deal with this by calculating g_m with a phenomenological Leuning-type model (Leuning, 1995), which allows g_m to change with C_i and with I_{inc}. Although this can be an effective method to estimate photosynthetic parameters, it does not explain why g_m varies with C_i. According to Tholen *et al.* (2012), the variability of g_m with C_i can be at least partially explained by the fact that (photo)respired CO_2 is released in the cytosol, interfering with the CO_2 diffusion pathway from ambient air into the chloroplast. Tholen *et al.* (2012) developed a framework in which the diffusion of CO_2 along the diffusion pathway is described by a resistance model that consists of two serial conductances. One of them is the

combined conductance of the cell wall and the plasma membrane, and the other is the combined conductance of the chloroplast envelope and the stroma. Between these two serial resistances, CO_2 produced by (photo)respiration is released in the cytosol by mitochondria. CO_2 produced by mitochondria shares the diffusion pathway of CO_2 from the cytosol to Rubisco. Unfortunately, this type of model either assumes that there is no CO_2 gradient in the cytosol (Tholen *et al.*, 2014) or that the mitochondria are located in a cytosol layer between the cell wall and the chloroplasts (Chapter 4). In Chapter 4, we explained that the first assumption is very unlikely. We also showed that assuming that (photo)respiration takes place in the outer cytosol potentially leads to an underestimation of the predicted net CO_2 assimilation rate.

The CO_2 diffusion pathway in the mesophyll is complicated, due to processes that add or remove CO_2 from the diffusion path, due to various structural barriers for CO_2 transport and due to the re-assimilation of (photo)respired CO_2, which can be affected by the position of mitochondria relative to the chloroplasts. Resistance models cannot fully capture this complexity. Therefore, we consider it necessary to use reaction-diffusion models to study how the CO_2 concentration in the atmosphere, the irradiance, leaf structural properties, diffusion and biochemical processes affect the efficiency of photosynthesis. Various reaction-diffusion models have been published to study the complex CO_2 diffusion pathway in mesophyll cells (Vesala *et al.*, 1996; Aalto and Juurola, 2002; Juurola *et al.*, 2005; Tholen and Zhu, 2011; Ho *et al.*, 2016). These models are potentially useful to answer questions that cannot be tackled by resistance models. However, they mostly use photosynthetic parameter values as input values that were previously estimated based on more simple models that implicitly assume that re-assimilation of CO_2 released from respiration does not take place (Laisk, 1977; Yin *et al.*, 2009), or that all CO_2 from (photo)respiration is released in the cytosol region between the plasma membrane and the chloroplast envelope (Chapter 3) and/or that mesophyll conductance is simply infinite (Aalto and Juurola, 2001). Only Juurola *et al.* (2005) used their 3-D model directly to estimate the maximum rate of RuBP carboxylation V_{cmax} and the maximum rate of electron transport J_{max}. One reason why reaction-diffusion models are seldom used to estimate

photosynthetic parameters is that these models can be demanding in computational time. In Chapter 3, we described the development and validation a 2-D CO_2 reaction-diffusion model that reduces the computational time considerably, but is still capable of describing how CO_2 consumption, production, re-assimilation and diffusion along the diffusion path affect the photosynthetic capacity. The reduced computational time makes it considerably more feasible to use this model for operations that require a large number of simulations, like optimization and parameter estimation. In this study, we will further explore the usefulness of this simple reaction-diffusion model in analysing re-assimilation of (photo)respired CO_2. First, we will assess whether the reaction-diffusion model indeed will produce higher estimates of R_d than the Kok and the Yin *et al*. methods. Next, we try to use the model to answer the following questions:

- How do physiological processes affect the re-assimilation of (photo)respired CO_2?

- How do atmospheric CO_2 concentrations, O_2 and irradiances affect the re-assimilation of (photo)respired CO_2 and the apparent mesophyll conductance?

- What is the most likely position of (photo)respired CO_2, and how does this position affect the apparent mesophyll conductance?

5.2 Material and methods

5.2.1 Plant material and experimental data

We used data sets from two experiments, both consisting of simultaneous measurements of gas exchange and chlorophyll fluorescence, with details given by Ho *et al.* (2016) and in Chapter 4, respectively. In brief, for the first experiment, measurements were conducted on leaves from three different tomato (*Solanum lycopersicum*) cultivars, Admiro, Doloress and Growdena (Ho *et al.*, 2016). For each cultivar, two types of leaflets were used for measurements. The first was the distal leaflet of the uppermost fully expanded leaf, which we will refer to as “upper leaf”. The second one was the most distal leaflet from a leaf four layer below the upper leaf, which we will refer to as “lower leaf”. For each leaflet, the gas exchange

measurements consisted of a CO_2 response curve measured at saturating light ($I_{\mathrm{inc}} = 1000\ \mu\mathrm{mol\ m^{-2}\ s^{-1}}$) in combination of either an ambient oxygen level ($O = 21$ kPa) or a low oxygen level ($O = 2$ kPa) and light response curves measured under photorespiratory ($C_{\mathrm{a}} = 38$ Pa, $O = 21$ kPa) and non-photorespiratory conditions ($C_{\mathrm{a}} = 100$ Pa, $O = 2$ kPa). In the second data set (Chapter 3), measurements were taken from the distal leaflet from 15-day and 25-day old leaves, using the same cultivars as in the experiment described by Ho *et al.* (2016). The measurements consisted again of CO_2 response curves at ambient ($O = 21$ kPa) and low ($O = 2$ kPa) oxygen levels under saturating light ($I_{\mathrm{inc}} = 1500\ \mu\mathrm{mol\ m^{-2}\ s^{-1}}$) and light response curves measured under photorespiratory ($C_{\mathrm{a}} = 40$ Pa, $O = 21$ kPa) and non-photorespiratory conditions ($C_{\mathrm{a}} = 100$ Pa, $O = 2$ kPa). Additionally, after measuring gas exchange and chlorophyll fluorescence, the leaflets were harvested and transversal sections were prepared for light microscopy (LM) and transmission electron microscopy (TEM). From the light microscopy images, S_{m}/S (surface area ratio of the mesophyll surface exposed to the intercellular air spaces to the leaf surface) was determined. From the TEM images, cell wall thickness (t_{wall}), cytosol thickness (t_{cyt}), stroma thickness (t_{str}) and the surface area ratio of the chloroplast surface exposed to the intercellular air spaces to the total exposed mesophyll surface ($S_{\mathrm{c}}/S_{\mathrm{m}}$) were determined.

5.2.2 Mesophyll microstructural model and CO_2 reaction-diffusion model

We used the anatomical properties measured from the TEM images to parameterize a 2-D model for the leaf microstructure. More details on the reconstruction of the leaf geometry can be found in Chapter 3 and Chapter 4. We meshed the geometry for CO_2 transport and solved a reaction-diffusion model that includes W in a stroma compartment as a sink term for CO_2 and $R_{\mathrm{d}} + R_{\mathrm{p}}$ as a source term. We assumed that release of CO_2 by (photo)respiration takes place either in the inner cytosol (region between inner chloroplast envelope and tonoplast), or in the outer cytosol (region between the outer chloroplast envelope and the plasma membrane), or in the cytosol gaps. From the steady state solution and the measurements from TEM and LM, we

calculated W, R_{d}, and R_{p} and applied equation (5.1) to calculate A_{N}. The model was implemented in the finite element software COMSOL Multiphysics 5.1 (COMSOL AB, Stockholm). More details on the reaction-diffusion model and its upscaling are explained in Chapter 4. In that study, we also demonstrated how the fraction of (photo)respired CO_2 that is re-assimilated, f_{rec}, can be calculated by solving a system of reaction-diffusion equations over the computational domain.

5.2.3 Determining *s* and *J*

For each leaf type, the lumped calibration factor s was determined according to the method described by Yin *et al*. (2009). This parameter can be defined as the slope of the relationship between A_{N} and $\frac{1}{4} I_{\mathrm{inc}} \Phi_2$, where Φ_2 is the quantum yield of Photosystem II. Subsequently, for each measurement the rate of electron transport J was calculated as $J = s I_{\mathrm{inc}} \Phi_2$, where I_{inc} is the irradiance (μmol m^{-2} s^{-1}) and Φ_2 is the quantum yield of Photosystem II.

5.2.4 Parameterization and validation of the 2-D reaction diffusion model

The reaction-diffusion model was used to estimate R_{d} for each leaf type in both data sets by minimizing the squared difference between the measured and the predicted net CO_2 assimilation rate, using the data from the light response curves under either photorespiratory or non-photorespiratory conditions. We only used the data for which the irradiance was 150 μmol m^{-2} s^{-1} or lower. We estimated R_{d} for each scenario for the location of the release of CO_2 produced by (photo)respiration. The values estimated by the reaction diffusion model will be compared with the values of R_{d} estimated by two more classical methods; the Yin *et al*. method and the Kok method. T_{p} was determined as $(A_{\mathrm{p}} + R_{\mathrm{d}})/3$, where A_{p} is the observed value at the highest C_{a} of the CO_2 response curve measured under photorespiratory conditions (Chapter 4). The reaction-diffusion model was also used to estimate V_{cmax} by minimizing the squared difference between the predicted and the measured net CO_2 assimilation rate. We estimated V_{cmax} for each scenario for the location of the release of CO_2 produced by (photo)respiration. For this analysis, only data from the CO_2 response curve

measured for $O = 21$ kPa and $C_a < 20$ Pa were used. We validated the model for each leaf type by predicting the net CO_2 assimilation rate for each combination of I_{inc}, C_a, and O in the measurements, which we did not use to estimate R_d and V_{cmax} or determine T_p.

5.2.5 Response of g_m to C_a and I_{inc}

We used the reaction-diffusion model to calculate the apparent mesophyll conductance g_m for each leaf type and each scenario. In order to do so, we first used the model to calculate A_N as described in Chapter 4. Next, we determined C_i and C_c:

$$C_i = C_a - \frac{A_N}{g_s} \tag{5.3}$$

$$C_c = H\left(\iint_{Stroma} [CO_2]\mathrm{d}x\,\mathrm{d}y\right)\left(\iint_{Stroma} \mathrm{d}x\,\mathrm{d}y\right)^{-1} \tag{5.4}$$

where $g_s$is stomatal conductance, and H is Henry's law constant for CO_2. Finally we re-arranged equation (5.2) to express g_m and use the values of C_i and C_c, determined by equations (5.3) and (5.4), to calculate g_m.

5.2.6 Response of f_{rec} to C_a and I_{inc}

We calculated the fraction of CO_2 produced by respiration and photorespiration that is re-assimilated, f_{rec}, for various levels of C_a, O and I_{inc}. In Chapter 4, we described how this fraction can be calculated by the reaction-diffusion model.

5.2.7 Sensitivity of f_{rec} and A_N to leaf physiological parameters

We calculated A_N and f_{rec} for a range of values of stomatal conductance g_s, R_d, the maximum rate of RuBP carboxylation V_{cmax}, and the rate of electron transport to investigate how these parameters affect f_{rec} and A_N under ambient CO_2 levels and irradiance.

5.2.8 Model selection

As stated, we assumed three scenarios for the position of releasing CO_2 by (photo)respiration (i.e., CO_2 released in inner cytosol, outer cytosol, or cytosol gaps). In order to identify the most likely scenario, we calculated the Akaike's Information Criterion (AIC) (Akaike, 1974) for each combination of measured and simulated response curves and for each scenario. In order to do so, we first minimized the negative log likelihood L for the standard deviation σ for each curve type (light response under non-photorespiratory conditions, light response curve under photorespiratory conditions and CO_2 response curve at $O = 21$ kPa. $O = 2$ kPa) and cultivar separately:

$$L_{\min} = \frac{N}{2}\ln(2\pi) + \frac{N}{2}\log(\sigma^2) + \frac{1}{2\sigma^2}\sum_{i=1}^{N}\left(A_{\mathrm{N},i} - \overline{A_{\mathrm{N},i}}\right)^2 \tag{5.5}$$

$$\mathrm{AIC} = 2L_{\min} + 2k \tag{5.6}$$

where L_{norm} is the negative log likelihood assuming normally distributed residuals. k is the number of estimated parameters in the maximum negative likelihood function. Since we optimized only for σ to obtain the maximum negative log likelihood, $k = 1$. $A_{\mathrm{N},i}$ is the measured net CO_2 assimilation rate i for a certain curve type for a certain cultivar and $\overline{A_{\mathrm{N},i}}$ and the modelled net CO_2 assimilation rate under the same circumstances. N is the total number of measurements for this curve type for this cultivar. For each scenario, curve type and cultivar, we calculated ΔAIC as:

$$\Delta\mathrm{AIC_i} = \mathrm{AIC_i} - \mathrm{AIC_{min}} \tag{5.7}$$

where AIC_{min} is the lowest AIC value among different scenarios. The model, for which $\Delta AIC = 0$, is considered the best model. According to Burnham and Anderson (2004), ΔAIC represents the information loss if an alternative model is fitted to the data, rather than the best model. They stated that the alternative model has "substantial support" if $\Delta AIC \leq 2$. We adopt this interpretation of ΔAIC in our study.

5.3 Results

5.3.1 Estimation of R_d

We used the reaction-diffusion model to estimate R_d from the dataset described in Chapter 3 and from leaves from the experiment described by Ho *et al.* (2016). Additionally, we estimated R_d by the Yin *et al.* and the Kok method for these leaves. For each method, we estimated separate R_d for photorespiratory and non-photorespiratory conditions. In all but one case ("Admiro upper leaf", Table 5.2), the R_d values estimated by the reaction-diffusion model under photorespiratory conditions were higher than the R_d values under non-photorespiratory conditions.

The values of R_d estimated by the reaction-diffusion model did not differ for different assumed positions of (photo)respiratory CO_2 release. In all instances, the values of R_d estimated by the Yin *et al*. method were higher than the R_d values estimated by the Kok method. In all cases, the values of R_d estimated by the Yin *et al*. method under non-photorespiratory conditions were close to the values estimated by the reaction-diffusion model. Under photorespiratory conditions, this was not always the case. The R_d values estimated by the reaction-diffusion model were sometimes more than 0.5 μmol m^{-2} s^{-1} higher (15-day old Doloress leaves, Table 5.1) than the R_d values estimated by the Yin *et al*. method.

5.3.2 Determination of T_p

There were almost no differences between the estimates of T_p for the same leaf types and different locations of (photo)respiratory CO_2 release (Table 5.3). This is not

Table 5.1: Estimates of the lumped calibration factor s and R_d, either estimated by the Kok (1948) method, the Yin *et al.* (2009) method or by the reaction diffusion model for three locations of (photo)respiration. Data from Chapter 3 of this dissertation for three cultivars and two leaf ages were used for estimation. Estimates were made both for photorespiratory (PR, i.e., $C_a = 40$ Pa, $O = 21$ kPa) and non-photorespiratory (NPR, i.e., $C_a = 100$ Pa, $O = 2$ kPa) conditions

Cultivar	**Leaf age (days)**	s	**Conditions**	R_d **(µmol m^{-2} s^{-1})**				
				Kok	**Yin**	**Reaction-diffusion model**		
						Inner[1]	**Outer**[2]	**Gap**[3]
Admiro	15	0.53	PR	2.94	3.17	3.44±0.36[4]	3.36±0.36	3.41±0.36
			NPR	1.72	2.14	2.04±0.61	2.04±0.61	2.04±0.61
	25	0.52	PR	2.54	2.76	3.43±0.36	3.36±0.36	3.41±0.36
			NPR	1.26	1.67	1.74±0.27	1.74±0.27	1.74±0.27
Doloress	15	0.51	PR	2.86	3.05	3.67±0.32	3.50±0.33	3.65±0.32
			NPR	1.91	2.31	2.24±0.33	2.24±0.33	2.24±0.33
	25	0.42	PR	3.45	3.66	3.51 ±0.31	3.46±0.33	3.50±0.32
			NPR	0.78	1.11	1.01±0.10	1.01±0.10	1.00±0.10
Growdena	15	0.46	PR	2.92	3.13	2.90±0.39	2.84±0.41	2.88±0.40
			NPR	0.85	1.21	1.15±0.66	1.15±0.66	1.15±0.66
	25	0.47	PR	2.56	2.77	2.22±0.41	2.16±0.42	2.20±0.42
			NPR	0.80	1.18	1.15±0.66	1.15±0.66	1.15±0.66

[1] Inner: This column contains the values of R_d estimated by the reaction-diffusion model for the scenario that assumed release of CO_2 from (photo)respiration in the inner cytosol.
[2] Outer: This column contains the values of R_d estimated by the reaction-diffusion model for the scenario that assumed release of CO_2 from (photo)respiration in the outer cytosol.
[3] Gaps: This column contains the values of R_d estimated by the reaction-diffusion model for the scenario that assumed release of CO_2 from (photo)respiration in the cytosol gaps between chloroplasts.
[4] Estimated value of R_d ± standard deviation.

surprising, since there were also almost no differences between the estimates of R_d for the same leaf type and different locations of (photo)respiratory CO_2 release.

5.3.3 Estimation of V_{cmax}

The estimate of V_{cmax} for each leaf type was lower if it was assumed that (photo)respiratory CO_2 release takes place in the inner cytosol than if it was assumed that (photo)respiratory CO_2 release takes place in the cytosol gaps. In case (photo)respiratory CO_2 release takes place in the outer cytosol, the estimate of V_{cmax} was always of the same order of magnitude as its standard error. Sometimes this standard error was larger than the estimate itself.

Table 5.2: Estimates of the lumped calibration factor s and R_d, either determined by the Kok (1948) method, the Yin *et al*. (2009) method or by the reaction-diffusion model. Data from Ho *et al*. (2016) were used for estimation. Estimates were done under both photorespiratory (PR, i.e., $C_a = 38$ Pa, $O = 21$ kPa) and non-photorespiratory (NPR, i.e., $C_a = 100$ Pa, $O = 2$ kPa) conditions

Cultivar	Leaf type	s	Conditions	R_d (µmol m^{-2} s^{-1})				
				Kok	Yin	Reaction-diffusion model		
						Inner[1]	Outer[2]	Gaps[3]
Admiro	Upper	0.52	PR	1.34	1.53	2.04±0.28	2.01±0.27	2.03±0.28
			NPR	2.05	2.18	1.99±0.49	1.99±0.49	1.99±0.49
	Lower	0.41	PR	0.98	1.20	1.54±0.27	1.54±0.26	1.54±0.26
			NPR	0.53	0.83	0.62±0.32	0.62±0.32	0.62±0.32
Doloress	Upper	0.49	PR	1.54	1.72	2.10±0.19	2.05±0.18	2.09±0.18
			NPR	1.64	1.83	1.56±0.36	1.56±0.36	1.56±0.36
	Lower	0.46	PR	0.77	0.94	1.96±0.07	1.89±0.12	1.94±0.09
			NPR	0.87	1.26	1.44±0.30	1.44±0.30	1.44±0.30
Growdena	Upper	0.50	PR	1.81	2.02	2.22±0.11	2.16±0.07	2.20±0.09
			NPR	1.64	1.74	1.42±0.25	1.42±0.25	1.42±0.25
	Lower	0.46	PR	0.46	0.67	2.19±0.07	2.12±0.12	2.16±0.09
			NPR	0.66	1.45	1.33±0.26	1.33±0.26	1.33±0.26

[1] Inner: This column contains the values of R_d estimated by the reaction-diffusion model for the scenario that assumed release of CO_2 from (photo)respiration in the inner cytosol.
[2] Outer: This column contains the values of R_d estimated by the reaction diffusion model for the scenario that assumed release of CO_2 from (photo)respiration in the outer cytosol.
[3] Gaps: This column contains the values of R_d estimated by the reaction diffusion model for the scenario that assumed release of CO_2 from (photo)respiration in the cytosol gaps between chloroplasts.
[4] Estimated value of R_d ± standard deviation.

Table 5.3: Values for T_p and V_{cmax} estimates for different scenarios of the location of (photo)respiratory CO_2 release

Data set	Cultivar	Leaf type	T_p (µmol m^{-2} s^{-1})			V_{cmax} (µmol m^{-2} s^{-1})		
			Inner[1]	Outer[2]	Gaps[3]	Inner[1]	Outer[2]	Gaps[3]
Chapter 3	Admiro	15 days old	11.61	11.61	11.61	174±29[4]	177±251	227±29
		25 days old	13.39	13.38	13.38	145±25	156±160	167±45
	Doloress	15 days old	11.92	11.92	11.92	188±31	177±296	249±23
		25 days old	10.61	10.61	10.61	131±31	167±212	167±29
	Growdena	15 days old	11.97	11.97	11.97	136±23	163±165	169±17
		25 days old	11.21	11.20	11.21	124±51	119±359	239±146
Ho *et al.* (2016)	Admiro	Upper	8.61	8.61	8.61	120±16	128±180	156±17
		Lower	6.96	6.96	6.96	70±7	92±64	82±10
	Doloress	Upper	9.21	9.21	9.21	99±12	117±140	175±6
		Lower	8.27	8.28	8.28	114±8	118±140	129±9
	Growdena	Upper	8.15	8.15	8.15	114±8	120±172	146±16
		Lower	7.81	7.81	7.81	94±5	110±134	115±11

[1] Inner: This column contains the estimates of T_p and V_{cmax} for the scenario that assumed release of CO_2 from (photo)respiration in the inner cytosol.
[2] Outer: This column contains the estimates T_p and V_{cmax} for the scenario that assumed release of CO_2 from (photo)respiration in the outer cytosol.
[3] Gaps: This column contains the estimates T_p and V_{cmax} for the scenario that assumed release of CO_2 from (photo)respiration the cytosol gaps between chloroplasts.
[4] Estimated value of V_{cmax} ± standard deviation.

5.3.4 Further validation

As stated earlier, we only used a part of the data for model parameter estimation, i.e., data from CO_2 curves for $C_a \leq 20$ Pa under photorespiratory conditions to estimate V_{cmax}, data from light response curves for $I_{inc} \leq 150$ µmol m^{-2} s^{-1} under both photorespiratory and non-photorespiratory conditions to estimate R_d, and data measured under photorespiratory conditions at the highest value of C_a to determine T_p. After calibration, we used the reaction-diffusion model to predict the net CO_2 assimilation rate for the remaining combinations of I_{inc}, C_a, and O that were used in the measurements. The solid curves in Figs 5.1 and 5.2 show these predicted net CO_2 assimilation rates for 15-day old Admiro leaves. Figs A5.1.1-A5.1.22 in the Appendix show the comparison between the predicted net CO_2 assimilation rates and the measured ones for the remaining leaves considered in this study.

The predicted net CO_2 assimilation rate generally agreed well with measured net CO_2 assimilation rates for all curve types, if it was assumed that the release of (photo)respired CO_2 takes place in the inner cytosol. There were barely differences between the predicted net CO_2 assimilation rates for different assumed locations of (photo)respired CO_2 release for the light response curve measured under non-photorespiratory conditions. For the CO_2 response curves under both normal and low oxygen levels, and for the light response curves at low normal oxygen levels, the net CO_2 assimilation rate was higher if (photo)respired CO_2 was released in the inner cytosol than if it was assumed that (photo)respired CO_2 is released in the cytosol gaps. Further, the net CO_2 assimilation rate was smaller if (photo)respired CO_2 was assumed to take place in the outer cytosol than if it is assumed that it takes place in the cytosol gaps. In case of T_p limitation, the predicted net CO_2 assimilation rate was the same for each scenario for the location of (photo)respired CO_2 release. The patterns described above can be found for each leaf type considered in this study (Figs A5.1.1-A5.1.22). There is one exception. For all scenarios, the model structurally underestimated the net CO_2 assimilation rate of 25-day old Doloress leaves in the CO_2 response curves. In Chapter 3, we explained that this underestimation probably stems from a possible underestimation of J due to errors in the calibration

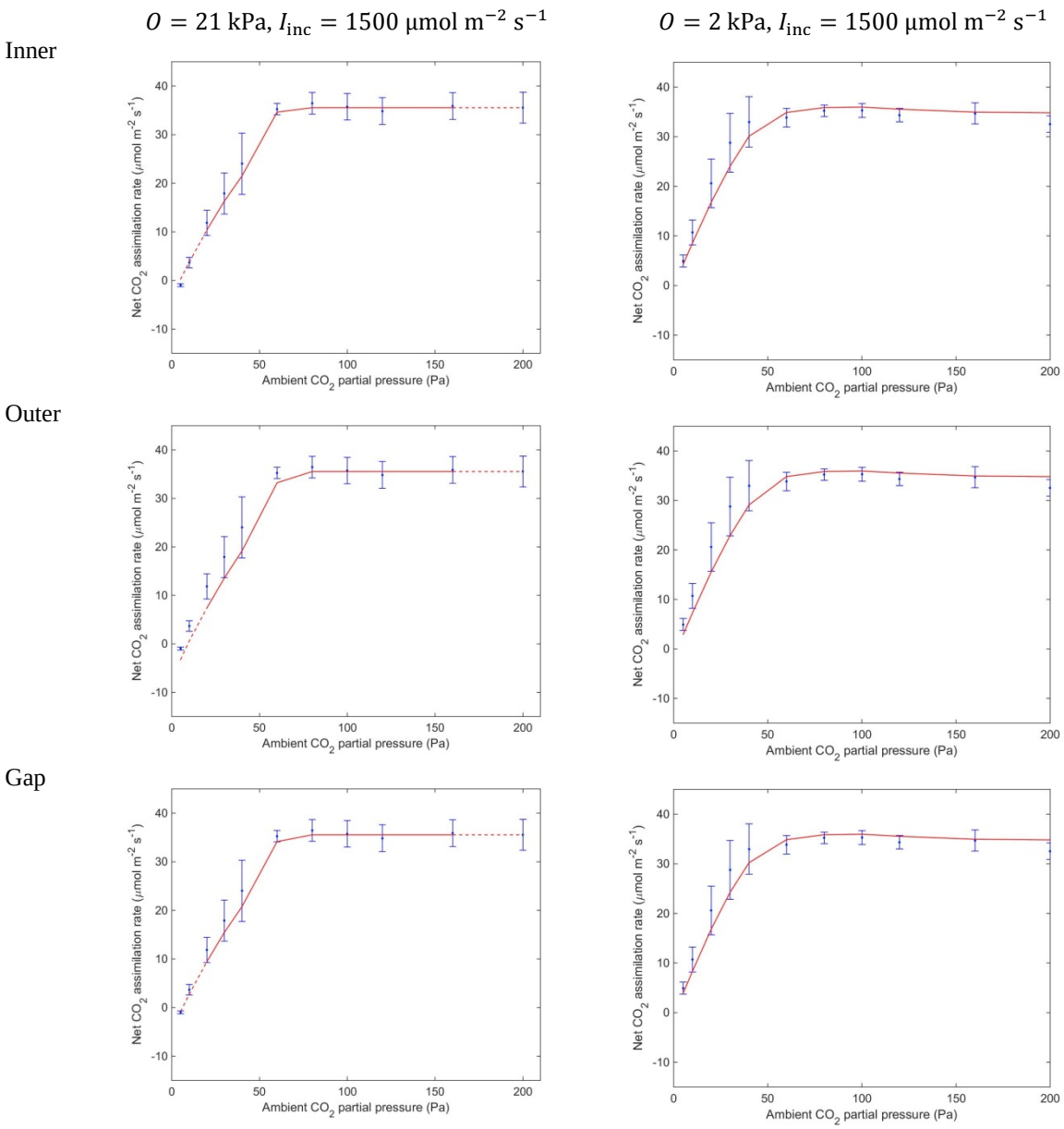

Figure 5.1: Measured (dots) and simulated (solid lines and dashed lines) CO_2 response curves for 15-day-old Admiro leaves. (Photo)respiration is assumed to take place in either the inner cytosol (top row), the outer cytosol (middle row) or the cytosol gaps (bottom row). Measurements were taken under saturating light ($I_{inc} = 1500$ µmol m^{-2} s^{-1}) and either an ambient O_2 partial pressure ($O = 21$ kPa) or a low O_2 partial pressure ($O = 2$ kPa). The error bar represents one standard error.

that was derived from measurements at 2 % O_2 on the quantum yield of photosystem II and the net CO_2 assimilation rate at low light levels.

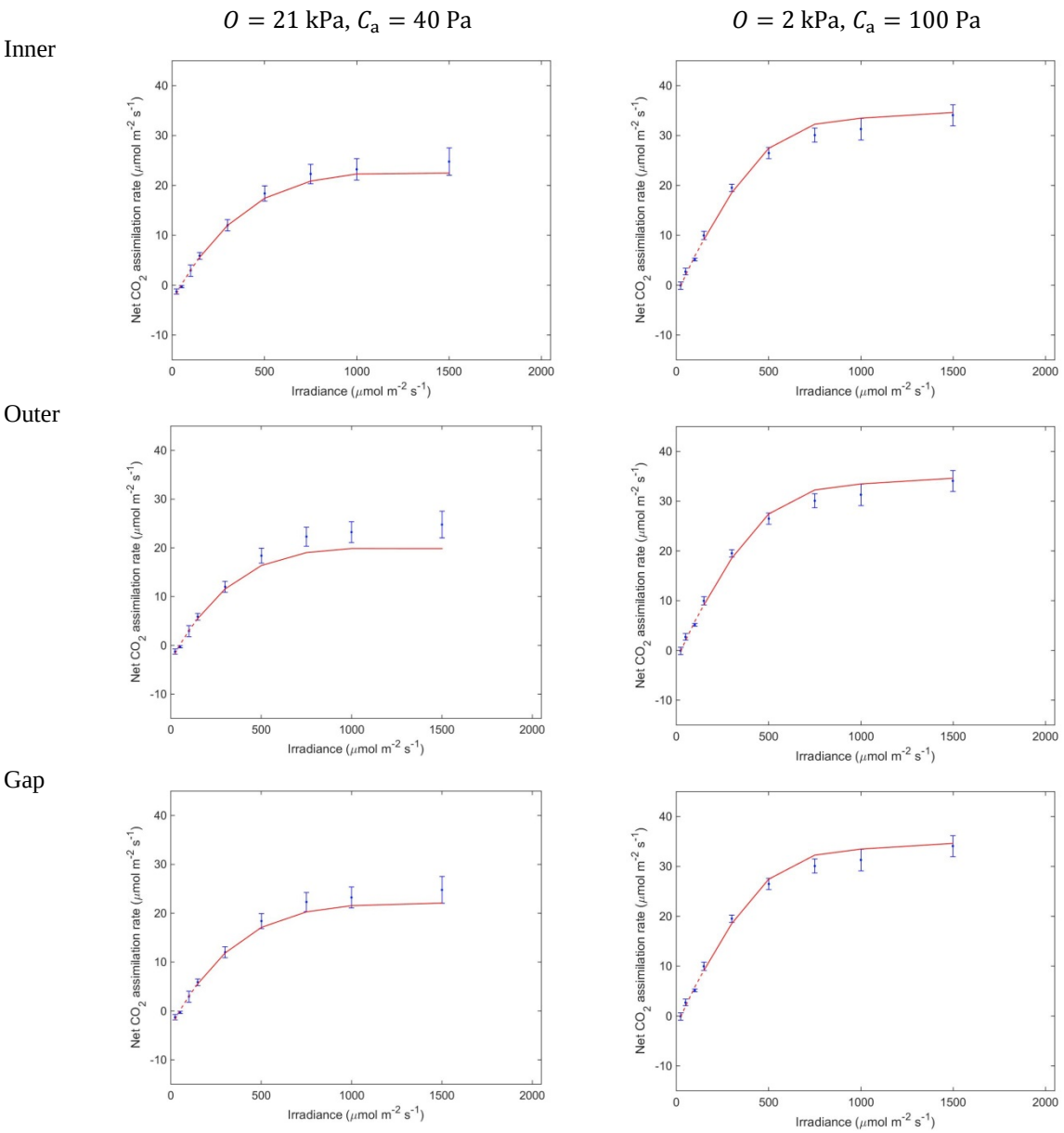

Figure 5.2: Measured (dots) and simulated (solid lines and dashed lines) light response curves for 15-day-old Admiro leaves. (Photo)respiration is assumed to take place in either the inner cytosol (top row), the outer cytosol (middle row) or the cytosol gaps (bottom row). Measurements were taken under either photorespiratory ($C_a = 40$ Pa, $O = 21$ kPa) or non-photorespiratory conditions ($C_a = 100$ Pa, $O = 2$ kPa). The errors bar respresent one standard error

5.3.5 Analysis of sensitivity of A_N and f_{rec} to physiological parameters

We simulated how the net CO_2 assimilation rate and f_{rec} respond to changes in stomatal conductance g_s (Fig. 5.3A-B), the normal rate of respiration R_d (Fig. 5.3C-D), the maximum rate of RuBP carboxylation V_{cmax} (Fig. 5.4A-B), the rate of electron transport J (Fig. 5.4C-D) and the rate of triose phosphate utilization T_p (Fig. 5.4E-F)

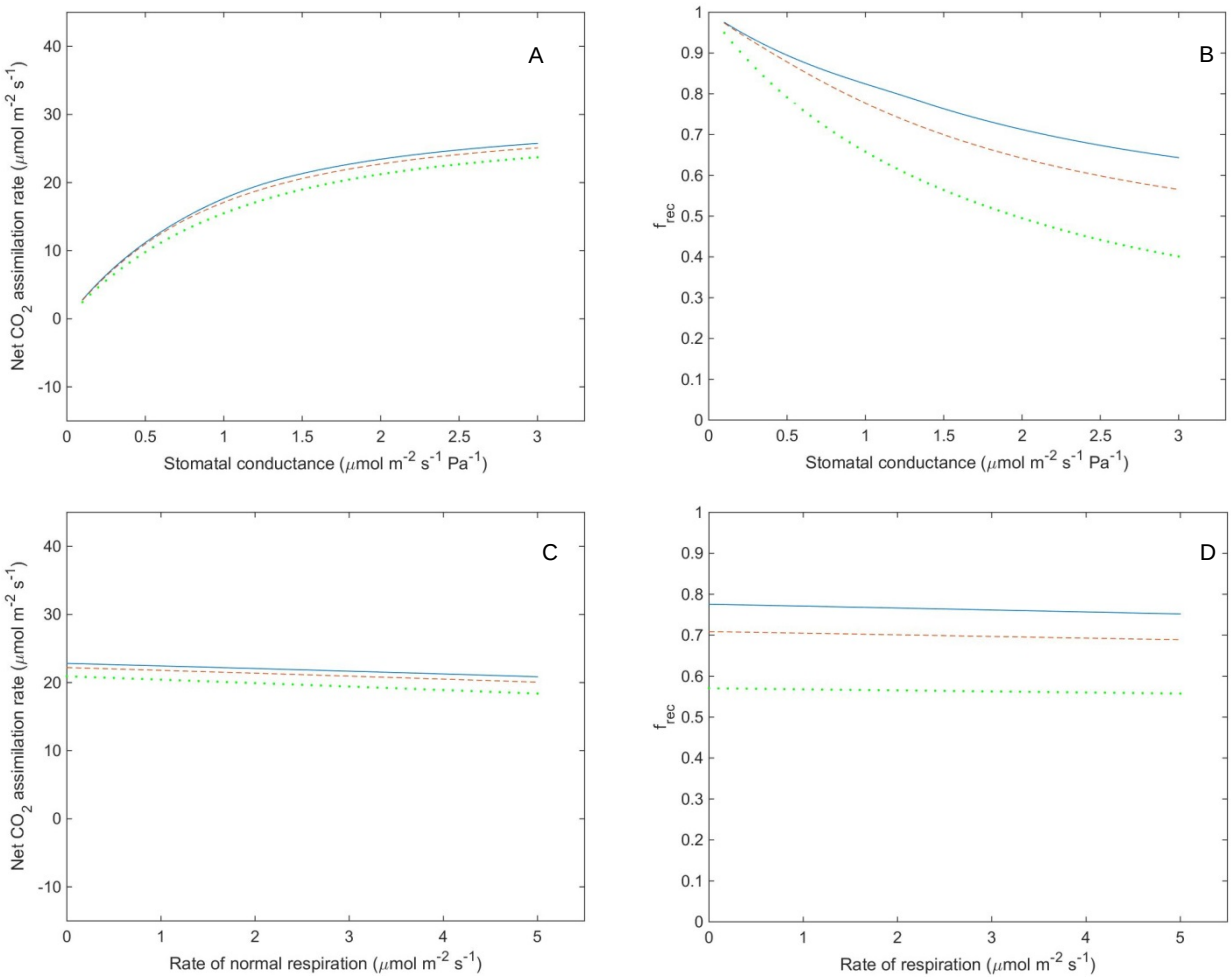

Figure 5.3: Response of the net CO_2 assimilation rate and the fraction of (photo)respired CO_2 that is re-assimilated to increasing stomatal conductance (A-B) or rate of respiration (C-D) under ambient O_2 levels ($O = 21$ kPa) and CO_2 levels ($C_a = 40$ Pa), and saturating light ($I_{inc} = 1500$ µmol m^{-2} s^{-1}) in 15-day-old Admiro leaves. The release of CO_2 produced by (photo)respiration is either assumed to take place in the inner cytosol (solid line), the outer cytosol (dotted line) or the cytosol gaps (dashed line).

under ambient CO_2 and O_2 levels, and saturating light. For each scenario, A_N increased with increasing g_s. The rate of this increase declined with increasing g_s. f_{rec} decreased with increasing g_s. The rate of this decrease declined with increasing g_s. Both A_N and f_{rec} decreased with increasing R_d. Although R_d was varied between 0 and 5 µmol m^{-2} s^{-1}, the net CO_2 assimilation rate decreased considerably less than 5 µmol m^{-2} s^{-1} over this interval of R_d. This can be explained by the re-assimilation of (photo)respired CO_2. We also simulated how the net CO_2 assimilation rate and f_{rec} responded to changes in V_{cmax}, J, and T_p. For each of these parameters, both f_{rec} and A_N increased with

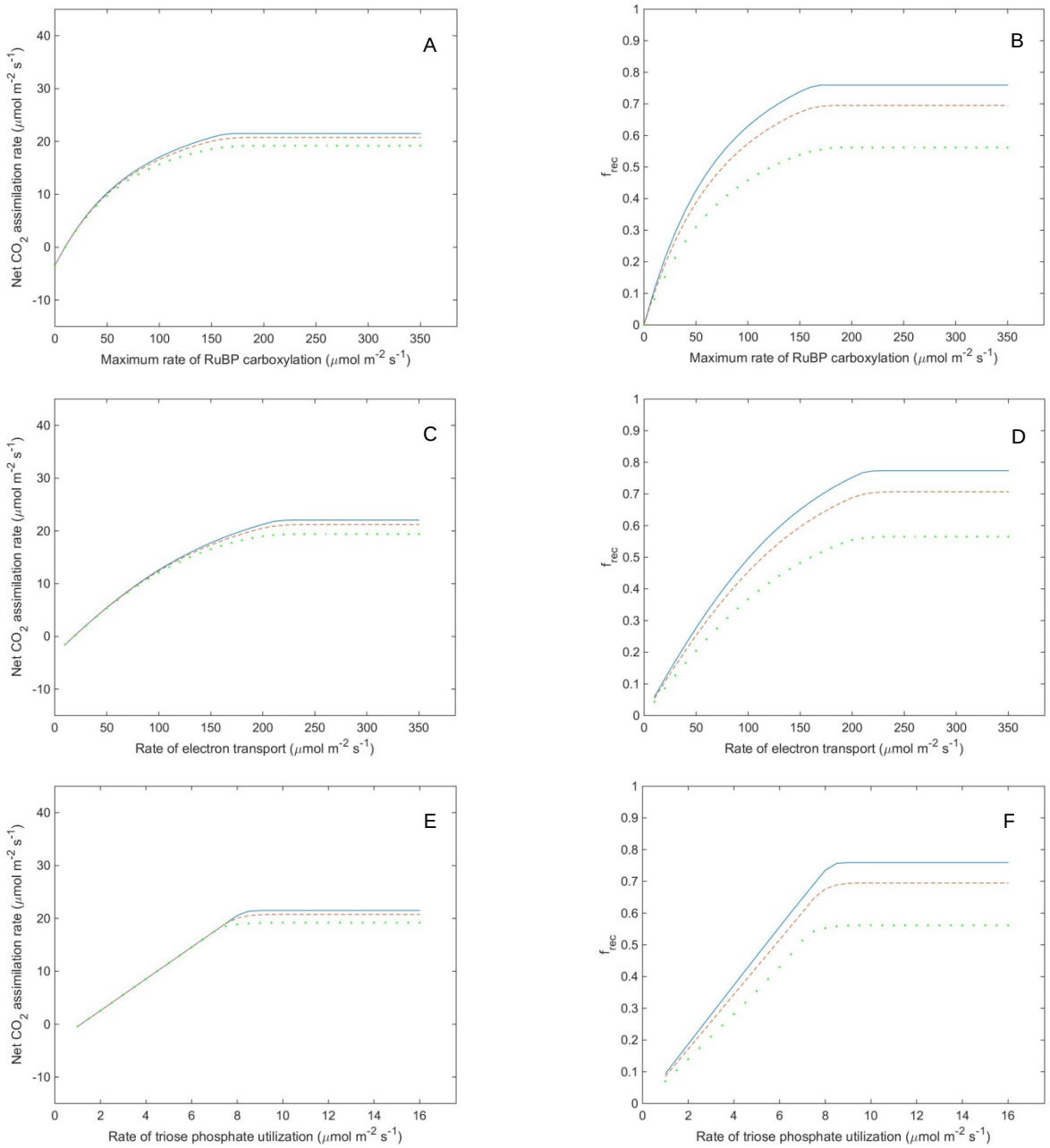

Figure 5.4: Response of the net CO_2 assimlation rate and the fraction of (photo)respired CO_2 that is re-assimilated to maximum rates of RuBP carboxylation (A-B), increasing rates of electron transport (C-D) or rates of triose phosphate utilization under ambient O_2 levels ($O = 21$ kPa) and CO_2 levels ($C_a = 40$ Pa), and saturating light ($I_{inc} = 1500$ µmol m^{-2} s^{-1}) in 15-day-old Admiro leaves. The release of CO_2 produced by (photo)respiration is either assumed to take place in the inner cytosol (solid line), the outer cytosol (dotted line) or the cytosol gaps (dotted line).

increasing these parameters. For each of them, the rate of decrease was decreasing and both A_N and f_{rec} approached an equilibrium value.

5.3.6 Response of f_{rec} to C_{a} and I_{inc}

We used the reaction-diffusion model to calculate f_{rec} for each measured combination of C_{a}, g_{s}, I_{inc}, and O measured in the CO_2- as well as light-response curves. Fig. 5.5 shows the response curve of f_{rec} to C_{a} if $O = 21$ kPa (A) and if $O = 2$ kPa (B) and saturating light. The relationship was sigmoidal under both oxygen levels. At low levels of C_{a}, f_{rec} did not change much with increased C_{a}. At intermediate C_{a} levels, f_{rec} decreased with an increase in C_{a}. At the highest C_{a} levels in these curves, the rate of decrease decreased and f_{rec} levelled off with an increase in C_a. f_{rec} was always higher if (photo)respired CO_2 release took place in the inner cytosol and if it took place in the outer cytosol for the same scenario and leaf type. If it took place in the cytosol gap, f_{rec} was between the f_{rec} values of the other two scenarios. However, it was closer to the f_{rec} value for the scenario that assumed (photo)respired CO_2 release in the inner cytosol. The differences in f_{rec} between the different scenarios decreased with an increase in C_{a}. The patterns described above can be seen in all other leaf types as well, although it was not always very clear that the f_{rec} levelled off at high C_{a} values, which may be explained by the fact that this levelling off took place at high C_{a} values that were outside the range of C_{a} used for the measurements. It should be noted that, although f_{rec} was higher under photorespiratory conditions than under non-photorespiratory conditions for the same scenario and leaf type, at high levels of C_{a} f_{rec} tended to approach the same value for both conditions.

Fig. 5.6 shows the response curve of f_{rec} to I_{inc}. The supplementary materials contain this relationship for the other leaf types. f_{rec} was always larger when (photo)respired CO_2 release took place in the inner cytosol and if it took place in the outer cytosol for the same light level. If it took place in the cytosol gap, f_{rec} was between the f_{rec} values of the other two scenarios. f_{rec} was increasing with increasing I_{inc} for any scenario. The rate of increase decreased with I_{inc} under both photorespiratory conditions and non-photorespiratory conditions. The same trend was observed in all other leaf types in the data set from Chapter 3 as well. However, in the Ho *et al*. (2016) data set, f_{rec} slightly decreased with an increase in I_{inc} for high light levels.

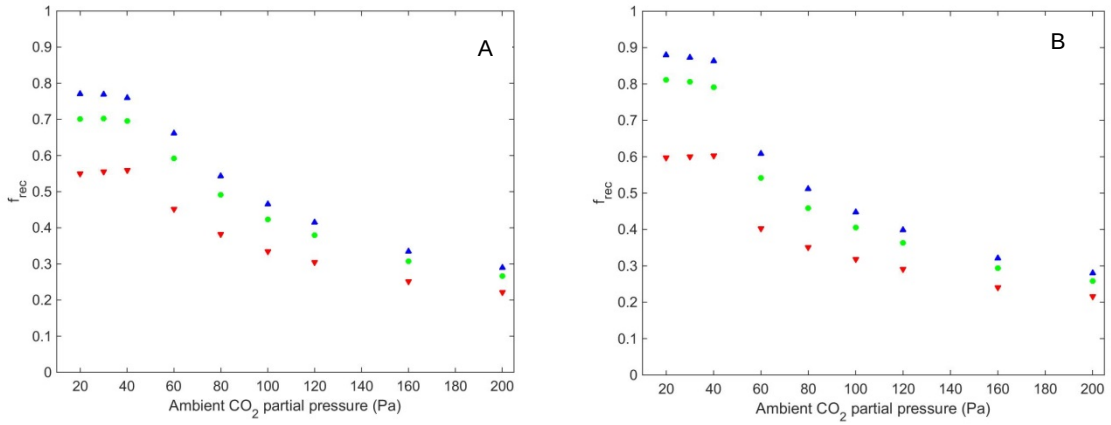

Figure 5.5: Response of the simulated appearant fraction of (photo)respired CO_2 that is re-assimilated (f_{rec}) to increased ambient CO_2 levels under ambient oxygen ($O = 21$ kPa) levels (A) and low oxygen ($O = 2$ kPa) and saturating light ($I_{\mathrm{inc}} = 1500$ µmol m^{-2} s^{-1}) levels (B) in 15-day-old Admiro leaves from the data set described in Chapter 3 of this dissertation. The release of (photo)respiratory CO_2 is assumed to either take place in the inner cytosol (upward pointing triangle), the outer cytosol (downward pointing triangle) or the cytosol gaps (dots).

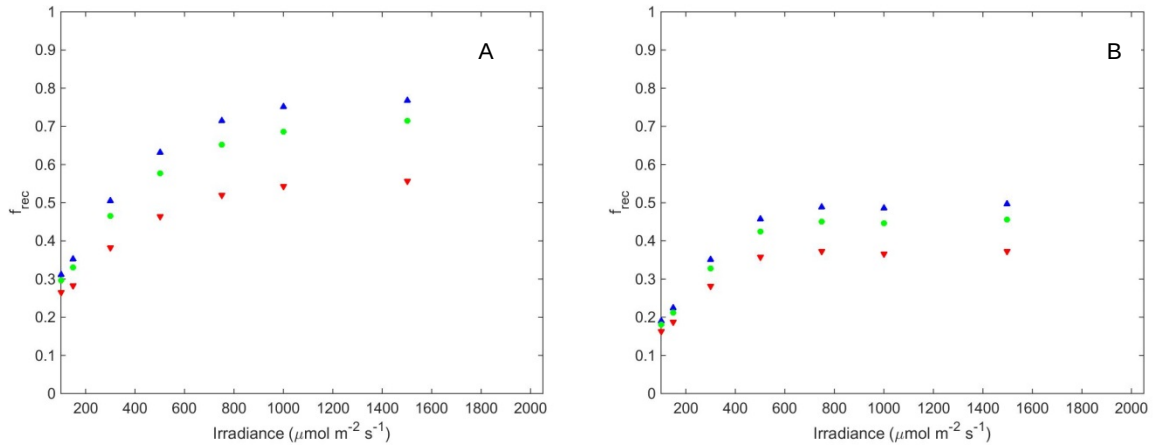

Figure 5.6: Response of the simulated appearant fraction of (photo)respired CO_2 that is re-assimilated (f_{rec}) to increased light levels under photorespiratory ($C_{\mathrm{a}} = 40$ Pa, $O = 21$ kPa) conditions (A) and non-photorespiratory ($C_{\mathrm{a}} = 100$ Pa, $O = 2$ kPa) conditions (B) in 15-day-old Admiro leaves from the data set described in Chapter 3 of this dissertation. The release of (photo)respiratory CO_2 is assumed to either take place in the inner cytosol (upward pointing triangle), the outer cytosol (downward pointing triangle) or the cytosol gaps (dots).

5.3.7 Response of g_{m} to C_{a} and I_{inc}

We used the model to calculate C_{c}, C_{i} and A_{N} and subsequently calculated g_{m} according to equation (5.2). Fig. 5.7 shows how g_{m} responded to C_{a} in 15-days old Admiro leaves. The supplementary materials contain this relationship for the other leaf types. The relationship between C_{a} and g_{m} shows the same trend for ambient O_2

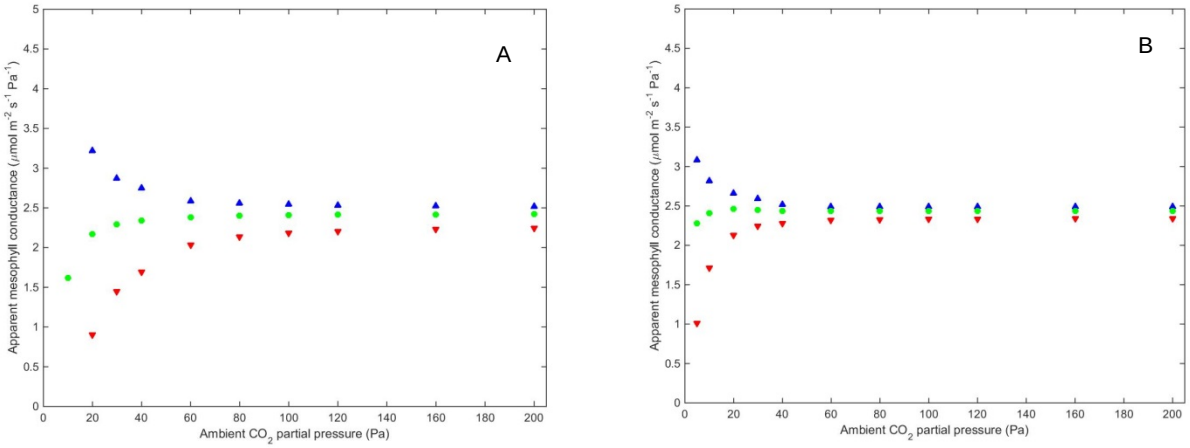

Figure 5.7: Response of the simulated appearant mesophyll conductance (g_m) to increased ambient CO_2 levels under ambient oxygen ($O = 21$ kPa) levels (A) and low oxygen ($O = 2$ kPa) levels (B) and saturating light ($I_\mathrm{inc} = 1500$ µmol $\mathrm{m^{-2}\ s^{-1}}$) in 15-day-old Admiro leaves from the data set described in Chapter 3 of this dissertation. The release of (photo)respiratory CO_2 is assumed to either take place in the inner cytosol (upward pointing triangle), the outer cytosol (downward pointing triangle) or the cytosol gaps (dots).

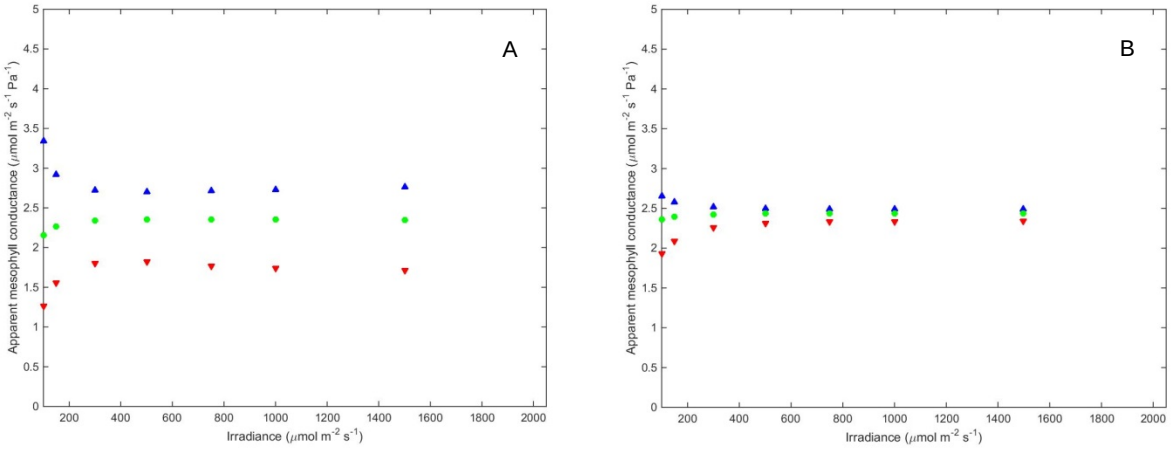

Figure 5.8: Response of the simulated appearant mesophyll conductance (g_m) to increased light levels under photorespiratory (A) conditions ($C_\mathrm{a} = 40$ Pa, $O = 21$ kPa) and non-photorespiratory (B) conditions ($C_\mathrm{a} = 100$ Pa, $O = 2$ kPa) in 15-day-old Admiro leaves from the data set described in Chapter 3 of this dissertation. The release of (photo)respiratory CO_2 is assumed to either take place in the inner cytosol (upward pointing triangle), the outer cytosol (downward pointing triangle) or the cytosol gaps (dots).

levels and low O_2 levels in all leaf types. If (photo)respired CO_2 release took place in the outer cytosol or in the cytosol gap, g_m increased with C_i. If (photo)respired CO_2 release took place in the inner cytosol, g_m decreased with C_a. g_m was always larger if (photo)respiratory CO_2 release took place in the inner cytosol than in the cytosol gaps. g_m was also always larger if (photo)respiratory CO_2 release took place in the cytosol gaps than in the outer cytosol. For each scenario, g_m tended to approach an equilibrium value. This equilibrium value was about the same for each scenario. It

should also be noted that, for the same leaf type, the equilibrium value was the same for photorespiratory and non-photorespiratory conditions. We also calculated how g_m responded to I_{inc}. The results are shown in Fig. 5.8 for 15-day old Admiro leaves and in the supplementary materials for the other leaf types. g_m increased with an increase in I_{inc} if (photo)respiratory CO_2 release took place in the outer cytosol or the cytosol gaps. The rate of increase decreased with I_{inc} and g_m tended to approach an equilibrium value. g_m decreased with an increase in I_{inc}, if (photo)respiratory CO_2 release took place in the inner cytosol. This rate of decrease decreased with an increase in I_{inc}. For each scenario, $g_m$tended to approach an equilibrium value at higher light levels. Under non-photorespiratory conditions, this equilbrium value was very similar for each scenario. Under photorespiratory conditions, there were substantial differences between the equilbrium values of g_m for each scenario.

5.3.8 Model selection

We calculated ΔAIC for each scenario for each measured light response curve and for each CO_2 response curve. Tables 5.4 and 5.5 show the results of this analysis. The ΔAIC values in the table are made bold if $\Delta AIC \leq 2$. This indicates that the corresponding scenario has substantial support. There was only one case (Table 5.5, Admiro lower leaf CO_2 response curves at ambient O_2) out of 48 in which the scenario that assumed that (photo)respiratory CO_2 release took place in the outer cytosol had substantially more support than the scenario that assumed that this took place in the inner cytosol. There was one case out of 48 in which the scenario that assumed that (photo)respiratory CO_2 took place in the cytosol gaps had more support than the other two scenarios (Table 5.1, 15-day old Growdena leaves, CO_2 response curves at low O_2). In all other 46 cases, the model that assumed that (photo)respired CO_2 release took place in the inner cytosol had either the most support or substantial support relative to the best model. In all cases, all three scenarios had substantial support for the light response curves measured under non-photorespiratory conditions.

Table 5.4: ΔAIC for different cultivars (Admiro, Doloress, Growena), leaf ages (15 days or 25 days after emergence), and scenarios (release of CO_2 from (photo)respiration in inner cytosol, outer cytosol or cytosol gaps). Experimental data were from the dataset described in Chapter 3 of this dissertation

Cultivar	Leaf age (d)	Curve	C_a (Pa)	O (kPa)	I_{inc} (µmol m^{-2} s^{-1})	ΔAIC Inner[2]	Outer[3]	Gaps[4]
Admiro	15	$A-I_{inc}$	40	21	var	**0**[5]	57.7	9.43
		$A-C_i$	var[1]	21	1500	**0**	32.3	5.47
		$A-I_{inc}$	100	2	var	**0.18**	**0**	**0.12**
		$A-C_i$	var	2	1500	**0.49**	13.1	**0**
	25	$A-I_{inc}$	40	21	var	**0.42**	43.04	**0**
		$A-C_i$	var	21	1500	3.72	9.48	**0**
		$A-I_{inc}$	100	2	var	**0.37**	**0**	**0.25**
		$A-C_i$	var	2	1500	**1.55**	4.11	**0**
Doloress	15	$A-I_{inc}$	40	21	var	**0**	45.47	10.01
		$A-C_i$	var	21	1500	**0**	42.31	7.85
		$A-I_{inc}$	100	2	var	**0.05**	**0**	**0.03**
		$A-C_i$	var	2	1500	**0.27**	14.14	**0**
	25	$A-I_{inc}$	40	21	var	**0**	26.29	7.05
		$A-C_i$	var	21	1500	**0**	7.48	**1.96**
		$A-I_{inc}$	100	2	var	**0**	**0.09**	**0.03**
		$A-C_i$	var	2	1500	**0**	**1.09**	**0.10**
Growdena	15	$A-I_{inc}$	40	21	var	**0**	27.06	7.00
		$A-C_i$	var	21	1500	**0**	18.14	4.29
		$A-I_{inc}$	100	2	var	**0**	**0.06**	**0.02**
		$A-C_i$	var	2	1500	3.23	6.64	**0**
	25	$A-I_{inc}$	40	21	var	**0**	13.62	2.51
		$A-C_i$	var	21	1500	**0**	7.28	**1.81**
		$A-I_{inc}$	100	2	var	**0**	**0.06**	**0.02**
		$A-C_i$	var	2	1500	**1.09**	5.31	**0**

[1] Variable; during the measurement of a response curve either C_a or I_{inc} was varied, while the other variable was kept constant.
[2] Inner: This column contains the ΔAIC values for the scenario that assumed release of CO_2 from (photo)respiration in the inner cytosol.
[3] Outer: This column contains the ΔAIC values for the scenario that assumed release of CO_2 from (photo)respiration in the outer cytosol.
[4] Gaps: This column contains the ΔAIC values for the scenario that assumed release of CO_2 from (photo)respiration the cytosol gaps between chloroplasts.
[5] Bolt values indicate that the corresponding model is either the best one from the three models ($\Delta AIC = 0$) or has substantial support relative to the best one ($0 < \Delta AIC \leq 2$).

5.4 Discussion

In this study, we used a reaction-diffusion model from our previous study directly to determine photosynthetic parameters (R_d and V_{cmax}) from data that consisted of simultaneous gas exchange and chlorophyll fluorescence measurements. These measurements were taken from leaves from three cultivars with different leaf layers or leaf ages. Next, we compared the estimates of R_d estimates for different scenarios for the localization of release of CO_2 from (photo)respiration: release of CO_2 from (photo)respiration takes either place in the inner cytosol, in the outer cytosol, or in the

Table 5.5: ΔAIC for different cultivars (Admiro, Doloress, Growena), leaf layers (upper leaf and lower leaf), and scenarios (release of CO_2 from (photo)respiration in inner cytosol, outer cytosol or cytosol gaps). Experimental data were from the Ho *et al.* (2016) data set.

Cultivar	Leaf layer	Curve	C_a (Pa)	O (kPa)	I_{inc} (µmol m^{-2} s^{-1})	ΔAIC Inner[2]	Outer[3]	Gaps[4]
Admiro	Upper	$A-I_{inc}$	38	21	var	**0**[5]	33.78	5.86
		$A-C_i$	var[1]	21	1000	**0**	9.63	3.09
		$A-I_{inc}$	100	2	var	**0**	**0.00**	**0.00**
		$A-C_i$	var	2	1000	**0.04**	**1.68**	**0**
	Lower	$A-I_{inc}$	38	21	var	**0.04**	**0.705**	**0**
		$A-C_i$	var	21	1000	3.26	**0**	**1.49**
		$A-I_{inc}$	100	2	var	**0.05**	**0**	**0.00**
		$A-C_i$	var	2	1000	**1.03**	**0**	**1.20**
Doloress	Upper	$A-I_{inc}$	38	21	var	**0**	19.65	5.39
		$A-C_i$	var	21	1000	**0**	68.71	13.8
		$A-I_{inc}$	100	2	var	**0.03**	**0**	**0.02**
		$A-C_i$	var	2	1000	**0**	3.49	**0.71**
	Lower	$A-I_{inc}$	38	21	var	**0**	8.11	2.35
		$A-C_i$	var	21	1000	**0**	11.31	2.17
		$A-I_{inc}$	100	2	var	**0**	**0.02**	**0.01**
		$A-C_i$	var	2	1000	**0**	**0.22**	**0.06**
Growdena	Upper	$A-I_{inc}$	38	21	var	**0**	10.49	2.91
		$A-C_i$	var	21	1000	**0**	18.12	3.24
		$A-I_{inc}$	100	2	var	**0.03**	**0**	**0.02**
		$A-C_i$	var	2	1000	**0.01**	**0.27**	**0**
	Lower	$A-I_{inc}$	38	21	var	**0**	2.48	**0.75**
		$A-C_i$	var	21	1000	**0**	2.45	**0.59**
		$A-I_{inc}$	100	2	var	**0.03**	**0**	**0.02**
		$A-C_i$	var	2	1000	**0.02**	**0.02**	**0**

[1] Variable; during the measurement of a response curve either C_a or I_{inc} was varied, while the other variable was kept constant.

[2] Inner: This column contains the ΔAIC values for the scenario that assumed release of CO_2 from (photo)respiration in the inner cytosol.

[3] Inner: This column contains the ΔAIC values for the scenario that assumed release of CO_2 from (photo)respiration in the outer cytosol.

[4] Gaps: This column contains the ΔAIC values for the scenario that assumed release of CO_2 from (photo)respiration the cytosol gaps between chloroplasts.

[5] Bolt values indicate that the corresponding model is either the best one from the three models ($\Delta AIC = 0$) or has substantial support relative to the best one ($0 < \Delta AIC \leq 2$).

cytosol gaps. We compared these estimates with estimates using traditional methods (Kok, 1948, 1949; Yin *et al.*, 2009; Yin *et al.*, 2011) to assess to what extent re-assimilation may affect the estimates of R_d by our model. After solving the model using the estimated parameters, we calculated the response of f_{rec} and g_m to different atmospheric partial pressures of CO_2 and O_2 and irradiances from our simulated results. Finally, we used model selection based on AIC (Akaike, 1974) to assess what

the most likely localization of release of CO_2 from (photo)respiration is, given the assumptions of the model.

5.4.1 Estimation of R_d

We hypothesized that the estimates of R_d by our model would be larger than the estimates by the Yin *et al*. method and the Kok method. Tables 5.1 and 5.2 show these estimates. In all but one case, the R_d values estimated by the Kok method were indeed smaller than the estimates by the reaction-diffusion model under photorespiratory conditions, but not always under non-photorespiratory conditions. The R_d values by the Yin *et al.* method were not consistently smaller than the R_d values estimated by the reaction-diffusion models. In fact, they were almost the same under non-photorespiratory conditions. Furthermore, there were almost no differences between the estimates of R_d by the reaction-diffusion models for the different assumed locations of (photo)respiratory CO_2 release. f_{rec} was very low under low light levels, which were used to estimate R_d. All these results suggest that the Yin *et al*. method predicts R_d reasonably well under non-photorespiratory conditions, because re-assimilation does not substantially affect A_N under these conditions and low light levels (Fig. 5.6). It was also noticeable that in almost all cases, R_d was higher under photorespiratory conditions than under non-photorespiratory conditions. This implies that R_d is oxygen dependent. This finding has consequences. It shows that R_d estimated by the Yin *et al.* method and the Kok method under non-photorespiratory conditions, which are the only conditions for which these methods are theoretically valid (see Yin *et al.* 2011), cannot be used to describe R_d under photorespiratory conditions.

5.4.2 Estimation of V_{cmax} and the likely location of (photo)respiratory CO_2 release

After estimating R_d and determining T_p, we estimated V_{cmax} (Table 5.3). We found that the estimate of V_{cmax} was always higher if (photo)respiratory CO_2 release took place in the cytosol gap than in the inner cytosol. Since the re-assimilation of (photo)respiratory CO_2 was higher if (photo)respiratory CO_2 was released in the inner

cytosol than in the cytosol gaps, the model compensated the lower re-assimilation by a more efficient RuBP carboxylation under Rubisco limited conditions by estimating a higher V_{cmax}. If (photo)respiratory CO_2 release took place in the outer cytosol, the standard error was very high. This indicates that for this scenario, V_{cmax} was very uncertain. An explanation could be that the model cannot fully compensate for the discrepancy between its prediction of A_{N} and the measured A_{N} for this scenario by estimating a high value for V_{cmax}. The latter explanation suggests that this scenario is less likely than the other two scenarios, which is supported by the $\Delta\mathrm{AIC}$ analysis. In only one of the 48 cases, the model that assumed (photo)respiratory CO_2 cytosol release in the outer cytosol had substantially more support than the model that assumed that (photo)respiratory CO_2 release takes place in the inner cytosol. In all other cases, this scenario had either less support than the other two scenarios or similar support (Table 5.4-5.5).

5.4.3 Re-assimilation and its relation to physiological and environmental factors

After parameterization and validation of the model, we did a sensitivity analysis for g_{s} and the FvCB parameters to assess how A_{N} and f_{rec} would respond to changes in these parameters. We found that g_{s} had a substantial influence on A_{N}; increasing g_{s} resulted in higher values of A_{N} (Fig. 5.3A). At the same time, opening the stomata will make it more likely that CO_2 molecules escape from the intercellular air spaces to the atmosphere, which explains the decrease of f_{rec} with increasing g_{s} (Fig 5.3B).

Next, we conducted a sensitivity analysis for R_{d}. We varied R_{d} between 0 and 5 μmol m^{-2} s^{-1} and calculated the response of A_{N} and f_{rec} (Fig. 5.3C-D). The net CO_2 assimilation rate and f_{rec} only slightly decreased with increasing R_{d}. The difference between the predicted A_{N} for $R_{\mathrm{d}} = 0\ \mu\mathrm{mol\ m^{-1}}$ and $R_{\mathrm{d}} = 5\ \mu\mathrm{mol\ m^{-1}}$ was considerably less than 5, which can be explained by the re-assimilation of respired CO_2 (Fig. 5.3C).

We also conducted sensitivity analyses of J, V_{cmax} and T_{p} (Fig. 5.4) to assess how the sink strength for CO_2 in the chloroplasts (i.e., the rate of RuBP carboxylation W) affects f_{rec}. Each of these parameters positively affects one of the potential rates of

RuBP carboxylation. These potential rates are the RuBP carboxylation rates limited by the capacity of Rubisco, electron transport and triose phosphate utilization, respectively. If the values of either J, V_{cmax} or T_{p} were high, A_{N} and f_{rec} did not change with a further increase in these parameters, because RuBP carboxylation was then no longer determined by the potential rate that is affected by this parameter. If the parameter values were low, both A_{N} and f_{rec} increased with an increase in one of these parameters. This demonstrates that the re-assimilation of (photo)respired CO_2 is determined by sink strength.

We also did a sensitivity analysis to investigate how f_{rec} changes with an increase in C_{a}, either at ambient O_2 levels or low O_2 levels and for I_{inc} under photorespiratory or non-photorespiratory conditions (Figs 5.5-5.6). This analysis showed that f_{rec} depends on the CO_2 partial pressure in the atmosphere at low CO_2 partial pressures. Depending on the scenario for (photo)respiratory CO_2 release, f_{rec} either decreased with C_{a} (CO_2 release in inner cytosol) or increased with C_{a} (both other scenarios). For high CO_2 partial pressures, f_{rec} no longer changed with C_{a}. Under low oxygen levels, f_{rec} was less sensitive to C_{a} than under ambient oxygen levels. We also found that f_{rec} at low light levels increased with an increase in I_{inc}, which can be explained by the fact that increasing I_{inc} increases J and, thereby, sink strength. However, at high light levels, f_{rec} slightly decreased with an increase in I_{inc} in the leaves from the (Ho *et al.*, 2016) data set. This can be explained by the increase in stomatal conductance with an increase in I_{inc}. This can affect C_{c}, even though RuBP carboxylation is not limited by the rate of electron transport under these light levels.

There are large differences between the different values of f_{rec} reported in literature (Loreto *et al.*, 1999; Haupt-Herting *et al.*, 2001; Pärnik and Keerberg, 2007; Tholen *et al.*, 2012; Busch *et al.*, 2013). The reported values for f_{rec} refer between 14%-18% (Pärnik and Keerberg, 2007) in sunflowers to 100% in tomato (Loreto *et al.*, 1999). The results of our sensitivity analyses prove that f_{rec} can be strongly affected by different physiological factors (stomatal conductance, sink strength, source strength) (Figs. 5.3 and 5.4), leaf anatomical properties (for instance, the position of mitochondria relative to the chloroplasts) (Figs 5.1 and 5.2, Figs A5.1.1-A51.22), and

environmental factors (CO_2 partial pressure in atmosphere, irradiance, Figs A5.1.24-A5.1.44). Additionally, Ho *et al.* (2016) demonstrated that (photo)respired CO_2 is also affected by S_c/S_m.

5.4.4 Apparent mesophyll conductance and its relation to likely positions of (photo)respired CO_2 release

Our reaction-diffusion model does not use mesophyll conductance models to determine physiological parameters, but it still considers that physical barriers for CO_2 transport in the leaves and biochemical processes affect the net CO_2 assimilation rate by modelling all these factors explicitly. We used our model to calculate the net CO_2 assimilation rate, the average CO_2 partial pressure in the chloroplasts and in the intercellular air spaces. Next, we used these calculated values to calculate g_m for different values of C_a and I_{inc} (Figs 5.5-5.6, Figs A5.1.45-A5.1.66). For all leaf types, we saw the same trend in the response of g_m to these environmental conditions. If (photo)respired CO_2 release was assumed to take place in the inner cytosol, g_m decreased with an increase in C_a, with an exception of the very lowest C_a values. The shape of this response was similar to the response of g_m to C_i observed in various other studies (Harley *et al.*, 1992; Flexas *et al.*, 2007; Yin and Struik, 2009; Tholen and Zhu, 2011). These models either implicitly assume that (photo)respired CO_2 release takes place in the same compartment as RuBP carboxylation does or in compartments between the chloroplasts and the vacuole (Tholen and Zhu, 2011; Ho *et al.*, 2016). The rate of decrease of g_m decreased with an increase in C_i and g_m approached an equilibrium value. If (photo)respired CO_2 release was assumed to take place in the outer cytosol or in the cytosol gaps, the shape of the response was more similar to the ones calculated by Tholen *et al.* (2012) and in Chapter 3 of this dissertation which predicted that g_m increased with C_i. These two studies implicitly assumed that (photo)respiratory CO_2 release takes place in the outer cytosol, unless there is no CO_2 gradient in the cytosol (Tholen *et al.*, 2014). In Chapter 3, we showed that there is a clear CO_2 gradient in the cytosol. Our ΔAIC analysis shows that (photo)respiratory CO_2 release in the outer cytosol is the least likely scenario of the three scenarios. It is more likely that (photo)respired CO_2 release takes place in the

inner cytosol. This is an important finding, because it shows that the classical model of g_m in equation (5.2) gives, at least in tomato, a better description of the response of g_m to C_i than some recent resistance models (Tholen *et al.*, 2012; Chapter 3). These recent models describe the diffusion of CO_2 by a model that consists of two resistances and a source of CO_2 production in between. It should be noticed though that the model that assumes that (photo)respiratory CO_2 release takes place in the cytosol gaps also predicts that g_m increases with C_i, but there are only two occasions (Table 5.4-5.5) where this model had substantially more support than the scenario that assumed (photo)respiratory CO_2 in the inner cytosol. The opposite was true for 14 other cases (Tables 5.4-5.5).

5.4.5 Future research needs

An advantage of using reaction-diffusion models for data analysis is that they do not require calculation of g_m in order to parameterize them, since factors that potentially affect g_m are modelled explicitly. Another advantage of using reaction-diffusion models over resistance models is that they are more flexible, since they can be used to explicitly define where various biochemical reactions take place. Their flexibility makes it also relatively easy to add features like the temperature sensitivity of Rubisco kinetic constants, other physiological parameters, solubility of CO_2 in water and the diffusion coefficient of CO_2 (Juurola *et al.*, 2005). Unlike a mesophyll conductance model, in which all these factors are lumped in $g_m$or in the temperature dependency of g_m, reaction-diffusion models allow studying the effect of each of these individual factors on the efficiency of CO_2 transport to Rubisco. This makes it possible to use these models to identify specific targets that can be altered to increase the net CO_2 assimilation rate.

Nevertheless, there are a few things that need to be considered if this model, or similar ones, are used as an alternative to resistance models. First, the reaction-diffusion model used in this study made various simplifications in both the leaf structure and biochemical processes taking place in the leaf. Second, it is implicitly assumed that there is full facilitation of CO_2 transport by carbonic anhydrase, which allowed us to

lump this process in the apparent diffusion coefficients of the cytosol and the stroma. Third, it is assumed that the leaf geometry can be modelled as a few rectangles. In order to assess to what extent these simplifications affect the predictions of the model, we compared a CO_2 response curve modelled by this model with the CO_2 response curve predicted by another model with a much more sophisticated 3D structure (Ho *et al.*, 2016) that does consider carbon anhydrase activity and HCO_3^- explicitly. In Chapter 4, we found that these simplifications barely affect the predicted net CO_2 assimilation rate in tomato. Also, we lumped the mitochondria and the cytosol compartment in which (photo)respiratory CO_2 release takes place, rather than modelling loose mitochondria explicitly. In our previous study, we found that modelling loose mitochondria does barely change the predicted values of A_N and f_{rec}. Although these simplifications of the model for the leaf microstructure can apparently be done for tomato, it does not necessarily mean that these simplifications are valid for other plant species as well. Therefore, we recommend validating the model again, if it is used in future research on other species. Furthermore, the diffusion coefficients in various locations of the CO_2 diffusion path are uncertain and hard to measure (Evans *et al.*, 2009). The apparent diffusion coefficients used in this study were adopted from literature (Gutknecht *et al.*, 1977; Fanta *et al.*, 2012; Ho *et al.*, 2016). The combination of assumed diffusion coefficients for different subcellular compartments resulted in reasonable predictions of the light and CO_2 response curves in tomato. However, this does not necessarily mean that each individual diffusion coefficient has a realistic value and therefore, again the model needs to be validated if it is applied to other species than tomato or they have to be measured directly. In future research, we therefore recommend to use this model to analyse data from other plant species as well to check which simplifications and assumptions can generally be made (i.e., which assumptions about diffusion coefficients, biochemical processes, and leaf structural properties do not substantially affect CO_2 diffusion in leaves) and which ones are essential to understand how leaf structural and biochemical properties affect its photosynthetic capacity.

Acknowledgements

Wageningen based authors thank the BioSolar Cells programme (project C3B3) for financial support. Leuven based authors thank the Research Council of the KU Leuven (project OT 12/055) for financial support. The authors thank Bob Douma, Pepijn van Oort, Wopke van der Werf, and Willemien Lommen (all Wageningen UR, Centre for Crop Systems Analysis, Wageningen, The Netherlands) for a useful discussion on the interpretation of Akaike's Information Criterion.

Appendix 5.1

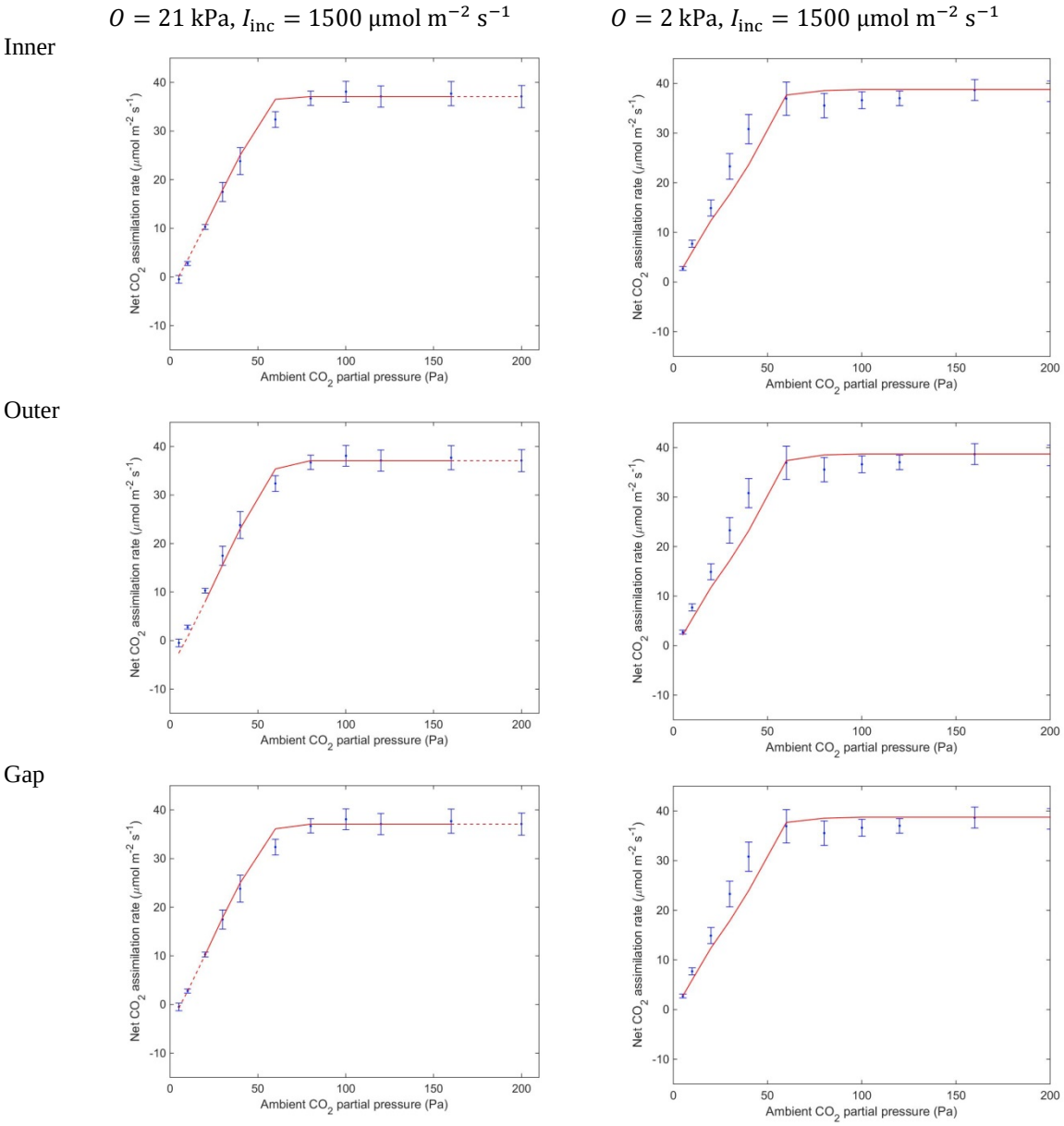

Figure A5.1.1: Measured (dots) and simulated (solid lines and dashed lines) CO_2-response curves for 25-days old Admiro leaves from the data set of Chapter 3. (Photo)respiration was assumed to take place in either the inner cytosol (top row), the outer cytosol (middle row) or the cytosol gaps (bottom row). Measurements were taken under saturating light and either an ambient O_2 partial pressure ($O = 21$ kPa) (left) or a low O_2 partial pressure ($O = 2$ kPa) (right). The error bars represent one standard deviation. The solid lines represent the predicted net CO_2 assimilation rates for values of C_a and I_{inc} that were neither used in the estimation procedure of R_d and V_{cmax} nor for the determination of T_p. The dashed lines connect the predicted net CO_2 assimilation rates under the remaining values of C_a with the solid lines.

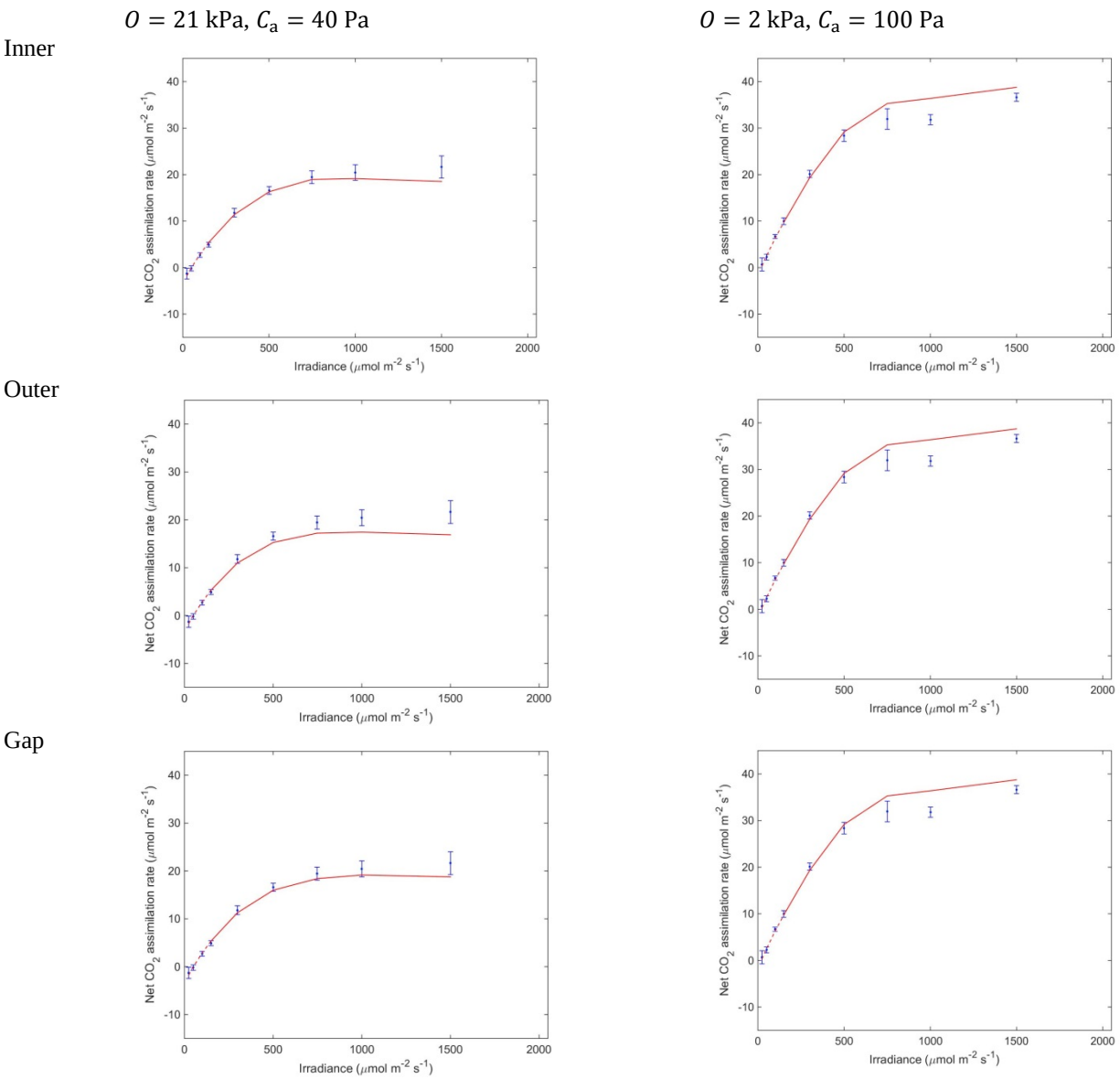

Figure A5.1.2: Measured (dots) and simulated (solid lines and dashed lines) light-response curves for 25-day-old Admiro leaves from the data set of Chapter 3. (Photo)respiration was assumed to take place in either the inner cytosol (top row), the outer cytosol (middle row) or the cytosol gaps (bottom row). Measurements were taken under either photorespiratory conditions ($O = 21$ kPa, $C_a = 40$ Pa) (left) or non-photorespiratory conditions ($O = 21$ kPa, $C_a = 100$ Pa) (right). The error bars represent one standard deviation. The solid lines represent the predicted net CO_2 assimilation rates for values of C_a and I_{inc} that were neither used in the estimation procedure of R_d and V_{cmax} nor for the determination of T_p. The dashed lines connect the predicted net CO_2 assimilation rates under the remaining values of I_{inc} with the solid lines.

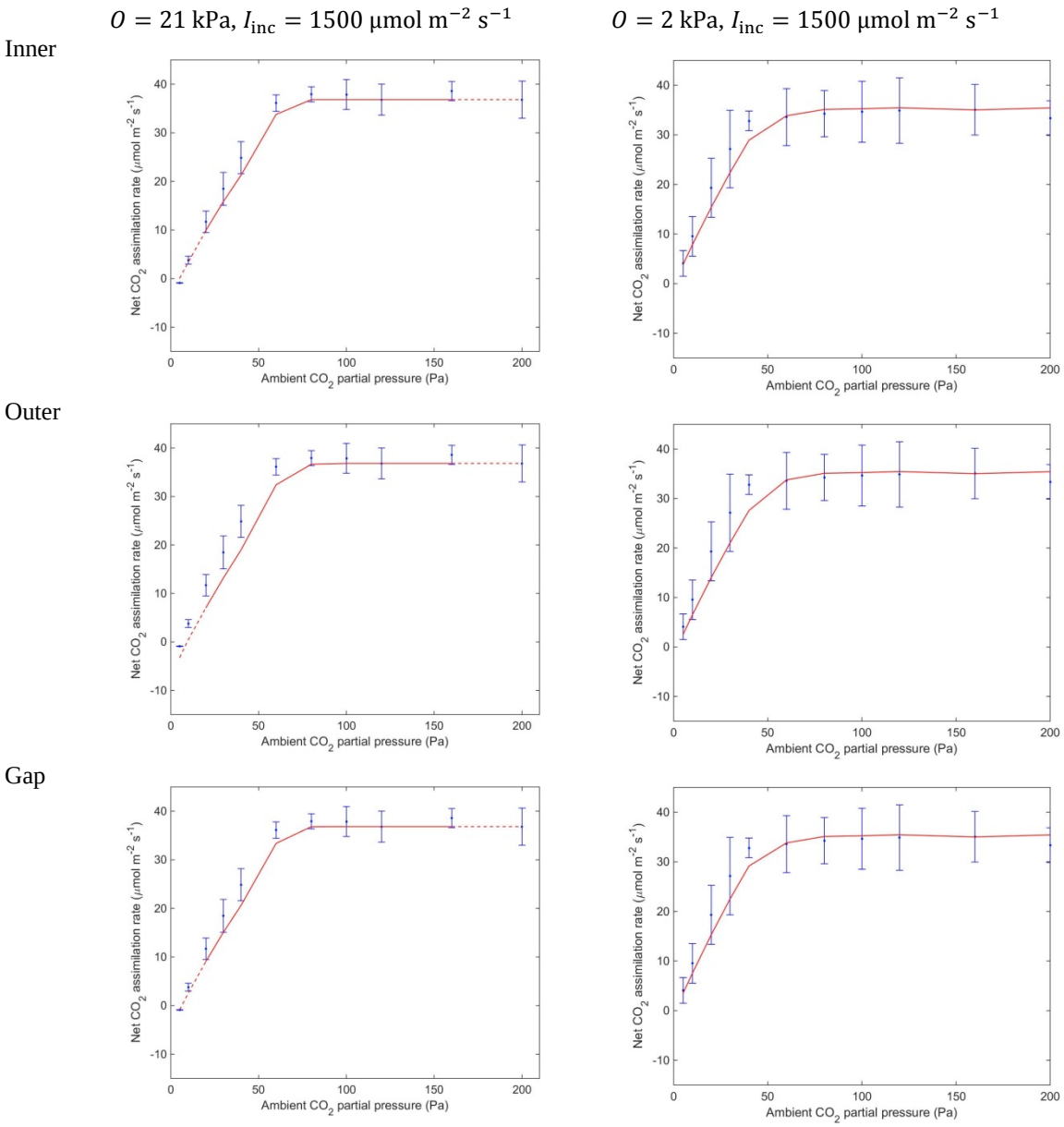

Figure A5.1.3: Measured (dots) and simulated CO_2 (solid lines and dashed lines) response curves for 15-day-old Doloress leaves from the data set of Chapter 3. (Photo)respiration was assumed to take place in either the inner cytosol (top row), the outer cytosol (middle row) or the cytosol gaps (bottom row). Measurements were taken under saturating light and either an ambient O_2 partial pressure ($O = 21$ kPa) (left) or a low O_2 partial pressure ($O = 2$ kPa) (right). The error bars represent one standard deviation. The solid lines represent the predicted net CO_2 assimilation rates for values of C_a and I_{inc} that were neither used in the estimation procedure of R_d and V_{cmax} nor for the determination of T_p. The dashed lines connect the predicted net CO_2 assimilation rates under the remaining values of C_a with the solid lines.

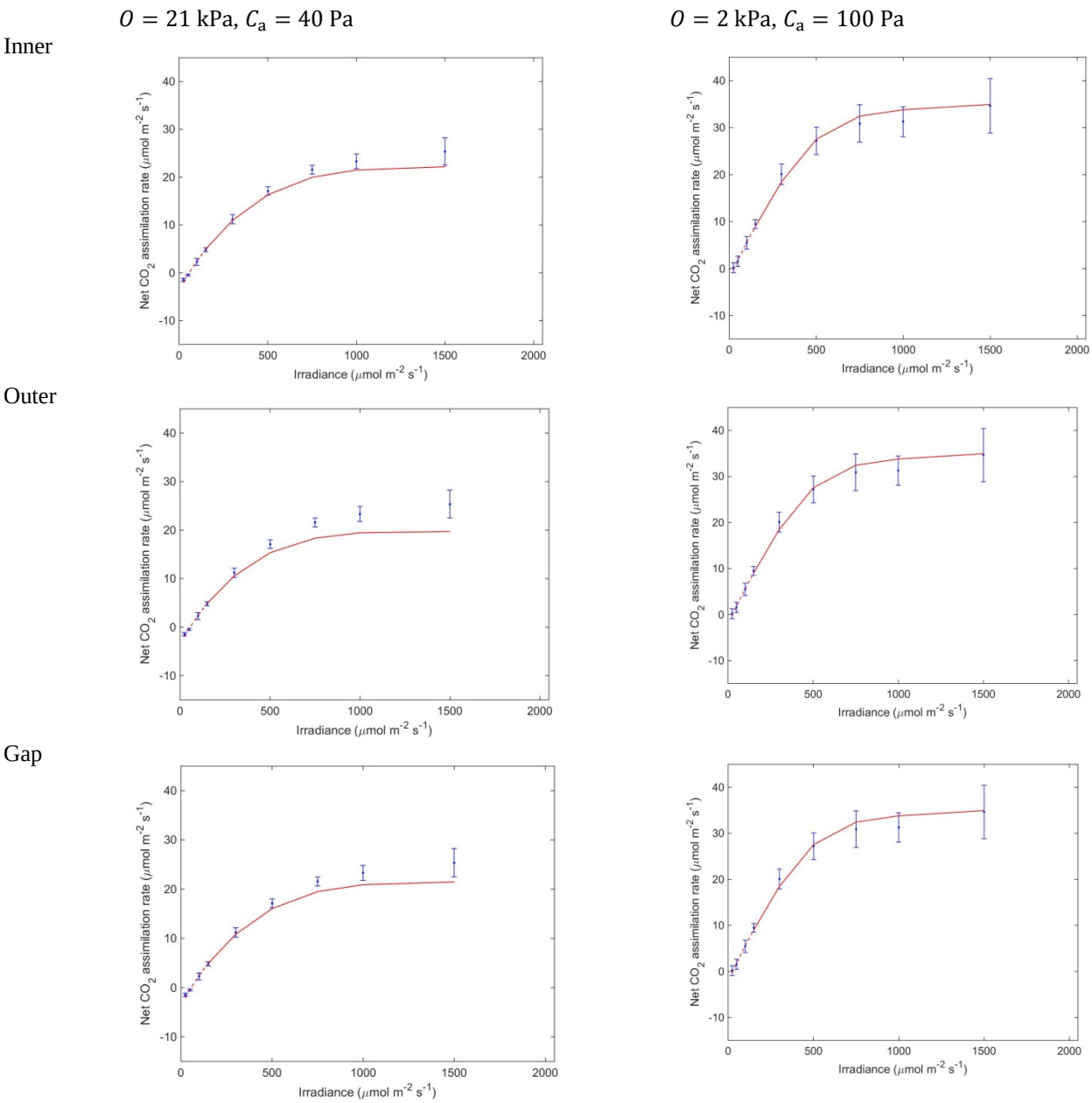

Figure A5.1.4: Measured (dots) and simulated light (solid lines and dashed lines) response curves for 15-day-old Doloress leaves from the data set of Chapter 3. (Photo)respiration was assumed to take place in either the inner cytosol (top row), the outer cytosol (middle row) or the cytosol gaps (bottom row). Measurements were taken under either photorespiratory conditions ($O = 21$ kPa, $C_a = 40$ Pa) (left) or non-photorespiratory conditions ($O = 21$ kPa, $C_a = 100$ Pa) (right). The error bars represent one standard deviation. The solid lines represent the predicted net CO_2 assimilation rates for values of C_a and I_{inc} that were neither used in the estimation procedure of R_d and V_{cmax} nor for the determination of T_p. The dashed lines connect the predicted net CO_2 assimilation rates under the remaining values of I_{inc} with the solid lines.

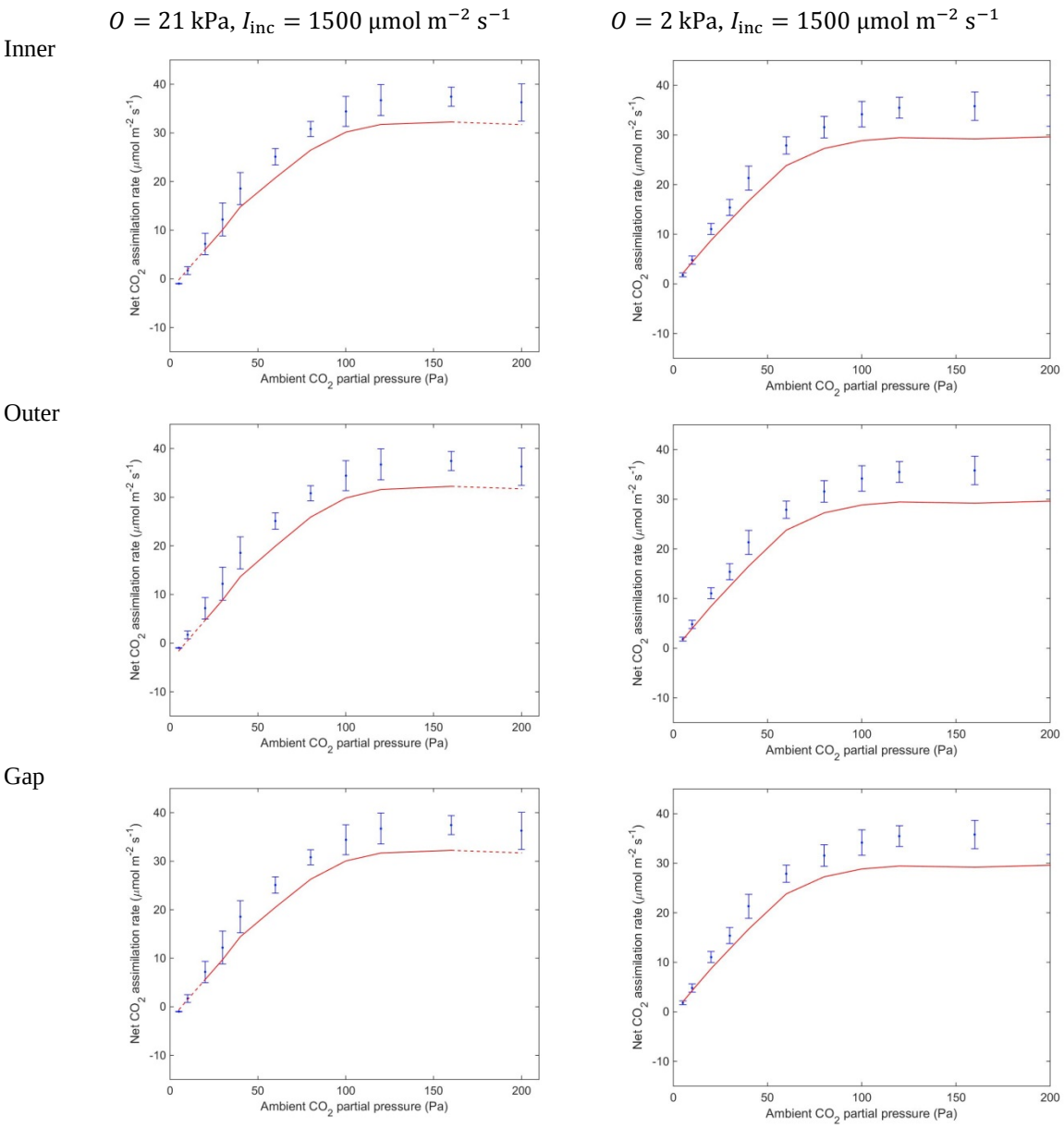

Figure A5.1.5: Measured (dots) and simulated CO_2 (solid lines and dashed lines) response curves for 25-day-old Doloress leaves from the data set of Chapter 3.. (Photo)respiration was assumed to take place in either the inner cytosol (top row), the outer cytosol (middle row) or the cytosol gaps (bottom row). Measurements were taken under saturating light and either an ambient O_2 partial pressure ($O = 21$ kPa) (left) or a low O_2 partial pressure ($O = 2$ kPa) (right). The error bars represent one standard deviation. The solid lines represent the predicted net CO_2 assimilation rates for values of C_a and I_{inc} that were neither used in the estimation procedure of R_d and V_{cmax} nor for the determination of T_p. The dashed lines connect the predicted net CO_2 assimilation rates under the remaining values of C_a with the solid lines.

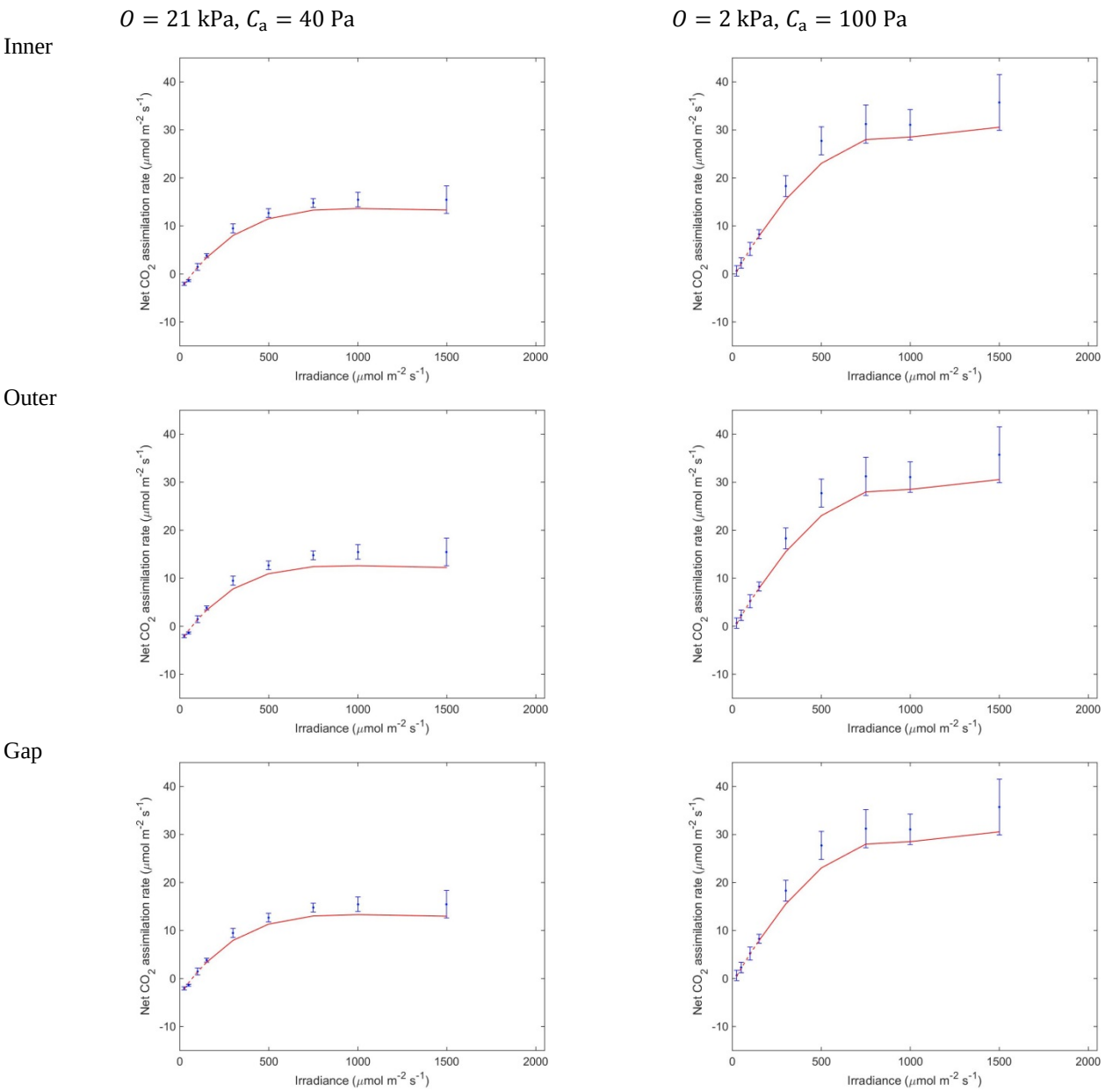

Figure A5.1.6: Measured (dots) and simulated light (solid lines and dashed lines) response curves for 25-day-old Doloress leaves from the data set of Chapter 3.. (Photo)respiration was assumed to take place in either the inner cytosol (top row), the outer cytosol (middle row) or the cytosol gaps (bottom row). Measurements were taken under either photorespiratory conditions ($O = 21$ kPa, $C_a = 40$ Pa) (left) or non-photorespiratory conditions ($O = 21$ kPa, $C_a = 100$ Pa) (right). The error bars represent one standard deviation. The solid lines represent the predicted net CO_2 assimilation rates for values of C_a and I_{inc} that were neither used in the estimation procedure of R_d and V_{cmax} nor for the determination of T_p. The dashed lines connect the predicted net CO_2 assimilation rates under the remaining values of I_{inc} with the solid lines.

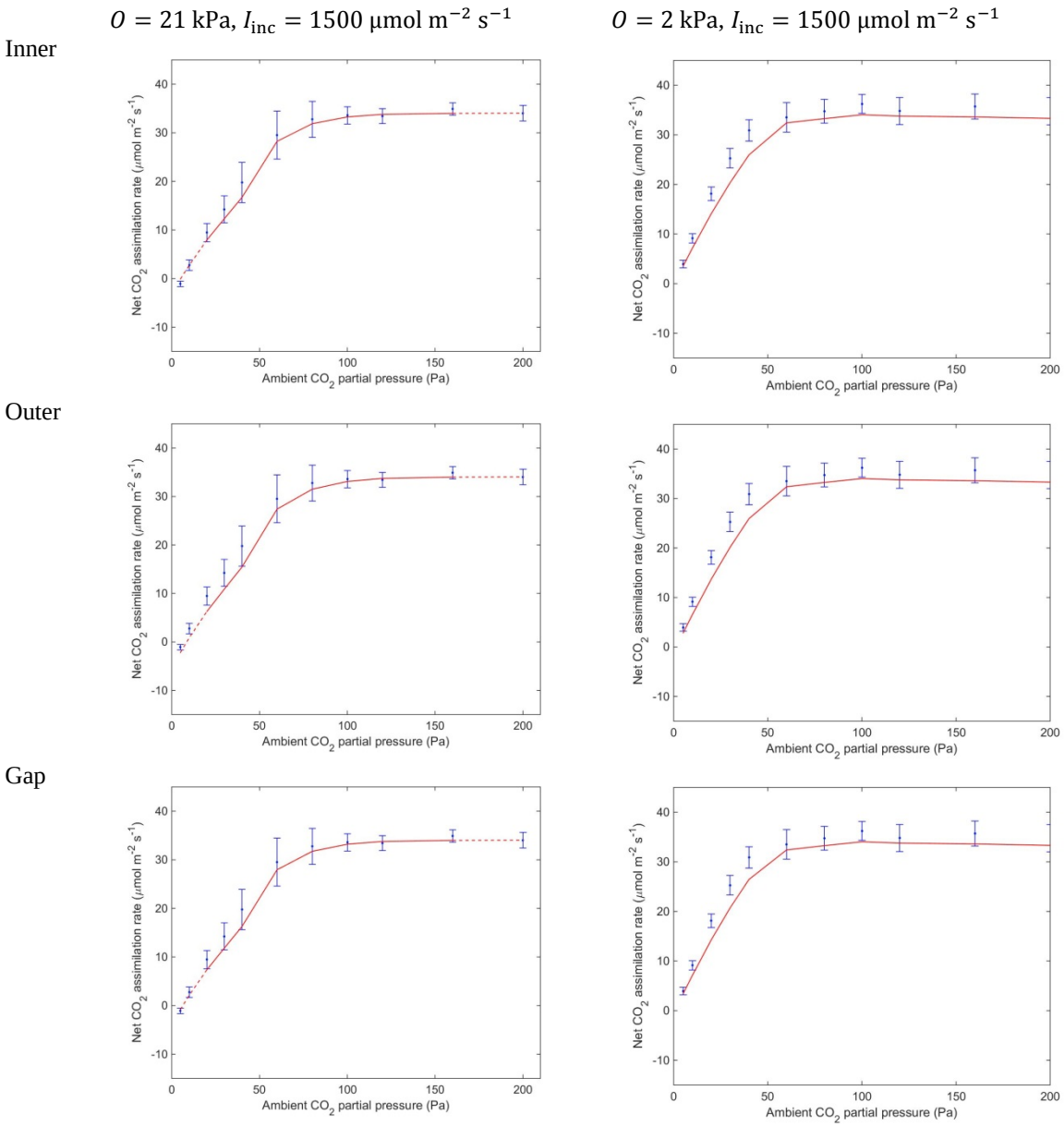

Figure A5.1.7: Measured (dots) and simulated CO_2 (solid lines and dashed lines) response curves for 15-day-old Growdena leaves from the data set of Chapter 3.. (Photo)respiration was assumed to take place in either the inner cytosol (top row), the outer cytosol (middle row) or the cytosol gaps (bottom row). Measurements were taken under saturating light and either an ambient O_2 partial pressure ($O = 21$ kPa) (left) or a low O_2 partial pressure ($O = 2$ kPa) (right). The error bars represent one standard deviation. The solid lines represent the predicted net CO_2 assimilation rates for values of C_a and I_{inc} that were neither used in the estimation procedure of R_d and V_{cmax} nor for the determination of T_p. The dashed lines connect the predicted net CO_2 assimilation rates under the remaining values of C_a with the solid lines.

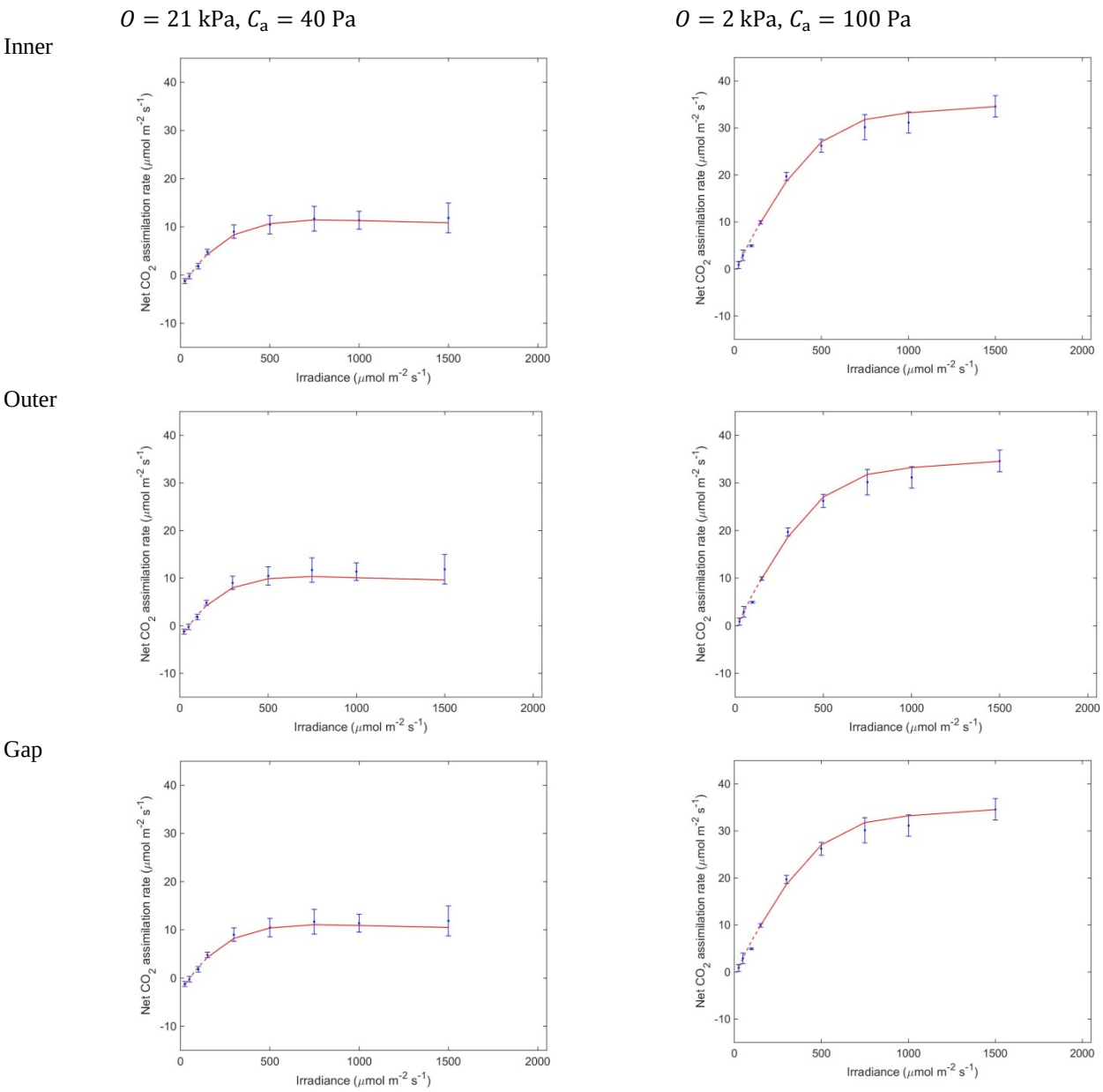

Figure A5.1.8: Measured (dots) and simulated light (solid lines and dashed lines) response curves for 15-day-old Growdena leaves from the data set of Chapter 3. (Photo)respiration was assumed to take place in either the inner cytosol (top row), the outer cytosol (middle row) or the cytosol gaps (bottom row). Measurements were taken under either photorespiratory conditions ($O = 21$ kPa, $C_a = 40$ Pa) (left) or non-photorespiratory conditions ($O = 21$ kPa, $C_a = 100$ Pa) (right). The error bars represent one standard deviation. The solid lines represent the predicted net CO_2 assimilation rates for values of C_a and I_{inc} that were neither used in the estimation procedure of R_d and V_{cmax} nor for the determination of T_p. The dashed lines connect the predicted net CO_2 assimilation rates under the remaining values of I_{inc} with the solid lines.

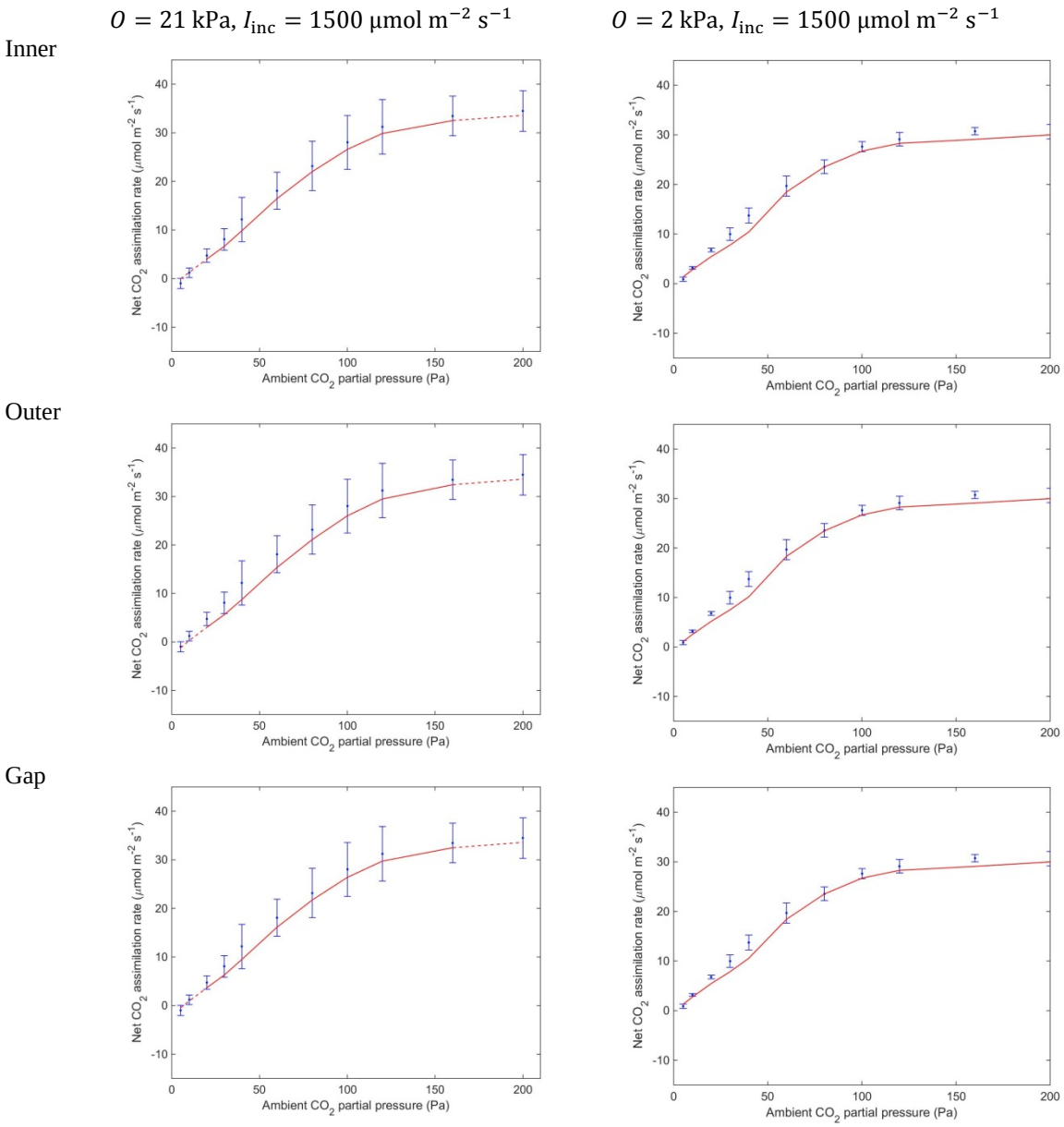

Figure A5.1.9: Measured (dots) and simulated CO_2 (solid lines and dashed lines) response curves for 25-day-old Growdena leaves from the data set of Chapter 3. (Photo)respiration was assumed to take place in either the inner cytosol (top row), the outer cytosol (middle row) or the cytosol gaps (bottom row). Measurements were taken under saturating light and either an ambient O_2 partial pressure ($O = 21$ kPa) (left) or a low O_2 partial pressure ($O = 2$ kPa) (right). The error bars represent one standard deviation. The solid lines represent the predicted net CO_2 assimilation rates for values of C_a and I_{inc} that were neither used in the estimation procedure of R_d and V_{cmax} nor for the determination of T_p. The dashed lines connect the predicted net CO_2 assimilation rates under the remaining values of C_a with the solid lines.

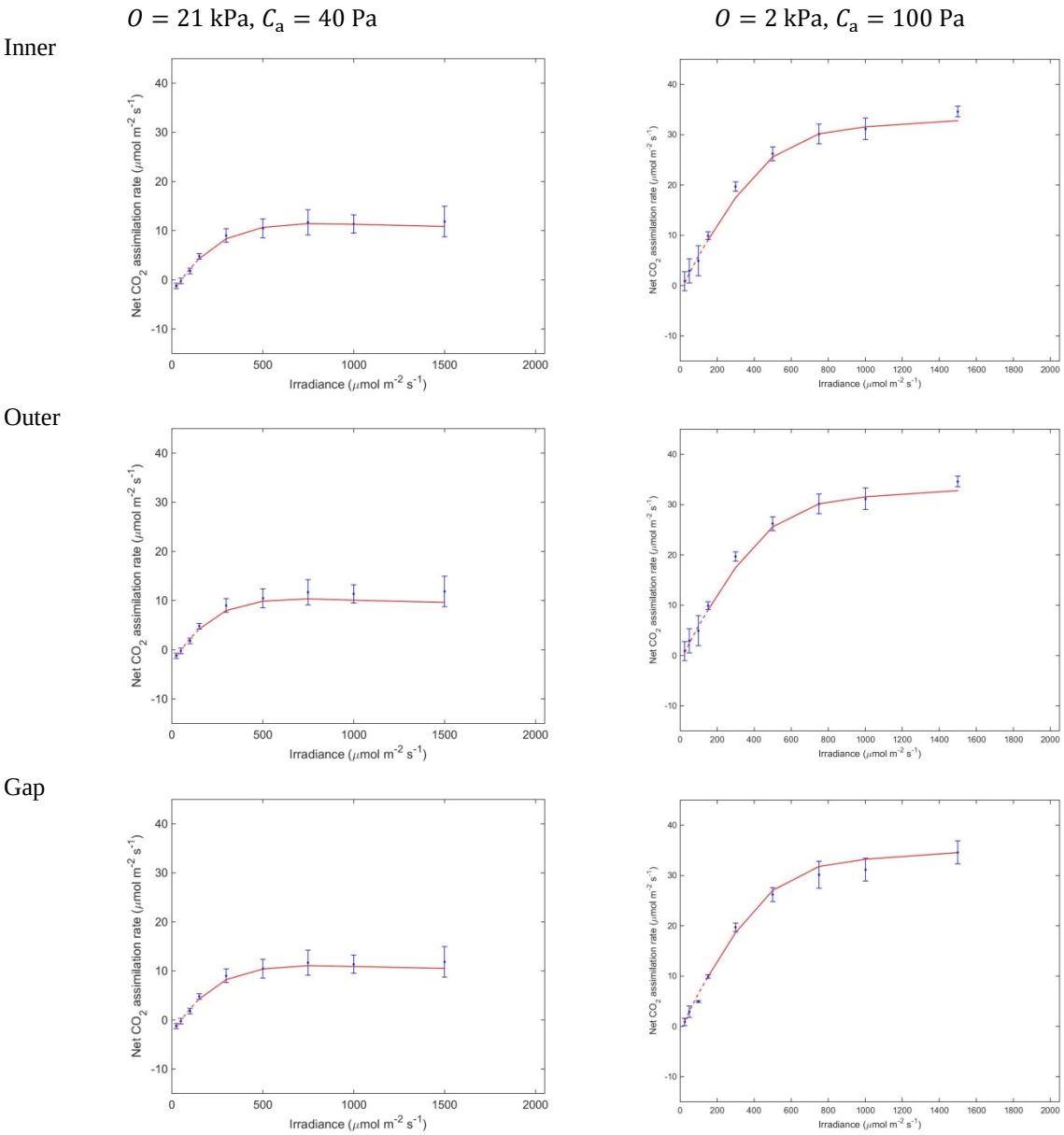

Figure A5.1.10: Measured (dots) and simulated light (solid lines and dashed lines) response curves for 25-day-old Growdena leaves from the data set of Chapter 3.. (Photo)respiration was assumed to take place in either the inner cytosol (top row), the outer cytosol (middle row) or the cytosol gaps (bottom row). Measurements were taken under either photorespiratory conditions ($O = 21$ kPa, $C_a = 40$ Pa) (left) or non-photorespiratory conditions ($O = 21$ kPa, $C_a = 100$ Pa) (right). The error bars represent one standard deviation. The solid lines represent the predicted net CO_2 assimilation rates for values of C_a and I_{inc} that were neither used in the estimation procedure of R_d and V_{cmax} nor for the determination of T_p. The dashed lines connect the predicted net CO_2 assimilation rates under the remaining values of I_{inc} with the solid lines.

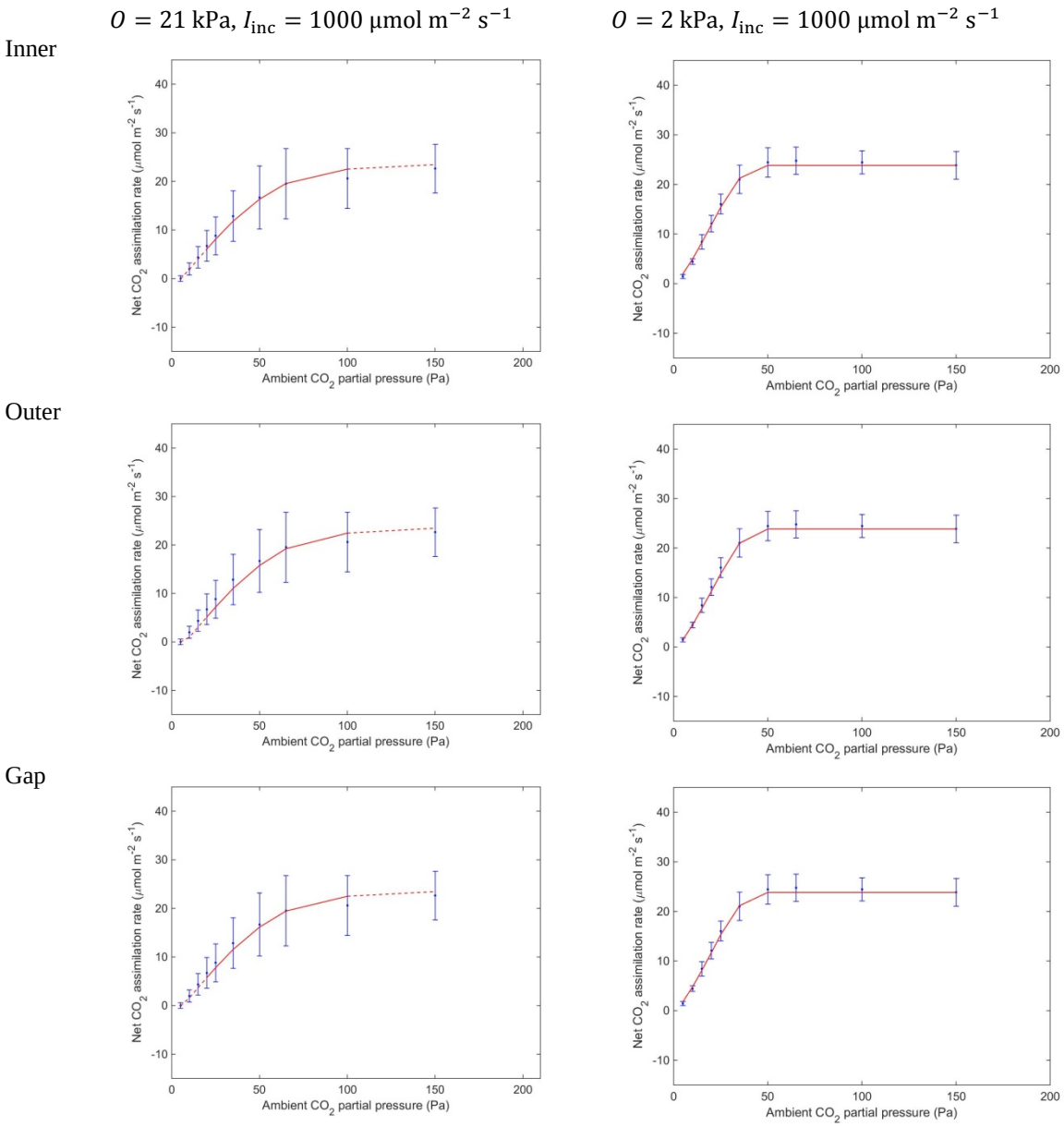

Figure A5.1.11: Measured (dots) and simulated CO_2 (solid lines and dashed lines) response curves Admiro upper leaves from the Ho *et al.* (2016) data set. (Photo)respiration was assumed to take place in either the inner cytosol (top row), the outer cytosol (middle row) or the cytosol gaps (bottom row). Measurements were taken under saturating light and either an ambient O_2 partial pressure ($O = 21$ kPa) (left) or a low O_2 partial pressure ($O = 2$ kPa) (right). The error bars represent one standard deviation. The solid lines represent the predicted net CO_2 assimilation rates for values of C_a and I_{inc} that were neither used in the estimation procedure of R_d and V_{cmax} nor for the determination of T_p. The dashed lines connect the predicted net CO_2 assimilation rates under the remaining values of C_a with the solid lines.

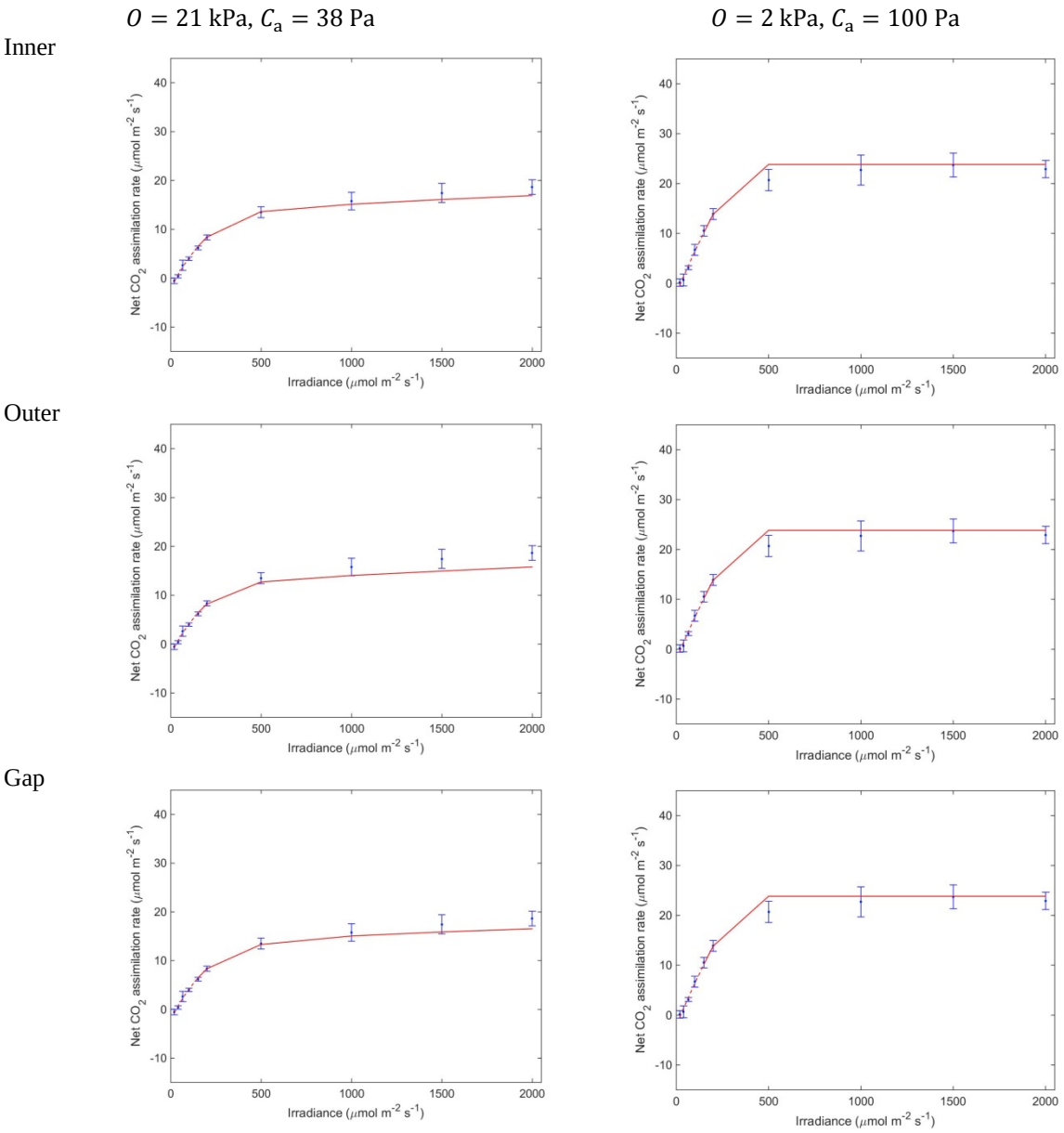

Figure A5.1.12: Measured (dots) and simulated light (solid lines and dashed lines) response curves for Admiro upper leaves from the Ho *et al.* (2016) data set. (Photo)respiration was assumed to take place in either the inner cytosol (top row), the outer cytosol (middle row) or the cytosol gaps (bottom row). Measurements were taken under either photorespiratory conditions ($O = 21$ kPa, $C_a = 100$ Pa) (left) or non-photorespiratory conditions ($O = 21$ kPa, $C_a = 40$ Pa) (right). The error bars represent one standard deviation. The solid lines represent the predicted net CO_2 assimilation rates for values of I_{inc} that were neither used in the estimation procedure of R_d and V_{cmax} nor for the determination of T_p. The dashed lines connect the predicted net CO_2 assimilation rates under the remaining values of I_{inc} with the solid lines.

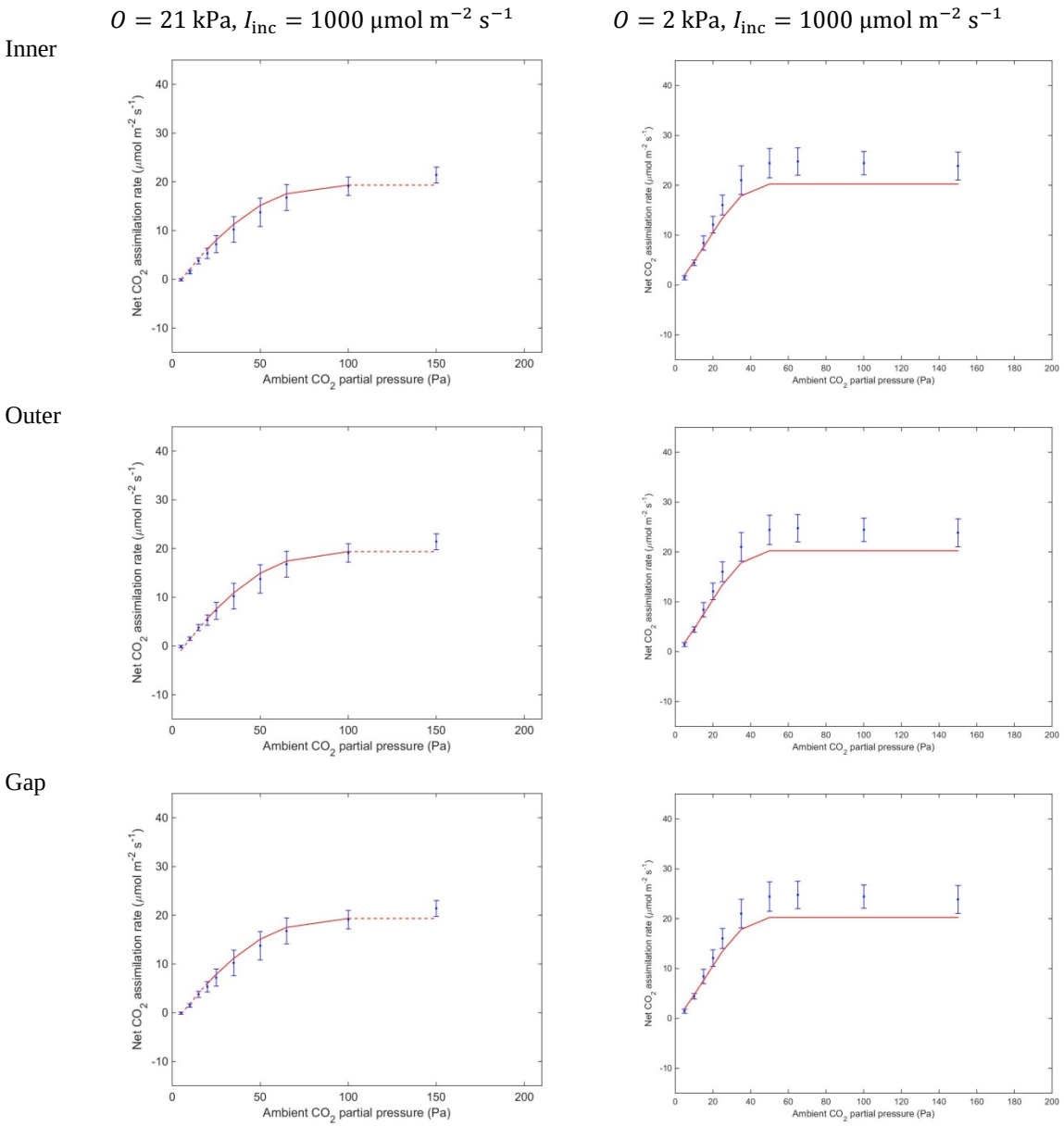

Figure A5.1.13: Measured (dots) and simulated CO_2 (solid lines and dashed lines) response curves for Admiro leaves from the from the Ho *et al.* (2016) data set. (Photo)respiration was assumed to take place in either the inner cytosol (top row), the outer cytosol (middle row) or the cytosol gaps (bottom row). Measurements were taken under saturating light and either an ambient O_2 partial pressure ($O = 21$ kPa) (left) or a low O_2 partial pressure ($O = 2$ kPa) (right). The error bars represent one standard deviation. The solid lines represent the predicted net CO_2 assimilation rates for values of C_a that were neither used in the estimation procedure of R_d and V_{cmax} nor for the determination of T_p. The dashed lines connect the predicted net CO_2 assimilation rates under the remaining values of C_a with the solid lines.

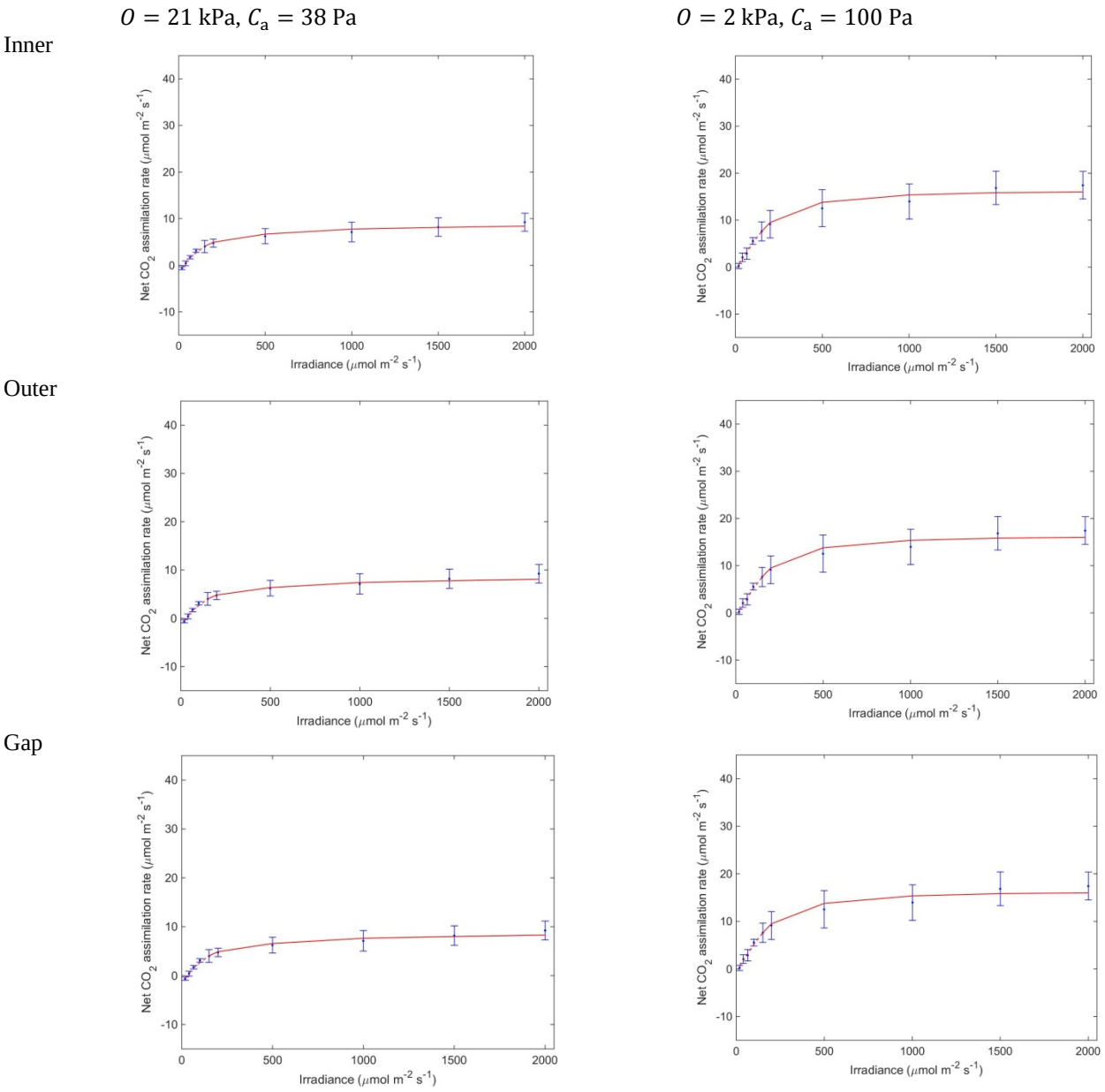

Figure A5.1.14: Measured (dots) and simulated CO_2 (solid lines and dashed lines) response curves for Admiro leaves lower from the from the Ho *et al.* (2016) data set. (Photo)respiration was assumed to take place in either the inner cytosol (top row), the outer cytosol (middle row) or the cytosol gaps (bottom row). Measurements were taken under either photorespiratory conditions ($O = 21$ kPa, $C_a = 40$ Pa) (left) or non-photorespiratory conditions ($O = 21$ kPa, $C_a = 100$ Pa) (right). The error bars represent one standard deviation. The solid lines represent the predicted net CO_2 assimilation rates for values of I_{inc} that were neither used in the estimation procedure of R_d and V_{cmax} nor for the determination of T_p. The dashed lines connect the predicted net CO_2 assimilation rates under the remaining values of I_{inc} with the solid lines.

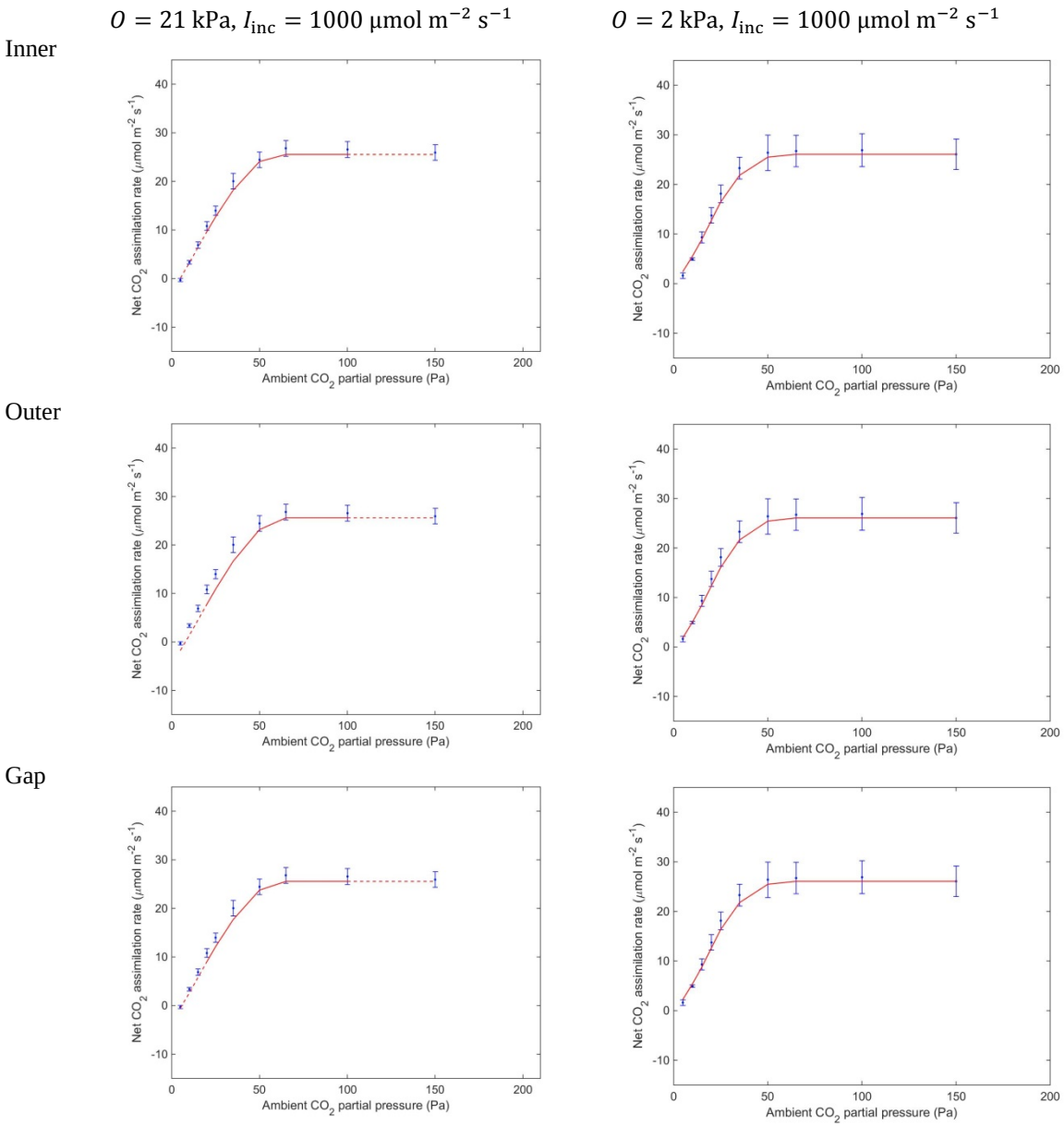

Figure A5.1.15: Measured (dots) and simulated CO_2 (solid lines and dashed lines) response curves for Doloress upper leaves from the from the Ho *et al.* (2016) data set. (Photo)respiration was assumed to take place in either the inner cytosol (top row), the outer cytosol (middle row) or the cytosol gaps (bottom row). Measurements were taken under saturating light and either an ambient O_2 partial pressure ($O = 21$ kPa) (left) or a low O_2 partial pressure ($O = 2$ kPa) (right). The error bars represent one standard deviation. The solid lines represent the predicted net CO_2 assimilation rates for values of C_a that were neither used in the estimation procedure of R_d and V_{cmax} nor for the determination of T_p. The dashed lines connect the predicted net CO_2 assimilation rates under the remaining values of C_a with the solid lines.

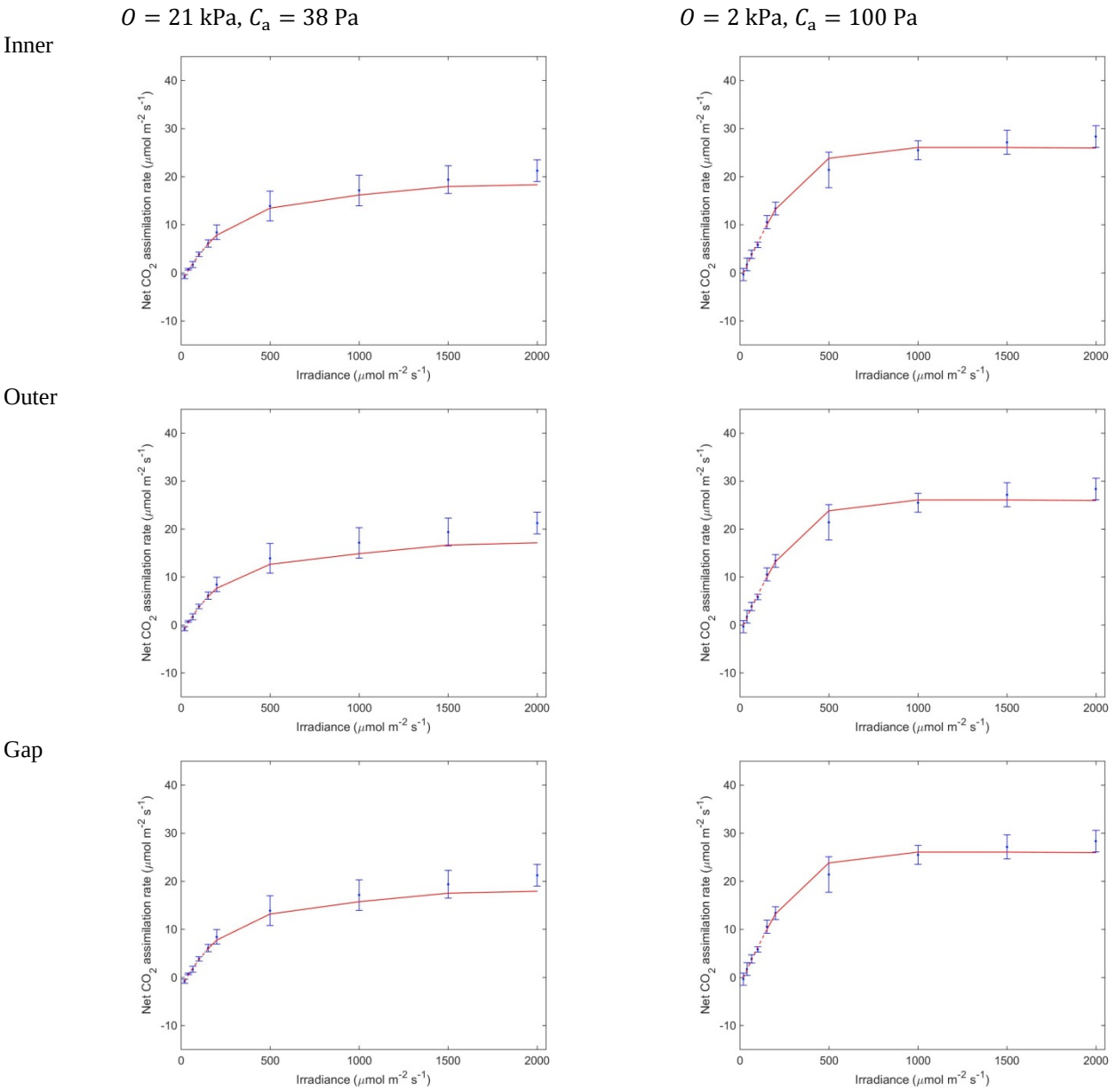

Figure A5.1.16: Measured (dots) and simulated CO_2 (solid lines and dashed lines) response curves for Doloress upper leaves from the from the Ho *et al.* (2016) data set. (Photo)respiration was assumed to take place in either the inner cytosol (top row), the outer cytosol (middle row) or the cytosol gaps (bottom row). Measurements were taken under either photorespiratory conditions ($O = 21$ kPa, $C_a = 40$ Pa) (left) or non-photorespiratory conditions ($O = 21$ kPa, $C_a = 100$ Pa) (right). The error bars represent one standard deviation. The solid lines represent the predicted net CO_2 assimilation rates for values of I_{inc} that were neither used in the estimation procedure of R_d and V_{cmax} nor for the determination of T_p. The dashed lines connect the predicted net CO_2 assimilation rates under the remaining values of I_{inc} with the solid lines.

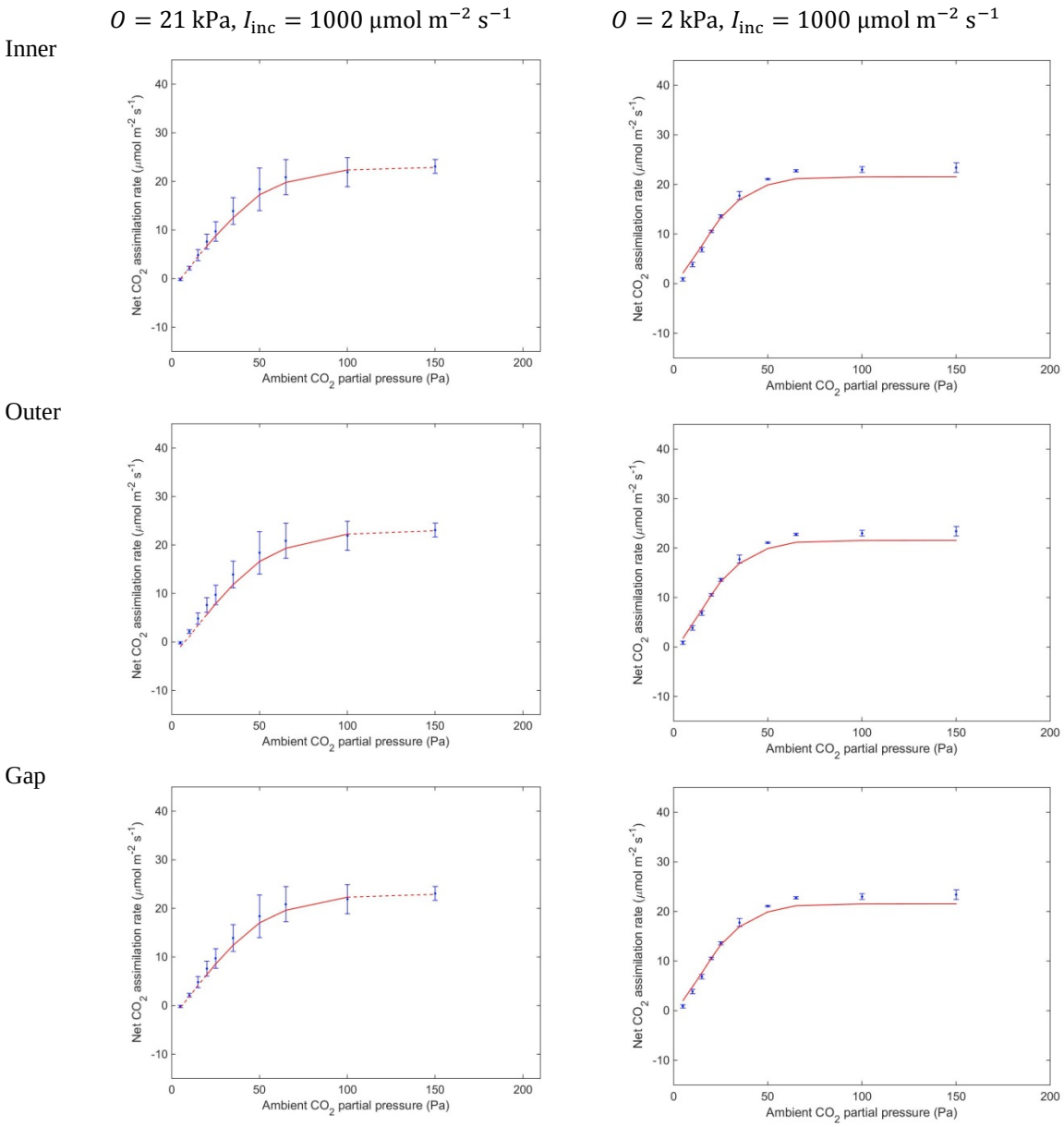

Figure A5.1.17: Measured (dots) and simulated CO_2 (solid lines and dashed lines) response curves for Doloress lower leaves from the from the Ho *et al.* (2016) data set. (Photo)respiration was assumed to take place in either the inner cytosol (top row), the outer cytosol (middle row) or the cytosol gaps (bottom row). Measurements were taken under saturating light and either an ambient O_2 partial pressure ($O = 21$ kPa) (left) or a low O_2 partial pressure ($O = 2$ kPa) (right). The error bars represent one standard deviation. The solid lines represent the predicted net CO_2 assimilation rates for values of C_a that were neither used in the estimation procedure of R_d and V_{cmax} nor for the determination of T_p. The dashed lines connect the predicted net CO_2 assimilation rates under the remaining values of C_a with the solid lines.

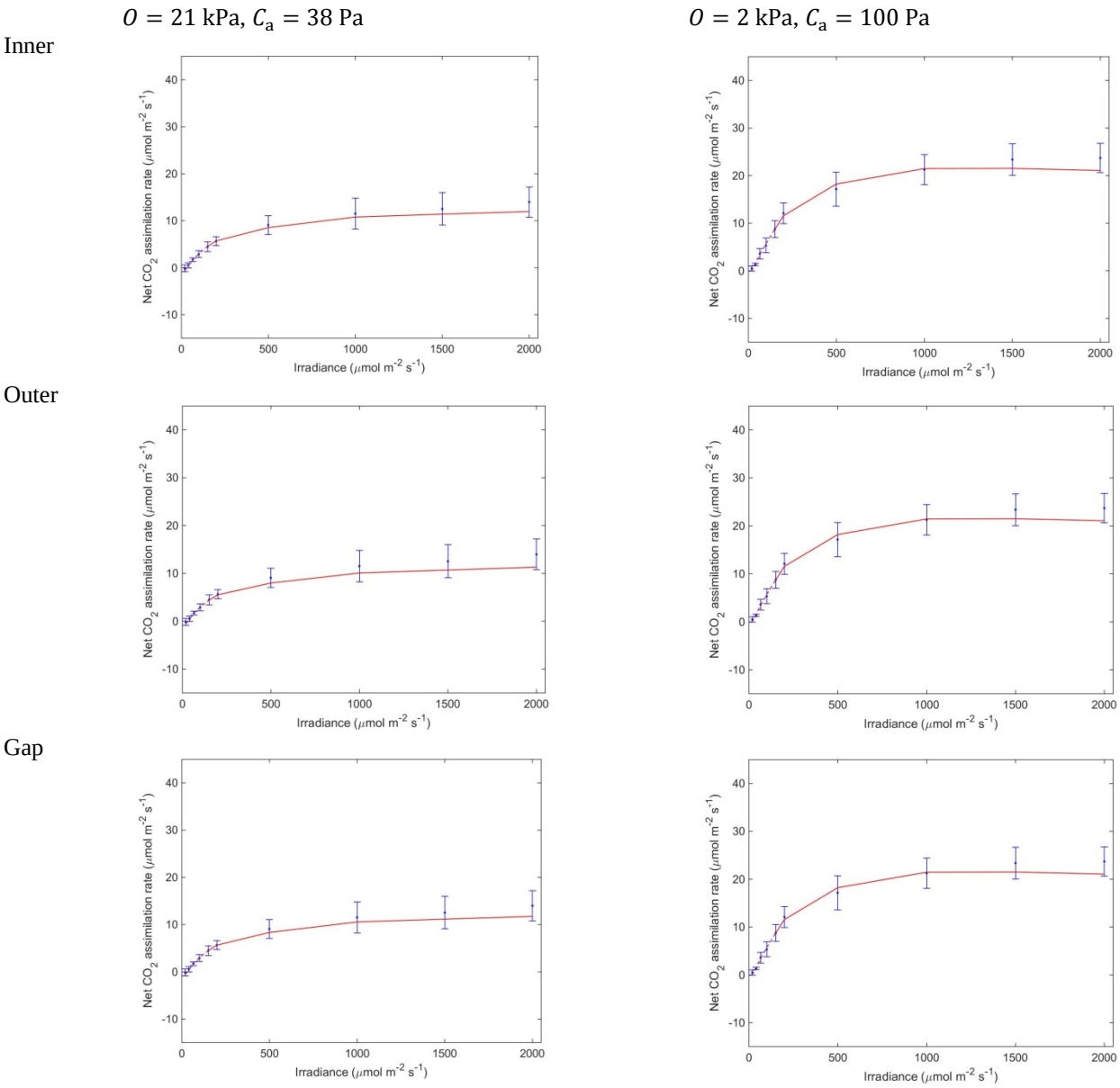

Figure A5.1.18: Measured (dots) and simulated light (solid lines and dashed lines) response curves for Doloress lower leaves from the from the Ho *et al.* (2016) data set. (Photo)respiration was assumed to take place in either the inner cytosol (top row), the outer cytosol (middle row) or the cytosol gaps (bottom row). Measurements were taken under either photorespiratory conditions ($O = 21$ kPa, $C_a = 40$ Pa) (left) or non-photorespiratory conditions ($O = 21$ kPa, $C_a = 100$ Pa) (right). The error bars represent one standard deviation. The solid lines represent the predicted net CO_2 assimilation rates for values of I_{inc} that were neither used in the estimation procedure of R_d and V_{cmax} nor for the determination of T_p. The dashed lines connect the predicted net CO_2 assimilation rates under the remaining values of I_{inc} with the solid lines.

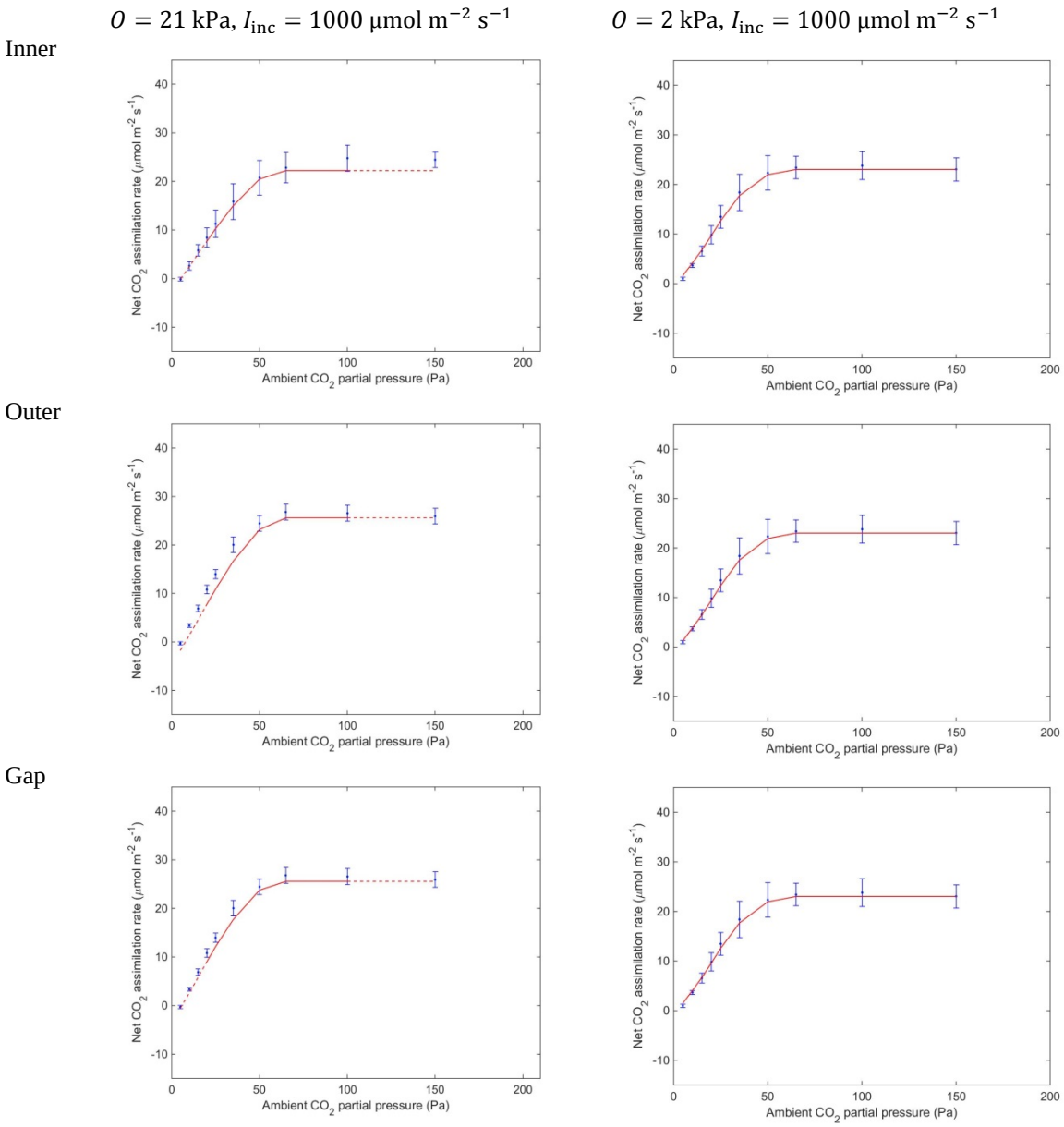

Figure A5.1.19: Measured (dots) and simulated CO_2 (solid lines and dashed lines) response curves for Growdena upper leaves from the Ho *et al.* (2016) data set. (Photo)respiration was assumed to take place in either the inner cytosol (top row), the outer cytosol (middle row) or the cytosol gaps (bottom row). Measurements were taken under saturating light and either an ambient O_2 partial pressure ($O = 21$ kPa) (left) or a low O_2 partial pressure ($O = 2$ kPa) (right). The error bars represent one standard deviation. The solid lines represent the predicted net CO_2 assimilation rates for values of C_a that were neither used in the estimation procedure of R_d and V_{cmax} nor for the determination of T_p. The dashed lines connect the predicted net CO_2 assimilation rates under the remaining values of C_a with the solid lines.

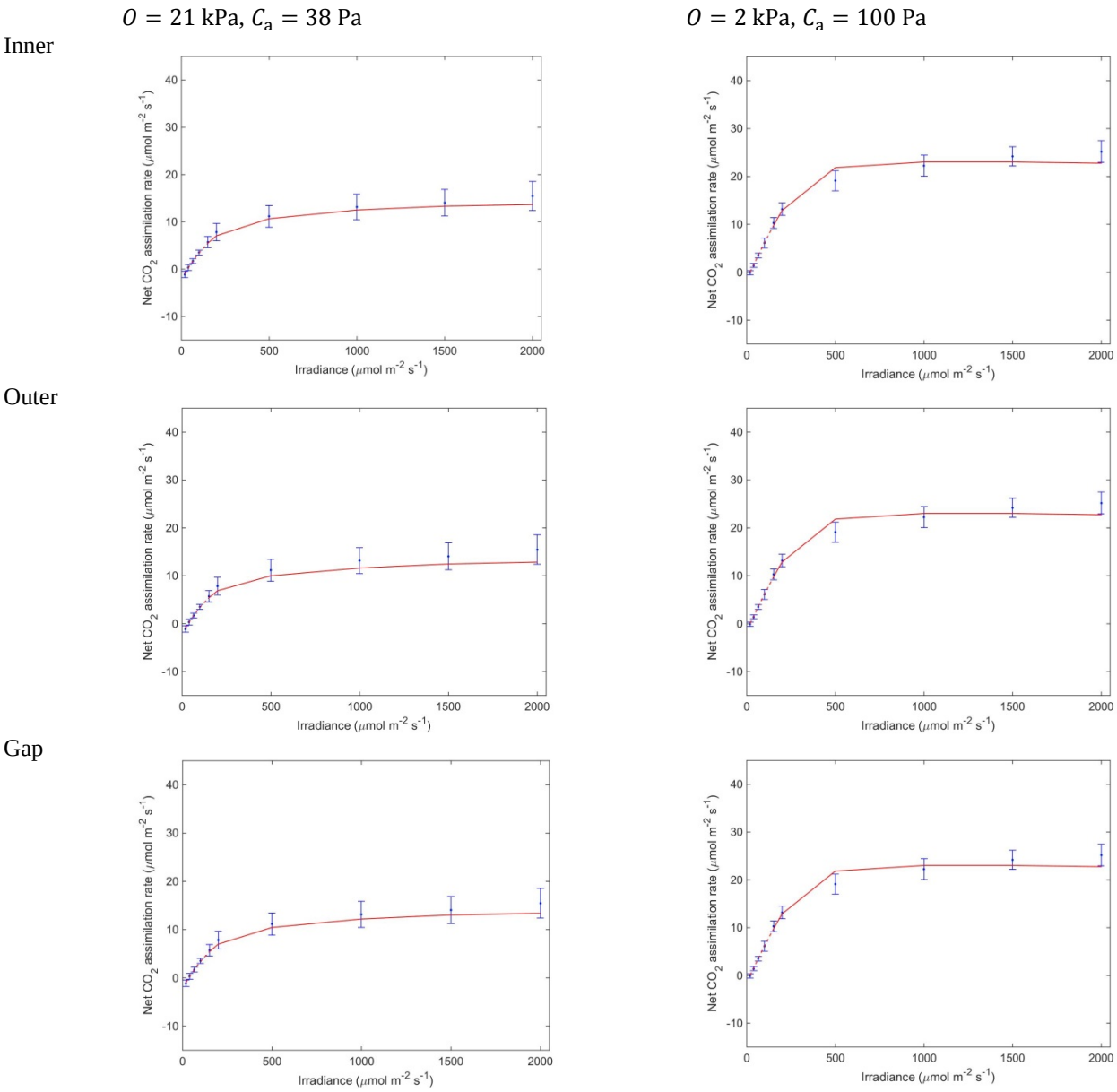

Figure A5.1.20: Measured (dots) and simulated light (solid lines and dashed lines) response curves for Growdena upper leaves from the from the Ho *et al.* (2016) data set. (Photo)respiration was assumed to take place in either the inner cytosol (top row), the outer cytosol (middle row) or the cytosol gaps (bottom row). Measurements were taken under either photorespiratory conditions ($O = 21$ kPa, $C_a = 40$ Pa) (left) or non-photorespiratory conditions ($O = 21$ kPa, $C_a = 100$ Pa) (right). The error bars represent one standard deviation. The solid lines represent the predicted net CO_2 assimilation rates for values I_{inc} that were neither used in the estimation procedure of R_d and V_{cmax} nor for the determination of T_p. The dashed lines connect the predicted net CO_2 assimilation rates under the remaining values of I_{inc} with the solid lines.

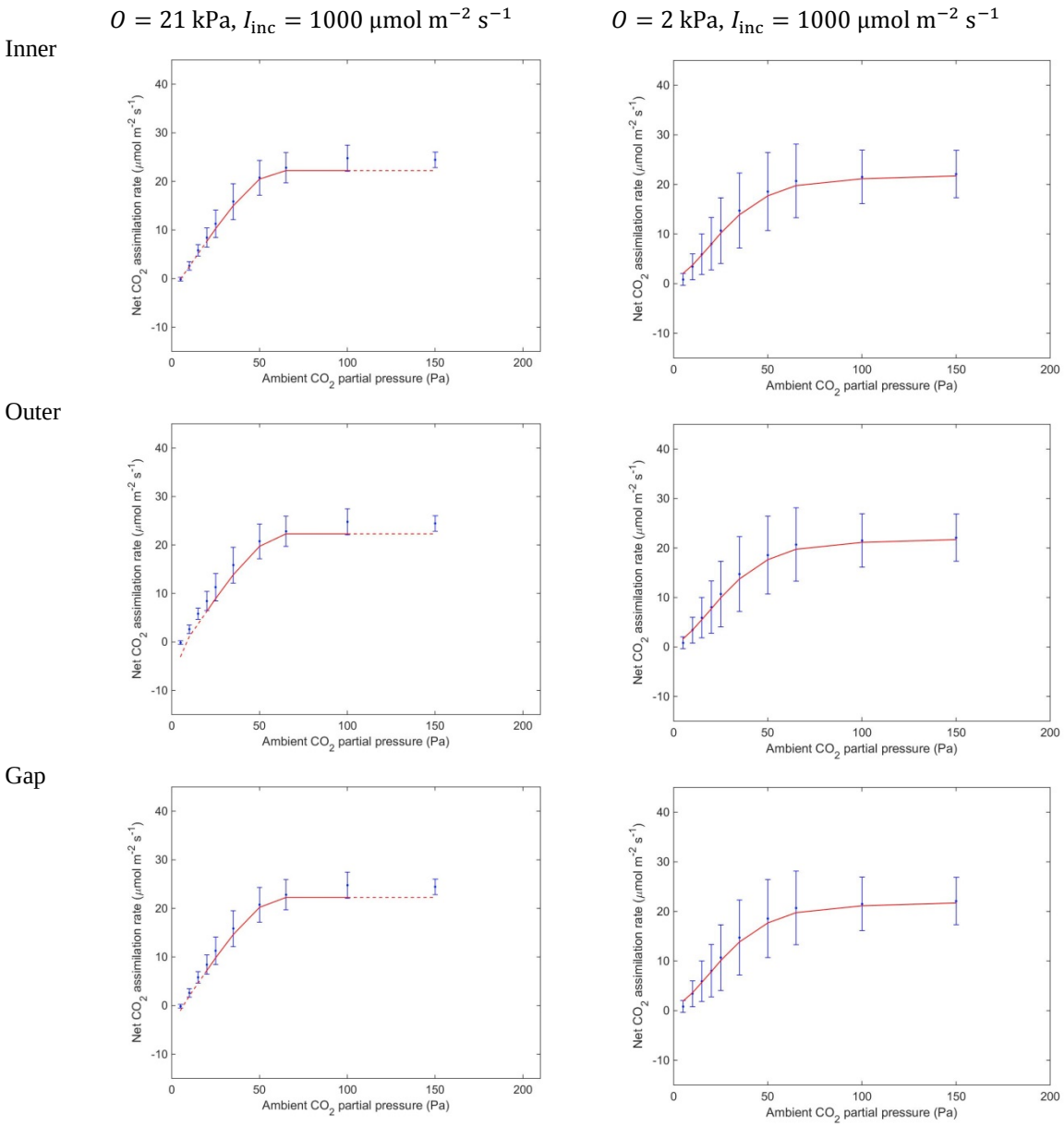

Figure A5.1.21: Measured (dots) and simulated CO_2 (solid lines and dashed lines) response curves for Growdena lower leaves from the Ho *et al.* (2016) data set. (Photo)respiration was assumed to take place in either the inner cytosol (top row), the outer cytosol (middle row) or the cytosol gaps (bottom row). Measurements were taken under saturating light and either an ambient O_2 partial pressure ($O = 21$ kPa) (left) or a low O_2 partial pressure ($O = 2$ kPa) (right). The error bars represent one standard deviation. The solid lines represent the predicted net CO_2 assimilation rates for values of C_a that were neither used in the estimation procedure of R_d and V_{cmax} nor for the determination of T_p. The dashed lines connect the predicted net CO_2 assimilation rates under the remaining values of C_a with the solid lines.

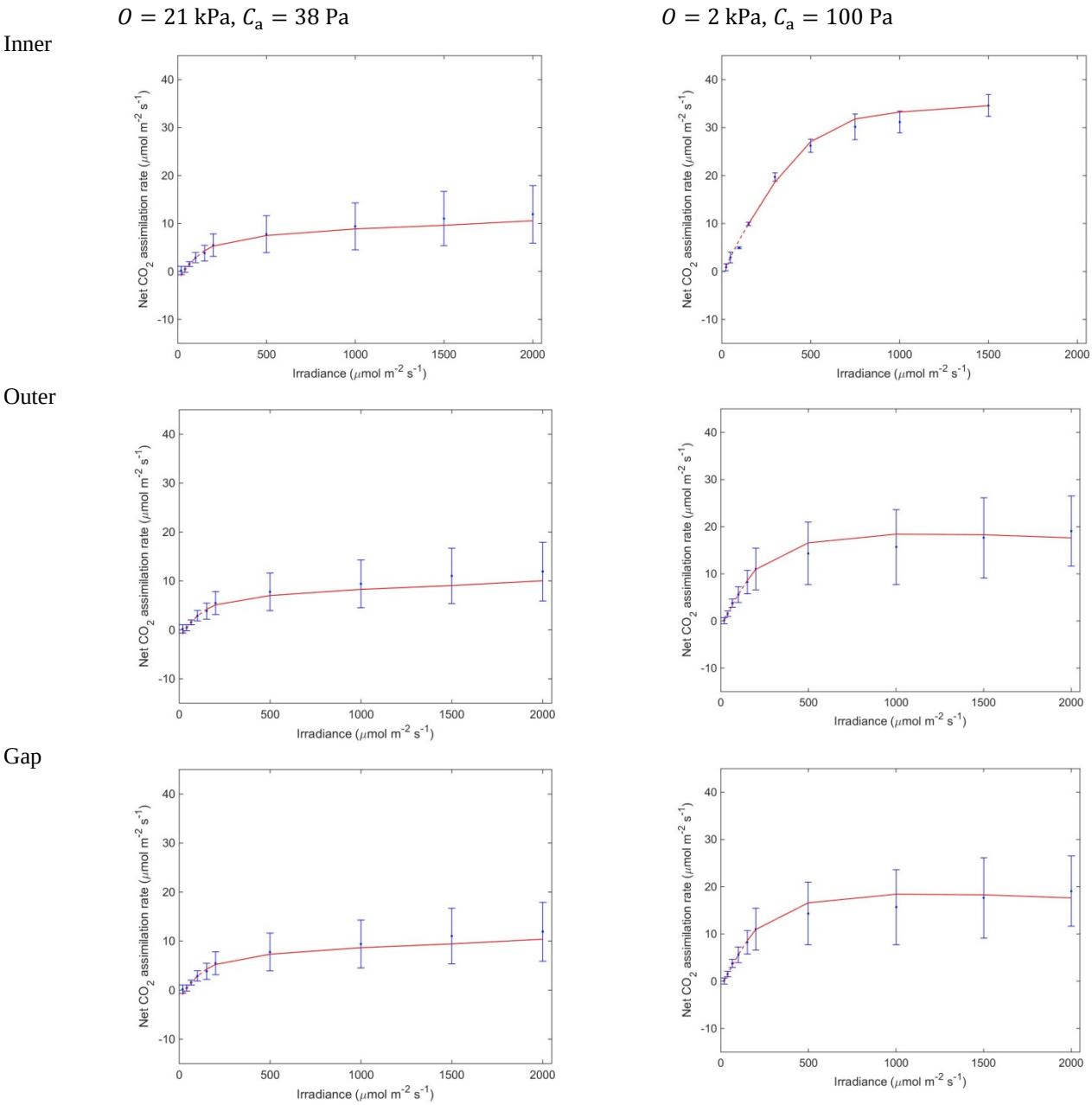

Figure A5.1.22: Measured (dots) and simulated light (solid lines and dashed lines) response curves for Growdena lower leaves from the from the Ho *et al.* (2016) data set. (Photo)respiration was assumed to take place in either the inner cytosol (top row), the outer cytosol (middle row) or the cytosol gaps (bottom row). Measurements were taken under either photorespiratory conditions ($O = 21$ kPa, $C_a = 40$ Pa) (left) or non-photorespiratory conditions ($O = 21$ kPa, $C_a = 100$ Pa) (right). The error bars represent one standard deviation. The solid lines represent the predicted net CO_2 assimilation rates for values of I_{inc} that were neither used in the estimation procedure of R_d and V_{cmax} nor for the determination of T_p. The dashed lines connect the predicted net CO_2 assimilation rates under the remaining values of I_{inc} with the solid lines.

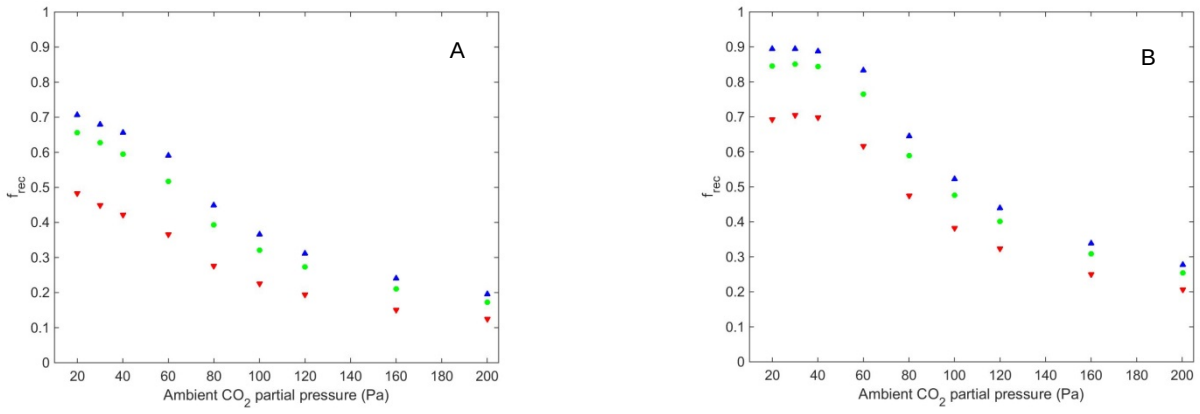

Figure A5.1.23: Response of the fraction of (photo)respired CO_2 that is re-assimilated f_{rec} to increased ambient CO_2 levels under ambient oxygen ($O = 21$ kPa) (A) and low oxygen levels ($O = 2$ kPa) (B) in 25-day-old Admiro leaves from the data set of Chapter 3. The release of (photo)respiratory CO_2 was assumed to either take place in the inner cytosol (upward pointing triangle), the outer cytosol (downward pointing triangle) or the cytosol gaps (dots).

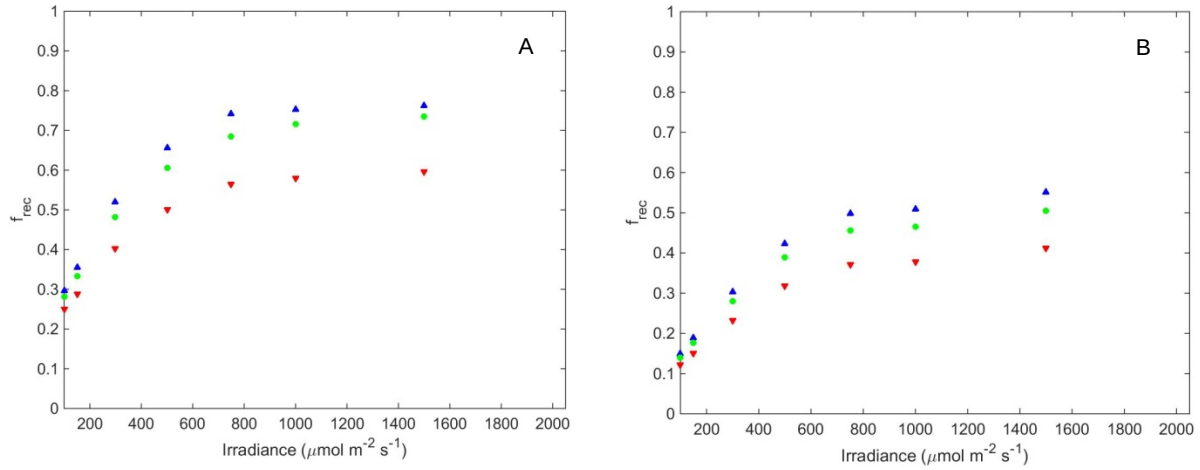

Figure A5.1.24: Response of the fraction of (photo)respired CO_2 that is re-assimilated f_{rec} to increased light levels under photorespiratory ($C_{\mathrm{a}} = 40$ Pa, $O = 21$ kPa) conditions (A) and non-photorespiratory ($C_{\mathrm{a}} = 100$ Pa, $O = 2$ kPa) conditions (B) in 25-day-old Admiro leavesfrom the data set of Chapter 3. The release of (photo)respiratory CO_2 was assumed to either take place in the inner cytosol (upward pointing triangle), the outer cytosol (downward pointing triangle) or the cytosol gaps (dots).

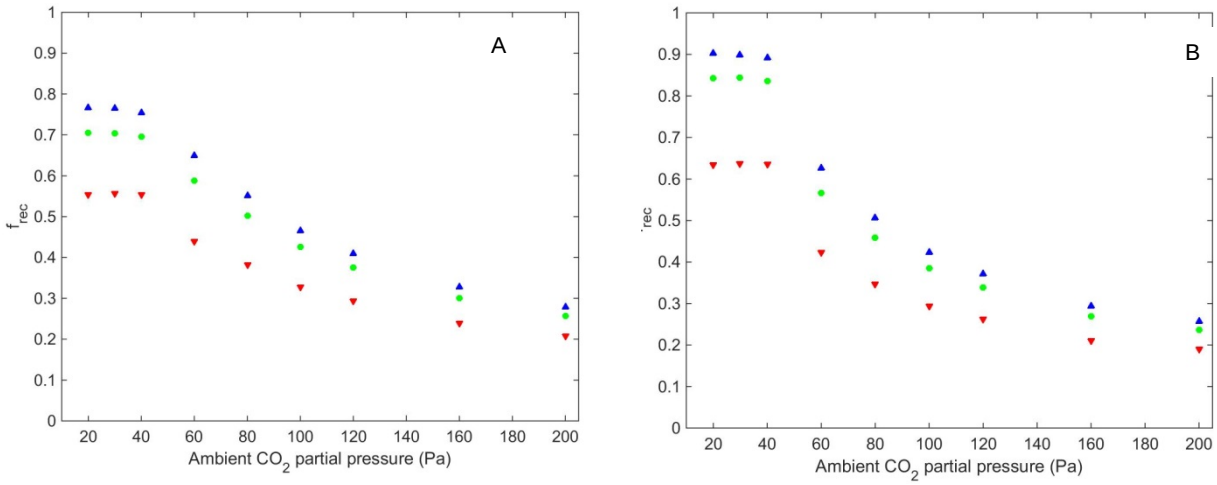

Figure A5.1.25: Response of the fraction of (photo)respired CO_2 that is re-assimilated f_{rec} to increased ambient CO_2 levels under ambient oxygen ($O = 21$ kPa) (A) and low oxygen levels ($O = 2$ kPa) (B) in 15-day-old Doloress leaves from the data set of Chapter 3. The release of (photo)respiratory CO_2 was assumed to either take place in the inner cytosol (upward pointing triangle), the outer cytosol (downward pointing triangle) or the cytosol gaps (dots).

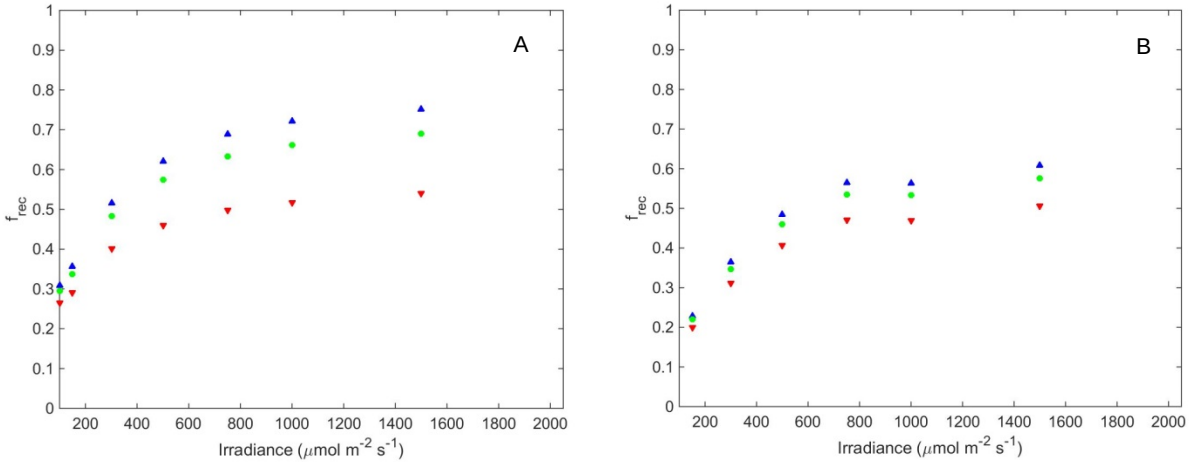

Figure A5.1.26: Response of the fraction of (photo)respired CO_2 that is re-assimilated f_{rec} to increased light levels under photorespiratory ($C_{\mathrm{a}} = 40$ Pa, $O = 21$ kPa) conditions (A) and non-photorespiratory ($C_{\mathrm{a}} = 100$ Pa, $O = 2$ kPa) conditions (B) in 15-day-old Doloress leaves from the data set of Chapter 3. The release of (photo)respiratory CO_2 was assumed to either take place in the inner cytosol (upward pointing triangle), the outer cytosol (downward pointing triangle) or the cytosol gaps (dots).

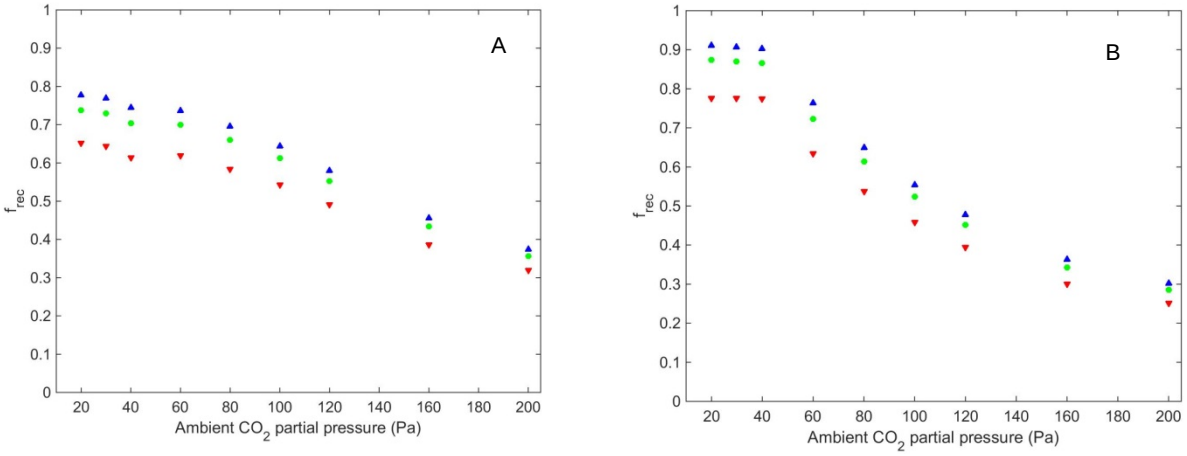

Figure A5.1.27: Response of the fraction of (photo)respired CO_2 that is re-assimilated f_{rec} to increased ambient CO_2 levels under ambient oxygen ($O = 21$ kPa) (A) and low oxygen levels ($O = 2$ kPa) (B) in 25-day-old Doloress leaves from the data set of Chapter 3. The release of (photo)respiratory CO_2 was assumed to either take place in the inner cytosol (upward pointing triangle), the outer cytosol (downward pointing triangle) or the cytosol gaps (dots).

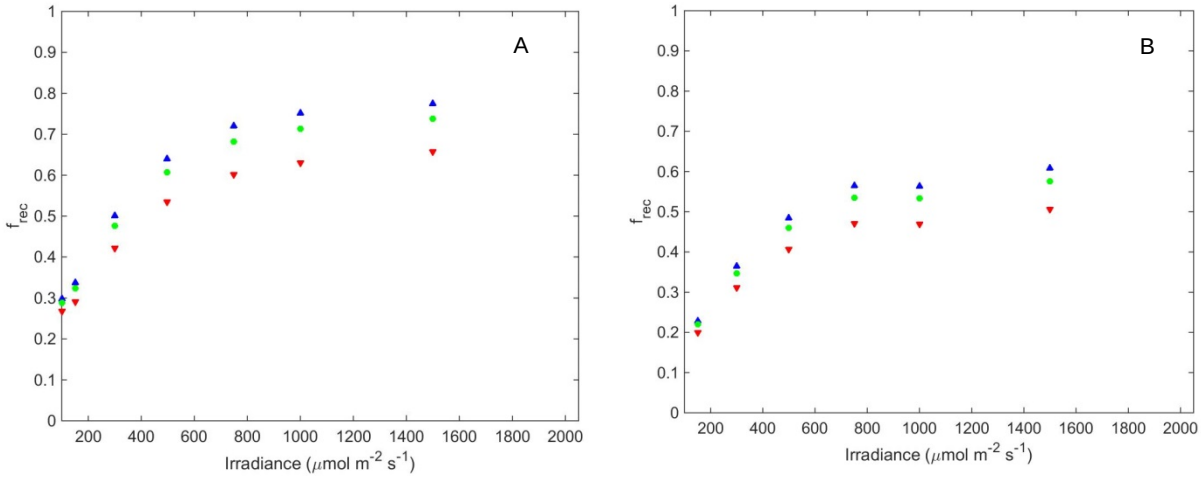

Figure A5.1.28: Response of the fraction of (photo)respired CO_2 that is re-assimilated f_{rec} to increased light levels under photorespiratory ($C_{\mathrm{a}} = 40$ Pa, $O = 21$ kPa) conditions (A) and non-photorespiratory ($C_{\mathrm{a}} = 100$ Pa, $O = 2$ kPa) conditions (B) in 25-day-old Doloress leaves from the data set of Chapter 3. The release of (photo)respiratory CO_2 was assumed to either take place in the inner cytosol (upward pointing triangle), the outer cytosol (downward pointing triangle) or the cytosol gaps (dots) .

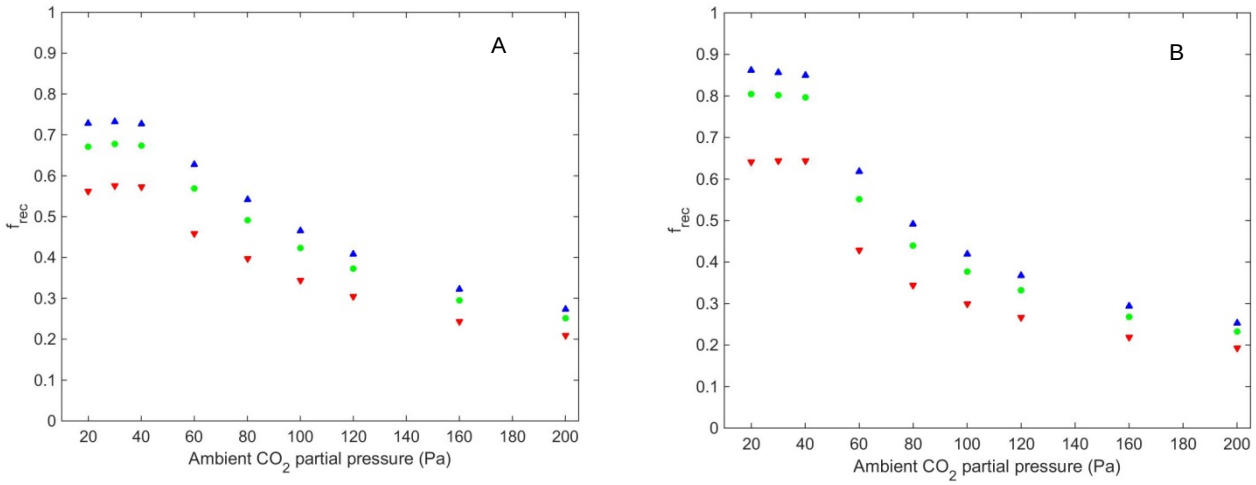

Figure A5.1.29: Response of the fraction of (photo)respired CO_2 that is re-assimilated f_{rec} to increased ambient CO_2 levels under ambient oxygen ($O = 21$ kPa) (A) and low oxygen levels ($O = 2$ kPa) (B) in 15-day-old Growdena leaves from the data set of Chapter 3. The release of (photo)respiratory CO_2 was assumed to either take place in the inner cytosol (upward pointing triangle), the outer cytosol (downward pointing triangle) or the cytosol gaps (dots).

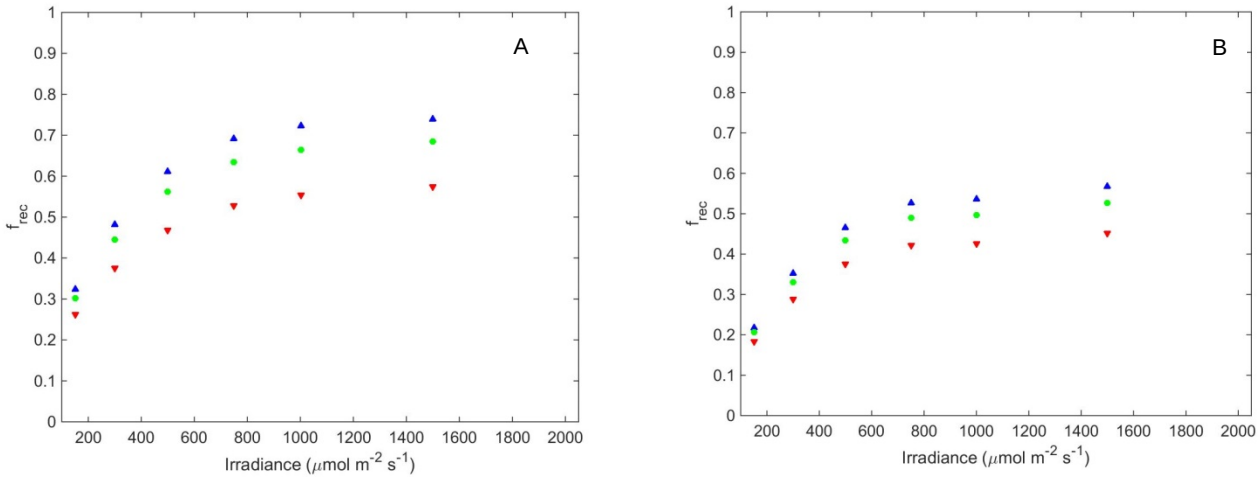

Figure A5.1.30: Response of the fraction of (photo)respired CO_2 that is re-assimilated f_{rec} to increased light levels under photorespiratory ($C_{\mathrm{a}} = 40$ Pa, $O = 21$ kPa) conditions (A) and non-photorespiratory ($C_{\mathrm{a}} = 100$ Pa, $O = 2$ kPa) conditions (B) in 15-day-old Growdena leaves from the data set of Chapter 3. The release of (photo)respiratory CO_2 was assumed to either take place in the inner cytosol (upward pointing triangle), the outer cytosol (downward pointing triangle) or the cytosol gaps (dots).

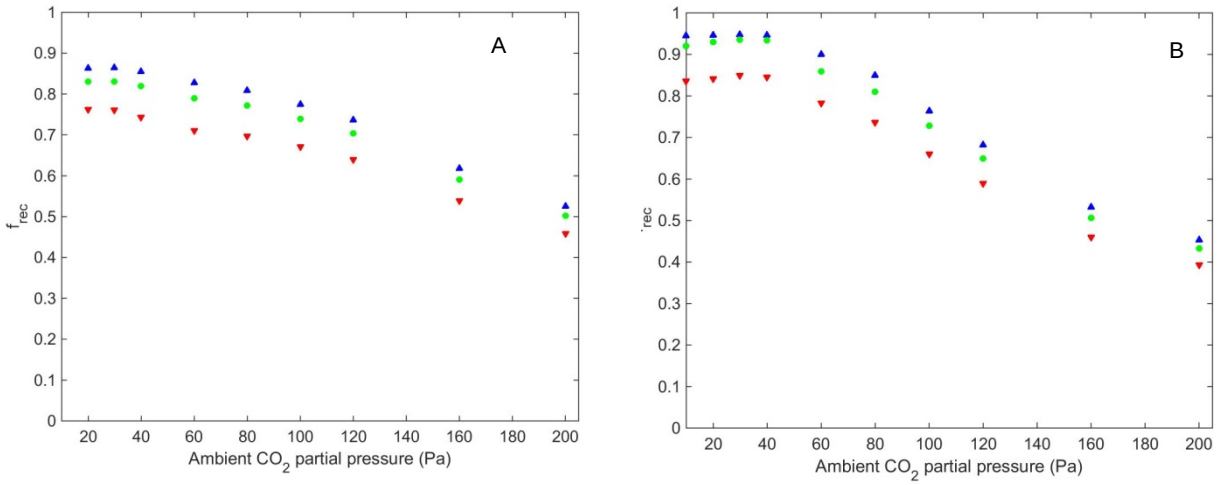

Figure A5.1.31: Response of the fraction of (photo)respired CO_2 that is re-assimilated f_{rec} to increased ambient CO_2 levels under ambient oxygen ($O = 21$ kPa) (A) and low oxygen levels ($O = 2$ kPa) (B) in 25-day-old Growdena leaves from the data set of Chapter 3. The release of (photo)respiratory CO_2 was assumed to either take place in the inner cytosol (upward pointing triangle), the outer cytosol (downward pointing triangle) or the cytosol gaps (dots).

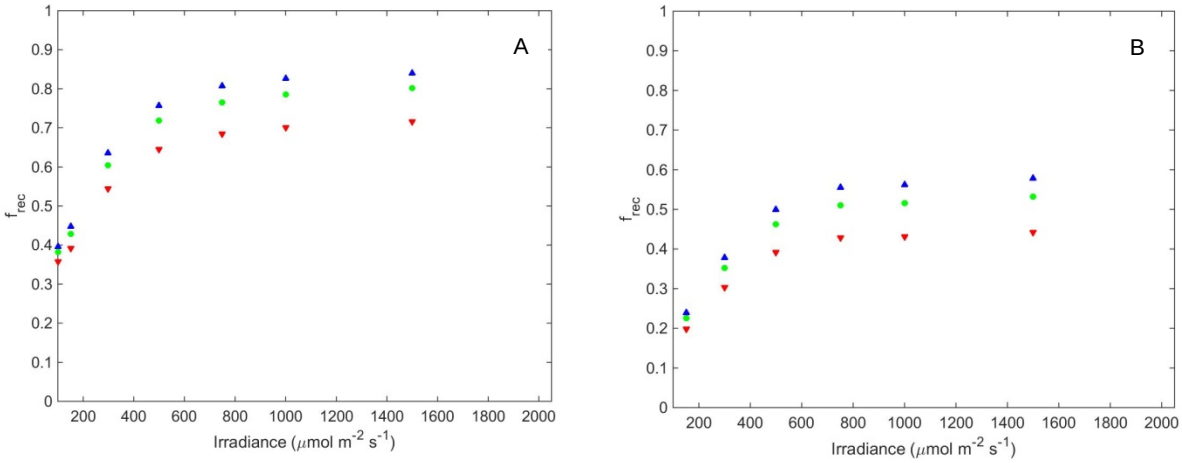

Figure A5.1.32: Response of the fraction of (photo)respired CO_2 that is re-assimilated f_{rec} to increased light levels under photorespiratory ($C_{\mathrm{a}} = 40$ Pa, $O = 21$ kPa) conditions (A) and non-photorespiratory ($C_{\mathrm{a}} = 100$ Pa, $O = 2$ kPa) conditions (B) in 25-day-old Growdena leaves from the data set of Chapter 3. The release of (photo)respiratory CO_2 was assumed to either take place in the inner cytosol (upward pointing triangle), the outer cytosol (downward pointing triangle) or the cytosol gaps (dots).

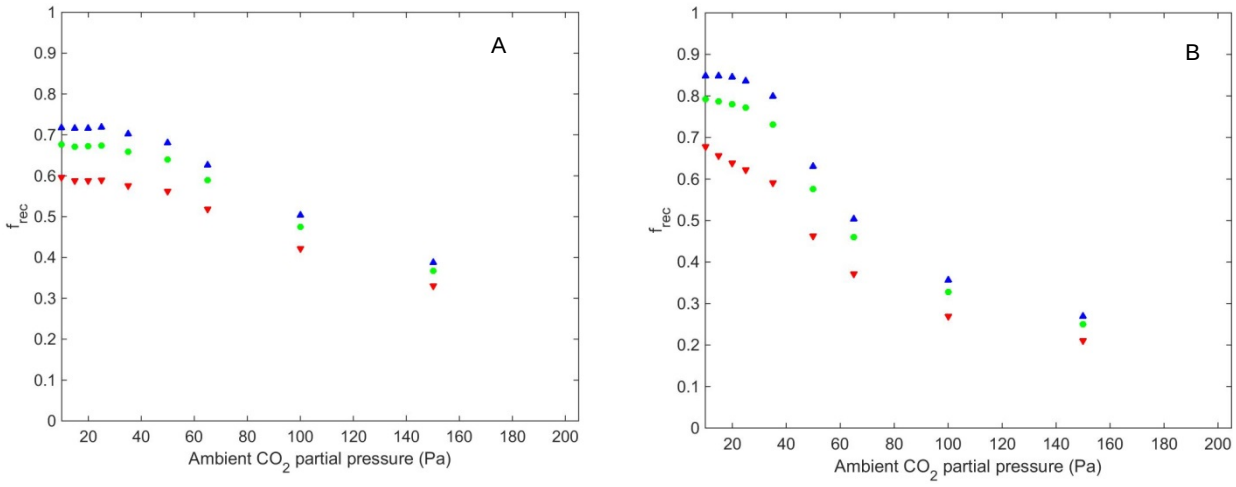

Figure A5.1.33: Response of the fraction of (photo)respired CO_2 f_{rec} that is re-assimilated f_{rec} to increased ambient CO_2 levels under ambient oxygen ($O = 21$ kPa) (A) and low oxygen levels ($O = 2$ kPa) (B) in Admiro upper leaves from the Ho *et al.* (2016) data set. The release of (photo)respiratory CO_2 was assumed to either take place in the inner cytosol (upward pointing triangle), the outer cytosol (downward pointing triangle) or the cytosol gaps (dots).

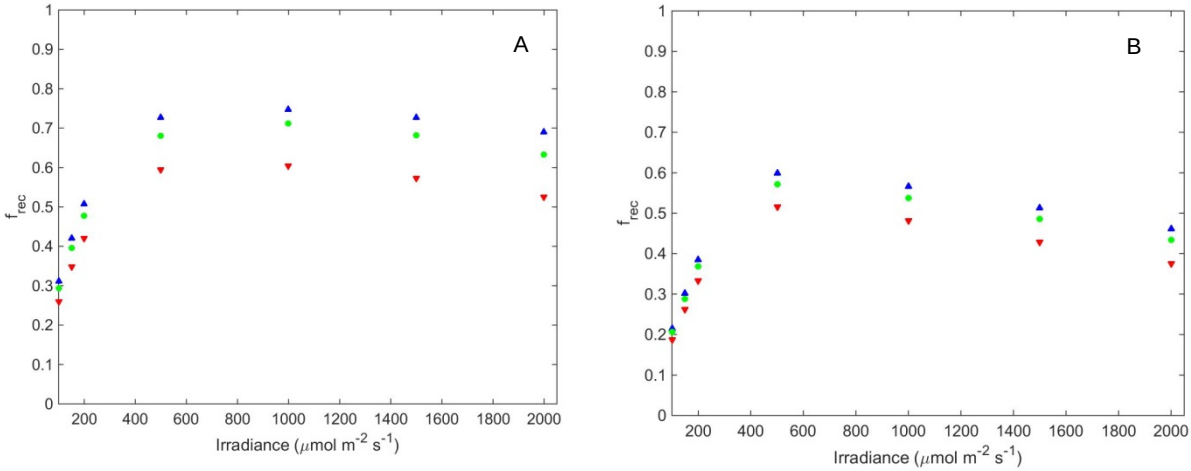

Figure A5.1.34: Response of the fraction of (photo)respired CO_2 that is re-assimilated f_{rec} to increased light levels under photorespiratory ($C_{\mathrm{a}} = 38$ Pa, $O = 21$ kPa) conditions (A) and non-photorespiratory ($C_{\mathrm{a}} = 100$ Pa, $O = 2$ kPa) conditions (B) in Admiro upper leaves from the Ho *et al.* (2016) data set. The release of (photo)respiratory CO_2 was assumed to either take place in the inner cytosol (upward pointing triangle), the outer cytosol (downward pointing triangle) or the cytosol gaps (dots).

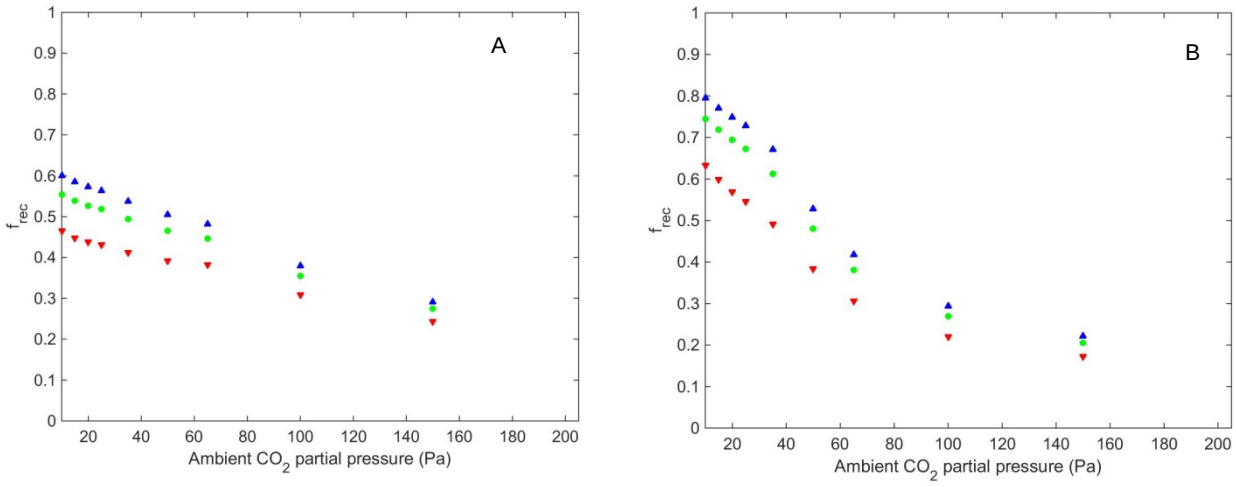

Figure A5.1.35: Response of the fraction of (photo)respired CO_2 that is re-assimilated f_{rec} to increased ambient CO_2 levels under ambient oxygen ($O = 21$ kPa) (A) and low oxygen levels ($O = 2$ kPa) (B) in Admiro lower leaves from the Ho *et al.* (2016) data set. The release of (photo)respiratory CO_2 was assumed to either take place in the inner cytosol (upward pointing triangle), the outer cytosol (downward pointing triangle) or the cytosol gaps (dots).

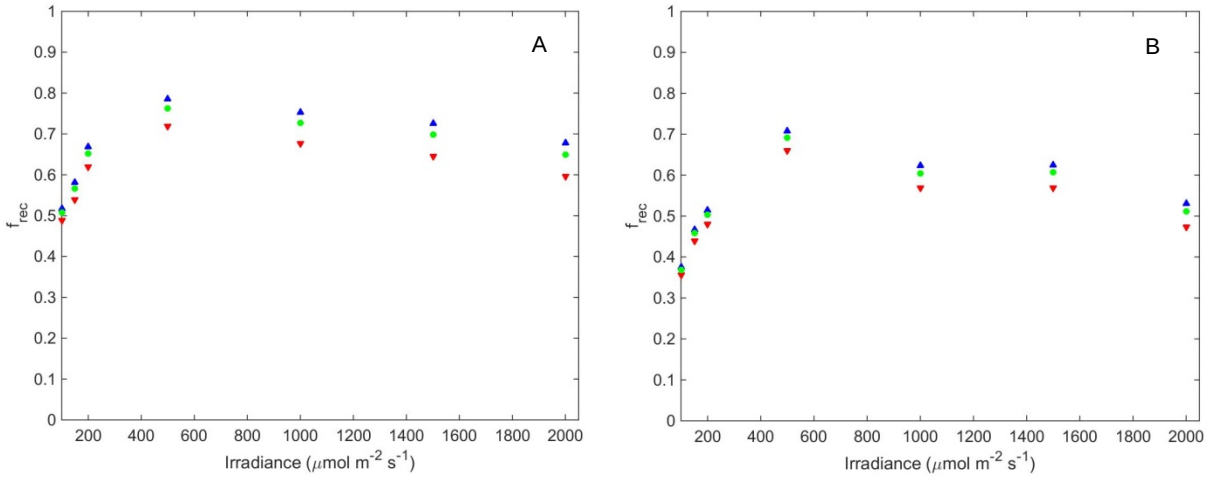

Figure A5.1.36: Response of the fraction of (photo)respired CO_2 that is re-assimilated f_{rec} to increased light levels under photorespiratory ($C_{\mathrm{a}} = 38$ Pa, $O = 21$ kPa) conditions (A) and non-photorespiratory ($C_{\mathrm{a}} = 100$ Pa, $O = 2$ kPa) conditions (B) in Admiro lower leaves from the Ho *et al.* (2016) data set. The release of (photo)respiratory CO_2 was assumed to either take place in the inner cytosol (upward pointing triangle), the outer cytosol (downward pointing triangle) or the cytosol gaps (dots).

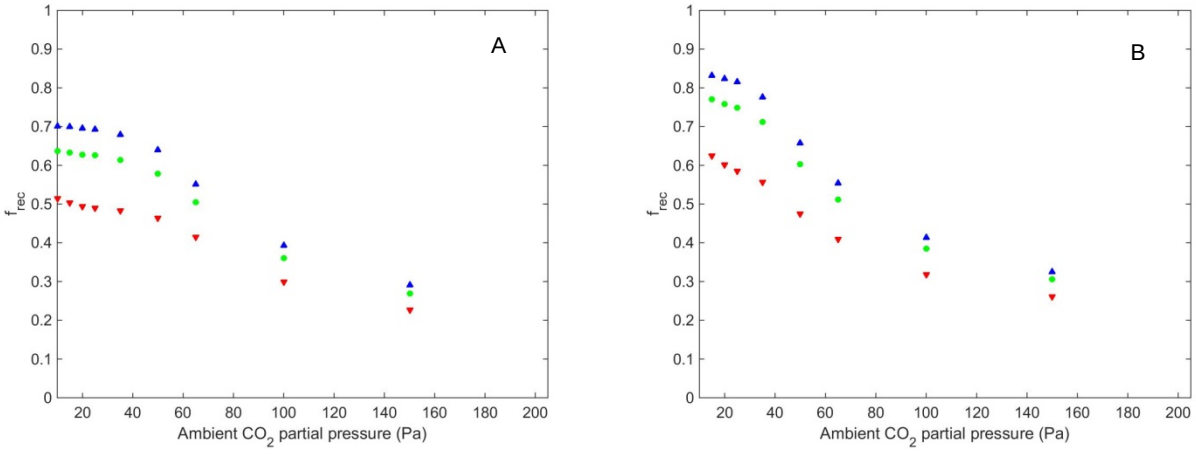

Figure A5.1.37: Response of the fraction of (photo)respired CO_2 f_{rec} that is re-assimilated f_{rec} to increased ambient CO_2 levels under ambient oxygen ($O = 21$ kPa) (A) and low oxygen levels ($O = 2$ kPa) (B) in Doloress upper leaves from the Ho *et al.* (2016) data set. The release of (photo)respiratory CO_2 was assumed to either take place in the inner cytosol (upward pointing triangle), the outer cytosol (downward pointing triangle) or the cytosol gaps (dots).

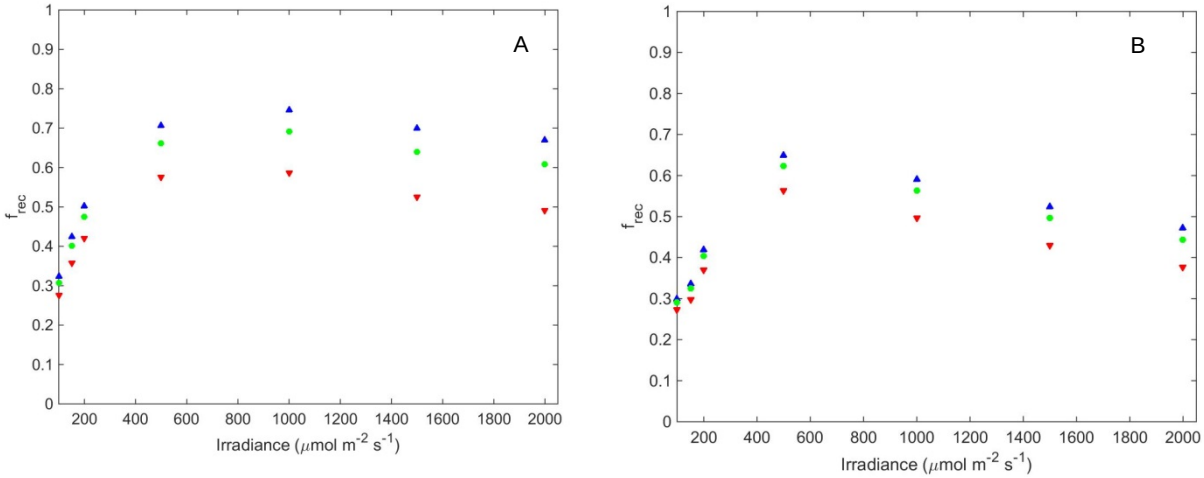

Figure A5.1.38: Response of the fraction of (photo)respired CO_2 that is re-assimilated f_{rec} to increased light levels under photorespiratory ($C_{\mathrm{a}} = 38$ Pa, $O = 21$ kPa) conditions (A) and non-photorespiratory ($C_{\mathrm{a}} = 100$ Pa, $O = 2$ kPa) conditions (B) in Doloress upper leaves from the Ho *et al.* (2016) data set. The release of (photo)respiratory CO_2 was assumed to either take place in the inner cytosol (upward pointing triangle), the outer cytosol (downward pointing triangle) or the cytosol gaps (dots).

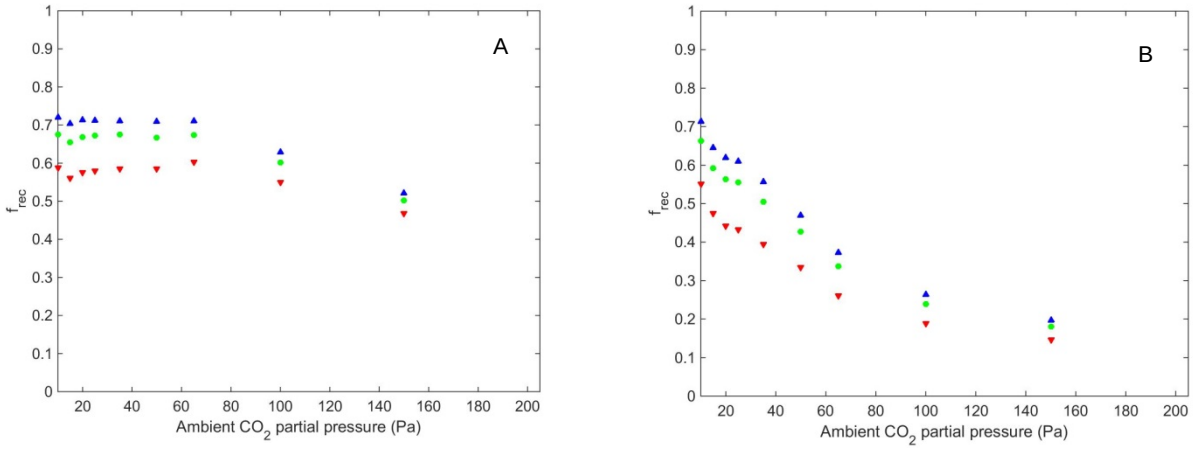

Figure A5.1.39: Response of the fraction of (photo)respired CO_2 that is re-assimilated f_{rec} to increased ambient CO_2 levels under ambient oxygen ($O = 21$ kPa) (A) and low oxygen levels ($O = 2$ kPa) (B) in Doloress lower leaves from the Ho *et al.* (2016) data set. The release of (photo)respiratory CO_2 was assumed to either take place in the inner cytosol (upward pointing triangle), the outer cytosol (downward pointing triangle) or the cytosol gaps (dots).

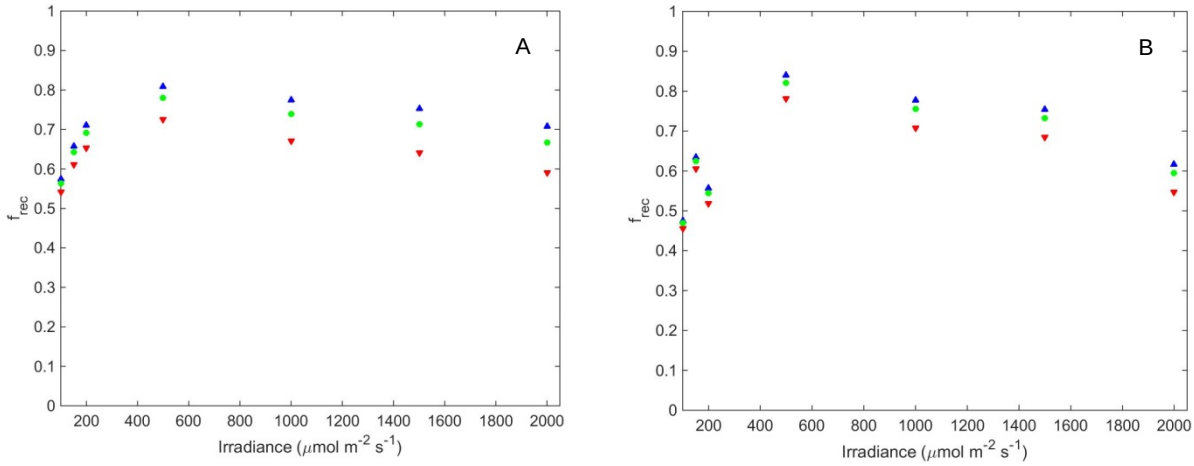

Figure A5.1.40: Response of the fraction of (photo)respired CO_2 that is re-assimilated f_{rec} to increased light levels under photorespiratory ($C_{\mathrm{a}} = 38$ Pa, $O = 21$ kPa) conditions (A) and non-photorespiratory ($C_{\mathrm{a}} = 100$ Pa, $O = 2$ kPa) conditions (B) in Doloress lower leaves from the Ho *et al.* (2016) data set. The release of (photo)respiratory CO_2 was assumed to either take place in the inner cytosol (upward pointing triangle), the outer cytosol (downward pointing triangle) or the cytosol gaps (dots).

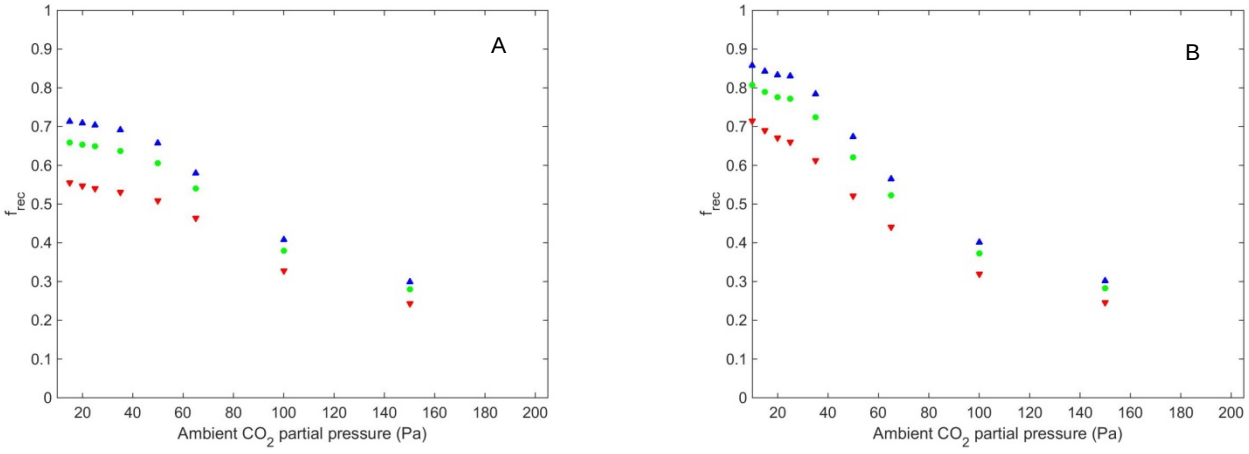

Figure A5.1.41: Response of the fraction of (photo)respired CO_2 that is re-assimilated f_{rec} to increased ambient CO_2 levels under ambient oxygen ($O = 21$ kPa) (A) and low oxygen levels ($O = 2$ kPa) (B) in Growdena upper leaves from the Ho *et al.* (2016) data set. The release of (photo)respiratory CO_2 was assumed to either take place in the inner cytosol (upward pointing triangle), the outer cytosol (downward pointing triangle) or the cytosol gaps (dots).

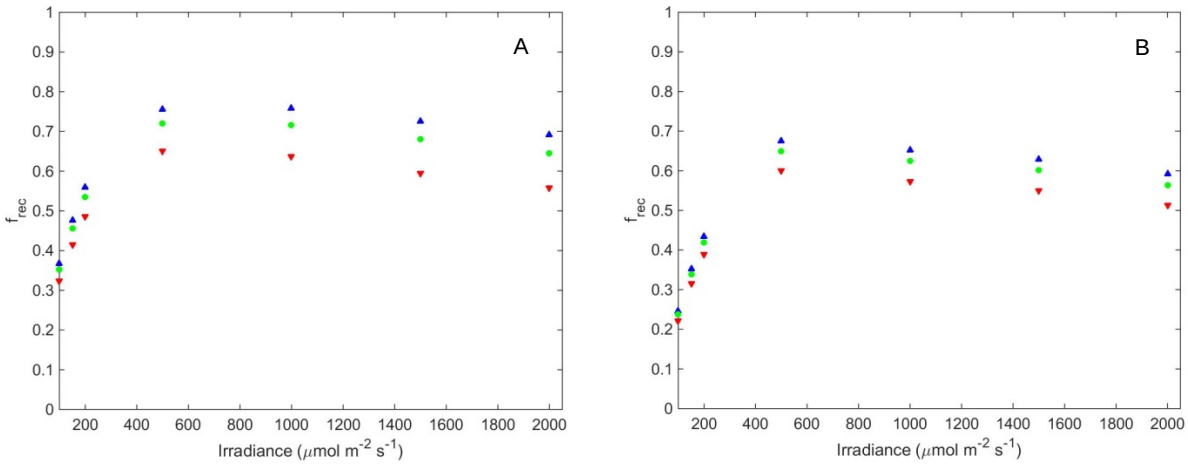

Figure A5.1.42: Response of the fraction of (photo)respired CO_2 that is re-assimilated f_{rec} to increased light levels under photorespiratory ($C_{\mathrm{a}} = 38$ Pa, $O = 21$ kPa) conditions (A) and non-photorespiratory ($C_{\mathrm{a}} = 100$ Pa, $O = 2$ kPa) conditions (B) in Growdena upper leaves from the Ho *et al.* (2016) data set. The release of (photo)respiratory CO_2 was assumed to either take place in the inner cytosol (upward pointing triangle), the outer cytosol (downward pointing triangle) or the cytosol gaps (dots).

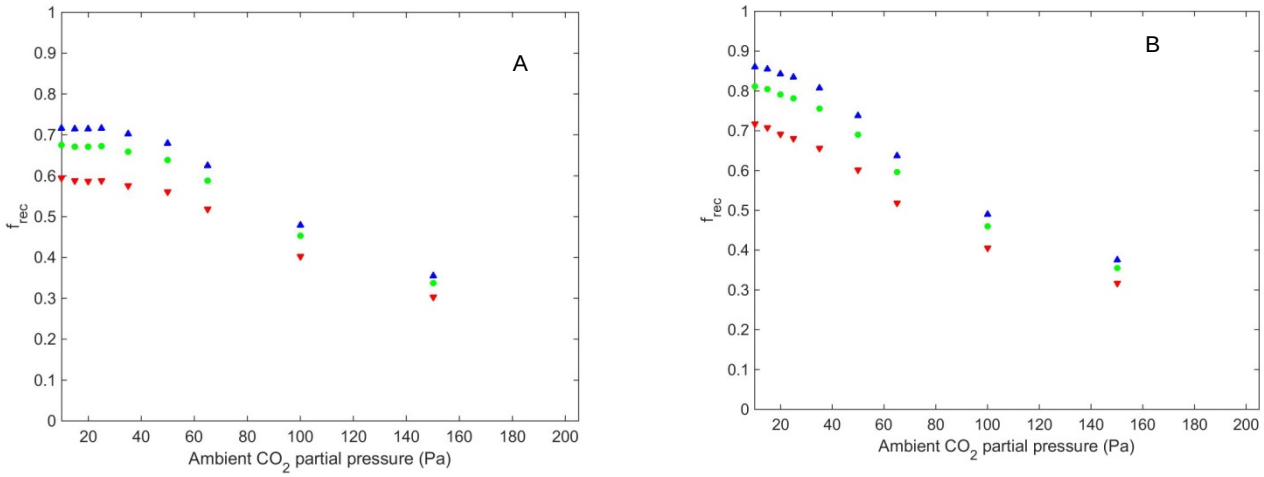

Figure A5.1.43: Response of the fraction of (photo)respired CO_2 that is re-assimilated f_{rec} to increased ambient CO_2 levels under ambient oxygen ($O = 21$ kPa) levels (A) and low oxygen ($O = 2$ kPa) levels (B) Growdena lower leaves from the Ho *et al.* (2016) data set. The release of (photo)respiratory CO_2 was assumed to either take place in the inner cytosol (upward pointing triangle), the outer cytosol (downward pointing triangle) or the cytosol gaps (dots).

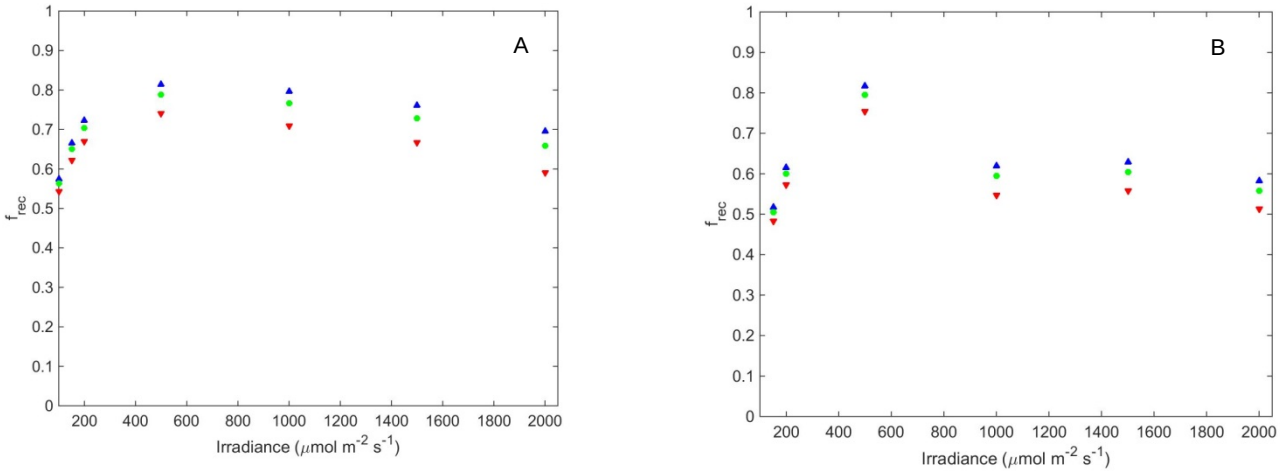

Figure A5.1.44: Response of the fraction of (photo)respired CO_2 that is re-assimilated f_{rec} to increased light levels under photorespiratory ($C_{\mathrm{a}} = 38$ Pa, $O = 21$ kPa) conditions (A) and non-photorespiratory ($C_{\mathrm{a}} = 100$ Pa, $O = 2$ kPa) conditions (B) in Growdena lower leaves from the Ho *et al.* (2016) data set. The release of (photo)respiratory CO_2 was assumed to either take place in the inner cytosol (upward pointing triangle), the outer cytosol (downward pointing triangle) or the cytosol gaps (dots).

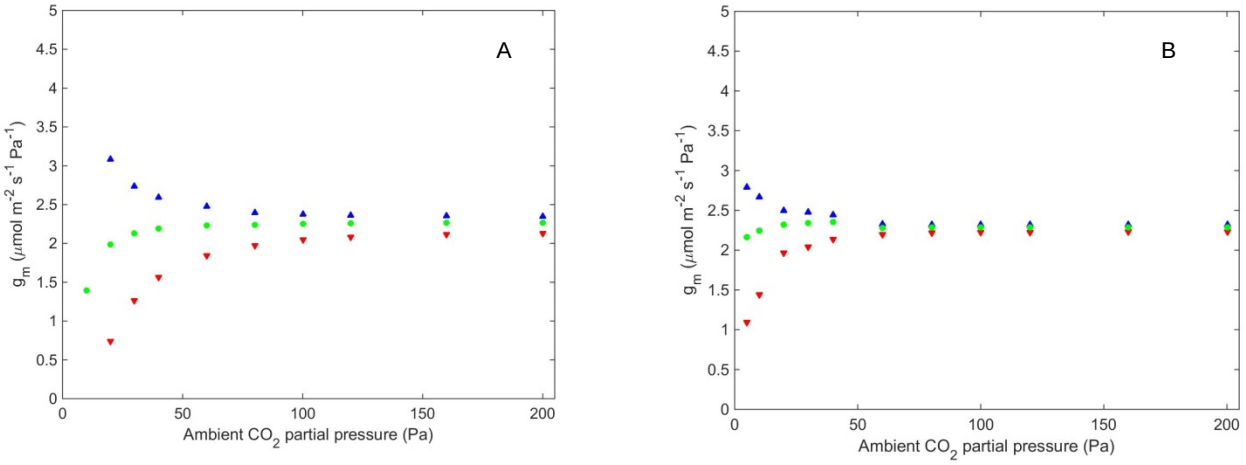

Figure A5.1.45: Response of the simulated apparent mesophyll conductance (g_m) to increased ambient CO_2 levels under ambient oxygen ($O = 21$ kPa) levels (A) and low oxygen ($O = 2$ kPa) levels (B) 25-day-old Admiro leaves from the data set of Chapter 3. The release of (photo)respiratory CO_2 was assumed to either take place in the inner cytosol (upward pointing triangle), the outer cytosol (downward pointing triangle) or the cytosol gaps (dots).

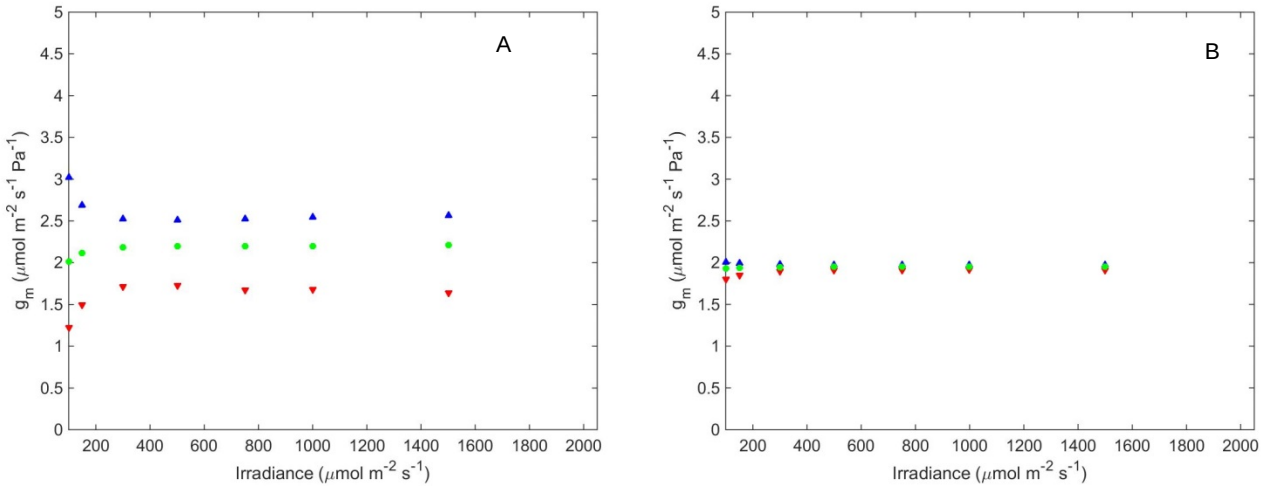

Figure A5.1.46: Response of the simulated apparent mesophyll conductance (g_m) to increased light levels under photorespiratory (A) conditions ($C_\mathrm{a} = 40$ Pa, $O = 21$ kPa) and non-photorespiratory (B) conditions ($C_\mathrm{a} = 100$ Pa, $O = 2$ kPa) in 25-day-old Admiro leaves from the data set of Chapter 3.. The release of (photo)respiratory CO_2 was assumed to either take place in the inner cytosol (upward pointing triangle), the outer cytosol (downward pointing triangle) or the cytosol gaps (dots).

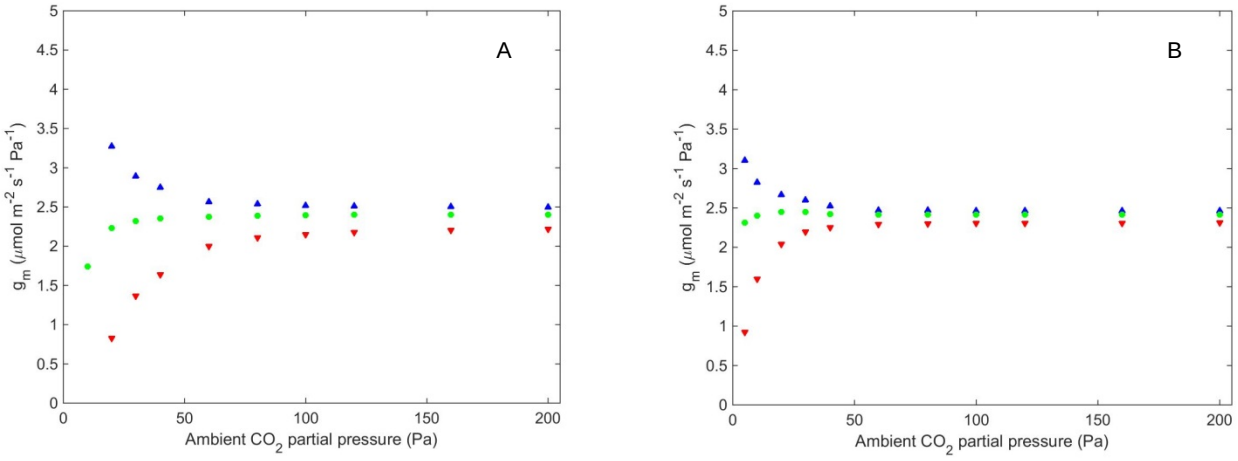

Figure A5.1.47: Response of the simulated apparent mesophyll conductance (g_m) to increased ambient CO_2 under ambient oxygen ($O = 21$ kPa) levels (A) and low oxygen ($O = 2$ kPa) levels (B) in 15-day-old Doloress leaves from the data set of Chapter 3. The release of (photo)respiratory CO_2 was assumed to either take place in the inner cytosol (upward pointing triangle), the outer cytosol (downward pointing triangle) or the cytosol gaps (dots).

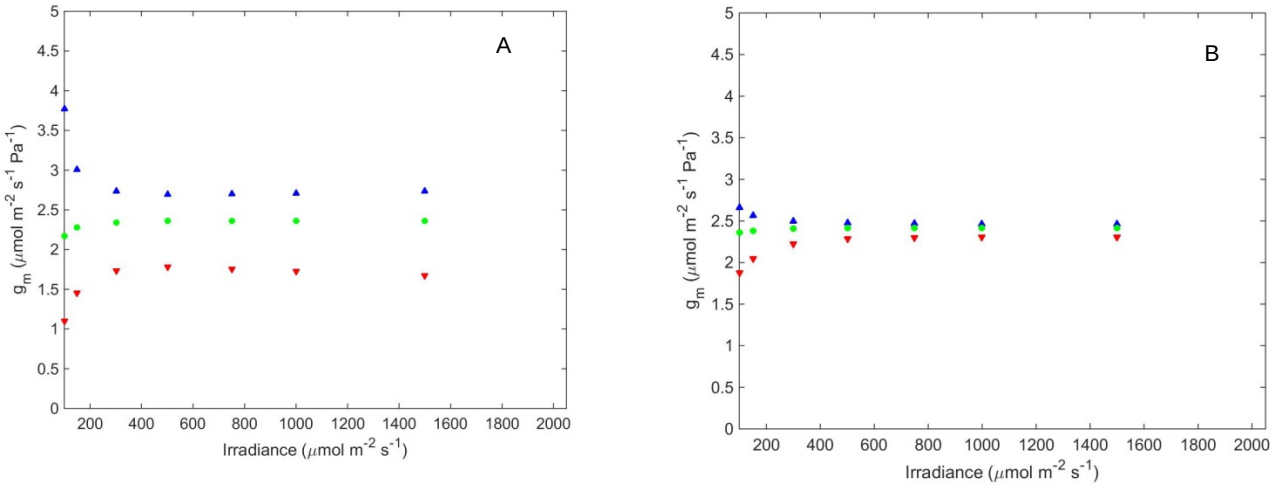

Figure A5.1.48: Response of the simulated apparent mesophyll conductance (g_m) to increased light levels under photorespiratory (A) conditions ($C_a = 40$ Pa, $O = 21$ kPa) and non-photorespiratory (B) conditions ($C_a = 100$ Pa, $O = 2$ kPa) in 15-day-old Doloress leaves from the data set of Chapter 3. The release of (photo)respiratory CO_2 was assumed to either take place in the inner cytosol (upward pointing triangle), the outer cytosol (downward pointing triangle) or the cytosol gaps (dots).

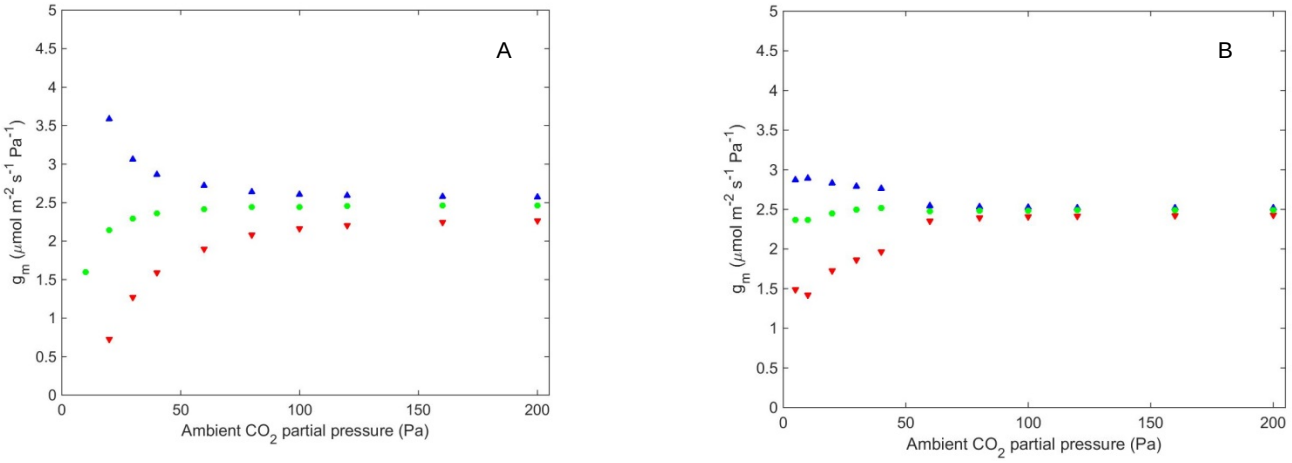

Figure A5.1.49: Response of the simulated apparent mesophyll conductance (g_m) to increased ambient CO_2 levels under ambient oxygen ($O = 21$ kPa) levels (A) and low oxygen ($O = 2$ kPa) levels (B) 25-day-old Doloress leaves from the data set of Chapter 3. The release of (photo)respiratory CO_2 was assumed to either take place in the inner cytosol (upward pointing triangle), the outer cytosol (downward pointing triangle) or the cytosol gaps (dots).

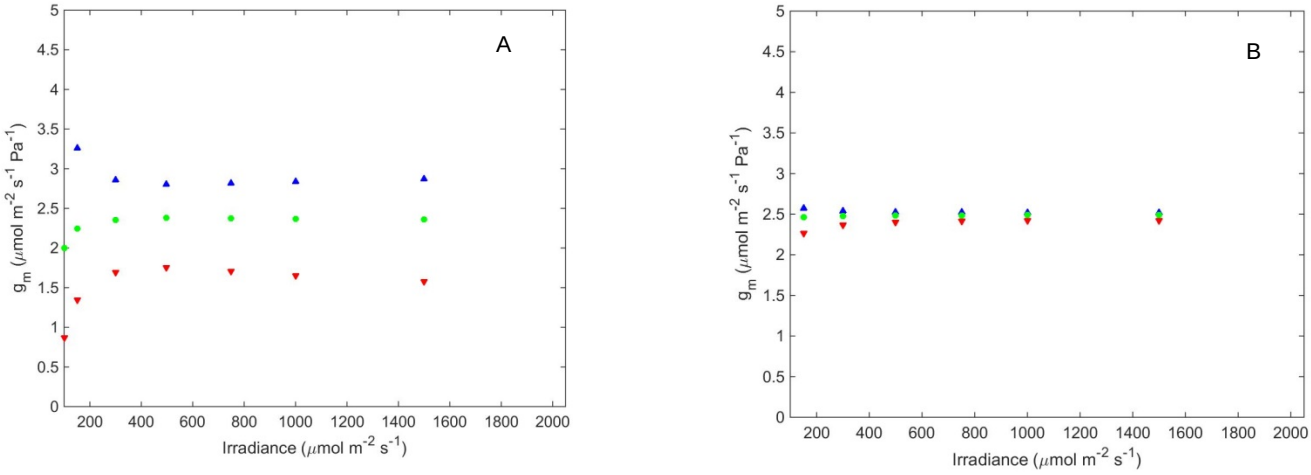

Figure A5.1.50: Response of the simulated apparent mesophyll conductance (g_m) to increased light levels under photorespiratory (A) conditions ($C_\mathrm{a} = 40$ Pa, $O = 21$ kPa) and non-photorespiratory (B) conditions ($C_\mathrm{a} = 100$ Pa, $O = 2$ kPa) in 25-day-old Doloress leaves from the data set of Chapter 3.. The release of (photo)respiratory CO_2 was assumed to either take place in the inner cytosol (upward pointing triangle), the outer cytosol (downward pointing triangle) or the cytosol gaps (dots).

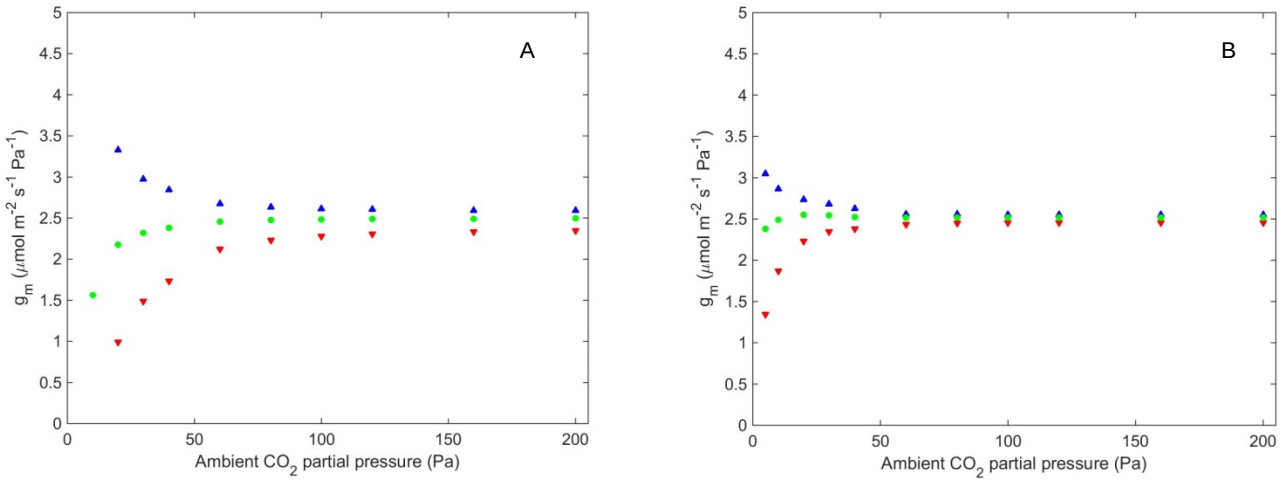

Figure A5.1.51: Response of the simulated apparent mesophyll conductance (g_{m}) to increased ambient CO_2 levels under ambient oxygen ($O = 21$ kPa) levels (A) and low oxygen ($O = 2$ kPa) levels (B) in 15-day-old Growdena leaves from the data set of Chapter 3.. The release of (photo)respiratory CO_2 was assumed to either take place in the inner cytosol (upward pointing triangle), the outer cytosol (downward pointing triangle) or the cytosol gaps (dots).

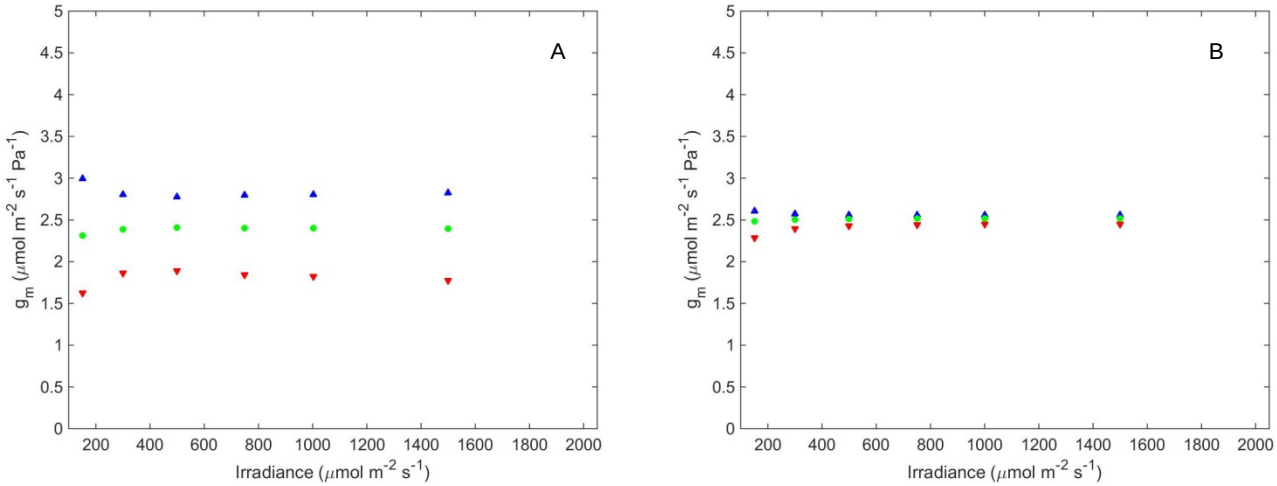

Figure A5.1.52: Response of the simulated apparent mesophyll conductance (g_{m}) to increased light levels under photorespiratory (A) conditions ($C_{\mathrm{a}} = 40$ Pa, $O = 21$ kPa) and non-photorespiratory (B) conditions ($C_{\mathrm{a}} = 100$ Pa, $O = 2$ kPa) in 15-day-old Growdena leaves from the data set of Chapter 3.. The release of (photo)respiratory CO_2 was assumed to either take place in the inner cytosol (upward pointing triangle), the outer cytosol (downward pointing triangle) or the cytosol gaps (dots).

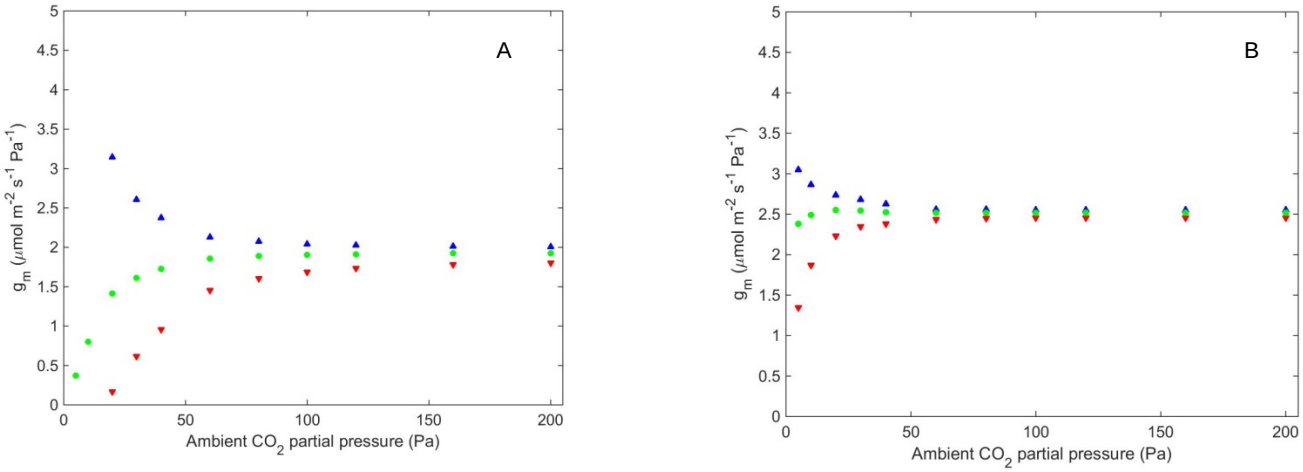

Figure A5.1.53: Response of the simulated apparent mesophyll conductance (g_m) to increased ambient CO_2 levels under ambient oxygen ($O = 21$ kPa) levels (A) and low oxygen ($O = 2$ kPa) levels (B) in 15-days old Growdena leaves from the data set of Chapter 3. The release of (photo)respiratory CO_2 was assumed to either take place in the inner cytosol (upward pointing triangle), the outer cytosol (downward pointing triangle) or the cytosol gaps (dots).

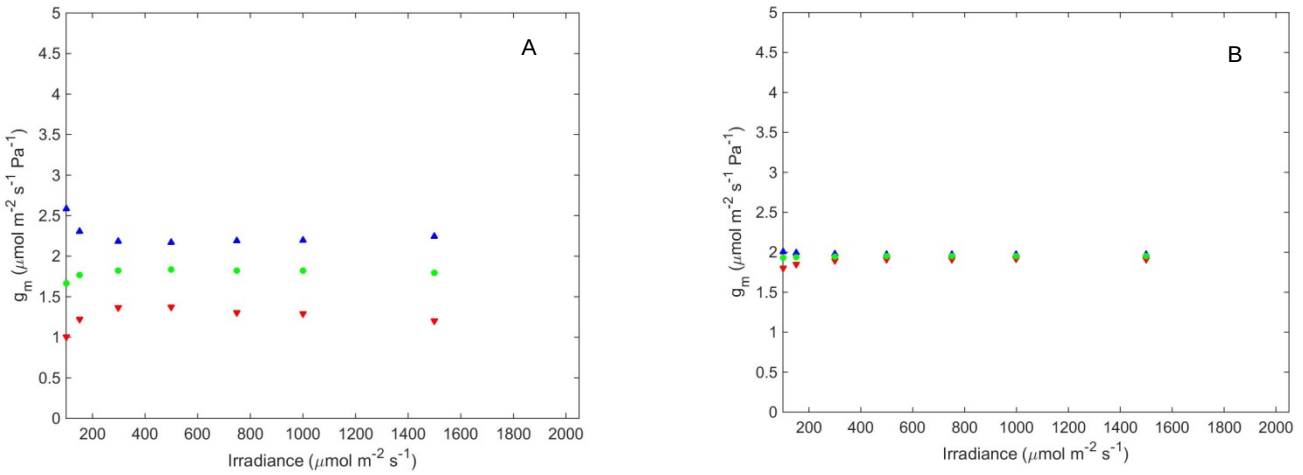

Figure A5.1.54: Response of the simulated apparent mesophyll conductance (g_m) to increased light levels under photorespiratory (A) conditions ($C_\mathrm{a} = 40$ Pa, $O = 21$ kPa) and non-photorespiratory (B) conditions ($C_\mathrm{a} = 100$ Pa, $O = 2$ kPa) in 25-day-old Growdena leaves from the data set of Chapter 3.. The release of (photo)respiratory CO_2 was assumed to either take place in the inner cytosol (upward pointing triangle), the outer cytosol (downward pointing triangle) or the cytosol gaps (dots).

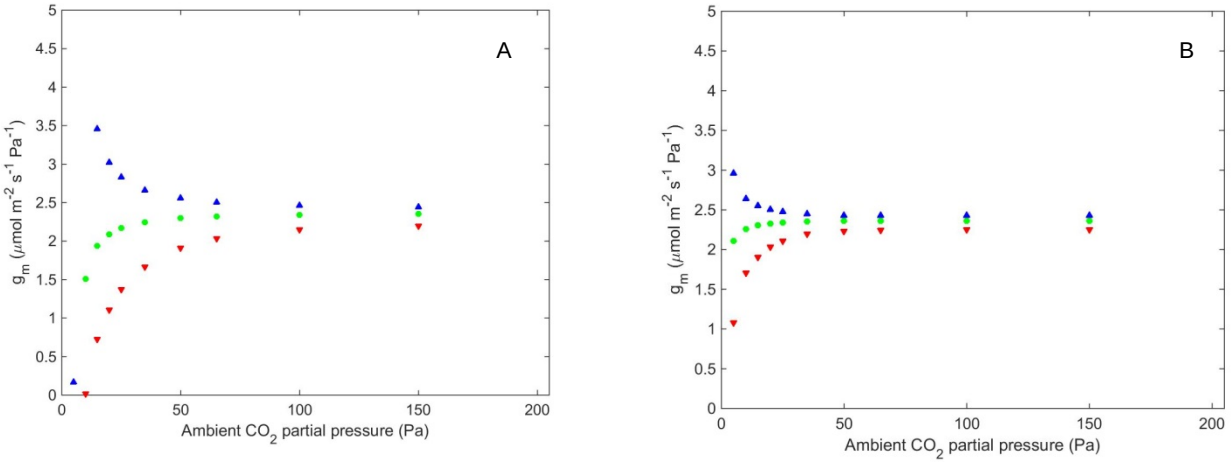

Figure A5.1.55: Response of the simulated apparent mesophyll conductance (g_{m}) to increased ambient CO_2 levels under ambient oxygen ($O = 21$ kPa) levels (A) and low oxygen ($O = 2$ kPa) levels (B) in Admiro upper leaves from the Ho *et al.* (2016) data set. The release of (photo)respiratory CO_2 was assumed to either take place in the inner cytosol (upward pointing triangle), the outer cytosol (downward pointing triangle) or the cytosol gaps (dots).

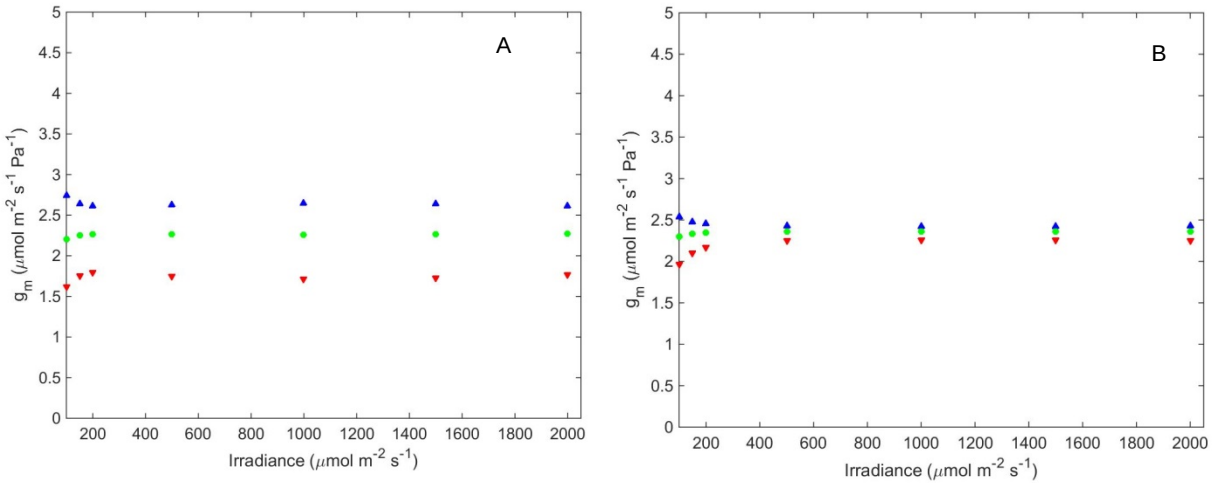

Figure A5.1.56: Response of the simulated apparent mesophyll conductance (g_{m}) to increased light levels under photorespiratory (A) conditions ($C_{\mathrm{a}} = 38$ Pa, $O = 21$ kPa) and non-photorespiratory (B) conditions ($C_{\mathrm{a}} = 100$ Pa, $O = 2$ kPa) in Admiro upper leaves from the Ho *et al.* (2016) data set. The release of (photo)respiratory CO_2 was assumed to either take place in the inner cytosol (upward pointing triangle), the outer cytosol (downward pointing triangle) or the cytosol gaps (dots).

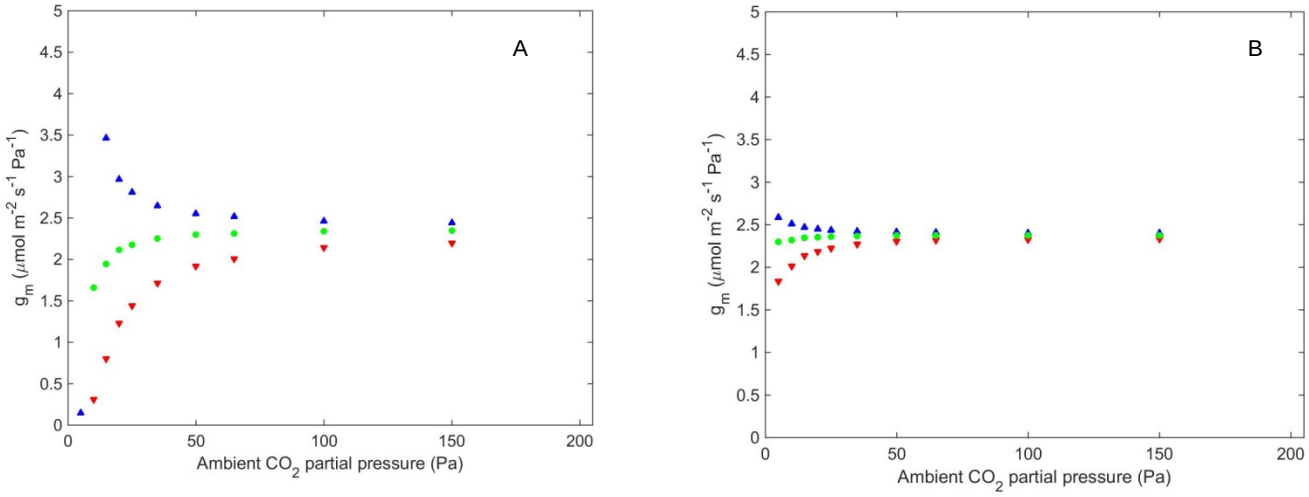

Figure A5.1.57: Response of the simulated apparent mesophyll conductance (g_m) to increased ambient CO_2 levels under ambient oxygen ($O = 21$ kPa) levels (A) and low oxygen ($O = 2$ kPa) levels (B) in Admiro lower leaves from the Ho *et al.* (2016) data set. The release of (photo)respiratory CO_2 was assumed to either take place in the inner cytosol (upward pointing triangle), the outer cytosol (downward pointing triangle) or the cytosol gaps (dots).

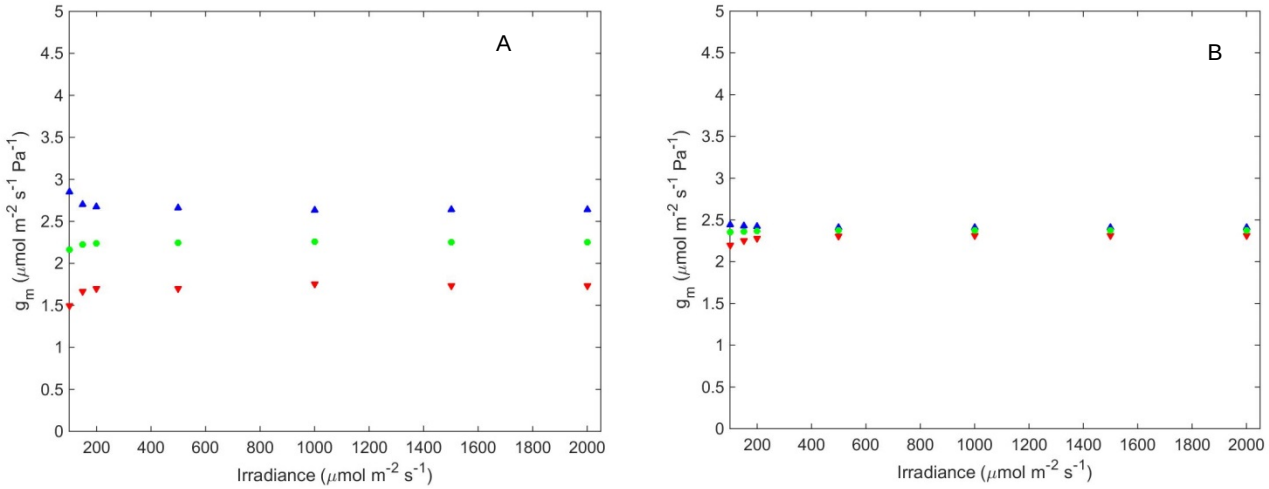

Figure A5.1.58: Response of the simulated apparent mesophyll conductance (g_m) to increased light levels under photorespiratory (A) conditions ($C_\mathrm{a} = 38$ Pa, $O = 21$ kPa) and non-photorespiratory (B) conditions ($C_\mathrm{a} = 100$ Pa, $O = 2$ kPa) in Admiro lower leaves from the Ho *et al.* (2016) data set. The release of (photo)respiratory CO_2 was assumed to either take place in the inner cytosol (upward pointing triangle), the outer cytosol (downward pointing triangle) or the cytosol gaps (dots).

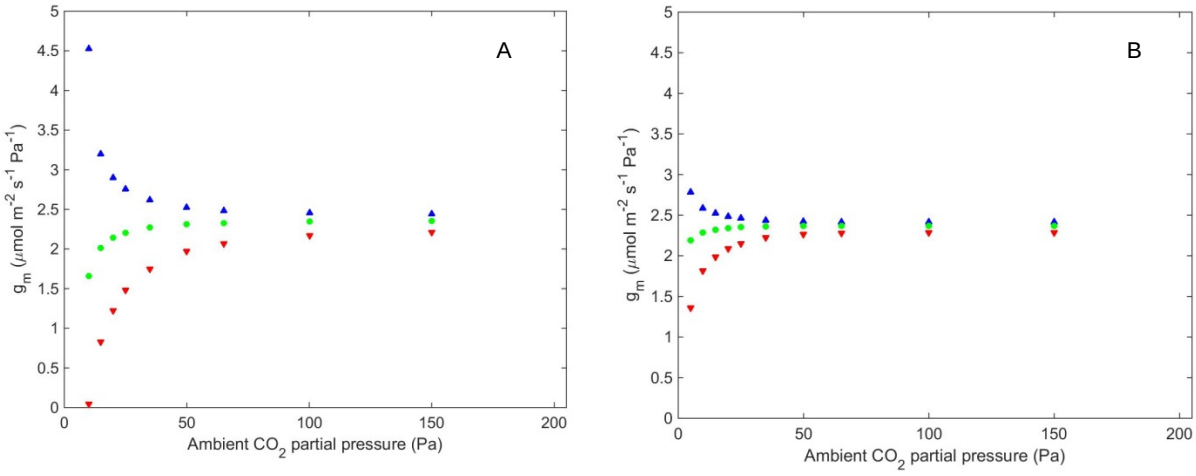

Figure A5.1.59: Response of the simulated apparent mesophyll conductance (g_m) to increased ambient CO_2 levels under ambient oxygen ($O = 21$ kPa) levels (A) and low oxygen ($O = 2$ kPa) levels (B) in Doloress upper leaves from the Ho *et al.* (2016) data set. The release of (photo)respiratory CO_2 was assumed to either take place in the inner cytosol (upward pointing triangle), the outer cytosol (downward pointing triangle) or the cytosol gaps (dots).

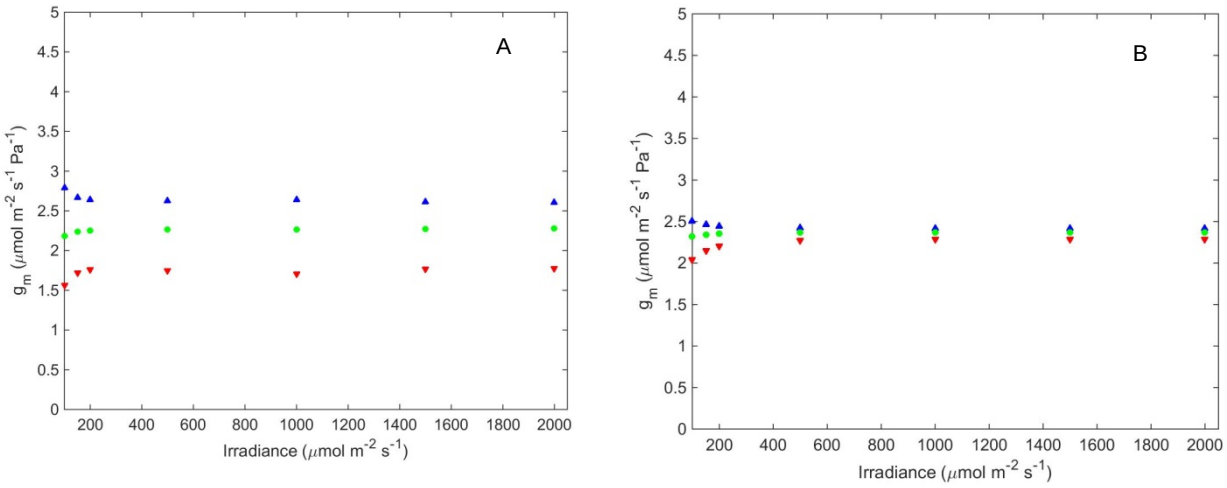

Figure A5.1.60: Response of the simulated apparent mesophyll conductance (g_m) to increased light levels under photorespiratory (A) conditions ($C_a = 38$ Pa, $O = 21$ kPa) and non-photorespiratory (B) conditions ($C_a = 100$ Pa, $O = 2$ kPa) in Doloress upper leaves from the Ho *et al.* (2016) data set. The release of (photo)respiratory CO_2 was assumed to either take place in the inner cytosol (upward pointing triangle), the outer cytosol (downward pointing triangle) or the cytosol gaps (dots).

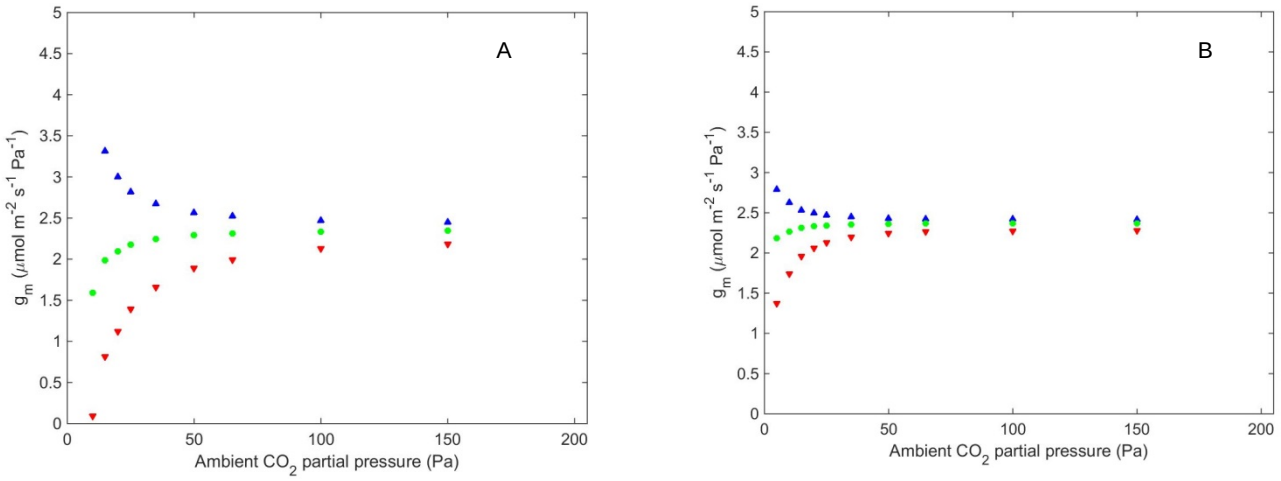

Figure A5.1.61: Response of the simulated apparent mesophyll conductance (g_m) to increased ambient CO_2 levels under ambient oxygen ($O = 21$ kPa) levels (A) and low oxygen ($O = 2$ kPa) levels (B) in Doloress lower leaves from the Ho *et al.* (2016) data set. The release of (photo)respiratory CO_2 was assumed to either take place in the inner cytosol (upward pointing triangle), the outer cytosol (downward pointing triangle) or the cytosol gaps (dots).

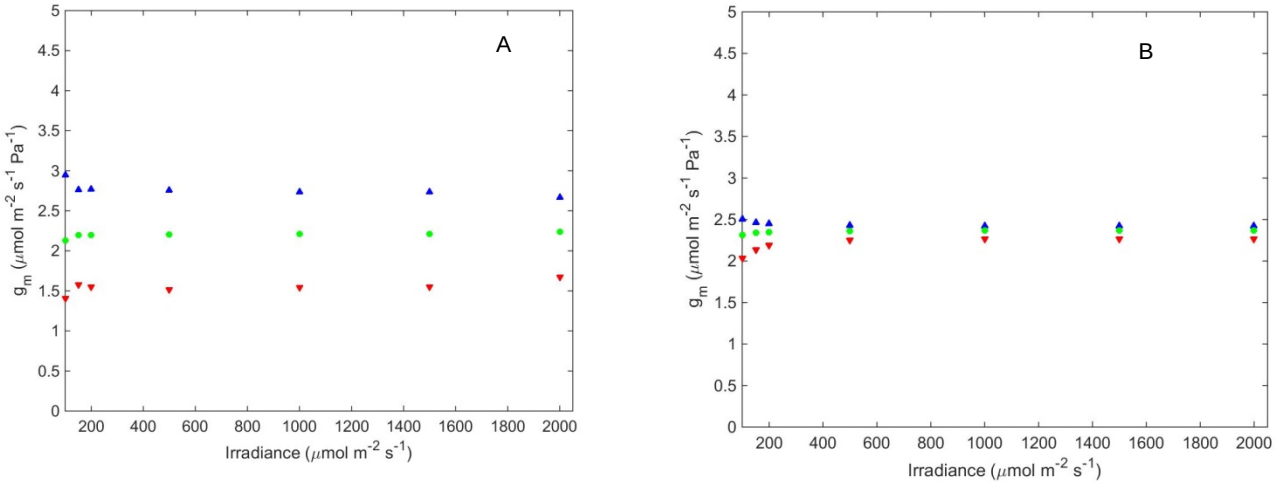

Figure A5.1.62: Response of the simulated apparent mesophyll conductance (g_m) to increased light levels under photorespiratory (A) conditions ($C_\mathrm{a} = 38$ Pa, $O = 21$ kPa) and non-photorespiratory (B) conditions ($C_\mathrm{a} = 100$ Pa, $O = 2$ kPa) in Doloress lower leaves from the Ho *et al.* (2016) data set. The release of (photo)respiratory CO_2 was assumed to either take place in the inner cytosol (upward pointing triangle), the outer cytosol (downward pointing triangle) or the cytosol gaps (dots).

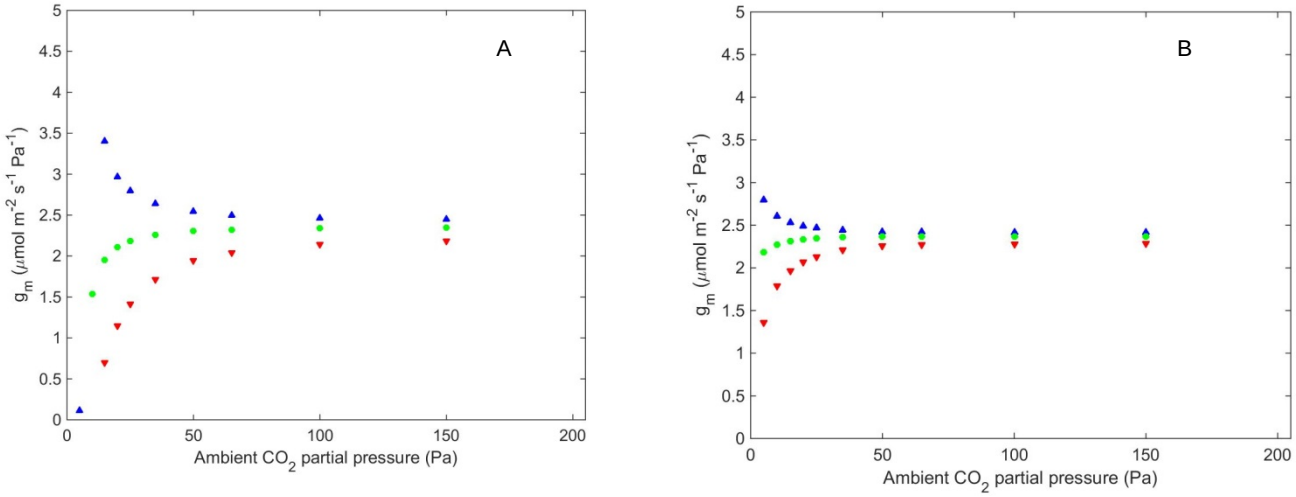

Figure A5.1.63: Response of the simulated apparent mesophyll conductance (g_m) to increased ambient CO_2 levels under ambient oxygen ($O = 21$ kPa) levels (A) and low oxygen ($O = 2$ kPa) levels (B) in Growdena upper leaves from the Ho *et al.* (2016) data set. The release of (photo)respiratory CO_2 was assumed to either take place in the inner cytosol (upward pointing triangle), the outer cytosol (downward pointing triangle) or the cytosol gaps (dots).

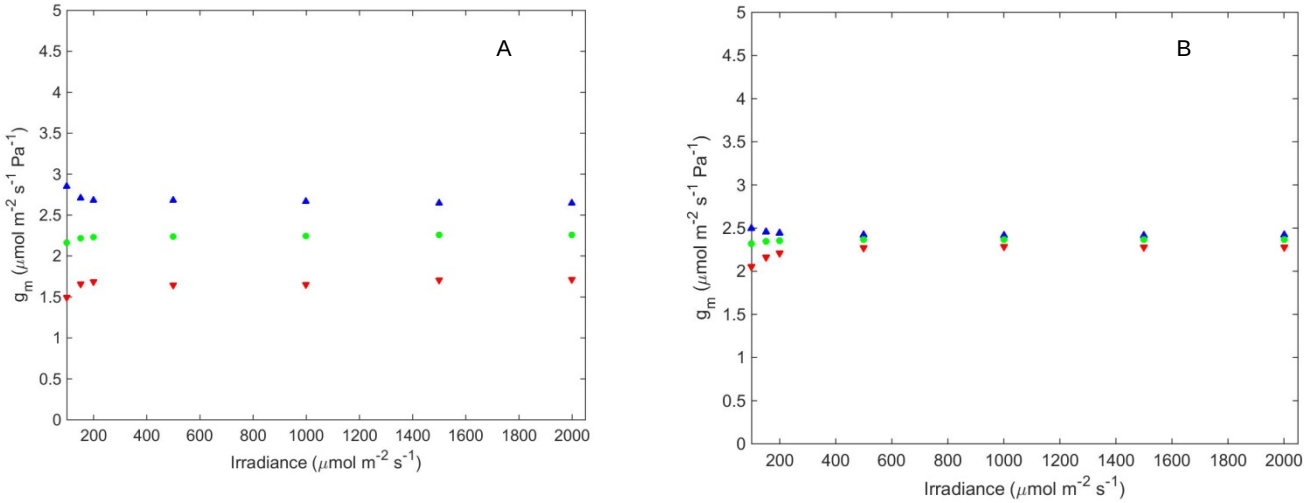

Figure A5.1.64: Response of the simulated apparent mesophyll conductance (g_m) to increased light levels under photorespiratory (A) conditions ($C_a = 38$ Pa, $O = 21$ kPa) and non-photorespiratory (B) conditions ($C_a = 100$ Pa, $O = 2$ kPa) in Growdena upper leaves from the Ho *et al.* (2016) data set. The release of (photo)respiratory CO_2 was assumed to either take place in the inner cytosol (upward pointing triangle), the outer cytosol (downward pointing triangle) or the cytosol gaps (dots).

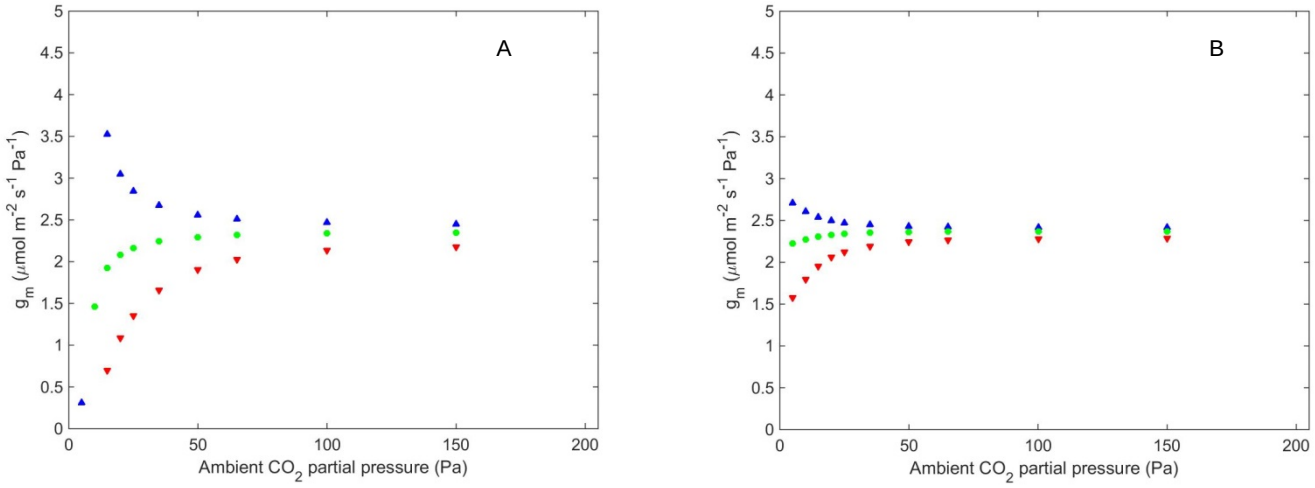

Figure A5.1.65: Response of the simulated apparent mesophyll conductance (g_m) to increased ambient CO_2 levels under ambient oxygen ($O = 21$ kPa) levels (A) and low oxygen ($O = 2$ kPa) levels (B) in Growdena lower leaves from the Ho *et al.* (2016) data set. The release of (photo)respiratory CO_2 was assumed to either take place in the inner cytosol (upward pointing triangle), the outer cytosol (downward pointing triangle) or the cytosol gaps (dots).

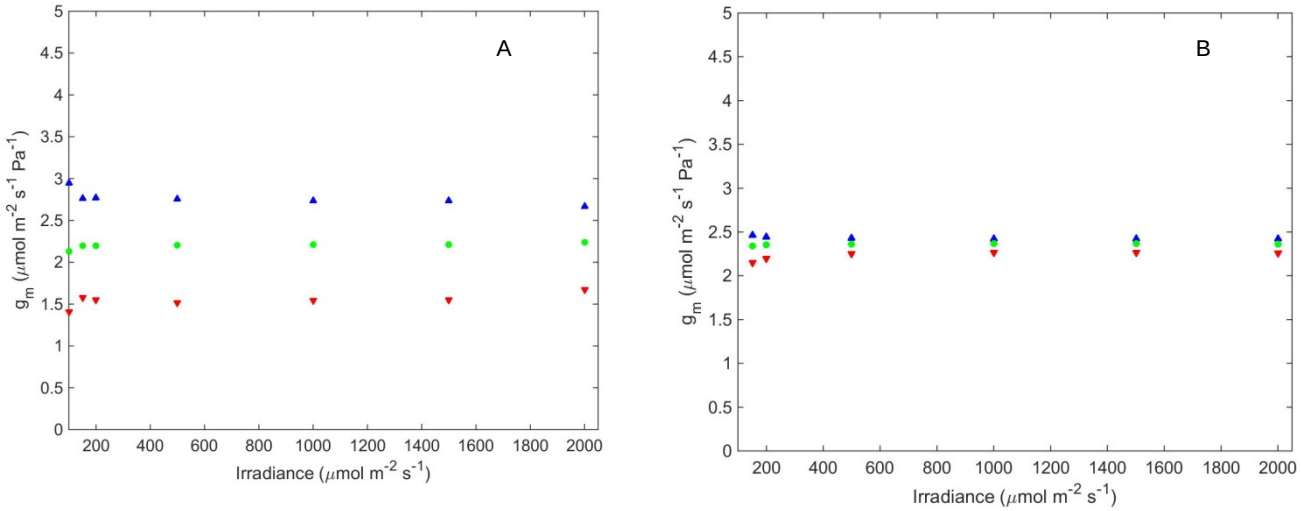

Figure A5.1.66: Response of the simulated apparent mesophyll conductance (g_m) to increased light levels under photorespiratory (A) conditions ($C_\mathrm{a} = 38$ Pa, $O = 21$ kPa) and non-photorespiratory (B) conditions ($C_\mathrm{a} = 100$ Pa, $O = 2$ kPa) in Growdena lower leaves from the Ho *et al.* (2016) data set. The release of (photo)respiratory CO_2 ws assumed to either take place in the inner cytosol (upward pointing triangle), the outer cytosol (downward pointing triangle) or the cytosol gaps (dots).

CHAPTER 6

General discussion

According to the widely used Farquhar-von Caemmerer-Berry model, abbreviated as FvCB model, the net CO_2 assimilation rate in C_3 plants depends on the CO_2 partial pressure near Rubisco, if RuBP carboxylation is either limited by Rubisco or by electron transport (Farquhar *et al.*, 1980). Due to various factors along the diffusion path, the CO_2 partial pressure near Rubisco is lower than in the atmosphere under most environmental conditions. In order to predict the net CO_2 assimilation rate of a C_3 plant correctly, it is important to calculate this drawdown of CO_2 partial pressure correctly. Although the CO_2 transport mechanism from the atmosphere to the intercellular air space is well understood and the CO_2 partial pressure in the intercellular air space can be readily calculated from gas exchange measurements at the leaf surface (Von Caemmerer and Farquhar, 1981), the mechanism that determines the efficiency of CO_2 on the remaining part of the diffusion pathway, is still unclear. Therefore, the main objective of my dissertation was to investigate how structural barriers along the CO_2 diffusion pathway in a C_3 leaf and biochemical processes that add or remove CO_2 to this diffusion path affect its photosynthetic capacity. In order to answer this question, I will pointwise answer the research questions that I stated in Chapter 1, the General Introduction, based on the findings in other Chapters of this thesis. Next, I will make some recommendations for further research.

6.1. How have mesophyll resistance models been used to study photosynthesis in previous work?

Chapter 2 is a critical literature review, in which I try to explain which factors may cause the difference between the CO_2 partial pressure in the intercellular air space and near Rubisco and how these factors were accounted for in photosynthesis models.

6.1.1 The mesophyll is an important barrier for CO_2 transport from the atmosphere to Rubisco

A very common way to deal with the drawdown of CO_2 from the intercellular air space to Rubisco is simply to assume that the drawdown is negligible and that the CO_2 partial pressure near Rubisco equals the one in the intercellular air space (Farquhar *et al.*, 1980; Harley *et al.*, 1992b; Wullschleger, 1993; Aalto and Juurola, 2001; Lenz *et*

al., 2010). In models that adopt this assumption, CO_2 transport from the intercellular air space from the mesophyll to Rubisco is only limited by the resistances for CO_2 transport of the boundary layer and the stomata. If these models are used to estimate parameters of the FvCB model from measured photosynthetic response curves, the predictions of these models may properly fit with the data. This good fit does not necessarily prove that the drawdown of CO_2 between the intercellular air space and Rubisco is negligible, as its effect may be lumped in the estimated FvCB model parameters. The most common type of models to describe the CO_2 drawdown from the intercellular air space to Rubisco is based on the mesophyll resistance concept. Niinemets *et al.* (2009) demonstrated how important it can be to validate whether or not mesophyll resistance does affect CO_2 transport. They parameterized both a model with a negligible mesophyll resistance and a model with a substantial mesophyll resistance. Next, they used both parameterized models to predict the diurnal variations in the net CO_2 assimilation rate in the evergreen species *Quercus ilex* and compared the predictions with measurements. They found that the model that assumed negligible mesophyll resistance performed considerably worse in predicting the diurnal net CO_2 assimilation than the model that did contain a substantial mesophyll resistance. Assuming a negligible mesophyll resistance can also affect long-term predictions of global carbon cycle models. Sun *et al.* (2014) showed that the long-term responsiveness of global terrestrial productivity to CO_2 fertilization is underestimated by these models, if it is assumed that mesophyll resistance is negligible. The conclusions of Niinemets *et al.* (2009) and Sun *et al.* (2014) in terms of model prediction may need to be critically assessed, as different *in vivo* Michaelis-Menten constants were obtained when using negligible mesophyll resistance and substantial mesophyll resistance models (Bernacchi *et al.*, 2001; Bernacchi *et al.*, 2002). The analyses of Niinemets *et al.* (2009) and Sun *et al.* (2014) gave little consideration of such a dependence of Michaelis-Menten constants on mesophyll resistance scenarios. Nevertheless, to understand the mechanisms with regard to photosynthesis-limiting factors, it is important to identify whether mesophyll resistance is significant, and if so, to quantify the magnitude of its variation.

6.1.2 Mesophyll resistance can be determined from gas exchange measurements, sometimes combined with chlorophyll fluorescence or carbon isotope discrimination measurements

Mesophyll resistance models are based on Fick's first law of diffusion (Fick, 1855). The formulation of this law can be that the net flux of a chemical species through a component is proportional to the concentration difference between both sides of this component. The proportionality constant is the conductance; the inverse of this conductance is the resistance. From the perspective of mesophyll resistance models, the net flux represents the net CO_2 assimilation rate and the resistance represents the mesophyll resistance. Often, methods to assess mesophyll resistance determine this one the latter from gas exchange measurements, sometimes combined with chlorophyll fluorescence measurements. Most of these methods are based on the following steps (Harley *et al.*, 1992a; Ethier *et al.*, 2006; Pons *et al.*, 2009; Yin and Struik, 2009; Yin *et al.*, 2009):

(1) rearrange Fick's first law to express CO_2 partial pressure near Rubisco as a function of the mesophyll resistance, the net CO_2 assimilation rate and the CO_2 partial pressure in the intercellular air space.

(2) substitute of this term in the FvCB model.

(3a) rearrange this term to either express mesophyll resistance directly, or

(3b) rearrange this term to express another variable in the FvCB model that can be measured.

In case 3a, the mesophyll resistance can be directly calculated. In case 3b, the mesophyll resistance can be determined by nonlinear regression. Gas exchange measurements, combined with isotope discrimination methods (Farquhar *et al.*, 1982; Evans *et al.*, 1986; Farquhar and Cernusak, 2012; Evans and Von Caemmerer, 2013), can also be used to determine the CO_2 partial pressure near Rubisco. Only in this case, this partial pressure is calculated directly from a number of fractionation coefficients of ^{12}C and ^{13}C. If necessary, one can determine the mesophyll resistance afterwards.

6.1.3 Mesophyll resistance may not be constant, but instead variable with the CO_2 partial pressure in the intercellular air space

All the above-mentioned methods implicitly assume that the resistance of the mesophyll does not change with the CO_2 partial pressure near Rubisco. However, various studies that used a method to calculate the mesophyll resistance directly under various environmental conditions showed that this assumption does not hold (Harley *et al.*, 1992a; Flexas *et al.*, 2007; Yin *et al.*, 2009; Tholen and Zhu, 2011; Tholen *et al.*, 2012). The mechanism of this variability is unclear, which makes it hard to model it. Yin *et al.* (2009) and Gu *et al.* (2012) dealt with this problem by using a phenomenological model, rather than a mechanistic model, to describe the mesophyll resistance and used this model for parameterization.

6.1.4 Mesophyll resistance models do not give a mechanistic description of the CO_2 diffusion pathway

The methods described above can be used to parameterize the FvCB model, without ignoring the contribution of the mesophyll to the overall resistance of the CO_2 transport from the atmosphere to Rubisco. Nevertheless, they do not give a mechanistic explanation for what factors determine the resistance of the mesophyll. With the exception of the Yin *et al.* (2009) model, which includes a phenomenological model for mesophyll resistance, they also do not provide a description of the variation of the mesophyll resistance with the CO_2 partial pressure near Rubisco. However, this phenomenological model does not provide information on the cause of the variability of mesophyll resistance. The lack of a mechanistic description of mesophyll resistance makes it hard to identify leaf traits that can be altered to increase the mesophyll resistance and thereby improve the efficiency of CO_2 diffusion in leaves and the photosynthesis. In this dissertation, I hope to contribute to identifying possible targets to decrease the mesophyll resistance by proposing a mechanistic model for mesophyll resistance.

6.2 What leaf anatomical properties can potentially affect the net CO_2 assimilation rate?

In Chapter 3, I present a resistance model that links the net CO_2 assimilation rate to various leaf anatomical properties that affect the mesophyll resistance models. In order to make this model, I first identified, in Chapter 2, various leaf anatomical properties that may substantially affect the mesophyll resistance and evaluated how these properties have been used in the past to make models for mesophyll resistance.

6.2.1 Mesophyll resistance is affected by various leaf anatomical structures and available surfaces for CO_2 uptake

CO_2 molecules have to diffuse to Rubisco in the chloroplast stroma in order to be assimilated. After CO_2 molecules from the atmosphere have passed the boundary layer at the leaf surface and the stomata, they diffuse dispersed throughout the network of intercellular air space surrounding the mesophyll cells. From there, they still have to cross various barriers to reach the stroma. First, they have to dissolve in the water filled pores of cell walls that are exposed to the intercellular air space. This makes the surface area of the mesophyll cells exposed to these air space in a leaf a potential determinant of the amount of CO_2 that can be taken up by this leaf (Nobel *et al.*, 1975; Nobel, 1977). From the cell wall, they have to cross the plasma membrane to enter the cytosol. From the cytosol, they have to cross the chloroplast envelope to enter the stroma. Since these mesophyll structures contribute to the total CO_2 diffusion path in the mesophyll, the individual resistance of each of these components contributes to the mesophyll resistance (Niinemets and Reichstein, 2003). While diffusing in the stroma, CO_2 molecules move a certain distance before they are assimilated. Therefore, the resistance of the stroma also contributes to the mesophyll resistance (Tosens *et al.*, 2012).

6.2.2 Mesophyll resistance can be partitioned into sub-resistances for various compartments in the mesophyll

Tosens *et al.* (2012) calculated the mesophyll resistance as a serial resistance, i.e. as the sum of individual resistances along the diffusion pathway of CO_2 in the mesophyll. Values for these resistances were either calculated from their assumed diffusion coefficients and their measured thickness or were set equal to an assumed value. In order to calculate the mesophyll resistance from the obtained liquid phase resistance, it has to be multiplied with the ratio of the exposed chloroplast surface to the leaf area and Henry's law has to be applied. The power of this approach is that it can be used to directly link mesophyll conductance to leaf anatomical properties. However, the Tosens *et al.* (2012)-model also does not give an explanation for the variability of the mesophyll conductance with the intercellular CO_2 partial pressure. Moreover, it requires a number of parameter values (diffusion coefficients, assumed resistances, diffusion path length in stroma) which are very uncertain. Tholen *et al.* (2012) developed a resistance model, in which they described CO_2 transport with two sub-resistances (i.e. resistance of combined cell wall and plasma membrane and resistance of chloroplast). Between these two sub-resistances, they placed a source of CO_2 which consists of CO_2 produced by respiration and photorespiration. According to this framework, the variability of mesophyll conductance can be partly explained by the release of photorespired CO_2 along the diffusion pathway, which depends on the CO_2 concentration near Rubisco, in the mesophyll.

6.2.3 The ratio of the exposed mesophyll surface area to the leaf area and the ratio of the exposed chloroplast surface area to the leaf area are main determinants of photosynthesis in tomato

The power of describing the CO_2 diffusion pathways by more than one resistance (Tholen *et al.*, 2012), is that it allows describing CO_2 transport along different parts of the CO_2 diffusion pathway explicitly. This also allows adding the source for CO_2 halfway the diffusion pathway, instead of assuming that respiration and photorespiration take place in the same compartment, making the model more

mechanistic than conventional mesophyll resistance models. The power of calculating individual resistances along the CO_2 diffusion pathways from curvature factors, diffusion coefficients and thicknesses (Tosens *et al.*, 2012), is that it allows to link leaf anatomical properties directly to mesophyll conductance. The power of the various FvCB parameter estimations described by Yin *et al.* (2009) is that it allows determining various photosynthetic parameters from chloroplast, before using the curve-fitting method. In Chapter 3, I combined the strengths of these three approaches. First, I quantified the rate of respiration and the rate of electron transport using the procedures described by Yin *et al.* (2009). Second, I used the Tosens *et al.* (2012) model to quantify the individual resistances of subcellular compartment along the CO_2 diffusion pathway. Third, I calculated the two sub-resistances from the Tholen *et al.* (2012) model from these individual sub-resistances. Fourth, I substituted the modified definition of the CO_2 partial pressure near Rubisco from Tholen *et al.* (2012) in the curve-fitting method described by Yin *et al.* (2009) (the version without a phenomenological model for mesophyll resistance) to determine the remaining FvCB parameters. Combining the models from Yin *et al.* (2009), Tholen *et al.* (2012), and Tosens *et al.* (2012) allowed me running a sensitivity analysis for the net CO_2 assimilation rate to assess the importance of various leaf anatomical properties. I found that the net CO_2 assimilation rate photosynthesis was most sensitive to (1) the ratio of the mesophyll surface area exposed to the intercellular air space to the leaf area and (2) the ratio of the exposed chloroplast surface area to the exposed mesophyll surface area.

6.2.4 Sensitivity of the net CO_2 assimilation rate to changes in leaf anatomy depends on the irradiance and the CO_2 partial pressure

The sensitivity analysis in Chapter 3 for the net CO_2 assimilation rate also showed that the extent of the response of the net CO_2 assimilation rate to leaf anatomical properties depends on the environmental conditions. First, the net CO_2 assimilation rate does not respond to changes in any leaf anatomical property if the net CO_2 assimilation rate is limited by the rate of triose phosphate utilization. This is not surprising, as the net CO_2 assimilation rate is not determined by CO_2 levels or irradiances under these conditions. If the net CO_2 assimilation rate is not limited by triose phosphate utilization, the

response of the net CO_2 assimilation rate to changes in leaf anatomical properties becomes stronger with increased irradiance. Under saturating light, the response of the net CO_2 assimilation rate to changes in leaf anatomy is strongest if the CO_2 partial pressure in the intercellular air space is about 25 Pa. My finding that the sensitivity of the net CO_2 assimilation rate to changes in leaf anatomy depends on the environmental conditions suggests that the success of attempts to increase the net CO_2 assimilation rate by altering the leaf anatomy in a crop depends on the environmental conditions in which this crop grows.

6.2.5 Resistance models cannot be used to mechanistically describe the effect of the placement of mitochondria relative to the stroma

In Chapter 3, I used a resistance model to describe the CO_2 diffusion pathway in the mesophyll. Unlike the conventional resistance model, this model is capable of studying the relationship between the leaf anatomy and the net CO_2 assimilation rate directly. However, it is important to realize that this model makes implicit assumptions about the location of the release of CO_2 produced by respiration and photorespiration. It is assumed that the diffusion paths of CO_2 from the intercellular air space and the CO_2 produced by (photo)respiration share their diffusion path in half the cytosol and in the chloroplast. Consequently, the source of CO_2 is placed in the middle of the cytosol layer between the plasma membrane and the part of the chloroplast envelope facing the intercellular air space ("outer cytosol"). If the mitochondria would be located in the cytosol layer between the tonoplast and the part of the chloroplast facing the vacuole ("inner cytosol") in reality, this approach may underestimate the fraction of (photo)respiratory CO_2 that is re-assimilated. The structure of the model in Chapter 3 is based on the model from Tholen *et al.* (2012). This model also assumes that there is CO_2 release in the cytosol and that there is a shared diffusion pathway of CO_2 from the atmosphere and CO_2 produced by (photo)respiration through the chloroplasts. This implies that they made the same assumption. Tholen *et al.* (2014) reflected on their earlier framework and claimed that the Tholen *et al.* (2012) model does not necessarily assume that mitochondria are placed in the outer cytosol, because it can also be assumed that there is no CO_2 gradient in the cytosol. However, this can only be true if

CO_2 diffusion in the cytosol is much faster than in the chloroplast. If this is the case, the location of the mitochondria will not have any effect on the re-assimilation.

6.2.6 Resistance models cannot be used to study the effect of the gap size between chloroplasts

The mesophyll surface is normally not fully covered with chloroplasts, which may make the effective area for CO_2 uptake smaller than the total mesophyll surface area (Von Caemmerer and Evans, 1991). In the model from Chapter 3, I dealt with this by assuming that, although the whole mesophyll surface is available for CO_2 transfer from the intercellular air space to the cytosol, only the chloroplast surface facing the intercellular air space is available for CO_2 transfer from the chloroplast envelope to Rubisco. However, another consequence of the presence of gaps between the chloroplasts is that these gaps provide a pathway for (photo)respired CO_2 to escape to the intercellular air space, in case that there are mitochondria in the inner cytosol. The resistance model from Chapter 3 is not capable of simulating this escape of (photo)respired CO_2 through the gaps. In order to study the effect of these gaps on the net CO_2 assimilation rate and the location of mitochondria relative to chloroplasts on the net CO_2 assimilation rate, I developed a more complex reaction-diffusion model in Chapter 4.

6.3 How have reaction-diffusion models been used to study photosynthesis in previous work?

Reaction-diffusion models normally need to be solved numerically and they are mathematically considerably more complex than the resistance models described above. This may be an important reason why they are not used often to study CO_2 transport in leaves. However, they are considerably more flexible than resistance models. Therefore, there are certain questions that these models can answer, which cannot be done by resistance models. In order to understand both the opportunities that these reaction-diffusion models can provide and their limitations, I reviewed reaction-diffusion models used to study CO_2 transport in leaves in Chapter 2.

6.3.1 In reaction-diffusion models for net CO_2 assimilation, the liquid phase and the gas phase should be modelled separately

Most early reaction-diffusion models (Parkhurst, 1977; Rand, 1978; Parkhurst, 1984; Parkhurst and Mott, 1990) used a porous volume approach to simulate CO_2 diffusion in the mesophyll. This means that they considered the mesophyll as a composed medium with one apparent diffusion coefficient. The models predict a clear CO_2 gradient between the adaxial and the abaxial leaf area. This gradient may not be there in reality in homobaric leaves. A major disadvantage of a porous volume approach is that it assumes that RuBP carboxylation can take place at any place in the leaf. In reality, the chloroplasts, in which this process takes place, fill only a fraction of the total mesophyll volume. Almost always, chloroplasts tend to be as close as possible to the exposed mesophyll surface (Haberlandt, 1904). As a consequence, the effective length of the CO_2 diffusion pathway is very small compared to the length of the intercellular air space. Since the intercellular air space, at least in tomato, are highly interconnected (Verboven *et al.*, 2015) and the diffusion coefficient of CO_2 in air is 10^4 as high as in water, I surmise that there is barely a gradient of CO_2 in the intercellular air space of homobaric leaves in reality. In contrast, there is a strong gradient between the intercellular air space to the inner chloroplast envelope. This view is confirmed in some more recent studies. A major step forward in the use of reaction-diffusion models to understand the CO_2 diffusion pathway in the mesophyll was the partitioning of the computational domain into a gas phase domain and a liquid phase domain, as proposed by Vesala *et al.* (1996). Aalto and Juurola (2002) also modelled the gas phase and the liquid phase for CO_2 transport separately. They used their reaction-diffusion model to show that there is almost no difference between the steady state CO_2 concentration at the abaxial and the adaxial leaf side in a homobaric and hypostomatous leaf. Further proof for the absence of a CO_2 gradient in a leaf was delivered by Ho *et al.* (2016). They solved a reaction-diffusion model over a tomography, which was partitioned into intercellular air space, epidermis, cytosol, vacuole, and chloroplasts. They also found that the CO_2 partial pressure was about the same throughout the intercellular air space.

6.3.2 Reaction-diffusion models can be used to study the effect of leaf anatomical properties and biochemical processes separately

Another major contribution in using reaction-diffusion models to understand the CO_2 diffusion pathway was the explicit modelling of loose chloroplasts, which was done for the first time by Aalto and Juurola (2002). Ho *et al.* (2016) used this approach in a reaction-diffusion model to assess how the light gradient and the net CO_2 assimilation rate within a leaf are affected by placing mitochondria in a face or a profile conformation (Tholen *et al.*, 2008) in mesophyll cells and to investigate how the net CO_2 assimilation and the re-assimilation of (photo)respired CO_2 are affected by the ratio of the exposed chloroplast surface area to the leaf area. The partitioning of the liquid phase into sub-compartments also allows modelling explicitly where in mesophyll cells various processes that add or remove CO_2 from the diffusion pathway (carbon anhydrases, respiration, photorespiration, RuBP carboxylation) occur. Since reaction-diffusion models describe all physical barriers, processes and their locations separately, they can be used to investigate the effect of each of these factors on photosynthesis separately, rather than lumping most of these processes in the mesophyll resistance.

6.3.3 Reaction-diffusion models always need to be validated due to uncertain values of the diffusion coefficients

An important disadvantage of reaction-diffusion models is that they require diffusion coefficients for each sub-compartment in the mesophyll. The values of these diffusion coefficients are hard to measure and the amount of data is very limited (Evans *et al.*, 2009). If a wrong combination of diffusion coefficients is used to parameterize the reaction-diffusion model, the model may produce errors that are worse than the ones produced by conventional mesophyll resistance models. Several reaction-diffusion models (Parkhurst, 1977; Rand, 1977; Rand and Cooke, 1980; Parkhurst, 1984; Vesala *et al.*, 1996; Aalto *et al.*, 1999; Aalto and Juurola, 2002) did not compare their predictions with actual data, which restricts them to strictly theoretical analysis. Conclusions drawn from the results of these studies may be wrong if the wrong

combination of diffusion coefficients is chosen. In some other studies, this problem was tackled by comparing measured CO_2 response curves with CO_2 response curves (Tholen and Zhu, 2011; Ho *et al.*, 2016) or light response curves (Ho *et al.*, 2016) simulated by the ones simulated by a reaction-diffusion models. It is important to realize that this only proves that the model correctly reproduces CO_2 response curves for the combination of assumed diffusion coefficients. This problem also applies to the resistance model presented in Chapter 3, since I calculated the individual resistances for CO_2 transport in the mesophyll from assumed diffusion coefficients. In Chapter 3, I conducted a sensitivity analysis for alternative values for the assumed diffusive properties. It was not possible to properly fit the model to the data using these alternative values for the diffusion coefficients. This does not necessarily mean that the each of the assumed diffusion coefficients for the mesophyll components has a realistic value. It is therefore controversial to use calculated resistances of individual components to conclude to what extent each individual component constrains CO_2 transport in leaves. Therefore, it has to be noticed that there is less uncertainty in sensitivity analysis for the mesophyll surface area to the leaf area and the chloroplast surface area to the leaf area than in the sensitivity analysis of the individual mesophyll components.

6.4. How can reaction-diffusion models be used as an alternative to resistance models?

In Chapter 4, I developed a reaction-diffusion model for CO_2 transport to analyse combined gas exchange and chlorophyll fluorescence data and to study how the position of mitochondria relative to the chloroplast affects the net CO_2 assimilation rate.

6.4.1 Reaction-diffusion model was used directly to determine FvCB model parameters

Since mesophyll resistance models are particularly useful for the parameterization of the FvCB model, the reaction-diffusion model should be capable of doing this as well, if it is used as an alternative to mesophyll resistance models. The reaction-diffusion

model from Ho *et al.* (2016) uses *a priori* estimated FvCB parameters to simulate CO_2 and light response curves. A disadvantage of this approach is that these *a priori* estimation methods make certain assumptions about the RuBP carboxylation and the CO_2 diffusion pathway. First, the estimates of the rate of respiration were obtained by the Yin *et al.* (2009) method. This method assumes, just like other commonly used methods to estimate this parameter (Kok, 1948; Laisk, 1977), that none of the respired CO_2 is re-assimilated. This assumption may considerably underestimate the rate of respiration. Therefore, I found it important to use the reaction-diffusion model directly to estimate this parameter for light response curves and described a method in Chapter 4 to do so. Second, Ho *et al.* (2016) estimated values for the maximum rate of RuBP carboxylation from a curve-fitting method, combined with a phenomenological model for mesophyll resistance. This model assumes that (photo)respiration and photosynthesis take place in the same compartment and, additionally, this parameter has to be estimated simultaneously with a parameter in the phenomenological model for mesophyll resistance from Yin *et al.* (2009). Given the strong correlation between mesophyll resistance and the maximum rate of RuBP carboxylation, the estimates may be biased. Therefore, I also described a procedure to use the reaction-diffusion model directly to estimate this parameter without the need to simultaneously estimate another parameter. I only used measured net CO_2 assimilation rates measured at the lowest light levels to determine the rate of respiration and measured net CO_2 assimilation rates measured at the lowest CO_2 levels to estimate the maximum rate of RuBP carboxylation. I validated the model by simulating the remaining parts of the light and CO_2 response curves and compare them with data that I did not use for the estimation of any parameters.

6.4.2 Reaction-diffusion model should be computational inexpensive, whenever possible

One of the attractive features of mesophyll resistance models is that they are analytical, which makes it possible to use these models for procedures that require a large number of simulations. This is particularly useful if these models are used for the estimation of FvCB model parameters within seconds. In contrast, reaction-diffusion

models have to be solved numerically and the time per simulation is much longer. Especially if the computational domain is complex, the amount of time per simulation is much higher in mesophyll resistance models. This makes it unfeasible to use reaction-diffusion models for most purposes. For instance, I run an early version (Ho *et al.*, 2012a) of the 3-D model from Ho *et al.* (2016) on my computer (Processor: Intel(R) Xeon CPU W3550 @ 3.07 GHz 3.06 GHz, Installed memory: 24 GB RAM) to simulate a CO_2 response curve. It took about 9 hours to simulate a single point in the curve. Consequently, it took several days to simulate a CO_2 response curve with 10 points. This can be considerably speeded up by the use of parallel computing using supercomputers, but even then it takes hours before a single curve is simulated. Therefore, it is currently not feasible to use this model for parameterization, which is a main application of mesophyll resistance models. In the model that I presented in Chapter 4, I presented a much simpler reaction-diffusion model. I tried to keep the time per simulation as low as possible by using various simplifications, compared to the approach from Tholen and Zhu (2011), Watté *et al.* (2015) and Ho *et al.* (2016):

(1) modelling the computational domain in 2-D.

(2) modelling the computational domain as rectangles.

(3) modelling the mitochondria and the cytosol layer that contains them as one single domain, rather than modelling loose mitochondria.

(4) not explicitly modelling carbon anhydrase activity.

(5) not modelling the transport of light explicitly.

(6) not modelling CO_2 transport in the intercellular air space explicitly.

The price of these simplifications is that oversimplification can potentially lead to wrong model predictions. Therefore, I validated the model extensively in both Chapter 4 and Chapter 5. In Chapter 4, I investigated whether the simplifications in both the processes and the leaf structure had an effect on the predicted net CO_2 assimilation rate by comparing a CO_2 response curve predicted by the model in Chapter 4 with a CO_2 response curve the model from Ho *et al.* (2016) for the same conditions. I found

that there was almost no difference between the predictions of both models. Since the model from Ho *et al.* (2016) does not contain mitochondria either, I did an additional validation by making a version of the model that contains mitochondria and I compared the net CO_2 assimilation rate with the predicted by the default model and the one by the model that contained loose mitochondria. Again, I did not find differences between the predictions of both models.

6.5 How does the position of mitochondria relative to the chloroplasts affect the net CO_2 assimilation rate?

Conventional mesophyll resistance models assume that CO_2 uptake by RuBP carboxylation and CO_2 release by (photo)respiration take place in the same compartment. In reality, RuBP carboxylation occurs in chloroplasts and the production of (photo)respired CO_2 takes place in the mitochondria. This CO_2 produced by (photo)respiration can either leave the leaf, or be re-assimilated after it has diffused into the chloroplast. Since conventional mesophyll resistance models do not describe this process explicitly, its effect on the drawdown between the CO_2 partial pressure in the intercellular air space and Rubisco is likely lumped in the estimate of the mesophyll resistance. Re-assimilation can be modelled explicitly by describing the CO_2 diffusion path by more than one resistance, like Tholen *et al.* (2012) did. The disadvantage of this approach is that it requires making assumptions about the location of the mitochondria. They are either located in the outer cytosol (Chapter 3), or it has to be assumed that CO_2 diffusion in cytosol is so much faster than in the chloroplasts (Tholen *et al.*, 2014) that the placement of mitochondria does not affect the re-assimilation of (photo)respired CO_2. These assumptions may affect the predicted net CO_2 assimilation rates. In Chapters 4 and 5, I used reaction-diffusion models to check whether the location of mitochondria affects the net CO_2 assimilation rate, while not making the assumption of very fast diffusion of CO_2 in the cytosol.

6.5.1 The position of the mitochondria relative to the chloroplasts affects the net CO_2 assimilation rate and the re-assimilation of (photo)respired CO_2

I parameterized and validated the reaction-diffusion model in Chapter 4 for three scenarios. I assumed that (photo)respiratory CO_2 takes place either in the inner cytosol, or in the outer cytosol, or in the cytosol gaps between the chloroplast. In all leaf types investigated, the predicted net CO_2 assimilation rate was higher if (photo)respired CO_2 takes place in the inner cytosol than in the outer cytosol. If I assumed that (photo)respired CO_2 release took place in the cytosol gaps, the net CO_2 assimilation was in between, but closer to the one predicted by the scenario assuming that (photo)respired CO_2 release takes place in the inner cytosol. In Chapter 4, I also described a method to use the reaction-diffusion model to calculate the fraction of (photo)respired CO_2 that is re-assimilated. I calculated this fraction for each scenario for (photo)respired CO_2 release under saturating light and ambient CO_2 and O_2 partial pressure in the atmosphere. This fraction was strongly affected by the position of the mitochondria. The scenario that assumed that (photo)respired CO_2 took place in the outer cytosol predicted that 56% of the (photo)respired CO_2 was re-assimilated, while the scenario that assumed that this took place in the inner cytosol predicted that 75% was re-assimilated. The scenario that assumed (photo)respired CO_2 release in the cytosol gap predicted 69%.

6.5.2 It is not likely that (photo)respired CO_2 is released in the outer cytosol

In Chapter 4, I validated the reaction-diffusion model by investigating whether the model was capable of predicting the light and CO_2 response curves for light and CO_2 levels that were not used for calibration. It appeared that the model that assumed (photo)respired CO_2 release in the inner cytosol performed best in predicting the net CO_2 assimilation rate, while the model that assumed (photo)respired CO_2 release in the outer cytosol performed worst. The latter model considerably underestimated the net CO_2 assimilation rate at low CO_2 levels or high irradiances. In Chapter 5, I used Akaike's Information Criterion (Akaike, 1974) to compare the predicted and measured CO_2, measured under low and ambient O_2 levels, and light response curves measured

under photorespiratory and non-photorespiratory conditions. There is not a single case in which the model that assumed (photo)respired CO_2 release in the outer cytosol performed substantially better than the other two models. In contrast, in 28 other curves it performed substantially worse than at least one of the other two scenarios. This implies that this scenario is not likely and that it should be avoided in models presented in future research, which use either reaction-diffusion models or models with a partitioned mesophyll resistance.

6.6 To what extent and under which combination of light, CO_2 and O_2 levels does the re-assimilation of CO_2 produced by respiration and photorespiration affect the net CO_2 assimilation rate of CO_2?

6.6.1 The fraction of (photo)respired CO_2 that is re-assimilated strongly depends on both environmental conditions and various leaf physiological traits

In order to assess the importance of re-assimilation of (photo)respired CO_2, in Chapter 5 I used the reaction-diffusion model developed in Chapter 4 to calculate the fraction of re-assimilated CO_2 produced by (photo)respiration under various combinations of irradiances and CO_2 partial pressures in the atmosphere and two O_2 partial pressures. I did these calculations for each scenario of the location of (photo)respired CO_2 release. The differences between the predicted fractions of re-assimilation of (photo)respired CO_2 were large, especially at high irradiances or low CO_2 partial pressures in the atmosphere. Nevertheless, for all 24 tomato leaf types from two experiments that I used in this study I found very similar trends. The relationship between the fraction of (photo)respired CO_2 that is re-assimilated with the ambient CO_2 level is S-shaped at any oxygen concentration. This fraction can vary considerably with the environmental conditions. For instance, while under intermediate CO_2 ambient conditions (20-40 Pa) this fraction is about 0.8 in 15-day old cv. Admiro tomato leaves, it is only 0.3 at very high CO_2 ambient conditions. I also found that the fraction of (photo)respired CO_2 that is re-assimilated increases with the irradiance, but this increase tends to level off at higher irradiances. We also conducted a sensitivity analysis under ambient CO_2 and

saturating light for this fraction to various FvCB model parameters. Although the response to changes in the rate of respiration in the light was rather weak, the fraction of (photo)respired CO_2 that is re-assimilated responded very strongly to changes in FvCB model parameters that determine the rate of RuBP carboxylation. In addition to the results of Chapters 4 and 5, various studies have attempted to determine the fraction of CO_2 that is re-assimilated. There is a wide variation in the reported values that were obtained by various methodologies. Loreto *et al.* (1999) determined that 100% of the CO_2 produced by respiration and photorespiration is re-assimilated in tomato. In contrast, Pärnik and Keerberg (2007) found percentages between 14% and 18% in sunflower. Various other studies reported values in between (Haupt-Herting *et al.*, 2001; Tholen *et al.*, 2012; Busch *et al.*, 2013; Ho *et al.*, 2016). The results from Chapter 5 suggest that these differences can likely be explained by the environmental conditions used in these different studies and/or by the different traits of the leaves that were used. Additionally, Busch *et al.* (2013) and Ho *et al.* (2016) showed that this fraction depends on the ratio between the exposed chloroplast surface area to the exposed mesophyll surface area. Since the fraction of (photo)respired CO_2 does not only depend on environmental conditions, but also on leaf specific properties, this fraction is likely to be species dependent as well.

6.6.2 The estimates for the rate of respiration are not affected by re-assimilation, but they do depend on oxygen partial pressure

Commonly used models to estimate the rate of respiration in the light (Kok, 1948, 1949; Yin *et al.*, 2009; Yin *et al.*, 2011) exploit the linear relationship between the irradiance and the net CO_2 assimilation rate to estimate the rate of respiration in the light. This assumption of a linear relationship is valid under conditions of low oxygen and light, because under these conditions RuBP carboxylation is limited by electron transport and there is no photorespiration (Yin *et al.*, 2011). However, none of these methods accounts for the re-assimilation of respired CO_2 and implicitly assumes that all respired CO_2 is lost to the atmosphere. This can potentially lead to an underestimation of the rate of respiration if these methods are used. In order to test this hypothesis, I estimated the rate of respiration under photorespiratory and non-

photorespiratory conditions with the reaction-diffusion models for three scenarios for (photo)respired CO_2 release in Chapter 5. I found that there were almost no differences between the estimates of the respiration rate in the light of the scenarios that assumed that (photo)respiration takes place in the inner cytosol, the outer cytosol or the cytosol gaps between the chloroplasts. Additionally, I showed that the fraction of (photo)respired CO_2 that is re-assimilated is low under low irradiances. I concluded that re-assimilation of respired CO_2 does not have much impact on the net CO_2 assimilation rate under the conditions in which Kok (1948) method and the Yin *et al.* (2009) method are used to estimate the rate of respiration. This conclusion is further supported by the fact that when I compared the estimates of the Yin *et al.* (2009)-method with the estimates of the reaction-diffusion models under non-photorespiratory conditions, the estimates by both methods were almost the same. When I compared the estimates of the rate of respiration by the reaction-diffusion model at non-photorespiratory conditions with the estimates at photorespiratory conditions, I found considerable differences between them. For all but one leaf type, the estimate of the rate of respiration was considerably higher at photorespiratory conditions than at non-photorespiratory conditions. This result strongly suggests that the rate of respiration in the light is oxygen dependent. This finding has implications for the use of the Kok (1948) method and Yin *et al.* (2009) method. These methods are strictly speaking not valid at ambient O_2 levels (Yin *et al.*, 2011) and may therefore only be used under low O_2 levels. However, if the respiration rate is oxygen dependent, the estimates obtained under low O_2 levels cannot be assumed equal to the estimates obtained under normal O_2 levels. In Chapter 3, I actually did make this assumption. This likely explains why there is generally a reasonable fit between the measured and the simulated net CO_2 assimilation by the resistance model from Chapter 3, even though this model assumed that (photo)respired CO_2 is released in the outer cytosol.

6.7 Concluding remarks

Zhu *et al.* (2010) estimated that decreasing the mesophyll resistance can potentially lead to an increase of the photosynthetic capacity by 20%. Attempts to decrease the mesophyll resistance can therefore potentially contribute to an increase in global crop

yield necessary to fulfil the growing demand for food, feed, fibres and bioenergy (FAO, 2009a; FAO, 2009b). Throughout this dissertation, I showed that mesophyll resistance is very complex. It violates the definition of a physical resistance, because it varies with the intercellular CO_2 concentration and should therefore be considered as an apparent parameter, instead of a resistance. It lumps the effects of physical barriers for CO_2 transport, biochemical processes that add or remove CO_2 along the CO_2 diffusion pathway and the re-assimilation of (photo)respired CO_2. In order to achieve the increase of photosynthetic efficiency by decreasing mesophyll resistance, it is necessary to identify specific targets to alter, and, therefore, to understand all factors that affect mesophyll resistance. In this dissertation, I contributed to this understanding by developing models that describe these factors explicitly and that are capable of simulating their effects on net CO_2 assimilation rate. The first approach I used was to develop a resistance model in Chapter 3. In this model, the mesophyll resistance is partitioned into sub-resistances for various leaf structures. The advantage of this approach is that it allowed directly linking leaf anatomical properties to net CO_2 assimilation rate, but important disadvantages were that respiration and photorespiration were assumed to take place in the outer cytosol and that the diffusion path length of CO_2 in the stroma was uncertain. Therefore, I developed a reaction-diffusion model in Chapter 4 that does not have these disadvantages. I showed in Chapter 5 that this model can be used to quantify the fraction of (photo)respired CO_2 that is re-assimilated and the mesophyll resistance, and to investigate how each individual component along the CO_2 diffusion path affects these factors.

Although these procedures cannot be done by a mesophyll resistance model, it does not necessarily mean that reaction-diffusion models are always preferable over mesophyll resistance models in future research. As long as one is not interested in identifying specific targets to decrease mesophyll resistance or find mechanistic explanations why mesophyll resistance differs along experimental treatments, mesophyll resistance models are a very powerful tool to estimate FvCB model parameters. However, if mesophyll resistance models are used, I want to recommend the use of a phenomenological model (Yin *et al.*, 2009; Gu *et al.*, 2012) These models

are capable of describing the variability of the mesophyll resistance with the intercellular CO_2 partial pressure, unlike mesophyll resistance models that assume a fixed value for this mesophyll resistance. In Chapter 5, I showed that the mesophyll conductance (inverse of mesophyll resistance) calculated by the reaction-diffusion model, assuming (photo)respired CO_2 release in the inner cytosol, has a very similar response to the response calculated by conventional (unpartitioned) mesophyll resistance models (Harley *et al.*, 1992a; Yin and Struik, 2009). This provides further proof that mesophyll resistance is variable and that a phenomenological model is necessary to properly deal with these variations, if one choses to use resistance models. A clear advantage of the phenomenological model for mesophyll resistance from Yin *et al.* (2009) over the reaction-diffusion model in Chapter 5 is that it does not require predefined diffusion coefficients or leaf anatomical parameters. However, both this framework and models with a constant mesophyll resistance are not able to describe the CO_2 diffusion pathway mechanistically. Therefore, I think that any attempt to partition the mesophyll resistance as defined in these models will constrain the mitochondria to the outer cytosol (Chapter 3), will assume that there is no CO_2 gradient in the cytosol, requires the estimation of more resistances than can be estimated from gas-exchange data, possibly combined with chlorophyll fluorescence or carbon isotope discrimination. In any case, it is not possible to study the position of mitochondria relative to the chloroplasts.

In order to use reaction-diffusion models to investigate how altering these targets can result in an increase in the photosynthetic efficiency, diffusion coefficients of various mesophyll components need to be quantified. Given the uncertainty of these diffusion coefficients, my first recommendation for further research is that more effort should be put on measuring these diffusion coefficients directly. Since these measurements are very challenging and there are very few available (Evans *et al.*, 2009), this may not be feasible in the short term. In order to still exploit the power of reaction-diffusion models as much as possible, my second recommendation is to validate the reaction-diffusion models. This is especially important, if assumed diffusion coefficients are used as input. In Chapters 4 and 5, I showed various examples to do so. Although the

diffusion coefficients of individual mesophyll components may not be realistic, I showed proof that the combination of them makes sense. In order to use the reaction-diffusion model from Chapters 4 and 5 in future studies, I recommend collecting a combination of leaf anatomical data and gas exchange from other C_3 species than tomato for further validation. Such a future study is especially interesting if the species that are used have considerably different leaf anatomical and/or physiological properties from tomato. This will contribute to a general understanding of the CO_2 diffusion pathway. My final recommendation is to extend the model with explicit descriptions of the temperature sensitivity of physical parameters (diffusion coefficients for CO_2, the solubility of CO_2 in water and in membranes) and physiological parameters (stomatal conductance, kinetic constants Rubisco, rates of respiration, electron transport, and triose phosphate utilization). Over the next decades, the ambient CO_2 partial pressure in the atmosphere and the temperature are both expected to rise (Meehl *et al.*, 2007). Such an extended model may be helpful to understand how leaf photosynthesis is affected by these climate change variables and how various components that affect mesophyll resistance may be altered for crops to adapt to climate change.

References

Aalto T, Juurola E. 2001. Parametrization of a biochemical CO_2 exchange model for birch (*Betula pendula* Roth.). *Boreal Environment Research* 6, 53-64.

Aalto T, Juurola E. 2002. A three-dimensional model of CO_2 transport in airspaces and mesophyll cells of a silver birch leaf. *Plant, Cell & Environment* **25**, 1399-1409.

Aalto T, Vesala T, Mattila T, Simbierowicz P, Hari P. 1999. A three-dimensional stomatal CO_2 exchange model including gaseous phase and leaf mesophyll separated by irregular interface. *Journal of Theoretical Biology* **196**, 115-128.

Akaike H. 1974. A new look at the statistical model identification. *IEE Transactions on Automatic Control* **19**, 716-723.

Bernacchi CJ, Portis AR, Nakano H, von Caemmerer S, Long SP. 2002. Temperature response of mesophyll conductance. Implications for the determination of Rubisco enzyme kinetics and for limitations to photosynthesis *in vivo*. *Plant Physiology* **130**, 1992-1998.

Bernacchi CJ, Singsaas EL, Pimentel C, Portis AR, Long SP. 2001. Improved temperature response functions for models of Rubisco-limited photosynthesis. *Plant, Cell & Environment* **24**, 253-259.

Bunce JA. 2010. Variable responses of mesophyll conductance to substomatal carbon dioxide concentration in common bean and soybean. *Photosynthetica* **48**, 507-512.

Burney JA, Davis SJ, Lobell DB. 2010. Greenhouse gas mitigation by agricultural intensification. *Proceedings of the National Academy of Sciences of the United States of America* **107**, 12052-12057.

Burnham KP, Anderson DR. 2004. Multimodel inference - understanding AIC and BIC in model selection. *Sociological Methods & Research* **33**, 261-304.

Busch FA. 2013. Current methods for estimating the rate of photorespiration in leaves. *Plant Biology* **15**, 648-655.

Busch FA, Sage TL, Cousins AB, Sage RF. 2013. C_3 plants enhance rates of photosynthesis by reassimilating photorespired and respired CO_2. *Plant, Cell & Environment*

Cano FJ, Lopez R, Warren CR. 2014. Implications of the mesophyll conductance to CO_2 for photosynthesis and water-use efficiency during long-term water stress and recovery in two contrasting *Eucalyptus* species. *Plant, Cell & Environment* **37**, 2470-2490.

Douthe C, Dreyer E, Epron D, Warren CR. 2011. Mesophyll conductance to CO_2, assessed from online TDL-AS records of (CO2)-^{13}C discrimination, displays small but significant short-term responses to CO_2 and irradiance in *Eucalyptus* seedlings. *Journal of Experimental Botany* **62**, 5335-5346.

Ethier GJ, Livingston NJ. 2004. On the need to incorporate sensitivity to CO_2 transfer conductance into the Farquhar-von Caemmerer-Berry leaf photosynthesis model. *Plant, Cell & Environment* **27**, 137-153.

Ethier GJ, Livingston NJ, Harrison DL, Black TA, Moran JA. 2006. Low stomatal and internal conductance to CO_2 versus Rubisco deactivation as determinants of the photosynthetic decline of ageing evergreen leaves. *Plant, Cell & Environment* **29**, 2168-2184.

Evans JR, Kaldenhoff R, Genty B, Terashima I. 2009. Resistances along the CO_2 diffusion pathway inside leaves. *Journal of Experimental Botany* **60**, 2235-2248.

Evans JR, Sharkey TD, Berry JA, Farquhar GD. 1986. Carbon isotope discrimination measured concurrently with gas exchange to investigate CO_2 diffusion in leaves of higher plants. *Australian Journal of Plant Physiology* **13**, 281-292.

Evans JR, Vogelmann TC. 2003. Profiles of ^{14}C fixation through spinach leaves in relation to light absorption and photosynthetic capacity. *Plant, Cell & Environment* **26**, 547-560.

Evans JR, von Caemmerer S. 1996. Carbon dioxide diffusion inside leaves. *Plant Physiology* **110**, 339-346.

Evans JR, Von Caemmerer S. 2013. Temperature response of carbon isotope discrimination and mesophyll conductance in tobacco. *Plant, Cell & Environment* **36**, 745-756.

Evans JR, Von Caemmerer S, Setchell BA, Hudson GS. 1994. The relationship between CO_2 transfer conductance and leaf anatomy in transgenic tobacco with a reduced content of Rubisco. *Australian Journal of Plant Physiology* **21**, 475-495.

Fanta SW, Vanderlinden W, Abera MK, Verboven P, Karki R, Ho QT, De Feyter S, Carmeliet J, Nicolaï BM. 2012. Water transport properties of artificial cell walls. *Journal of Food Engineering* **108**, 393-402.

FAO. 2009a. FAO's Director-General on How to Feed the World in 2050. *Population and Development Review* **35**, 837-839.

FAO. 2009b. How to feed the world in 2050. *How to feed the world in 2050; high level expert forum*. Rome.

Farquhar GD, Cernusak LA. 2012. Ternary effects on the gas exchange of isotopologues of carbon dioxide. *Plant, Cell & Environment* **35**, 1221-1231.

Farquhar GD, Oleary MH, Berry JA. 1982. On the relationship between carbon isotope discrimination and the inter-cellular carbon-dioxide concentration in leaves. *Australian Journal of Plant Physiology* **9**, 121-137.

Farquhar GD, von Caemmerer S, Berry JA. 1980. A biochemical model of photosynthetic CO_2 assimilation in leaves of C_3 species. *Planta* **149**, 78-90.

Fick A. 1855. Über Diffusion. *Poggendorff's Annalen der Physik und Chemie* **94**, 59-86.

Flexas J, Barbour MM, Brendel O, Cabrera HM, Carriqui M, Diaz-Espejo A, Douthe C, Dreyerc E, Ferrio JP, Gago J, Galle A, Galmes J, Kodama N, Medrano H, Niinemets U, Peguero-Pina JJ, Poua A, Ribas-Carbo M, Tomas M, Tosens T, Warren CR. 2012. Mesophyll diffusion conductance to CO_2: An unappreciated central player in photosynthesis *Plant Science* **193**, 70-84.

Flexas J, Diaz-Espejo A, Berry JA, Cifre J, Galmes J, Kaidenhoff R, Medrano H, Ribas-Carbo M. 2007a. Analysis of leakage in IRGA's leaf chambers of open gas exchange systems: quantification and its effects in photosynthesis parameterization. *Journal of Experimental Botany* **58**, 1533-1543.

Flexas J, Diaz-Espejo A, Galmes J, Kaldenhoff R, Medrano H, Ribas-Carbo M. 2007b. Rapid variations of mesophyll conductance in response to changes in CO_2 concentration around leaves. *Plant, Cell & Environment* **30**, 1284-1298.

Flexas J, Ribas-Carbo M, Diaz-Espejo A, Galmes J, Medrano H. 2008. Mesophyll conductance to CO_2: current knowledge and future prospects. *Plant, Cell & Environment* **31**, 602-621.

Gaastra P. 1959. Photosynthesis of crop plants as influenced by light, carbon dioxide, temperature, and stomatal diffusion resistance. *Mededelingen van Landbouwhogeschool te Wageningen, Nederland* **59**, 1-68.

Galmes J, Ochogavia JM, Gago J, Roldan EJ, Cifre J, Conesa MA. 2013. Leaf responses to drought stress in Mediterranean accessions of *Solanum lycopersicum*: anatomical adaptations in relation to gas exchange parameters. *Plant, Cell & Environment* **36**, 920-935.

Genty B, Briantais JM, Baker NR. 1989. The relationship between the quantum yield of photosynthetic electron-transport and quenching of chlorophyll fluorescence. *Biochimica et Biophysica Acta* **990**, 87-92.

Gielwanowska I, Pastorczyk M, Kellmann-Sopyla W, Gorniak D, Gorecki RJ. 2015. Morphological and ultrastructural changes of organelles in leaf mesophyll cells of the Arctic and Antarctic plants of Poaceae family under cold influence. *Arctic Antarctic and Alpine Research* **47**, 17-25.

Gillon JS, Yakir D. 2000. Internal conductance to CO_2 diffusion and (COO)-^{18}O discrimination in C_3 leaves. *Plant Physiology* **123**, 201-213.

Gu JF, Yin X, Stomph TJ, Wang HQ, Struik PC. 2012. Physiological basis of genetic variation in leaf photosynthesis among rice (*Oryza sativa* L.) introgression lines under drought and well-watered conditions. *Journal of Experimental Botany* **63**, 5137-5153.

Gu LH, Sun Y. 2014. Artefactual responses of mesophyll conductance to CO_2 and irradiance estimated with the variable *J* and online isotope discrimination methods. *Plant, Cell & Environment* **37**, 1231-1249.

Gutknecht J, Bisson MA, Tosteson FC. 1977. Diffusion of carbon dioxide through lipid bilayer membranes - effects of carbonic anhydrase. *Journal of General Physiology* **69**, 779-794.

Haberlandt GFJ. 1904. Das Assimilationsystem. In: Engelmann VvW, ed. *Physiologische Pflanzenanatomie*. Leipzig.

Hall AE, Schulze ED. 1980. Stomatal response to environment and a possible interrelation between stomatal effects on transpiration and CO_2 asimilation. *Plant, Cell & Environment* **3**, 467-474.

Harley PC, Loreto F, Dimarco G, Sharkey TD. 1992a. Theoretical considerations when estimating the mesophyll conductance to CO_2 flux by analysis of the response of photosynthesis to CO_2. *Plant Physiology* **98**, 1429-1436.

Harley PC, Thomas RB, Reynolds JF, Strain BR. 1992b. Modeling photosynthesis of cotton grown in elevated CO_2. *Plant, Cell & Environment* **15**, 271-282.

Hassiotou F, Ludwig M, Renton M, Veneklaas EJ, Evans JR. 2009. Influence of leaf dry mass per area, CO_2, and irradiance on mesophyll conductance in sclerophylls. *Journal of Experimental Botany* **60**, 2303-2314.

Haupt-Herting S, Klug K, Fock HP. 2001. A new approach to measure gross CO_2 fluxes in leaves. Gross CO_2 assimilation, photorespiration, and mitochondrial respiration in the light in tomato under drought stress. *Plant Physiology* **126**, 388-396.

Ho QT, Berghuijs HNC, Watté R, Verboven P, Herremans E, Yin X, Retta MA, Aernouts B, Saeys W, Helfen L, Farquhar GD, Struik PC, Nicolaï BM. 2016. 3-D microscale modeling of CO_2 transport and light propagation in tomato leaves enlightens photosynthesis. *Plant, Cell & Environment* **39**, 50-61.

Ho QT, Verboven P, Herremans E, Retta MA, Defraeye T, Nicolaï BM, Yin X, Thapa RK, Struik PC. 2012a. A 3-D microscale model for CO_2 gas transport in tomato leaves during photosynthesis. *Acta Horticulturae 957*. Nanjing.

Ho QT, Verboven P, Verlinden BE, Nicolaï BM. 2010. A model for gas transport in pear fruit at multiple scales. *Journal of Experimental Botany* **61**, 2071-2081.

Ho QT, Verboven P, Yin X, Struik PC, Nicolaï BM. 2012b. A microscale model for combined CO_2 diffusion and photosynthesis in leaves. *Plos One* **7**.ARTN e48376 10.1371/journal.pone.0048376

Ivanova LA. 2012. Restructuring of the leaf mesophyll in a series of plant life forms. *Doklady Biological Sciences* **477**, 386-389.

Ivanova LA, Petrov MS, Kadushikov RM. 2006. Determination of mesophyll diffusion resistance in *Chamaerion angustifolium* by the method of three-

dimensional reconstruction of the leaf cell packing. *Russian Journal of Plant Physiology* **53**, 316-324.

Ivanova LA, Pyankov VI. 2002. Structural adaptation of the leaf mesophyll to shading. *Russian Journal of Plant Physiology* **2002**, 467-480.

Johnson IR, Thornley JHM. 1984. A model of instantaneous and daily canopy photosynthesis. *Journal of Theoretical Biology* **107**, 531-545.

Juurola E, Aalto T, Thum T, Vesala T, Hari P. 2005. Temperature dependence of leaf level CO_2 fixation: revising biochemical coefficients through analysis of leaf three-dimensional structure. *New Phytologist* **166**, 205-215.

Kok B. 1948. A critical consideration of the quantum yield of *Chlorella* photosynthesis. *Enzymologia* **13**, 1-56.

Kok B. 1949. On the interrelation of respiration and photosynthesis in green plants. *Biochimica et Biophysica Acta* **3**, 625-631.

Laisk AK. 1977. Kinetics of photosynthesis and photorespiration in C_3 plants. *Nauka Moscow (in Russian).*

Lenz KE, Host GE, Roskoski K, Noormets A, Sober A, Karnosky DF. 2010. Analysis of a Farquhar-von Caemmerer-Berry leaf level photosynthetic rate model for *Populus tremuloides* in the context of modeling and measurement limitations. *Environmental Pollution* **158**, 1015-1022.

Leuning R. 1995. A critical appraisal of a combined stomatal-photosynthesis model for C_3 Plants. *Plant, Cell & Environment* **18**, 339-355.

Lewis RW, Nithiarasu P, Seetharamu KN. 2004. *Fundamentals of the Finite Element Method for Heat and Fluid Flow*: Wiley.

LI-COR I. 1999. 1. System description; what it is, what it does, and how it does it. In: LI-COR I, ed. *Using the LI-6400 portable photosynthesis system.* Lincoln, Nebraska,USA. 1-15.

Long SP, Bernacchi CJ. 2003. Gas exchange measurements, what can they tell us about the underlying limitations to photosynthesis? Procedures and sources of error. *Journal of Experimental Botany* **54**, 2393-2401.

Long SP, Zhu XG, Naidu SL, Ort DR. 2006. Can improvement in photosynthesis increase crop yields? *Plant, Cell & Environment* **29**, 315-330.

Loreto F, Delfine S, Di Marco G. 1999. Estimation of photorespiratory carbon dioxide recycling during photosynthesis. *Australian Journal of Plant Physiology* **26**, 733-736.

Mebatsion HK, Verboven P, Verlinden BE, Ho QT, Nguyen TA, Nicolaï BM. 2006. Microscale modelling of fruit tissue using Voronoi tessellations. *Computers and Electronics in Agriculture* **52**, 36-48.

Meehl GA, Stocker TF, Collins WD, Friedlingstein P, Amadou TG, Gregory JM, Kitoh A, Knutti R, Murphy JM, Noda A, Raper SCB, Watterson IG, Weaver AJ, Zhao ZC. 2007. Global climate projections. In: Press CU, ed. *Climate Change 2007: The Physical Science Basis.* Cambridge, United Kingdom and New York,NY,USA.

Moser T, Holzinger A, Buchner O. 2015. Chloroplast protrusions in leaves of Ranunculus glacialisL. respond significantly to different ambient conditions, but are not related to temperature stress. *Plant, Cell & Environment* **38**, 1347-1356.

Niinemets U, Diaz-Espejo A, Flexas J, Galmes J, Warren CR. 2009. Importance of mesophyll diffusion conductance in estimation of plant photosynthesis in the field. *Journal of Experimental Botany* **60**, 2271-2282.

Niinemets U, Reichstein M. 2003. Controls on the emission of plant volatiles through stomata: A sensitivity analysis. *Journal of Geophysical Research-Atmospheres* **108**.

Nobel PS. 1977. Internal leaf area and cellular CO_2 resistance - Photosynthetic implications of variations with growth-conditions and plant species. *Physiologia Plantarum* **40**, 137-144.

Nobel PS. 2009. *Physicochemical and Environmental Plant Physiology*. Oxford, United Kingdom: Elsevier Inc.

Nobel PS, Zaragoza LJ, Smith WK. 1975. Relation between mesophyll surface-area, photosynthetic rate, and illumination level during development for leaves of *Plectranthus parviflorus* Henckel. *Plant Physiology* **55**, 1067-1070.

Ort DR, Merchant SS, Alric J, Barkan A, Blankenship RE, Bock R, Croce R, Hanson MR, Hibberd JM, Long SP, Moore TA, Moroney J, Niyogi KK, Parry MAJ, Peralta-Yahya PP, Prince RC, Redding KE, Spalding MH, van Wijk KJ, Vermaas WFJ, von Caemmerer S, Weber APM, Yeates TO, Yuan JS, Zhu XG.

2015. Redesigning photosynthesis to sustainably meet global food and bioenergy demand. *Proceedings of the National Academy of Sciences of the United States of America* **112**, 8529-8536.

Pachepsky LB, Haskett JD, Acock B. 1995. A two-dimensional model of leaf gas exchange with special reference to leaf anatomy. *Journal of Biogeography* **22**, 209-214.

Parkhurst DF. 1977. 3-dimensional model for CO_2 uptake by continuously distributed mesophyll in leaves. *Journal of Theoretical Biology* **67**, 471-488.

Parkhurst DF. 1984. Mesophyll resistance to photosynthetic carbon dioxide uptake in leaves - dependence upon stomatal aperture. *Canadian Journal of Botany-Revue Canadienne De Botanique* **62**, 163-165.

Parkhurst DF. 1994. Diffusion of CO_2 and other gases inside leaves. *New Phytologist* **126**, 449-479.

Parkhurst DF, Mott KA. 1990. Intercellular diffusion limits to CO_2 uptake in leaves. *Plant Physiology* **94**, 1024-1032.

Pärnik T, Keerberg O. 2007. Advanced radiogasometric method for the determination of the rates of photorespiratory and respiratory decarboxylations of primary and stored photosynthates under steady-state photosynthesis. *Physiologia Plantarum* **129**, 34-44.

Peguero-Pina JJ, Flexas J, Galmes J, Niinemets U, Sancho-Knapik D, Barredo G, Villarroya D, Gil-Pelegrin E. 2012. Leaf anatomical properties in relation to differences in mesophyll conductance to CO_2 and photosynthesis in two related Mediterranean Abies species. *Plant, Cell & Environment* **35**, 2121-2129.

Pons TL, Flexas J, von Caemmerer S, Evans JR, Genty B, Ribas-Carbo M, Brugnoli E. 2009. Estimating mesophyll conductance to CO_2: methodology, potential errors, and recommendations. *Journal of Experimental Botany* **60**, 2217-2234.

Price GD, Voncaemmerer S, Evans JR, Yu JW, Lloyd J, Oja V, Kell P, Harrison K, Gallagher A, Badger MR. 1994. Specific reduction of chloroplast carbonic-anhydrase activity by antisense RNA in transgenic tobacco plants has a minor effect on photosynthetic CO2 assimilation. *Planta* **193**, 331-340.

Rand RH. 1977. Gaseous-diffusion in leaf interior. *Transactions of the ASAE* **20**, 701-704.

Rand RH. 1978. Theoretical analysis of CO_2 absorption in sun versus shade leaves. *Journal of Biomechanical Engineering* **100**, 20-24.

Rand RH, Cooke JR. 1980. A comprehensive model for CO_2 assimilation in leaves. *Transactions of the ASAE* **23**, 601-607.

Raschke K. 1956. Über die physikalischen Beziehungen zwischen Warmeübergangszahl, Strahlungsaustausch, Temperatur und Transpiration eines Blattes. *Planta* **48**, 200-238.

Reece JB, Urry LA, Cain ML, Wasserman SA, Minorsky PVM, Jackson RB. 2011. Photosynthesis. *Campbell Biology 9th edition*. Berkeley, California: Benjamin Cummings/Pearson. 184-205.

Sage TL, Sage RF. 2009. The functional anatomy of rice leaves: implications for refixation of photorespiratory CO_2 and efforts to engineer C_4 photosynthesis into rice. *Plant and Cell Physiology* **50**, 756-772.

Sander R. 2014. Compilation of Henry's law constants, version 3.99. *Atmospheric Chemistry and Physics* **14**, 29615-30521.

Scafaro AP, Von Caemmerer S, Evans JR, Atwell BJ. 2011. Temperature response of mesophyll conductance in cultivated and wild Oryza species with contrasting mesophyll cell wall thickness. *Plant, Cell & Environment* **34**, 1999-2008.

Sharkey TD. 1985. Photosynthesis in intact leaves of C_3 plants - physics, physiology and rate limitations. *Botanical Review* **51**, 53-105.

Sharkey TD. 2015. What gas exchange data can tell us about photosynthesis. *Plant, Cell & Environment,* in press. doi: 10.1111/pce.12641.

Sinclair TR, Goudriaan J, De Wit CT. 1977. Mesophyll resistance and CO_2 compensation concentration in leaf photosynthesis models. *Photosynthetica* **11**, 56-65.

Spurr AR. 1969. A low-viscosity epoxy resin embedding medium for electron microscopy. *Journal of Ultrastructure Research* **26**, 31-43.

Sun JD, Feng ZZ, Leakey ADB, Zhu XG, Bernacchi CJ, Ort DR. 2014a. Inconsistency of mesophyll conductance estimate causes the inconsistency for the

estimates of maximum rate of Rubisco carboxylation among the linear, rectangular and non-rectangular hyperbola biochemical models of leaf photosynthesis-A case study of CO_2 enrichment and leaf aging effects in soybean. *Plant Science* **226**, 49-60.

Sun JD, Nishio JN, Vogelmann TC. 1998. Green light drives CO_2 fixation deep within leaves. *Plant and Cell Physiology* **39**, 1020-1026.

Sun Y, Gu LH, Dickinson RE, Norby RJ, Pallardy SG, Hoffman FM. 2014b. Impact of mesophyll diffusion on estimated global land CO_2 fertilization. *Proceedings of the National Academy of Sciences of the United States of America* **111**, 15774-15779.

Sun Y, Gu LH, Dickinson RE, Pallardy SG, Baker J, Cao YH, DaMatta FM, Dong XJ, Ellsworth D, Van Goethem D, Jensen AM, Law BE, Loos R, Martins SCV, Norby RJ, Warren J, Weston D, Winter K. 2014c. Asymmetrical effects of mesophyll conductance on fundamental photosynthetic parameters and their relationships estimated from leaf gas exchange measurements. *Plant, Cell & Environment* **37**, 978-994.

Tazoe Y, von Caemmerer S, Badger MR, Evans JR. 2009. Light and CO_2 do not affect the mesophyll conductance to CO_2 diffusion in wheat leaves. *Journal of Experimental Botany* **60**, 2291-2301.

Tazoe Y, von Caemmerer S, Estavillo GM, Evans JR. 2011. Using tunable diode laser spectroscopy to measure carbon isotope discrimination and mesophyll conductance to CO_2 diffusion dynamically at different CO_2 concentrations. *Plant, Cell & Environment* **34**, 580-591.

Terashima I, Hanba YT, Tazoe Y, Vyas P, Yano S. 2006. Irradiance and phenotype: comparative eco-development of sun and shade leaves in relation to photosynthetic CO2 diffusion. *Journal of Experimental Botany* **57**, 343-354.

Terashima I, Hanba YT, Tholen D, Niinemets U. 2011. Leaf functional anatomy in relation to photosynthesis. *Plant Physiology* **155**, 108-116.

Thain JF. 1983. Curvature correction factors in the measurement of cell-surface areas in plant-tissues. *Journal of Experimental Botany* **34**, 87-94.

Tholen D, Boom C, Noguchi K, Ueda S, Katase T, Terashima I. 2008. The chloroplast avoidance response decreases internal conductance to CO_2 diffusion in Arabidopsis thaliana leaves. *Plant, Cell & Environment* **31**, 1688-1700.

Tholen D, Boom C, Zhu XG. 2012a. Opinion: Prospects for improving photosynthesis by altering leaf anatomy. *Plant Science* **197**, 92-101.

Tholen D, Ethier G, Genty B. 2014. Mesophyll conductance with a twist. *Plant, Cell & Environment* **37**, 2456-2458.

Tholen D, Ethier G, Genty B, Pepin S, Zhu XG. 2012b. Variable mesophyll conductance revisited: theoretical background and experimental implications. *Plant, Cell & Environment* **35**, 2087-2103.

Tholen D, Zhu XG. 2011. The mechanistic basis of internal conductance: a theoretical analysis of mesophyll cell photosynthesis and CO_2 diffusion. *Plant Physiology* **156**, 90-105.

Tomas M, Flexas J, Copolovici L, Galmes J, Hallik L, Medrano H, Ribas-Carbo M, Tosens T, Vislap V, Niinemets U. 2013. Importance of leaf anatomy in determining mesophyll diffusion conductance to CO_2 across species: quantitative limitations and scaling up by models. *Journal of Experimental Botany* **64**, 2269-2281.

Tomas M, Medrano H, Brugnoli E, Escalona JM, Martorell S, Pou A, Ribas-Carbo M, Flexas J. 2014. Variability of mesophyll conductance in grapevine cultivars under water stress conditions in relation to leaf anatomy and water use efficiency. *Australian Journal of Grape and Wine Research* **20**, 272-280.

Tosens T, Niinemets U, Vislap V, Eichelmann H, Diez PC. 2012a. Developmental changes in mesophyll diffusion conductance and photosynthetic capacity under different light and water availabilities in *Populus tremula*: how structure constrains function. *Plant, Cell & Environment* **35**, 839-856.

Tosens T, Niinemets U, Westoby M, Wright IJ. 2012b. Anatomical basis of variation in mesophyll resistance in eastern Australian sclerophylls: news of a long and winding path. *Journal of Experimental Botany* **63**, 5105-5119.

Uehlein N, Otto B, Hanson DT, Fischer M, McDowell N, Kaldenhoff R. 2008. Function of Nicotiana tabacum aquaporins as chloroplast gas pores challenges the concept of membrane CO_2 permeability. *Plant Cell* **20**, 648-657.

Verboven P, Herremans E, Helfen L, Ho QT, Abera M, Baumbach T, Wevers M, Nicolaï BM. 2015. Synchrotron X-ray computed laminography of the three-dimensional anatomy of tomato leaves. *Plant Journal* **81**, 169-182.

Verboven P, Kerckhofs G, Mebatsion HK, Ho QT, Temst K, Wevers M, Cloetens P, Nicolaï BM. 2008. Three-dimensional gas exchange pathways in pome fruit characterized by synchrotron X-ray computed tomography. *Plant Physiology* **147**, 518-527.

Vesala T, Ahonen T, Hari P, Krissinel E, Shokhirev N. 1996. Analysis of stomatal CO_2 uptake by a three-dimensional cylindrically symmetric model. *New Phytologist* **132**, 235-245.

Vesala T, Hameri K, Ahonen T, Kulmala M, Hari P, Pohja T, Krissinel E, Shokhirev N, Lushnikov AA. 1995. Experimental and numerical analysis of stomatal absorption of sulfur dioxide and transpiration by pine needles. *Atmospheric Environment* **29**, 825-836.

Vogelmann TC, Evans JR. 2002. Profiles of light absorption and chlorophyll within spinach leaves from chlorophyll fluorescence. *Plant, Cell & Environment* **25**, 1313-1323.

von Caemmerer S, Evans JR. 1991. Determination of the average partial pressure of CO_2 in chloroplasts from leaves of several C_3 plants. *Australian Journal of Plant Physiology* **18**, 287-305.

von Caemmerer S, Farquhar GD. 1981. Some relationships between the biochemistry of photosynthesis and the gas exchange of leaves. *Planta* **153**, 376-387.

von Caemmerer S, Furbank RT. 2003. The C_4 pathway: an efficient CO_2 pump. *Photosynthesis Research* **77**, 191-207.

Vrabl D, Vaskova M, Hronkova M, Flexas J, Santrucek J. 2009. Mesophyll conductance to CO_2 transport estimated by two independent methods: effect of

variable CO_2 concentration and abscisic acid. *Journal of Experimental Botany* **60**, 2315-2323.

Watté R, Aernouts B, Van Beers R, Herremans E, Ho QT, Verboven P, Nicolaï B, Saeys W. 2015. Modeling the propagation of light in realistic tissue structures with MMC-fpf: a meshed Monte Carlo method with free phase function. *Optics Express* **23**, 17467-17486.

Williams TG, Flanagan LB, Coleman JR. 1996. Photosynthetic gas exchange and discrimination against CO_2 -^{13}C and (COO)-^{18}O-^{16}O in tobacco plants modified by an antisense construct to have low chloroplastic carbonic anhydrase. *Plant Physiology* **112**, 319-326.

Wullschleger SD. 1993. Biochemical limitations to carbon assimilation in C_3 plants - a retrospective analysis of the A/C_i curves from 109 species. *Journal of Experimental Botany* **44**, 907-920.

Yin X, Belay DW, van der Putten P, Struik PC. 2014. Accounting for the decrease of photosystem photochemical efficiency with increasing irradiance to estimate quantum yield of leaf photosynthesis. *Photosynthesis Research* **122**, 323-335.

Yin X, Struik PC. 2009. Theoretical reconsiderations when estimating the mesophyll conductance to CO_2 diffusion in leaves of C_3 plants by analysis of combined gas exchange and chlorophyll fluorescence measurements. *Plant, Cell & Environment* **32**, 1513-1524.

Yin X, Struik PC. 2015. Constraints to the potential efficiency of converting solar radiation into phytoenergy in annual crops: from leaf biochemistry to canopy physiology and crop ecology. *Journal of Experimental Botany* **32**, 448-464.

Yin X, Struik PC, Romero P, Harbinson J, Evers JB, Van Der Putten PEL, Vos J. 2009. Using combined measurements of gas exchange and chlorophyll fluorescence to estimate parameters of a biochemical C_3 photosynthesis model: a critical appraisal and a new integrated approach applied to leaves in a wheat (*Triticum aestivum*) canopy. *Plant, Cell & Environment* **32**, 448-464.

Yin X, Sun ZP, Struik PC, Gu JF. 2011. Evaluating a new method to estimate the rate of leaf respiration in the light by analysis of combined gas exchange and

chlorophyll fluorescence measurements. *Journal of Experimental Botany* **62**, 3489-3499.

Yin X, Van Oijen M, Schapendonk AHCM. 2004. Extension of a biochemical model for the generalized stoichiometry of electron transport limited C_3 photosynthesis. *Plant Cell and Environment* **27**, 1211-1222.

Zhu XG, Long SP, Ort DR. 2010. Improving photosynthetic efficiency for greater yield. *Annual Review of Plant Biology* **61**, 235-261

Summary

Photosynthesis can be defined as the process in which light energy is converted into chemical energy. This process is of vital importance for life on Earth, as it allows plants to convert sun light and inorganic carbon (CO_2) into biomass. A better understanding of photosynthesis is important from an agronomic perspective. In 2009, the Food and Agriculture Organization of the United Nations estimated that the global crop yield has to be increased by 70% by 2050 to meet the global demand for food, fibres and bioenergy due to the increase of the global population. Increasing the efficiency of photosynthesis is necessary to meet this increasing demand, because other measures (increasing the harvest index, the efficiency of light absorption) can only further increase to a small extent and the availability of arable land is limited.

According to the widely used Farquhar-von Caemmerer-Berry model ("FvCB model"), the net rate of CO_2 assimilation is determined by the CO_2 partial pressure near Rubisco under both Rubisco and electron-transport limited conditions. This CO_2 partial pressure is smaller than the CO_2 partial pressure in the atmosphere due to various structural barriers that CO_2 has to cross to reach Rubisco and various processes that add or remove CO_2 along this diffusion pathway. The CO_2 partial pressure in the intercellular air spaces of leaves can be directly calculated from gas exchange measurements of CO_2 and water vapour. The drawdown of the CO_2 partial pressure from the intercellular air spaces to Rubisco is more challenging to determine, as it cannot be determined directly from gas exchange measurements. It is commonly modelled by Fick's first law of diffusion. A formulation of this law is that the flux of a chemical species over a barrier is proportional to the difference in partial pressure of this species at both sides of this barrier. The proportionality constant is the conductance. The inverse of a conductance is a resistance. Commonly, mesophyll resistance models are used to calculate the CO_2 partial pressure near Rubisco. Decreasing the mesophyll resistance can potentially increase the crop yield by 20%, which can be a major contribution to reach the required 70% increase in crop yield. However, mesophyll resistance is a complex trait. It lumps various barriers for CO_2 transport and involves various processes that add or remove CO_2 to the diffusion

pathway. This complexity makes it challenging to identify targets to decrease mesophyll resistance. Therefore, it is necessary to find a more mechanistic description of CO_2 transport in the mesophyll. The aim of this dissertation is to investigate how leaf anatomical properties along the CO_2 diffusion pathway in C_3 leaves and biochemical processes that add CO_2 to this diffusion path or remove it affect the photosynthetic capacity of this leaves. In this study, I used *Solanum lycopersicum* (tomato) as a model plant.

Chapter 2 is a literature review, in which I discuss how mesophyll resistance models have been used in previous work and what the advantages and disadvantages of various approaches are. The simplest approach is to assume that the mesophyll resistance is negligible such that the CO_2 partial pressure in the intercellular air spaces equals the CO_2 partial pressure near Rubisco. The disadvantage of this approach is that if these simple models are used to estimate parameters of the FvCB model, the potential effect of mesophyll resistance will be lumped in these biochemical parameters. It has been shown in previous work that this could lead to wrong results, if this model is used for predictions after parameterization. Various methods have been proposed to estimate mesophyll resistance from gas exchange measurements, sometimes combined with chlorophyll fluorescence. These methods are based on (1) Fick's first law to express the CO_2 partial pressure near Rubisco as a function of the intercellular CO_2 partial pressure and the net CO_2 assimilation rate. (2) substitute this term in the FvCB model. (3a) either rewrite this term to express the mesophyll resistance directly or (3b) rewrite this term to a term that can be determined from gas exchange measurements or chlorophyll fluorescence measurements. Alternatively, the CO_2 partial pressure near Rubisco can be determined by combined measurements of gas exchange and carbon isotope discrimination. Subsequently, the mesophyll resistance can be calculated. Finally, some models use measurements of leaf anatomical properties and assumed values of diffusion coefficients for CO_2 of the subcomponents of the mesophyll to calculate the resistance of each subcomponent. These values are used to calculate the overall mesophyll resistance. Each of these methods assumes that the mesophyll resistance is a serial physical resistance. This

means that it is only determined by the temperature and by the thicknesses and the diffusion coefficients for CO_2 of various mesophyll components. However, several studies showed that the mesophyll resistance obtained by these methods depends on the intercellular CO_2 partial pressure. Consequently, mesophyll resistance must be considered as an apparent variable, rather than a physical resistance. One way to deal with this problem is to use a phenomenological model to describe the mesophyll resistance for parameterization of the FvCB model. Although such a model does consider the variability of the mesophyll resistance, it does not provide any mechanistic explanation for the variability of the mesophyll resistance with the intercellular CO_2 partial pressure.

A possible partial explanation for this variability is the release of CO_2 produced by respiration and photorespiration half way the CO_2 diffusion path. This can be modelled by partitioning the mesophyll resistance into two sub-resistances. These are the combined resistance of the cell wall and the plasma membrane and the combined resistance of the chloroplast envelope and the stroma. Between these two resistances, i.e. the cytosol, it is assumed that the release of CO_2 produced by respiration and photorespiration takes place. In Chapter 3, I used this approach to model CO_2 transport in the mesophyll. I quantified the sub-resistances based on leaf anatomical properties. This combined use this model and the partitioning of the mesophyll resistance into two sub-resistances allowed me to directly simulate how changes in leaf anatomical properties affect the net CO_2 assimilation rate. I showed that the net CO_2 assimilation rate is most sensitive to changes in the ratio of the exposed mesophyll surface area to the leaf area and to the ratio of the the exposed chlorophyll surface area to the exposed mesophyll surface area.

This approach has some limitations. It needs assumed values of diffusion coefficients for CO_2 and the ratio of the length of the CO_2 diffusion path in the stroma to the stroma thickness. These values area uncertain. The approach of two sub-resistances with a CO_2 source in between either assumes that (1) CO_2 produced by respiration and photorespiration is released in the outer cytosol (cytosol layer between plasma membrane and chloroplast envelope) or (2) there is no CO_2 gradient in the cytosol. In

case (1), the fraction of CO_2 produced by respiration and photorespiration that is re-assimilated may be underestimated. This can result in an underestimation of the net CO_2 assimilation rate. In case (2), the position of mitochondria relative to the stroma does not have any effect on the re-assimilation of CO_2 produced by (photo)respiration which is not realistic. It is also not possible to use this model to study CO_2 diffusion in the cytosol gaps between the chloroplast. These gaps may be used in reality as a pathway for CO_2 produced by respiration and photorespiration to escape to the intercellular air spaces. Finally, photosynthesis models that include mesophyll resistance are algebraically complex. This makes it both hard to make adjustments and to understand the model's behaviour.

Reaction-diffusion models can be used as an alternative to mesophyll resistance models, since they avoid certain assumptions. First, reaction-diffusion models do not need a predefined ratio of the length of the diffusion pathway in the stroma to the stroma thickness. Second, they allow to specify the position of the mitochondria relative to the chloroplast. In Chapter 2, I describe a literature study in which I investigated the use of these models in previous photosynthesis research. The earliest reaction-diffusion models often used a porous medium approach. A disadvantage of this approach is that it assumes that CO_2 assimilation can take place at any location of the leaf. However, in reality the CO_2 assimilation only occurs in the chloroplasts. Chloroplasts only fill a small fraction of the mesophyll and are concentrated near the exposed mesophyll surface area. Using a porous medium approach results in a predicted CO_2 gradient between the adaxial and the abaxial sides which may not be there in reality. This issue was solved by the modelling CO_2 transport in the gas phase and the liquid phase separately in more recent reaction-diffusion models. Other important improvements are the explicit modelling of individual chloroplasts and restricting RuBP carboxylation to these chloroplasts and respiration and photorespiration outside them. In Chapter 4, I developed a reaction-diffusion model, which I used to analyse gas exchange data combined with chlorophyll fluorescence data. I also used it to study how the position of mitochondria affects the net CO_2 assimilation rate. I found that the predicted net CO_2 assimilation under high

irradiances or low ambient CO_2 partial pressure is considerably higher if it is assumed that respiration and photorespiration take place in the inner cytosol than in the outer cytosol. If these processes take place in the cytosol gaps, the predicted net CO_2 assimilation is in between. I only used gas exchange and chlorophyll fluorescence data measured at low irradiances or low CO_2 partial pressures to estimate of FvCB model parameters with the reaction-diffusion model. In Chapters 4 and 5, I tested the model by predicting the net CO_2 assimilation rate for the remaining combination of oxygen levels, irradiances and CO_2 partial pressures. In almost all cases, the model that assumed that CO_2 release by respiration and photorespiration take place in the inner cytosol predicted the measurements reasonably well. The models that assumed that these processes take place in the outer cytosol performed worse in predicting CO_2 response curves under photorespiratory conditions, and light response curves in almost all leaf types.

In Chapter 4, I also presented a method to calculate the fraction of (photo)respired CO_2 that is re-assimilated. In Chapter 5, I further used this method to investigate how re-assimilation responds to changes in environmental conditions and leaf physiological parameters. I found that the relationship between the ambient CO_2 partial pressure and the fraction of (photo)respired CO_2 that is re-assimilated has an inverse S shape. It is high at low and intermediate ambient CO_2 levels. For higher CO_2 levels, it strongly decreases. At high ambient CO_2 levels it stabilizes again. The fraction of (photo)respired CO_2 that is re-assimilated is low at low irradiances and it increases with increased irradiance. The rate of this increase decreased with increased irradiance. I found that increases in the stomatal conductance and the FvCB parameters that determine the sink strength of CO_2 in the chloroplasts can strongly increase the fraction of CO_2 produced by (photo)respiration that is re-assimilated under saturating light and ambient CO_2 levels. In contrast, the fraction of (photo)respired CO_2 that was re-assimilated only slightly decreased with increased rates of respiration under these conditions.

Commonly used methods to estimate the rate of respiration in the light implicitly assume that all CO_2 produced by respiration is released in the atmosphere. This

assumption can potentially underestimate the respiration rate. In Chapter 5, I investigated this by using the reaction-diffusion model to estimate the rate of respiration directly for each of the scenarios of (photo)respired CO_2 release. Under both photorespiratory and non-photorespiratory conditions, the estimate was not affected by the position of the mitochondria relative to the chloroplasts. This can be explained by the low fraction of (photo)respired CO_2 that is reassimilated at low light levels. However, I did find that the estimates of the rate of respiration were considerably higher than under non-photorespiratory conditions. This is an indication that the rate of respiration depends on the oxygen partial pressure and that estimates of the rate of respiration obtained under non-photorespiratory conditions should not be assumed equal to the rate of respiration under photorespiratory conditions.

Based on the results of this dissertation, I do not think that mesophyll resistance models are capable of identifying the targets to decrease mesophyll resistance. It is an apparent variable that lumps various structural barriers for CO_2 transport and biochemical processes. In order to explain the drawdown of the CO_2 partial pressure between the intercellular air spaces and Rubisco, it is necessary to make models that are capable of studying all these factors separately. This can only be done to a limited extent with resistance models that partition the mesophyll resistance into sub-resistances. However, these models either constrain the location of mitochondria in the outer cytosol, and assume that there is no CO_2 gradient in the cytosol or require more sub-resistances than can be determined by gas exchange measurements combined with either chlorophyll fluorescence or carbon isotope discrimination measurements. In order to use reaction-diffusion models in further studies, I recommend to put more effort in the measurement of diffusion coefficients for CO_2 of various mesophyll components and/or to validate the model from Chapters 4 and 5 for more plant species to check whether the combination of assumed diffusion coefficients makes sense. I want to emphasize that an important disadvantage of reaction-diffusion models is that they may have long computational times, due to the fact that they have to be solved numerically in almost all cases. This limits the number of simulations that can be done by these models within an acceptable time frame. Therefore, I want to recommend to

keep these models simple, whenever possible, to minimize the computational time. Finally, I recommend to extend the model with explicit descriptions of the temperature sensitivity of physical and physiological parameters. This may help to understand how leaf photosynthesis may be affected by the expected rise in both the CO_2 partial pressure and temperature.

Samenvatting

Fotosynthese is een proces, waarin lichtenergie wordt omgezet in chemische energie. Dit proces is van vitaal belang voor het leven op aarde, aangezien het planten in staat stelt om geabsorbeerd zonlicht en anorganische koolstof, in de vorm van CO_2, om te zetten in biomassa. Vanuit een landbouwkundig gezichtspunt is het belangrijk om dit proces goed te begrijpen. De Food and Agriculture Organization van de Verenigde Naties heeft geschat dat in 2050 de globale gewasopbrengst moet toenemen met 70% ten opzichte van 2009 om te kunnen voldoen aan de globale vraag voor voedsel, vezels en bio-energie vanwege de groeiende wereldbevolking en veranderende voedingspatronen. Het is daarom noodzakelijk dat de efficiëntie van fotosynthese hoger wordt, aangezien andere ingrepen slechts zeer beperkt kunnen bijdragen aan het verhogen van de gewasopbrengst. Ook is er maar een beperkte hoeveelheid landbouwgrond beschikbaar.

Volgens het veel gebruikte model van Farquhar, Von Caemmerer en Berry ("FvCB-model"), hangt de netto snelheid van CO_2-opname af van de CO_2-partieeldruk bij Rubisco – het sleutelenzym van de koolstoffixatie. Dit geldt zowel als de CO_2-opname wordt gelimiteerd door de capaciteit van Rubisco als door de snelheid van elektronentransport. De CO_2-partieeldruk bij Rubisco is kleiner dan de CO_2-partieeldruk onder de meeste omstandigheden vanwege verschillende barrières die CO_2 moet passeren om Rubisco te bereiken en vanwege verschillende processen die CO_2 kunnen toevoegen of verwijderen van het diffusiepad. De CO_2-partieeldruk in de intercellulaire ruimte binnen bladeren kan direct worden bepaald van gasuitwisselingsmetingen voor CO_2 en waterdamp op het bladoppervlak. Het verschil in de CO_2-partieeldruk in de intercellulaire ruimte en Rubisco is moeilijker om te onderzoeken, omdat dit niet direct kan worden bepaald met gaswisselingsmetingen. Gewoonlijk wordt dit verschil bepaald met behulp van de eerste wet van Fick voor diffusie. Volgens deze wet is de flux van een stof over een barrière evenredig met het verschil in partieeldruk aan beide zijdes van deze barrière. De evenredigheidsconstante van dit verband is de geleidbaarheid. De inverse van de geleidbaarheid is de weerstand. Gewoonlijk worden modellen voor mesofylweerstand gebruikt om de CO_2-

partieeldruk bij Rubisco te bepalen. Het verkleinen van de mesofylweerstand kan mogelijk leiden tot een toename van de gewasopbrengst met 20%, wat een belangrijke bijdrage kan zijn om de noodzakelijke 70% toename van de globale gewasopbrengst te behalen. De mesofylweerstand is echter een ingewikkelde bladeigenschap. Hij wordt bepaald door de weerstand van allerlei barrières voor CO_2-transport en wordt ook beïnvloed door verschillende processen die CO_2 toevoegen of verwijderen van het CO_2-diffusiepad in het mesofyl. Deze complexiteit maakt het moeilijk om specifieke eigenschappen of processen aan te wijzen die kunnen worden worden veranderd om de mesofylweerstand te verlagen. Daarom is het nodig om een meer mechanistische beschrijving voor CO_2-transport in bladeren te vinden. Het doel van dit proefschrift is om uit te zoeken hoe de efficiëntie van fotosynthese wordt beïnvloed door anatomische eigenschappen van bladeren van C_3-planten en biochemische processen die CO_2 toevoegen of verwijderen van het diffusiepad. In dit onderzoek heb ik tomaat als modelplant gebruikt.

Hoofdstuk 2 is een literatuuroverzicht, waarin ik bespreek hoe het concept mesofylweerstand werd toegepast in eerder onderzoek en wat de voor- en nadelen van verschillende benaderingen zijn. De makkelijkste benadering is om aan te nemen dat de weerstand van het mesofyl verwaarloosbaar is. De CO_2-partieeldruk bij Rubisco is dan gelijk aan die van de intercellulaire ruimte. Het nadeel van deze benadering is dat het effect van de mesofylweerstand invloed heeft op geschatte waardes van parameters van het FvCB model. Uit eerder onderzoek is gebleken dat deze benaderingen kunnen leiden tot verkeerde resultaten, als zo een model wordt gebruikt voor voorspellingen nadat de FvCB parameters zijn geschat. Er zijn verschillende methoden beschreven om de weerstand van het mesofyl te schatten met behulp van gaswisselingsmetingen, soms in combinatie met metingen van chlorofylfluorescentie. Deze methodes zijn gebaseerd op (1) het uitdrukken van de CO_2-partieeldruk bij Rubisco als een functie van de CO_2-partieeldruk in de intercellulaire ruimte, (2) substitutie van deze term in het FvCB model, en (3a) het herschrijven van deze term naar de mesofylweerstand ofwel (3b) het herschrijven van deze term naar een andere term die met metingen van gaswisseling en chlorofylfluorescentie kan worden bepaald. In plaats van deze

benaderingen kan de CO_2-partieeldruk worden bepaald met behulp van een combinatie van gaswisselingsmetingen en metingen van de discriminatie van koolstofisotopen. Vervolgens kan de mesofylweerstand worden berekend. Tenslotte worden in een aantal onderzoeken bladantomische eigenschappen en aangenomen waarden van diffusiecoëfficiënten voor CO_2 van verschillende individuele onderdelen van het mesofyl gebruikt om de weerstand van elk onderdeel uit te rekenen. Vervolgens kan de mesofylweerstand worden berekend. Elk van de bovengenoemde methoden gaat er vanuit dat de mesofylweerstand een samengestelde weerstand is. Dit betekent dat zijn waarde slechts afhangt van de temperatuur en van de diffusiecoëfficiënten van de verschillende onderdelen van het mesofyl. Uit verschillende onderzoeken bleek echter dat de waarde van de mesofylweerstand, die met deze methoden is bepaald, afhangt van de CO_2-partieeldruk in de intercellulaire ruimte. Dit geef aan dat de mesofyl weerstand moet worden beschouwd als een functie die afhangt van de de CO_2-partieeldruk in de intercellulaire ruimte en niet als een fysische weerstand. Een manier om met de variabiliteit van de mesofylweerstand om te gaan is om een fenomenologisch model te gebruiken om de mesofylweerstand te beschrijven om de parameters van het FvCB model te kunnen schatten. Hoewel zo een model in staat is om de variabiliteit van de mesofylweerstand te beschrijven, geeft het geen mechanistische uitleg waarom de mesofylweerstand varieert met de CO_2-partieeldruk in de intercellulaire ruimte.

Een mogelijke uitleg voor deze variabiliteit is het vrijkomen van CO_2, geproduceerd door ademhaling en fotorespiratie. Dit vindt halverwege het CO_2-diffusiepad in het mesofyl plaats. Een manier om dit te modelleren is het opdelen van de mesofylweerstand in twee individuele weerstanden. Dit zijn de samengestelde weerstand van de celwand en het plasmamembraan en de samengestelde weerstand van de chloroplastenveloppe en de stroma van chloroplasten. Tussen deze weerstanden bevindt zich het cytosol, waarin CO_2 vrijkomt dat is geproduceerd door ademhaling en fotorespiratie. In Hoofdstuk 3 heb ik deze benadering gebruikt om de mesofylweerstand te modelleren en ik heb de twee individuele weerstanden bepaald door ze te berekenen met aangenomen diffusiecoëfficiënten en bladanatomische

eigenschappen. Door deze benadering toe te passen kon ik direct simuleren hoe de netto CO_2-opname wordt beïnvloed door veranderingen van bladanatomische eigenschappen. Ik heb zo laten zien dat de netto CO_2 het meest afhangt van de verhouding van de oppervlakte van het mesofyl dat blootgesteld is aan de intercellulaire ruimte en de oppervlakte van het blad en van de verhouding van de oppervlakte van de chloroplasten aan de kant van de intercellulaire ruimte en het oppervlakte van het blootgestelde mesofyl.

De benadering heeft een aantal beperkingen. Het is noodzakelijk om waardes aan te nemen voor de diffusiecoëfficiënten van CO_2 en voor de verhouding van de lengte van het CO_2-diffusiepad in de stroma en de totale dikte van de stroma. Deze waarden zijn onzeker. Verder gaat de benadering van twee weerstanden er van uit dat ofwel (1) CO_2 geproduceerd door ademhaling en fotorespiratie vrijkomt in het buitencytosol (de laag cytosol tussen het plasmamembraan en de chloroplastenveloppe aan de kant van de intercellulaire ruimte), ofwel (3) dat er geen CO_2-gradiënt in het cytosol is. In het eerste geval (1) kan het percentage van CO_2 dat door ademhaling en fotorespiratie wordt geproduceerd en opnieuw wordt opgenomen worden onderschat. In het tweede geval (2) zal de positie van mitochondriën geen enkel effect hebben op de re-assimilatie van CO_2 geproduceerd door ademhaling en fotorespiratie. Dit is niet realistisch. Het is ook niet mogelijk om met dit model CO_2-diffusie te modelleren in de cytosolruimtes tussen de chloroplasten. In werkelijkheid vormen deze gaten een pad, waarover CO_2 geproduceerd door ademhaling en fotorespiratie kan ontsnappen naar intercellulaire ruimte. Tenslotte zijn fotosynthesemodellen met mesofylweerstand algebraïsch complex. Dit maakt het zowel moeilijk om het model aan te passen als om het gedrag van het model te begrijpen.

Reactie-diffusiemodellen kunnen worden gebruikt als alternatief voor modellen met mesofylweerstand, aangezien bepaalde aannames niet door deze modellen worden gemaakt. Ten eerste hebben reactie-diffusiemodellen geen aangenomen verhouding van de lengte van het diffusiepad in de stroma en de dikte van het stroma nodig als invoerparameter. Ten tweede is het in reactie-diffusiemodellen wel mogelijk om aan te geven waar de mitochondriën zich bevinden ten opzichte van de chloroplasten.

Hoofdstuk 2 bevat een literatuuronderzoek, waarin ik beschrijf hoe reactie-diffusiemodellen in het verleden werden toegepast in onderzoek over fotosynthese. De vroegste reactie-diffusiemodellen gebruikten vaak de benadering van een poreus medium om de structuur van het mesofyl te modelleren. Het nadeel van deze benadering is dat wordt aangenomen dat CO_2-opname op elke mogelijke plaats in het mesofyl kan plaatsvinden. In werkelijkheid vindt CO_2-opname slechts plaats in de chloroplasten. Deze nemen slechts een klein deel van het totale volume mesofyl in en bevinden zich voornamelijk vlakbij het oppervlakte van het mesofyl dat is blootgesteld aan de intercellulaire ruimte. Wanneer de benadering van poreuze media wordt toepast, kan er een CO_2-gradiënt worden voorspeld tussen de bovenkant en de onderkant van het blad die er in werkelijkheid niet is, er vanuit gaande dat er slechts huidmondjes zijn aan de onderkant van het blad. Dit probleem werd opgelost door de gasfase en de vloeibare fase van CO_2-diffusie in het mesofyl in gescheiden compartimenten te modelleren. Een andere belangrijke verbetering in meer recente modellen is dat chloroplasten als losse compartimenten werden gemodelleerd en dat RuBP carboxylatie slechts in deze compartimenten plaatsvindt en CO_2-productie door ademhaling en fotorespiratie daarbuiten. In Hoofdstuk 4 beschrijf ik een reactie-diffusiemodel dat ik gebruikte om data van metingen van gaswisseling en chlorofylfluorescentie te analyseren. Ik heb dit model ook gebruikt om na te gaan hoe de positie van de mitochondriën invloed heeft op de netto CO_2-opname. Ik heb gevonden dat de snelheid van netto CO_2-opname hoger is als wordt aangenomen dat CO_2 productie door ademhaling en fotorespiratie plaatsvindt in het binnencytosol dan als deze processen plaatsvinden in het buitencytosol. Dit verschil is vooral duidelijk waar te nemen bij lage CO_2- niveaus of hoge lichtintensiteiten Als deze processen plaatsvinden in de cytosolruimtes tussen de chloroplasten, dan ligt de snelheid van netto CO_2-opname daar tussenin. Ik heb bij de schatting van de parameters van het FvCB model met het reactie-diffusiemodel slechts gebruik gemaakt van data van gaswisseling en chlorofylfluorescentie gemeten bij lage CO_2-niveaus en lichtintensiteiten. In Hoofdstuk 4 en 5 heb ik het reactie-diffusiemodel gevalideerd voor de overgebleven data gemeten onder andere combinaties van zuurstofniveaus, CO_2-niveaus en lichtintensiteiten. In vrijwel alle gevallen was het model voldoende in

staat om deze metingen te beschrijven, als werd wordt aangenomen dat CO_2 geproduceerd door ademhaling en fotorespiratie vrij komt in het binnencytosol.

In Hoofdstuk 4 heb ik een methode beschreven waarmee het percentage kan worden berekend van de CO_2 geproduceerd door ademhaling en fotorespiratie die opnieuw wordt opgenomen. In Hoofdstuk 5 heb ik deze methode verder gebruikt om uit te zoeken hoe re-assimilatie afhangt van het milieu en van bladfysiologische parameters. Ik heb gevonden dat de relatie tussen dit percentage en de CO_2-partieeldruk in de atmosfeer een sigmoïdaal verloop heeft. Bij lage en gemiddelde CO_2-niveaus ligt het percentage hoog. Daarna vindt er een sterke daling plaats als de CO_2-partieeldruk in de atmosfeer verder wordt verlaagd. Bij hoge CO_2-partieeldruk stabiliseert het percentage weer. Het percentage van CO_2, geproduceerd door ademhaling en fotorespiratie, is laag bij lage lichtniveaus en stijgt met een toenemende lichtintensiteit. Ik heb ook gevonden dat de het percentage sterk toeneemt onder standaard CO_2-niveaus in de atmosfeer en verzadigde lichtintensiteit met toenemende geleidbaarheid van de huidmondjes en toenemende waardes van parameters van het FvCB model die de snelheid van CO_2-verbruik voor RuBP carboxylatie bepalen.

De gebruikelijk methoden om de snelheid van CO_2-productie door ademhaling gaan er impliciet vanuit dat alle CO_2, geproduceerd door ademhaling in het licht, verloren gaat aan de atmosfeer. Mogelijk kan deze aanname de snelheid van ademhaling in het licht onderschatten. In Hoofdstuk 5 heb ik dit onderzocht door het reactie-diffusiemodel direct te gebruiken om de snelheid van ademhaling in het licht te schatten van data van gaswisseling en chlorofylfluorescentie. Onder zowel omstandigheden met fotorespiratie als zonder fotorespiratie, heb ik gevonden dat de positie van de mitochondriën ten opzichte van de chloroplasten geen invloed heeft op de schattingen van de snelheid van ademhaling in het licht. Dit kan worden verklaard doordat het percentage van CO_2, geproduceerd door ademhaling en fotorespiratie, zeer laag is onder lage lichtniveaus. Ik heb echter wel gevonden dat de schattingen van de snelheid van ademhaling substantieel hoger zijn onder omstandigheden met fotorespiratie dan bij omstandigheden zonder fotorespiratie. Dit is een indicatie dat de snelheid van ademhaling afhangt van de O_2-partieeldruk en dat schattingen van de snelheid van

ademhaling onder omstandigheden zonder fotorespiratie niet zonder meer gelijk kunnen worden gesteld aan de snelheid van ademhaling onder omstandigheden met fotorespiratie.

Op basis van de resultaten in dit proefschrift denk ik niet dat modellen voor de weerstand van het mesofyl in staat zijn om factoren te identificeren die kunnen worden veranderd om de mesofylweerstand te veranderen. Mesofylweerstand is een CO_2-afhankelijke functie die barrières voor CO_2-transport en biochemische processen samenvoegt. Het is noodzakelijk om deze barrières en processen expliciet te modelleren om een verklaring te vinden voor de afname van de CO_2-partieeldruk tussen de intercellulaire ruimte en Rubisco. Dit doel kan in beperkte mate worden bereikt met weerstandsmodellen die de mesofylweerstand opdelen in twee individuele weerstanden. Deze modellen gaat er echter vanuit dat mitochondriën zich slechts in het buitencytosol bevinden, of ze nemen aan dat er geen CO_2-gradiënt in het cytosol bestaat, of ze zullen meer weerstanden nodig hebben dan dat er kunnen worden bepaald aan de hand van gaswisselingmetingen gecombineerd met metingen van chlorofylfluorescentie of discriminatie van koolstofisotopen. Als reactie-diffusiemodellen in toekomstig fotosynthese onderzoek worden gebruikt, dan raad ik aan om meer prioriteit te geven aan het meten van de diffusiecoëfficiënten van de verschillende onderdelen van het mesofyl en/of om modellen, zoals die in Hoofdstuk 4 en 5, verder te valideren voor andere plantensoorten dan tomaat om te zien of combinatie van aangenomen diffusiecoëfficiënten nog steeds resulteert in correcte voorspellingen van de netto-snelheid van CO_2-opname. Ik wil benadrukken dat een belangrijk nadeel van reactie-diffusiemodellen is dat ze lange rekentijden kunnen hebben, aangezien ze vrijwel altijd numeriek moeten worden opgelost. Dit beperkt het aantal simulaties dat met deze modellen kan worden gedaan binnen een aanvaardbare tijdsduur. Daarom raad ik sterk aan om deze modellen, waar mogelijk, zo eenvoudig mogelijk te houden om de rekentijd te minimaliseren. Tenslotte wil ik aanraden om het model uit te breiden met expliciete beschrijvingen van de reactie van fysische en fysiologische parameters ten opzichte van de temperatuur. Dit kan helpen om beter te

begrijpen hoe de bladfotosynthese wordt beïnvloed door de in de toekomst verwachte stijgingen van de CO_2-partieeldruk in de atmosfeer en de temperatuur.

Acknowledgements

I am very grateful to my supervisory team, which consisted of prof. dr. ir. Paul Struik (Centre for Crop Systems Analysis, Wageningen University and Research Centre), prof. dr. ir. Bart M. Nicolaï (Mechanotronics, Biostatistics and Sensors, KU Leuven) and dr. Xinyou Yin (Centre for Crop Systems Analysis, Wageningen University and Research Centre).

Paul, I am very grateful for your never-ending trust in my capability to successfully finish this PhD thesis. I really appreciated that I could always walk into your office if I needed help or encouragement. I also appreciated your fast response to and accurate comments on all texts that I wrote.

Xinyou, I am deeply grateful for all support you provided me. You are open-minded, very analytical and you have an immensely detailed knowledge on leaf photosynthesis. Your advices and our discussions were incredibly useful for me to move in the right direction and they made me very eager to further explore the mechanisms of leaf photosynthesis.

Bart, I am very grateful for all the support that you provided during my stays in Leuven. It was the first time in my life that I spent a long period abroad. This was not always easy for me. I appreciate that you were always there during this period, when this was necessary. You have a very strong capability to look beyond the boundaries of different scientific fields. Your advices were very helpful to successfully finish this interdisciplinary project.

I am also very grateful to dr. Quang Tri Ho (Mechanotronics, Biostatistics, and Sensors, KU Leuven). Tri, you are a very good modeller. I learned a lot from you. I especially appreciate our discussions about the implementation of re-assimilation in my model. I would not have been able to finish this extremely challenging task without your help, your patience and your immense experience.

I am grateful to dr. ir. Steven Driever (Centre for Crop Systems Analysis, Wageningen University and Research Centre) for the brainstorm sessions that we had and his

willingness to be a co-author of my literature review. Thanks to his deep knowledge on measurement techniques in photosynthesis research and his excellent advices related to scientific writing, this chapter improved a lot.

I want to thank Moges Retta (Mechanotronics, Biostatistics, and Sensors, KU Leuven) for his support and patience when he helped me to find my way in the KU Leuven during my first stay and introduced me to COMSOL Multiphysics. I also want to thank him for all discussions that we had during the last years and his constructive criticism on my manuscripts. I learned a lot from them.

I want to thank dr. ir. Pieter Verboven (Mechanotronics, Biostatistics and Sensors, KU Leuven) for his supervision during my stays in Leuven and for granting me access to the facilities for light and transmission electron microscopy at KU Leuven. Access to these facilities was crucial for me to successfully finish the experimental work.

I express my gratitude to dr. Metadel Abera (Mechanotronics, Biostatistics and Sensors, KU Leuven) for his help during the digitization of my microscopic images and for our collaboration to design a virtual leaf generator.

I want to thank to dr. Jeremy Harbinson (Horticulture and Product Physiology, Wageningen University and Research Centre) for the brainstorm sessions that we had during the first year of my PhD. These brainstorm sessions helped me to further develop my ideas.

Cor Langeveld (Centre for Crop Systems Analysis, Wageningen University and Research Centre) recommended me two textbooks that I could borrow from him for years. Especially the textbook Physicochemical Plant Physiology (Nobel, 2009) was extremely useful for me to bridge the gap between biophysics and plant biology. Cor, thank you so much!

This PhD project included a huge amount of experimental work. I would never have been able to finish this on my own and I want to thank all the people that helped me with this. Especially Peter van der Putten (Centre for Crop Systems Analysis, Wageningen University and Research Centre) contributed a lot to the experimental

work. Peter, you took great effort to successfully guide me through my greenhouse experiments. This was not always easy for you, because I probably do not belong to the most skilled persons that you have supervised. I am very grateful for all your hard work and your patience. I also want to thank Tiny Franssen-Verheijen (Laboratory of Virology, Wageningen University and Research Centre), dr. Norbert de Ruiter (Laboratory of Cell Biology, Wageningen University and Research Centre), An Verdoren (Laboratory of Socioecology and Social Evolution, KU Leuven), prof. dr. Johan Billen (Laboratory of Socioecology and Social Evolution, KU Leuven), dr. Arjen Bader (Laboratory of Biophysics, Wageningen University and Research Centre), Arjen van der Peppel (Horticulture and Product Physiology, Wageningen University and Research Centre), Maarten Wassenaar (Horticulture and Product Physiology, Wageningen University and Research Centre), prof. dr. Herbert van Amerongen (Laboratory of Biophysics, Wageningen University and Research Centre), Nele Schoutede (Laboratory of Tropical Crop Improvement, KU Leuven), Victor Baiye Mfortaw Mbong (Mechanotronics, Biostatistics, and Sensors, KU Leuven), Wenjing Ouyang (Centre for Crop Systems Analysis, Wageningen University and Research Centre), Daniel Belay and all people from Unifarm for their assistance during the experimental work and discussing the protocols.

For me, doing a PhD meant that I had to do a lot of work on my own. This is a lonely business. I sometimes tended to focus so much on my own project that I was not able to see the overall picture anymore. The CSA Photosynthesis Discussion Group was a great opportunity for me to interact with other PhD students, postdocs, and permanent staff in CSA, who are working on photosynthesis. This platform helped me significantly to develop my ideas and improve my research. I want to thank my supervisors prof. dr. ir. Paul Struik and dr. Xinyou Yin for stimulating me to establish this discussion group. I also want to thank Peter van der Putten, Alejandro Morales Sierra and dr. ir. Tjeerd-Jan Stomph for their willingness to actively participate in this discussion group for years. Tjeerd-Jan, I appreciated your very broad interest, your enthusiasm and your useful advices during these discussion group meetings. Alejandro, I am really impressed by your modelling skills. I am also impressed by

your capability to ask exactly the right questions to help me to reconsider my ideas. This was sometimes confronting, but it benefited my research a lot at the end. I also want to thank all other people (dr. ir. Steven Driever, dr. Wouter Kegge, dr. Vicky Aerts, Laurens Krah, Kailei Tang, Wanju Shi, dr. Elias Kaiser, dr. Quang Tri Ho, Moges Retta, Wenjing Ouyang, Martin Sikma), who joined some of the meetings for their active contribution when they were in Wageningen. I want to thank Alejandro and Laurens for proofreading one of my manuscripts.

I want to thank Pepijn van Oort, Wopke van der Werf, and Willemien Lommen for their advice about the AIC analysis in Chapter 5 of this thesis.

I want to thank the secretaries of both the Mechanotronics, Biostatistics and Sensors (Inge Cenes) and the Centre for Crop Systems Analysis (Sjanie van Wetten, Nicole Wolffensperger) for their help to arrange all formalities during the course of this PhD project. Nicole, I am thankful for your assistance to combine all loose manuscripts into this booklet. This is not a trivial task, but you helped me to go through this very smoothly. Sjanie, I know you already for more than 6 years. During all this time your door was always open for me, both if I needed to fulfil some formality and if I needed encouragement. I am very grateful for this.

When I approached the end of my PhD, I struggled both with the last steps to finish my thesis and to decide how to proceed my career. I am grateful to Barend van den Broek and Jessica Tummers for both their advice how to properly schedule the last steps of my PhD and how to face life after my PhD. For the latter, I also want to thank prof. dr. ir. Paul Struik, dr. Xinyou Yin, dr. Peter Leffelaar, Cor Langeveld, prof. dr. ir. Bart Nicolaï, dr. ir. Wopke van der Werf, dr. Claudius van de Vijver, dr. Jeremy Harbinson, prof. dr. Niels Anten, and Rien Geuze for their advices.

As I mentioned before, doing a PhD is a lonely business. Especially during the first two years of my PhD, I often felt isolated. I am therefore very grateful to Gou Fang for stimulating the other PhD students to meet to discuss each other's research and other issues, for stimulating to have lunch together and for organizing activities outside work. Because of this, I felt much happier during the last two years of my PhD. This

was very important for me to successfully finish my PhD. I feel privileged that you are willing to be my paranymph.

Finally, I want to thank my sister Marij Berghuijs and my parents dr. Joantine Berghuijs and Gerrit-Klaas Berghuijs for all the love and support they gave to me during the last 4.5 years. Marij, I cannot imagine to have a better cover for my thesis than the one that you designed for me. I am thankful for all your hard work. Papa, I am very grateful for all the support you gave to me, even though I sometimes said that I did not need it. I am grateful for your help to prepare some of my stays in Leuven. Mama, I am also very grateful for all the support you gave to me and that we could share our struggles related to research and doing a PhD. Furthermore, you have a unique ability to understand very complex things, even if they are a way outside your own expertise. Therefore, I thank you for proofreading some of my work and I am happy to have you as my paranymph.

Curriculum vitae

Herman Nicolaas Cornelis Berghuijs was born no November 29 1986 in Voorburg, the Netherlands. He grew up in Zoetermeer, the Netherlands. There, he graduated from high school in 2005. In 2008, he obtained his BSc degree Biology at Leiden University (the Netherlands), in which he specialized in molecular microbiology. During his BSc thesis, he examined whether *Bacillus subtilis* strains can be used as a biocontrol agent to prevent from infection of tomato roots by the soil-borne pathogenic fungus *Fusarium oxysporum* sp. *lycorpersici*. This research was done under the supervision of dr. Floricia Constantinescu and prof. Cees van den Hondel. Afterwards, he started his MSc Biology at Wageningen University, in which he specialized in mathematical biology. During his MSc, he finished two theses. In his first thesis, he developed a mathematical model to compare weed seed bank dynamics in a crop rotation system and in a monoculture system. This research was done under the supervision of dr. Lammert Bastiaans and dr. Wopke van der Werf in the Crop and Weed Ecology group of the Centre for Crop Systems Analysis. During his second thesis, he developed a reaction-diffusion model to simulate the dispersal of the predator carabid beetle *Pterostichus melanarius* on arable lands. This research was done under the supervision of dr. Bas Allema, dr. Lia Hemerik in Biometris and dr. Wopke van der Werf. Both theses have resulted in papers that have been presented at international conferences. In 2011, he obtained his MSc degree. Afterwards, he started his joined PhD at Wageningen University and the Katholieke Universiteit Leuven (Belgium) under supervision of prof. dr. Paul Struik, prof. dr. Bart Nicolaï and dr. Xinyou Yin. During this period, he worked both in the Centre for Crop Systems Analysis (Wageningen University) and the MeBioS division (Katholieke Universiteit Leuven). He examined how leaf anatomy and various biochemical processes that add or remove CO_2 from the CO_2 diffusion pathway in the mesophyll affect the photosynthetic capacity of C_3 leaves. The details of his PhD research can be found in this thesis.

List of publications

Bastiaans L, Berghuijs HNC. 2011. Delivering the barebones for designing more weed suppressive crop rotations. *Proceedings of the Conference on Making Crop Rotations fit for the Future, 20-21 December 2011, Hancock, Newcastle-upon-Tyne, UK*, Vol. 113. Warwick, UK: Association of Applied Biologists, 45-52.

Berghuijs HNC, Allema AB, Hemerik L, Van der Werf W, Groot JCJ, Rossing WAH. 2012. Fokker-Planck model for movement of the carabid beetle Pterostichus melanarius in arable land: Model selection and parameterization. *Proceedings of the Netherlands Entomological Society meeting* **23**, 21-28.

Abera M, Retta MA, Berghuijs HNC, Verboven P, Struik PC, Nicolaï BM. 2014. Virtual microstructural leaf tissue generation based on cell growth modeling. *29th International Horticultural Congress*. Brisbane, Australia.

Berghuijs HNC, Yin X, Ho QT, Van der Putten PEL, Retta MA, Verboven P, Nicolaï BM, Struik PC. 2015. Modeling the relationship between CO_2 assimilation and leaf anatomical properties in tomato leaves. *Plant Science* **238**, 297-311.

Ho QT, Berghuijs HNC, Watté R, Verboven P, Herremans E, Yin X, Retta MA, Aernouts B, Saeys W, Helfen L, Farquhar GD, Struik PC, Nicolaï BM. 2016. 3-D microscale modeling of CO_2 transport and light propagation in tomato leaves enlightens photosynthesis. *Plant Cell and Environment* **39**, 50-61.

Retta MA, Ho QT, Yin X, Verboven P, Berghuijs HNC, Struik PC, Nicolaï BM. 2016 A two-dimensional model of gas exchange during photosynthesis in maize (*Zea mays* L.) leaves. Accepted by *Plant Science*

PE&RC Training and Education Statement

With the training and education activities listed below the PhD candidate has complied with the requirements set by the C.T. de Wit Graduate School for Production Ecology and Resource Conservation (PE&RC) which comprises of a minimum total of 32 ECTS (= 22 weeks of activities)

Review of literature (6 ECTS)

- Reaction-diffusion models extend our understanding of C_3 leaf photosynthesis: opportunities and challenges

Writing of project proposal (4.5 ECTS)

- Physiological and genetic analysis of 3D microscale gas exchange and light penetration

Post-graduate courses (6.8 ECTS)

- Photosynthesis, climate and change; PE&RC (2012)
- Theoretical ecology; RSEE (2012)
- Biofluidics; KU Leuven (2013)

Laboratory training and working visits (1.5 ECTS)

- LICOR Training; LICOR BioScience (2012)
- Various work visits; COMSOL Multiphysics (2012-2014)

Invited review of (unpublished) journal manuscript (1 ECTS)

- PlosOne: relationship between mesophyll conductance and patchy stomatal closure (2015)

Competence strengthening / skills courses (2.4 ECTS)

- Project and time management; WGS (2015)
- Interpersonal communication skills; WGS (2015)
- Career assessment; WGS (2015)

PE&RC Annual meetings, seminars and the PE&RC weekend (1.5 ECTS)

- PE&RC Weekend, first year (2012)
- PE&RC Weekend, last year (2014)

Discussion groups / local seminars / other scientific meetings (7.5 ECTS)

- Modelling and statistics discussion group (2012-2014)
- CSA Photosynthesis discussion group; including the coordination (2012-2015)

International symposia, workshops and conferences (8.3 ECTS)

- COMSOL Conference (2015)
- Biosolar cells cluster meeting (2012, 2014)
- Biosolar cells annual meeting (2012- 2014)

Lecturing / supervision of practical's / tutorials (1.5 ECTS)

- Plant adaptation and plasticity (2012)
- Crop systems analysis (2012, 2013)

Funding

This work was carried out within the research programme of Biosolar Cells, co-financed by the Dutch Ministry of Economic Affairs.